Lactate Metabolism in Cancer Cell Lines

by

Kelly M. Kennedy

Department of Pathology
Duke University

Date:_____

Approved:

_____
Mark W. Dewhirst, Supervisor

_____
Donald P. McDonnell

_____
Laura P. Hale

_____
Robin E. Bachelder

_____
Jen-Tsan Ashley Chi

Dissertation submitted in partial fulfillment of
the requirements for the degree of Doctor
of Philosophy, in the Department of
Pathology in the Graduate School
of Duke University

2013

ABSTRACT

Lactate Metabolism in Cancer Cell Lines

by

Kelly M. Kennedy

Department of Pathology
Duke University

Date:_____

Approved:

_____
Mark W. Dewhirst, Supervisor

_____
Donald P. McDonnell

_____
Laura P. Hale

_____
Robin E. Bachelder

_____
Jen-Tsan Ashley Chi

An abstract of a dissertation submitted in partial fulfillment of the requirements for the degree of Doctor of Philosophy in the Department of Pathology in the Graduate School of Duke University

2013

Abstract

Pathophysiologic lactate accumulation is characteristic of solid tumors and has been associated with metastases and poor overall survival in cancer patients. In recent years, there has been a resurgence of interest in tumor lactate metabolism. In the past, our group has shown that lactate can be used as a fuel in some cancer cell lines; however, survival responses to exogenous lactate alone are not well-described. We hypothesized that lactate utilization and cellular responses to exogenous lactate were varied and dynamic, dependent upon factors such as lactate concentration, duration of lactate exposure, and of expression of the lactate transporter, monocarboxylate transporter 1 (MCT1). We hypothesized that pharmacological inhibition of MCT1 with a small molecule, competitive MCT1 inhibitor, α-cyano-4-hydroxycinnamic acid (CHC), could elicit cancer cell death in high lactate conditions typical of that seen in breast cancer.

My work focused on defining: 1. Lactate levels in locally advanced breast cancer (LABC); 2. Lactate uptake and catabolism in a variety of cancer cell lines; 3. The effect of exogenous lactate on cancer cell survival; 4. Whether the lactate-transporters, MCT1 and MCT4 can be used as markers of cycling hypoxia.

Lactate levels in LABC biopsies were assessed *ex vivo* by bioluminescence. NMR techniques were employed extensively to determine metabolites generated from ^{13}C-

labeled lactate. Cell viability in response to extracellular lactate (± glucose and ± CHC) was measured with Annexin V / 7-AAD staining to assess acute survival responses and clonogenic assays to evaluate long-term colony forming ability after lactate treatment. MCT1 and MCT4 protein expression was evaluated in cancer cell lines with Western blots after exposure to chronic or cycling hypoxia. Immunofluorescence was employed to assess MCT1 and MCT4 expression in head and neck cancer biopsies, and the expression patterns of the transporters were correlated to areas of hypoxia, as indicated by hypoxia marker EF5.

Lactate concentrations in LABC biopsied ranged from 0 – 12.3 μmol/g of tissue. The LABC dataset was too small to derive statistical power to test if lactate accumulation in LABC biopsies was associated with poor patient outcome or other clinical parameters of known prognostic significance. All cell lines tested (normal and cancer) showed uptake and metabolism of labeled lactate, with dominant generation of alanine and glutamate; however, relative rates and the diversity of metabolites generated was different among cell lines. MCF7 cells showed greater overall lactate uptake (mean = 18mM) over five days than MDA-MB-231 cells (mean = 5.5mM). CHC treatment effectively prevented lactate uptake in cancer cells when lactate concentrations were ≤20mM.

Cell survival was dependent upon lactate concentration and glucose availability. Acute responses to exogenous lactate did not reflect the long-term consequences of

lactate exposure. Acutely, HMEC and R3230Ac cells were tolerant of all lactate concentrations tested (0-40mM) regardless of presence or absence of glucose. MCF7 and MDA-MB-231 cells were tolerant of lactate within the concentration ranges seen in biopsies. Cytotoxicity was seen after 24 hr incubation with 40mM lactate (-glucose), but this concentration is three times higher than any measurement made in human biopsies of LABC. Similarly, HMEC and MCF7 cells showed significantly decreased colony formation in response to 40mM exogenous lactate (+ glucose) while R3230Ac and MDA-MB-231 cells showed no impairment in colony-forming abilities with any lactate concentration (+ glucose). 5mM CHC significantly increased cell death responses independent of lactate treatment, indicating off-target effects at high concentrations.

MCT1 was found to be expressed in a majority of the cell lines tested, except for MDA-MB-231 cells. Cancer cells exposed to exogenous lactate showed upregulation of MCT1 but not MCT4. Chronic hypoxia resulted in an increase in protein expression of MCT4 but a decrease in MCT1 expression in cancer cell lines. The time course of regulation of protein levels of each transporter suggested the possibility of expression of both transporters during cycling hypoxia. When cancer cells were exposed to cycling hypoxia, both transporters showed upregulation. In head and neck tumor biopsies, MCT1 expression was significantly positively correlated to aerobic tumor regions and inversely correlated to hypoxic tumor regions.

Cancer cell responses to exogenous lactate were not uniform. Some cell lines demonstrated a lactate-tolerant and/or a lactate-consuming phenotype while other cell lines demonstrated lactate-intolerant and/or non-lactate-consuming phenotype. My work indicates that exogenous lactate was well-tolerated at clinically relevant concentrations , especially in the presence of glucose. Evidence of glutamate metabolism from lactate indicated that exogenous lactate partially progresses through the TCA cycle, suggesting that lactate may be utilized for fuel. The cell death elicited from 5mM CHC treatment was not dependent upon presence of lactate, indicating that manipulation of lactate metabolism may not be the best option for targeting cancer metabolism. When attempting to manipulate lactate metabolism in tumors, microenvironmental factors, such as hypoxia and glucose, must be taken into account in order to ensure a predictable and favorable outcome. Together, these results illustrate the importance of characterizing tumor metabolism before therapeutic intervention.

Dedication

This work is dedicated to my grandparents:

Arlene Sghiatti: The loving and generous nurturer that cooks her way into everyone's heart.

Juliano Sghiatti: An inspiration in dedication and resourcefulness in pulling oneself up by one's own bootstraps.

Leona Kennedy: The head lioness of the pride, exemplifying inner strength and devotion.

Thomas Kennedy: A salt-of-the-earth guardian of our family and country.

I'm fighting the enemy that stole many of you from me too soon in the hopes of lessening the suffering of other grandchildren.

Contents

Abstract iv

List of Tables xvi

List of Figures xix

Abbreviations xxviii

Acknowledgements xxxi

1. Introduction 1

1.1 Introduction to Lactate in Cancer 4

1.1.2 Characteristics of the Tumor Microenvironment and Cancer Metabolism 7

1.1.2.1 Hypoxia and the Pasteur Effect 9

1.1.2.2 The Warburg Effect 12

1.1.2.3 HIF and c-Myc regulation of metabolism 15

1.1.2.4 Spatial distribution of lactate in tumors 17

1.2 Lactate Metabolism 19

1.2.1 Lactate Consumption in Normal Tissue 21

1.2.1.1 Lactate Utilization in Muscle 22

1.2.1.2 Lactate Utilization in Brain 23

1.2.2 Lactate Utilization in Tumors 24

1.2.3 Lactate Uptake Rates 28

1.2.4 Lactosis versus Acidosis 29

1.3 The monocarboxylate transporter (MCT) family 34

1.3.1 MCT1 and MCT4 expression and regulation 36

1.3.2 MCTs and cancer 39

1.3.2.1 Inhibition of MCT1 as a potential therapeutic option in cancer treatment 42

1.4 The epithelial to mesenchymal transition (EMT) in cancer and connections to tumor metabolism 46

1.4.1 The potential importance of lactate signaling in EMT 48

1.5 Objective 51

2. Methods 52

2.1 Lactate and CHC 52

2.2 Cell Culture 52

2.3 Protein extractions and concentration assay 53

2.3.1 Total Protein (RIPA buffer) 53

2.3.2 Total Protein (Triton X lysis buffer) 54

2.3.3 Protein concentration assay 54

2.4 Western Blots 54

2.4.1 MCT blots 54

2.4.1.1 MCT1/4 expression regulation 55

2.4.2 Snail, Slug and Twist Western blots 56

2.5 Human LABC and HNSCC samples 58

2.5.1 Sample Storage 58

2.5.2 Cryosectioning 58

2.5.3 Immunohistochemistry on LABC biopsies 59

2.5.4 LABC genomics 60
2.5.5 Data analysis and statistics for LABC samples 61
2.6 Immunofluorescence in cells and tissue 63
2.6.1 Preparation of Coverslips for Staining 63
2.6.2 Membrane Expression of MCT1/4 63
2.6.3 Immunohistochemistry for MCT1 and MCT4 on tissue samples 64
2.6.4 Confocal Microscopy 65
2.7 Bioluminescence 65
2.8 NMR for 13C-lactate in vitro 67
2.9 Cell survival assays 68
2.9.1 Clonogenic Survival Assays 68
2.9.1.1 Clonogenic Survival Assay Protocol 1 68
2.9.1.2 Clonogenic Survival Assay Protocol 2 70
2.9.2 Apoptosis/Cell Death Assays: Annexin V / 7-AAD staining 71
2.9.3 Cell Cycle/Propidium Iodide staining 73
2.9.4 Assessment of Cell Survival after Detachment 75
2.10 Statistics 75
3 Lactate levels in Locally Advanced Breast Cancer (LABC) 77
3.1 Introduction 77
3.2 Results 81
3.2.1 Patient clinical parameters 81

3.2.2 Lactate accumulation occurs in LABC biopsies, but higher lactate concentrations do not significantly correlate with greater % invasive cancer 84

3.2.3 Lactate levels show intratumoral heterogeneity 86

3.3 Discussion 88

4. Lactate uptake and catabolism occurs *in vitro* in cancer cells and normal cells 93

4.1 Introduction 93

4.2 Results 97

4.2.1 MCT1 expression in breast cell lines 97

4.2.2 Preliminary lactate consumption experiments *in vitro* show greater lactate uptake in MCF7 cells compared to MDA-MB-231 98

4.2.3 ^{13}C NMR *in vitro* 102

4.2.3.1 All cell lines tested take up ^{13}C-lactate 106

4.2.3.2 Most cell lines show common lactate-derived metabolites 108

4.2.3.3 HepG2 and MEF cells convert ^{13}C-lactate to produce a diverse metabolic profile 111

4.2.3.4 Cell lines transport lactate-generated metabolites out of the cell 114

4.2.4 CHC does not effectively inhibit lactate uptake in HUVEC cells but does inhibit uptake in R3230Ac rat mammary carcinoma for lactate concentrations ≤20mM 116

4.3 Discussion 124

5. Cell Viability after Lactate Exposure 131

5.1 Introduction 131

5.2 Results 134

5.2.1 High pathophysiologic lactate levels and prolonged lactate exposure significantly decrease clonogenicity and increase cell death 134

5.2.1.1 Breast cancer cell lines MCF7 and MDA-MB-231 showed clonogenic decline after lactate exposure 136

5.2.1.2 Glucose-deprived breast cancer cell lines MCF7 and MDA-MB-231 but not normal breast cells (HMEC) or R3230Ac cells showed a significant increase in cell death after 24 hr exposure to very high lactate levels (≥40mM) 144

5.2.1.3 Normal liver cells WRL-68 showed clonogenic decline after lactate exposure; hepatocellular carcinoma cells HepG2 showed a varied clonogenic response to lactate exposure 148

5.2.1.4 Normal liver cells (WRL-68) and liver cancer cells (HepG2) showed a significant increase in cell death and early apoptosis events (HepG2 only) after 24 hr exposure to very high lactate levels (≥40mM) 152

5.2.1.5 Comparison of clonogenic assay and flow cytometry results 154

5.2.3 Glucose deprivation has a greater influence on cell cycle than treatment with exogenous lactate 155

5.2.4 The effect of MCT1-inhibitor (CHC) on cell survival 158

5.3 Discussion 164

6. MCT1 and MCT4 as Potential Markers of Cycling Hypoxia 170

6.1 Introduction 170

6.2 Results 171

6.2.1 MCT1 and MCT4 regulation with lactate exposure and hypoxia 172

6.2.1.1 Coverslip IF shows positive MCT1 expression in normoxic conditions and positive MCT4 expression in hypoxic conditions 172

6.2.1.2 MCT1 and MCT4 are regulated by lactate and hypoxia *in vitro*; cycling hypoxia upregulates both MCT1 and MCT4 174

6.2.2 MCT1 and MCT4 expression in human cancer biopsies 179

6.2.2.1 Seventy percent of LABC biopsies show positive expression of MCT1 ... 179

6.2.2.2 MCT1 and MCT4 expression in HNSCC ... 180

6.3 Discussion ... 184

7. Conclusions and Future Directions ... 189

7.1 Consequences of lactate metabolism ... 189

7.2 Tumor metabolism manipulation as a therapeutic strategy ... 191

Appendix A ... 200

Additional Tables for Section 3 ... 200

Appendix B ... 210

Cell Detachment after Lactate Treatment ... 210

Appendix C ... 213

MCT1 Regulation by ERRα ... 213

Appendix D ... 216

Proteomics and phosphoproteomics in liver cell lines reveal cytoskeletal protein regulation by lactate ... 216

Appendix E ... 227

Assessment of EMT Signaling After Lactate Treatment ... 227

References ... 239

Biography ... 274

List of Tables

Table 1: Classification of tumors 3

Table 2: Lactate in solid tumors 4

Table 3: Cellular pH regulators 31

Table 4: MCT1 and MCT4 expression in solid tumors 41

Table 5: Markers of epithelial and mesenchymal cells 47

Table 6: Potential relevance of lactate to different EMT subtypes 50

Table 7: Conditions for cell survival experiments with CHC treatment 72

Table 8: Clinical characteristics of LABC patients 81

Table 9: Comparison of patient clinical parameters and specimen lactate concentrations in the low (Lo [L]) vs. high (Hi [L]) lactate groups 83

Table 10: Lactate distribution in LABC biopsies 84

Table 11: Cell lines used for *in vitro* ^{13}C-lactate metabolism experiments 102

Table 12: Chemical shifts for anticipated metabolites generated from 3-^{13}C-lactate 106

Table 13: Statistical analysis of lactate concentrations that significantly decrease clonogenic survival of breast cancer cells 138

Table 14: Increased duration of lactate exposure significantly decreases clonogenic survival of breast cancer cell lines 139

Table 15: Increased duration of lactate exposure significantly influences clonogenic survival of liver cell lines 151

Table 16: Clonogenic survival response to lactate is significantly different in HepG2 cells 152

Table 17: Summary of breast cell line responses to exogenous lactate 168

Table 18: Genes and pathways of interest for LABC analysis 200

Table 19: Mean lactate concentrations in inflammatory vs. noninflammatory LABC specimens 204

Table 20: Mean lactate concentrations in ER+ vs. ER- LABC specimens 205

Table 21: Mean lactate concentrations in PR+ vs. PR- LABC specimens..... 205

Table 22: Mean lactate concentrations in Her2+ vs. Her2- LABC specimens 205

Table 23: Mean lactate concentrations in LABC specimens from patients with triple negative breast cancer vs. not triple negative breast cancer 206

Table 24: Mean lactate concentrations in LABC specimens from patients with relapse vs. no relapse 206

Table 25: Mean lactate concentrations in LABC specimens from patients with TMN staging ≥ 3 vs. TMN staging < 3 206

Table 26: Mean lactate concentrations in LABC specimens from patients with nodal involvement (+) vs. no nodal involvement (-)..... 207

Table 27: Mean lactate concentrations in LABC specimens from patients with distant metastases vs. no distant metastases..... 207

Table 28: Mean lactate concentrations in LABC specimens from patients with a positive (alive) or negative (dead) outcome..... 207

Table 29: Mean lactate concentrations in LABC specimens from patients with cCR, cPR or cSD..... 208

Table 30: Mean lactate concentrations in LABC specimens from patients with pCR, pPR or pSD 208

Table 31: Mean lactate concentrations in LABC specimens from patients with IIb, IIIa or IIIb tumors 208

Table 32: Mean lactate concentrations in LABC specimens from patient tumors displaying MPTS 4-6 vs. MPTS 0-3..... 209

Table 33: Mean lactate concentrations in LABC specimens from patient tumors displaying a centrifugal (CF) vs. centripetal (CP) DCE-MRI parameters..... 209

Table 34: Highly regulated proteins in HepG2 cells after 24 hr treatment with 10mM of sodium lactate.....220

Table 35: Commonly upregulated phosphoproteins in HepG2 and WRL-68 cells after lactate treatment.....223

Table 36: Commonly downregulated phosphoproteins in HepG2 and WRL-68 cells after lactate treatment.....224

Table 37: Differentially regulated phosphoproteins in HepG2 and WRL-68 cells after lactate treatment.....225

List of Figures

Figure 1: High lactate in solid tumors is associated with poor patient outcome and increased metastases in head and neck cancer (top) and colorectal cancer (bottom). Top: Patients with H&N tumors with high lactate show significantly decreased OS (left) and DFS (right) compared to patients with low tumor lactate levels. Bottom: Metastatic rectal adenocarcinoma shows significantly higher lactate concentrations than nonmetastatic adenocarcinoma (left); metabolite levels as measured by bioluminescence show high lactate *ex vivo* (right). Reprinted with permission [22, 24]. 6

Figure 2: Theoretical representation of oxygen and metabolite concentrations in relation to intervessel distance in solid tumors. Tumor vessels = red bars, [lactate] = green line, [glucose] = purple line, [ATP] = orange line, pH_e = black line, pO_2 = blue line. Areas of hypoxia are represented by the light blue box. Areas of anoxia are represented by the dark blue box. As intervessel distance increases, pO_2, ATP, pH_e and glucose levels decrease while extracellular lactate increases, resulting in a hypoxic and acidic microenvironment. Adapted from [45]. 8

Figure 3: "Tides" of oxygen during cycling hypoxia. Microregions of tissue experience varying severity of hypoxia due to temporal fluctuations in pO_2 levels. "Low tide" is an analogy describing lack of oxygen surrounding a region of tumor tissue when pO_2 is low (left). In regions of the tumor in which pO_2 is higher, microregions experience adequate oxygenation. Adapted from [64]. 11

Figure 4: Spatial distribution of lactate in rat tumors. Lactate (green) accumulates in hypoxic (yellow), necrotic (n) and viable (v) tumor regions of rat tumors, R3230 Ac (top) and FSA (bottom). The tumor edge is indicated (e). Ranges of lactate measurements in microregions of represented tumor slices are indicated on the right. Reprinted from [104] with permission. 18

Figure 5: Representative images of the lactate distribution in LABC biopsies. Tumor regions ("T") are indicated in H&E (A&C) sections of LABC biopsies. Lactate bioluminescence (B&D) shows lactate accumulation in the stroma (B) and tumor (D) region of LABC biopsies. For each sample, lactate measurements are n=3-4 sections. 85

Figure 6: Waterfall chart of lactate concentrations in each individual LABC biopsy with accompanying clinical information. Biopsies with invasive cancer are denoted as "LABC," but biopsies without invasive cancer are marked as "bb." The median concentration is represented by the middle line of the boxplot. Ranges of the 25th and 75th

percentile concentrations are represented by the black and gray portions of the box, respectively. Error bars indicate 95% confidence intervals. †p<0.05 87

Figure 7: Metabolic pathways in which lactate (yellow) participates are marked in pink. 94

Figure 8: Lactate uptake and intracellular metabolism. Lactate enters the cell through a MCT (green cylinder) and is converted to pyruvate before being transported into the mitochondria via the MPC (purple cylinder). Pyruvate can complete oxidative phosphorylation or generate glutamate from α-ketoglutarate after partial completion of the Kreb's Cycle. Alanine can be generated from the reversible reaction of pyruvate + glutamate → α-ketoglutarate + alanine..... 96

Figure 9: Representative Western blot showing MCT1 expression in total protein samples from MCF7, MDA-MB-231 and HMEC cells. MCF7 and HMEC show MCT1 expression, but MDA-MB-231 showed very little to no MCT1 expression. 98

Figure 10: Lactate concentration measurements over five days showed a greater decline in the cell media of MCF7 cells than in the cell media of MDA-MB-231 cells. Lines in the plots represent individual experiments. Samples were taken from cell media of a cell-free plate (Media, A), MDA-MB-231 (B) and MCF7 cells (C) over a period of 5 days (n=5). Rate coefficients of lactate consumption as determined by a linear regression model are significantly different for MCF7 compared to MDA-MB-231 cells..... 100

Figure 11: MCF7 cells show a significantly different relative rate of lactate consumption compared to MDA-MB-231 cells. Total drop in lactate concentration (mM) in the cell media of MCF7 and MDA-MB-231 cells after 5 days of 20mM lactate exposure. Mean lactate concentration decrease in the media of MCF7 cells was 18.3mM, significantly greater than the mean decrease in lactate concentration in the media of MDA-MB-231 cells (5.5mM, *p = 0.0006, n = 5) (A). Relative rates of lactate consumption for breast cancer cell lines reported as mM of lactate consumed per cell show significantly more lactate is consumed by MCF7 cells compared to MDA-MB-231 cells (*p < 0.05, n = 5) (B). 101

Figure 12: ^{1}H NMR plots of known metabolites to acquire chemical shifts. Starting from the bottom, the spiked metabolites are lactate, alanine, pyruvate, glutamate, and α-ketoglutarate. 103

Figure 13: Biochemical pathways of labeled lactate generate labeled metabolites. A ^{13}C enrichment label is represented by the stars. 3-^{13}C-lactate can generate 3-^{13}C-pyruvate, 3-

^{13}C-alanine, 4-^{13}C-citrate, 4-^{13}C-α-ketoglutarate and 4-^{13}C-glutamate. Modified with permission from [292]..... 105

Figure 14: HMQC and ^{13}C NMR plots of metabolites generated from labeled lactate. HMQC (A, B, D) or ^{13}C (C) NMR plots of cell extracts treated for 4.5 hr with 10mM ^{13}C-lactate showing ^{13}C-lactate (L) uptake and ^{13}C-glutamate (G), ^{13}C-alanine (A), and ^{13}C-pyruvate (P) generation in HMEC (A), MCF7 (B), MDA-MB-231 (C) and WRL-68 cells (D)..... 107

Figure 15: HMQC NMR plots of cell extracts of CCD1112Sk and SNU-182 cells. CCD1112sk (A) and SNU-182 (B) cells treated for 4.5 hr (A) or 24 hr (B) with 10mM ^{13}C-lactate showing ^{13}C-lactate (L) uptake and ^{13}C-glutamate (G), and ^{13}C-alanine (A) generation..... 108

Figure 16: HMQC NMR plots of cell extracts of HMEC, MDA-MB-231, MCF7 and WRL-68 cells. Each cell line was treated for 24 hr with 10mM ^{13}C-lactate. Cell extracts revealed ^{13}C-lactate (L) uptake and ^{13}C-glutamate (G), ^{13}C-alanine (A), and ^{13}C-pyruvate (P) generation in HMEC (A), MDA-MB-231 (B), MCF7 (C) and WRL-68 cells (D) 109

Figure 17: Overlaid HMQC NMR plots of breast cell extracts. HMQC NMR plots from breast cells treated for 24 hr with 10mM ^{13}C-lactate were overlaid to identify common metabolites generated from labeled lactate in HMEC and MDAMB231 cells (A), HMEC and MCF7 cells (B) and MDAMB231 and MCF7 cells (C)..... 111

Figure 18: HMQC NMR plots of HepG2 and MEF cell extracts. After 24 hr treatment with 10mM lactate cell extracts showed ^{13}C-lactate (L) uptake and ^{13}C-glutamate (G), ^{13}C-alanine (A), ^{13}C-pyruvate (P) and unknown ^{13}C metabolite species generation in MEF (A) and HepG2 cells (B) 113

Figure 19: ^{13}C-labeled metabolites generated from lactate catabolism are transported out of the cell. Labeled metabolites (^{13}C-glutamate “1, 2”, ^{13}C-lactate “3”, and ^{13}C-alanine “4”) were observed in the cell culture media after 24 hr incubation with ^{13}C-lactate. Each cell line shows different relative rates and amount of lactate utilization. Studies conducted in collaboration with and Figure made by Dr. Thies Schroeder. 116

Figure 20: Expected ^{13}C-lactate metabolism with high (5mM) and low (0.1mM) CHC treatments. Labeled lactate metabolism in the absence of CHC will show generation of labeled alanine and glutamate. High CHC will prevent lactate uptake via MCT1-inhibition; low CHC will prevent lactate catabolism to alanine and glutamate via MPC-inhibition. Stars indicate ^{13}C enrichment. 117

Figure 21: 5mM CHC does not prevent lactate uptake in HUVEC cells. 1D ^{13}C NMR plots of HUVEC cell extracts after 6 hr treatment with 10mM ^{12}C-lactate (bottom), 10mM ^{13}C-lactate (second from bottom), 10mM ^{13}C-lactate + DMSO (second from top), and 10mM ^{13}C-lactate + 5mM CHC (top). ^{13}C-lactate (L) is present in all 13C-lactate treatments despite the presence of CHC, a putative MCT1 inhibitor. 119

Figure 22: R3230Ac cells treated with 20mM ^{13}C-lactate + Low (0.1mM) or high (5mM) CHC treatment show no intracellular labeled metabolites in ^{1}H NMR spectra of the cell extract. Cell extracts from R3230 Ac cells treated for 4hrs (A&B) or 24hrs (C&D) with 0.1mM CHC (A&C) or 5mM CHC (B&D) and 20mM of ^{13}C-lactate. Metabolites in the cell extract included endogenous lactate (L_{en}) and endogenous alanine (A_{en}). DMSO is indicated by D. 121

Figure 23: R3230Ac cells treated with 20mM ^{13}C-lactate + Low (0.1mM) or high (5mM) CHC treatment show abundant ^{13}C-lactate and endogenous lactate in the ^{1}H NMR spectra of the cell media. Cell media from R3230 Ac cells treated for 4hrs (A&B) or 24hrs (C&D) with 0.1mM CHC (A&C) or 5mM CHC (B&D) and 20mM of ^{13}C-lactate. Metabolites in the cell media included ^{13}C-lactate (^{13}C-L) and endogenous lactate (L_{en}). DMSO is indicated by D. 123

Figure 24: Lactate treatment significantly decreased colony forming abilities of breast cancer cell lines (protocol 1). Clonogenic survival assays using protocol 1 showed a significant decrease in the colony-forming abilities of MCF7 (A, B) and MDA-MB-231 (C, D) cells with increasing lactate concentrations and duration of lactate exposure in glucose-deprived (A, C) and glucose-available (B, D) conditions. All results are reported after normalizing to the untreated control. Detached cells were excluded from these assays, per clonogenic survival assay protocol 1. 137

Figure 25: High lactate treatment for 24 hr significantly decreased colony formation of HMEC cells. HMEC cells seeded at a density of 100 (A) or 500 (B) show a significant decrease in clonogenic survival (protocol 2) with 24 hr treatment with 40mM lactate (One-Way ANOVA, $p<0.05$) in the presence of glucose. Detached cells included. 140

Figure 26: Lactate treatment of 10mM and 40mM for 24 hr showed significantly decreased colony formation of MCF7 cells. MCF7 cells seeded at a density of 500 (A) or 1500 (B) show a significant decrease in clonogenic survival (protocol 2) at lactate concentrations of 10mM and 40mM (One-Way ANOVA, $*p<0.05$) in the presence of glucose. Detached cells included. 142

Figure 27: Lactate treatment for 24 hr did not significantly influence the colony-forming abilities of MDA-MB-231 or R3230Ac cells. MDA-MB-231 (A, B) and R3230Ac (C, D) cells seeded at a density of 200 (A, C) or 1000 (B, D) do not show significant changes in clonogenic survival (protocol 2) in response to 24 hr exogenous lactate treatment in the presence of glucose. Detached cells included. 143

Figure 28: Cell viability as measured by Annexin V / 7-AAD labeling (n=3) in lactate-treated (+glucose) breast cell lines. HMEC (A), MCF7 (B), MDA-MB-231 (C), and R3230Ac (D) cells show no significant changes after 24 hr exposure to exogenous lactate (0-40mM) in the context of available glucose. No significant changes in cell death responses (Annexin V+ / 7-AAD-, Annexin V- / 7-AAD+, or Annexin V+ / 7-AAD+) were observed in HMEC (E), MCF7 (F), MDA-MB-231 (G) or R3230Ac cells (H) after 24 hr exposure to exogenous lactate (0-40mM) in the context of available glucose. 145

Figure 29: Cell viability as measured by Annexin V / 7-AAD labeling (n=3) in lactate-treated (-glucose) breast cell lines HMEC (A) and R3230Ac (D) cells show no loss of cell viability with 24 hr lactate treatment. MCF7 (B) and MDA-MB-231 (C) showed a significant decrease in live cells after 24 hr exposure 40mM lactate (no glucose). There were no cell death responses in HMEC (E) and R3230Ac cells (H) after 24 hr exposure to exogenous lactate (0-40mM, no glucose). The percentage of Annexin V+ / 7-AAD+ MCF7 (F) and MDA-MB-231 (G) cells increased significantly with 24 hr 40mM lactate treatment in the absence of glucose. CNT = complete media (including glucose), no lactate. # $p < 0.001$, * $p < 0.05$ One-Way ANOVA 147

Figure 30: Lactate treatment significantly decreased colony forming abilities of WRL-68 cells, but HepG2 cells showed a variable response to lactate treatment (protocol 1). Clonogenic survival (protocol 1) decreases in WRL-68 (A, B) increasing lactate concentrations and duration of lactate exposure in glucose-deprived (A) and glucose-available (B) conditions. HepG2 cells (C, D) show decreasing clonogenic survival with 48 hr exposure but show highly variable responses at different lactate concentrations and exposure times. 149

Figure 31: Cell viability and death as measured by Annexin V / 7-AAD labeling (n=3) in liver cell ines. WRL-68 (A, B) and HepG2 cells (C, D) showed a significant decrease in Annexin V- / 7-AAD- labeled cells after 24 h exposure to 40mM exogenous lactate in the context of glucose deprivation (A, C). Percentage of Annexin V- / 7-AAD+ WRL-68 cells (B) increased significantly with 24 h 40mM lactate treatment in the absence of glucose. Percentage of Annexin V+ / 7-AAD- HepG2 cells showed a significant increase with 24 h

40mM lactate treatment (-glucose) (D). CNT = complete media (including glucose), no lactate. *p < 0.01, #p < 0.0033, One-Way ANOVA. 153

Figure 32: Five-day lactate treatment impairs breast cancer cell line growth. Treatment with 20mM of lactate in the context of glucose deprivation for 5 days decreased MCF7 cell growth and significantly decreased MDA-MB-231(p < 0.05, One-Way ANOVA) cell growth *in vitro,* as measured by hemocytometer cell counts, compared to high glucose DMEM control. 156

Figure 33: Cell cycle distribution of cell lines after 48 hr lactate exposure. Cell cycle distribution of MCF7 (A), MDA-MB-231 (B), HMEC (C), WRL-68 (D) and HepG2 (E) cells were measured by P.I. staining, after 48 hr treatment with lactate (0-20mM) in the context of no glucose or 5mM of glucose. There were no significant changes in cell cycle distribution except in glucose-deprived HMEC cells compared to glucose-sufficient HMEC cells (*p < 0.05, One-Way ANOVA). Lactate was not found to be a significant factor in cell cycle regulation. CNTRL = complete media, no lactate. 157

Figure 34: High CHC significantly decreases breast cancer cell viability. Percent of viable (Annexin V- / 7-AAD-) MCF7 (A) or R3230Ac (B) cells significantly decreases after 24 hr treatment with high (5mM) CHC independent of exogenous lactate (40mM) supplementation. *p < 0.05 high CHC compared to all other groups, †p < 0.0001 high CHC compared to 0mM CHC groups, One-Way ANOVA. 162

Figure 35: High CHC significantly increased cell death responses in breast cancer cell lines. Cell death responses to 24 h treatment with high (5mM) or low (0.1mM) CHC in MCF7 (A-C) or R3230Ac (D-F) cells showed that high CHC significantly increased the percent of MCF7 cells with Annexin V+ / 7-AAD+ staining (C) and the percent of R3230Ac cells undergoing apoptosis (D). *p < 0.05, One-Way ANOVA 163

Figure 36: Coverslip IF demonstrating reliable detection of MCT1. SiHa cells (positive MCT1 control, top) but not MDA-MB-231 cells (negative control, bottom) displayed membrane expression of MCT1 (red) when grown on glass coverslips. 173

Figure 37: Coverslip IF demonstrating reliable detection of MCT4. WiDr cells (positive MCT4 control, top) but not SiHa cells (negative control, bottom) displayed membrane expression of MCT4 (red) when grown on glass coverslips. 174

Figure 38: MCT1 expression increased after treatment with exogenous lactate. Representative Western blots of the time course of MCT1 and MCT4 expression changes

in A549 (top) and HT1080 cells (bottom) after exposure to 10mM lactate. MCT1 increased in each cell line as the duration of lactate exposure increased. 175

Figure 39: MCT1 expression decreased and MCT4 expression increased after exposure to chronic hypoxia. Representative Western blots of the time course of MCT1 and MCT4 expression changes in A549 (top) and HT1080 cells (bottom) after exposure to 0.5% O_2. In both cell lines, MCT1 protein expression was downregulated and MCT4 protein expression was upregulated after prolonged exposure to hypoxia. 177

Figure 40: MCT1 and MCT4 expression increased with exposure to cycling hypoxia and re-oxygenation. Representative Western blots of MCT1 and MCT4 protein expression changes in A549 (top) and HT1080 cells (bottom) in response to cycling hypoxia. After 3-5 cycles of hypoxia and 12 hr re-oxygenation, MCT1 and MCT4 protein was upregulated in both cell lines..... 178

Figure 41: Seventy percent of LABC biopsies showed expression of MCT1. Representative image (n=3) of positive MCT1 (red) IF in a locally advanced breast cancer biopsy..... 179

Figure 42: Demonstration of IF artifacts in head and neck patient biopsies. EF5 (red) signal bleed-through to the MCT channel (green) is marked by the white arrows. High background in the MCT channel from secondary antibody is marked by the yellow arrows. 181

Figure 43: Representative images (n=3) demonstrating of the inverse relationship between MCT1 expression (green) and hypoxia (EF5, red) in human head and neck cancer samples..... 183

Figure 44: MCT1 expression is significantly correlated to normoxic regions of human head and neck cancer specimens. Positive MCT1 staining (n=3 per section) in HNSCC biopsies (n=9) is significantly higher in normoxic regions than in hypoxic regions ($p<0.0001$, A), and MCT1 signal is highly correlated with normoxia (negative EF5 staining) ($r=0.9$, $p<0.0001$, B). 184

Figure 45: Breast cancer cell detachment after lactate treatment. MCF7 (top), MDA-MB-231 (middle), and T47D (bottom) cells show cellular detachment from the culture plate after treatment with 0-40mM of lactate (+glucose) for 24 h, 48 h, or 1 week. 211

Figure 46: Viability of breast cancer cells post-detahment as assessed by the Trypan Blue Exclusion assay. A majority of MCF7 (top) and T47D (bottom) cells retain viability after detaching from the culture plate post-lactate treatment. 212

Figure 47: MCT1 regulation by ERRα. ERRα and MCT1 induction in MCF7 (top) and MDA-MB-231 cells (bottom) after transfection with ERRα-specific plasmids. MCT1 shows upregulation with ERRα/PGC-1α stimulation. 215

Figure 48: Representative image of F-actin changes after 24 hr lactate treatment. Phalloidin staining was conducted for detection of F-actin in MCF7 (A-D), MDA-MB-231 (E-H) and HepG2 (I-L) cells (n=2). F-actin expression varied between cell lines with 24 hr glucose deprivation ("-G") (B-C, F-G, J-K) and lactate supplementation (C-D, G-H, K-L). Lactate (+G) enhances F-actin expression in MCF7 cells but suppresses F-actin expression in HepG2 cells. 222

Figure 49: Network of lactate-regulated phosphoproteins common to WRL-68 and HepG2 cells. Processes affected by lactate include ion channels, solute carrier transporters, calcium signaling, metabolism and cytoskeletal rearrangement. 226

Figure 50: Schematic of mammosphere assays. "Pre" lactate treatment indicates lactate supplementation while cells were grown in monolayer; "Post" lactate treatment indicate lactate supplementation while cells were grown as primary and secondary spheres. 230

Figure 51: Stacked bar graphs (% of cells) of CD24 and CD44 expression changes in breast cancer cell lines after 24 hr exposure to lactate. There were no significant changes in CD24 or CD44 expression after 24 hr treatment with exogenous lactate (+ or – glucose) in MDA-MB-231 (A) and MCF7 cells (B). 232

Figure 52: Stacked bar graphs (% of cells) of CD24 and CD44 expression changes in breast cancer cell lines after 10 day exposure to lactate. There were no significant changes in CD24 and CD44 expression after 10 day treatment with exogenous lactate (+ or – glucose) in MDA-MB-231 (A) and MCF7 cells (B). 233

Figure 53: High endogenous Snail-1 expression in MCF7 cells. MCF7 cells exposed to lactate for 3 days (n=2) showed high endogenous Snail-1 mRNA (top) and low E-cadherin (bottom). 234

Figure 54: Snail-1 mRNA expression but not protein expression increased with 3-day lactate treatment in T47D cells. Representative images of Snail-1 mRNA (top) and protein expression (bottom) in T47D cells after lactate treatment (n=3). Increased mRNA

expression of Snail-1 and decreased E-cadherin after 3-day lactate treatment (A). Quantified Snail-1 mRNA relative to 10mM lactate-treated group (B) and quantified E-cadherin mRNA (C) for results pictured in A. Representative Western blot of Snail-1 and Twist in T47D cells shows slight increase after lactate exposure (D); quantified protein expression of Snail-1 relative to the control (E). 236

Figure 55: Primary mammosphere formation was significantly increased with 3-day 10mM and 40mM lactate treatments in T47D cells. Representative independent experiments of primary (A) and secondary (B) mammosphere formation in T47D cells after 3-day treatment with exogenous lactate. 10mM and 40mM lactate significantly increase primary mammosphere formation (*$p<0.05$, One-Way ANOVA, A). No significant changes were seen in secondary mammosphere formation after lactate treatment (B). 238

Abbreviations

ALT = alanine transferase

AMPK = ‘5-AMP-activated protein kinase

ATCC = America Type Culture Collection

CA = carbonic anhydrase

CHC = α-cyano-4-hydroxycinnamic acid

CSC = cancer stem cell

DFS = disease-free survival

ECM = extracellular matrix

EMT = epithelial to mesenchymal transition

ERR-α = estrogen-related receptor alpha

ETC = electron transport chain

FBS = fetal bovine serum

FGFR = fibroblast growth factor receptor

GLUT = glucose transporter

HIF = hypoxia-inducible factor

HMEC = human mammary epithelial cell

HUVEC = human umbilical vein endothelial cell

IHC = immunohistochemistry

IF = immunofluorescence

K_m = the Michaelis constant

LABC = locally advanced breast cancer

LDH = lactate dehydrogenase

MCT = monocarboxylate transporter (proton-coupled)

MET = mesenchymal to epithelial transition

MMP = matrix metalloproteinases

MPC = mitochondrial pyruvate carrier

NF-κB = nuclear factor kappa-light-chain-enhancer of activated B cells

NMR = nuclear magnetic resonance

OS = overall survival

OXPHOS = oxidative phosphorylation

PDC = pyruvate dehydrogenase complex

PDH = pyruvate dehydrogenase

PDK = pyruvate dehydrogenase kinase

PFK = phosphofructokinase

PGC-1α = peroxisome proliferator-activated receptor gamma coactivator-1 alpha

pH_e = extracellular pH

pH_i = intracellular pH

PTM = posttranslational modification

ROS = reactive oxygen species

RT-PCR = real time reverse transcriptase polymerase chain reaction

SLC = solute carrier

SMCT = sodium-coupled monocarboxylate transporter

TCA = tricarboxylic acid

TME = tumor microenvironment

Acknowledgements

Many people helped me along the way, and I would like to take a moment to thank them.

My loving boyfriend, Nikola Kilibarda: He has been a source of joy, support and relief during the long process of finishing my degree, adding light and beauty to my life. His intellectual contributions to my work have provided insight and new ideas. (And I thank him for humoring me, as he has been subjected to longer conversations about lactate than he may have ever wanted.)

My supportive parents, Florene and Thomas Kennedy: They have been an endless source of moral support and have provided me with encouragement and comfort. Their examples of hard work, dedication and loyalty have been an inspiration for me.

My awesome brothers, Thomas and Donald Kennedy: They have kept me smiling and laughing. New interests and hobbies they have introduced me to have kept me balanced.

My friends:

Justin Wisner and Ethan Dale: For entertaining my whimsical side and providing insightful discussions on literature, philosophy, art, nature and design.

Kenneth Young, Chelsea Landon, Peter Scarbrough, PhD, Rhea Brooking-Dixon, PhD, Yvonne Mowery, MD, PhD and Andrew Fontanella: For providing friendship and encouragement. They have added color and fun to the lab environment and/or the grad school experience and have contributed to experimental design and assisted with statistical analysis and/or interpretations of results.

My advisor, Mark W. Dewhirst, DVM, PhD: He has taught me the importance of collaborating and interacting with scientists from different disciplines, striving for clarity in scientific writing and always remembering to keep the big picture in mind. His guidance has prepared me for the scientific challenges that lie ahead.

My thesis committee members:

Donald McDonnell, PhD: He has provided an excellent example of honesty and directness and instilled the importance of transparency in science. He has made me a better scientist and skeptic by presenting challenges and pushing me to meet high standards.

Robin Bachelder, PhD: She has been an important source of encouragement for me personally and professionally. Always up on current information and deeply involved

in the search for scientific knowledge, I consider her a role model in dedication and fortitude.

Laura Hale, MD, PhD: Her practical approach, attention to detail and wealth of knowledge is admirable, and her influence has helped to keep me grounded and focused. Her care for and involvement with students provides direction and moral support.

Jen-Tsan (Ashley) Chi, MD, PhD: His influence and collaboration has provided me with perspective and new insights. With his advisement on limitations and opportunities, substantial improvements in my project have followed.

Salvatore Pizzo, MD, PhD: For taking a personal interest in my success and career development, providing moral support, assistance and a shared rapport on many topics. His contributions to manuscript revisions are valued.

Rachel Richardson, DVM, PhD and Hong Yuan, PhD: For their advice and examples, and for collaborating on the lactate project and providing *in vivo* data for a 2013 publication.

Sturgis Payne: Assisting with Snail-1 and Slug experiments.

Lan Lan, PhD and Kouros Owzar, PhD: Assisted with statistical analyses.

Mike Cook, PhD: Conducted a majority of the flow cytometry in my project.

Arthur Moseley, PhD and Brenna Richardson, PhD: Conducted proteomic and phosphoproteomic analysis.

Dewhirst lab members for their contributions, discussions and support.

The Garcia-Blanco Lab, especially Jason Somarelli, PhD: For providing T47D reporter cell lines and assisting with these EMT experiments.

Kimberly Blackwell, MD and Joseph Geradts, MD: For providing LABC samples and tissue analysis.

Shara Reihani, PhD: Assisting with access to LABC clinical data and patient de-identification.

The Pizzo Lab: Provided access to lab space and instruments.

1. Introduction

In 2008, the estimated number of new cancer cases was 12.7 million worldwide [1, 2]. 40% of these new cases can be attributed to lung, female breast, colorectal and stomach cancers. Cancer is the leading cause of death in developed countries and the second leading cause of death in developing countries [3]. 13% of all deaths that occurred in 2008 were due to cancer; the percentage is equivalent to 7.6 million people [2]. This year, over half a million Americans are expected to die from cancer [4]. Future projections of cancer burden in the world population for 2030 estimates a 75% increase compared with 2008, which is roughly 22 million cases each year [5].

Breast cancer is one of the most common cancers diagnosed in women (23% of all new cancer cases) and is the leading cause of cancer death in females worldwide (14% of total cancer deaths in women)[1, 2]. One in eight women will be diagnosed with breast cancer during her lifetime [6], and, in the U.S., breast cancer accounts for one third of cancer diagnoses in women. While a 7% decline in breast cancer incidence rates in the U.S. was reported in 2002-2003 [7], this trend has not continued [8].

Though not restricted to elderly individuals, cancer is a disease of the aging population [9].The world population continues to rise, and, in developed countries, life expectancy is also increasing. In the U.S., life expectancy has increased by 8 years since 1970. As individuals live longer, the risk for cancer incidence also increases [9]. While medical science has made considerable progress in cancer treatment and prevention, this

disease not only has an personal and emotional impact on individual lives, but it also carries a heavy economic burden: the economic cost of premature death and disability from cancer worldwide is equivalent to $895 billion [10].

The greatest gift we could give to future generations is freedom from the burdens of cancer. If such an idealistic goal is not within reach just yet, we can continue to strive to lessen the load. Cancer is the enemy, and wisdom regarding war against one's enemy comes from Sun Tzu's *Art of War*:

> "If you know the enemy and know yourself, you need not fear the result of a hundred battles. If you know yourself but not the enemy, for every victory gained you will also suffer a defeat. If you know neither the enemy nor yourself, you will succumb in every battle." [11]

We must know our enemy.

"Cancer" is the more common term for what is known medically as malignant neoplasms (new growth). Tumors consist of proliferating neoplastic cells (the parenchyma) and the supporting connective tissue and blood vessels (the stroma). Tumors are classified as benign or malignant based on distinct features (Table 1, [12]). Progression to a malignant phenotype involves four basic steps: 1. Transformation, 2. Growth, 3. Local invasion, and finally 4. Metastases [12]. Metastatic spread greatly reduces the possibilities of tumor control, effective treatment and patient survival [12].

Table 1: Classification of tumors

Benign	Malignant
Well differentiated	Poorly differentiated
Slow, progressive growth	Rapid and/or erratic growth
Usually smaller	Larger
Demarcated	Poorly demarcated
Noninvasive	Invasive and infiltrating normal tissue
Nonmetastatic	Metastatic

Neoplasms are considerably heterogeneous and diverse, which poses a challenge when it comes to accurately defining cancer. In 2000, Hanahan and Weinberg published the six hallmarks of cancer, compiling the insights and discoveries in the previous 25 years of cancer research into an organized outline defining features of the disease [13]. In 2011, they updated the list, adding two "enabling features" and two "emerging hallmarks," one of which happens to be "deregulating cellular energetics" (or altered metabolism) [14]. With the rampant and unchecked proliferation that occurs in tumors, nutrients, energetic substrates and ATP production are in high demand. The observation of altered tumor metabolism was made over 80 years ago [15], indicating that glycolysis, rather than oxidative phosphorylation, was the favored metabolic pathway for tumor cells [16, 17]. The end product of the glycolytic pathway is lactate, the focus of this dissertation.

1.1 Introduction to Lactate in Cancer[1]

Several clinical studies have linked high lactate levels found in solid tumors with poor patient prognosis, poor overall survival and increased incidence of metastases (Table 2).

Table 2: Lactate in solid tumors

Type of cancer	Lactate levels
Cervical	↑ with metastases [19], poor DFS, OS [20] (bioluminescence)
Head & Neck	↑ with metastases [21], poor DFS, OS [22]. (bioluminescence) HMRS studies: lactate SI did not correlate with tumor pO2, treatment response or locoregional response [23]
Colorectal	↑ with metastases [24] (bioluminescence)
Liver	Utilization in rat hepatomas [25, 26] (NMR)
Breast	unknown
Brain	↑ in gliomas [27-29] utilization in rat glioma [30-32] (NMR)
Lung	[Lactate] significantly ↑ in patients with recurrence and correlates with poorer mean survival [33]

Otto Warburg was the first to discover high concentrations of lactate within solid tumors [15, 34, 35]. Since the pioneering work of Warburg, production and accumulation of lactate has been documented to have clinical significance in a number of different cancer types (Table 2). In the 1970s, lactate metabolism in malignant metastatic carcinomas and colorectal cancers was beginning to be explored with blood samples

[1] A majority of Sections 1.1 – 1.3 are excerpts from review article: 18. Kennedy, K.M. and M.W. Dewhirst, *Tumor metabolism of lactate: the influence and therapeutic potential for MCT and CD147 regulation.* Future Oncol, 2010. **6**(1): p. 127-48.

from patients who were injected or infused with radiolabeled glucose and pyruvate [36, 37]. These studies indicated that lactate levels in plasma and venous blood were elevated in patients with metastatic cancer [37].

In the 1980s, quantitative bioluminescence imaging was used to assess metabolites such as lactate and glucose from flash-frozen biopsies to study ischemia in brain tissue [27, 38]. This technique was later applied to assess these same metabolites in cancer [28, 39, 40] (Figure 1). More recent studies investigating lactate accumulation in human tumors has found that cervical tumors, head and neck cancers and rectal adenocarcinomas with metastatic spread exhibited a wider range and significantly higher levels of lactate than non-metastatic tumors [19, 21, 24] (Figure 1). Subsequently, it was found that elevated lactate levels correlate with worse patient prognosis, poor disease-free or metastasis-free survival and overall survival in human cervical cancers [20], head and neck cancer [22], high grade gliomas [28, 41, 42], rectal adenocarcinoma [24] and non-small-cell lung cancer [33] (Table 2). Mean lactate content can vary widely between individual tumors even if tumors are of the same size, grade or entity [20, 21]. The underlying mechanisms that give rise to these different metabolic phenotypes are actively being studied currently (Section 1.1.2).

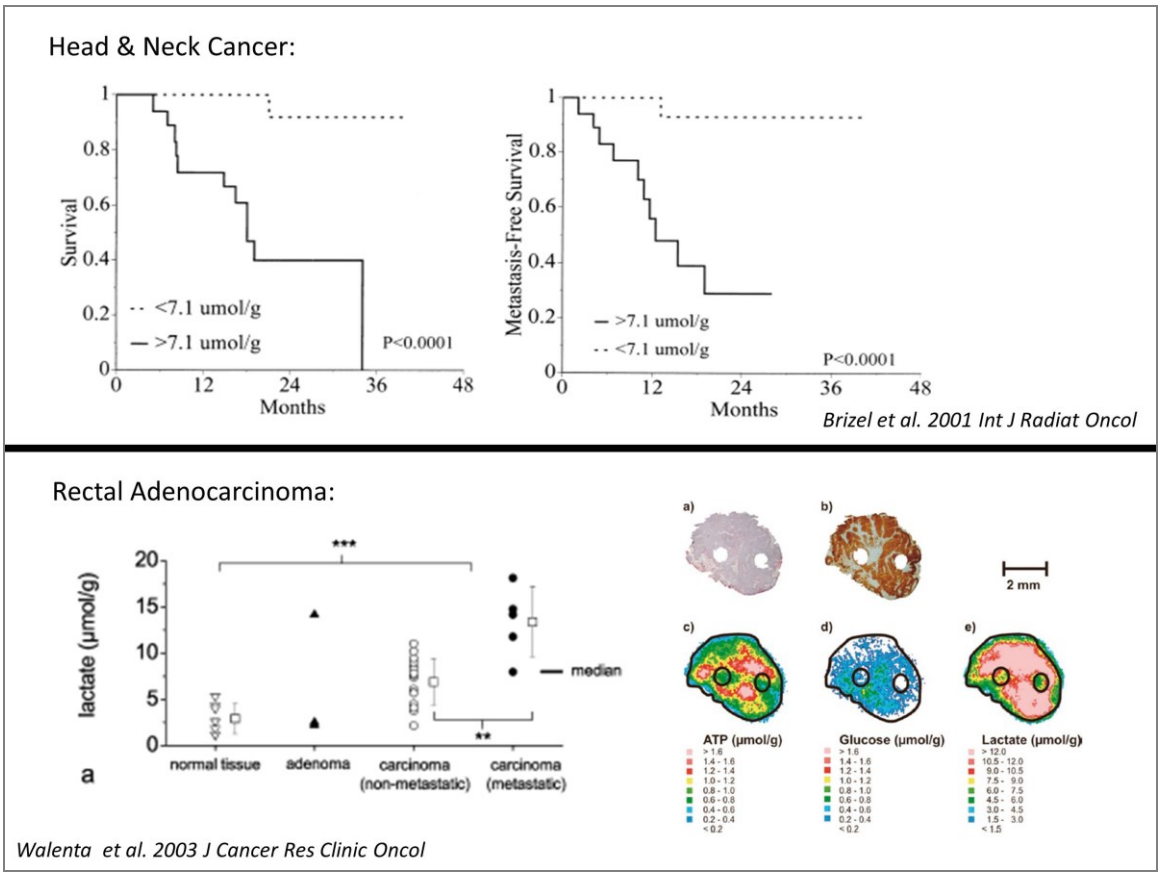

Figure 1: High lactate in solid tumors is associated with poor patient outcome and increased metastases in head and neck cancer (top) and colorectal cancer (bottom). Top: Patients with H&N tumors with high lactate show significantly decreased OS (left) and DFS (right) compared to patients with low tumor lactate levels. Bottom: Metastatic rectal adenocarcinoma shows significantly higher lactate concentrations than nonmetastatic adenocarcinoma (left); metabolite levels as measured by bioluminescence show high lactate *ex vivo* (right). Reprinted with permission [22, 24].

For nearly a century it has been known that tumors demonstrate high lactate levels compared to normal tissue. Yet, we still know little about lactate metabolism within the tumor. Elucidating the intricacies of lactate metabolism, we may have the potential to modify the metabolism of the tumor. Manipulating tumors to utilize lactate

(decreasing its accumulation) or finding ways to reduce glycolysis and lactate formation may affect tumor aggressiveness and invasiveness. In summary, lactate has been shown to be a prognostic indicator across a wide variety of tumors and types of cancer; this feature makes lactate metabolism of interest for further investigation as not only a biological marker but also as a potential therapeutic endpoint or target.

1.1.2 Characteristics of the Tumor Microenvironment and Cancer Metabolism

The tumor microenvironment (TME) consists of cancer, immune and stromal cells, blood vessels, cytokines and chemokines, the ECM, and nutrients, chemicals and metabolites. TME pathology is influenced by several key factors: oxygen and biochemical transport, vascular structure/perfusion, pH, and oncogenic and tumor suppressor regulation [43, 44]. Tumors do not grow as functional organ systems. The arrangement of vessels and the red blood cell flux is haphazard and unorganized [45]. This affects transport of oxygen, substrates and metabolites. The high proliferative demands of tumor cells are often not met due to diffusion limits imposed by the vascular structure (Figure 2) and the constant, inefficient metabolism of neighboring tumor cells. Tumor cells have adapted their metabolism to suppress oxidative phosphorylation in favor of glycolysis [46-48].

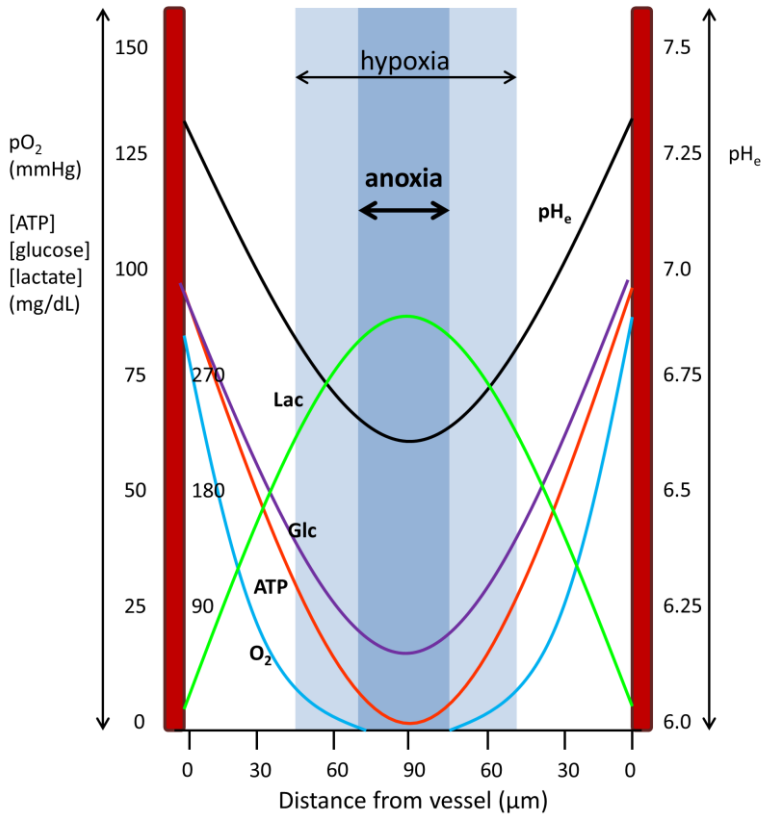

Figure 2: Theoretical representation of oxygen and metabolite concentrations in relation to intervessel distance in solid tumors. Tumor vessels = red bars, [lactate] = green line, [glucose] = purple line, [ATP] = orange line, pH_e = black line, pO_2 = blue line. Areas of hypoxia are represented by the light blue box. Areas of anoxia are represented by the dark blue box. As intervessel distance increases, pO_2, ATP, pH_e and glucose levels decrease while extracellular lactate increases, resulting in a hypoxic and acidic microenvironment**.** Adapted from [45].

Glycolysis is an ancient metabolic pathway, as it occurs in almost all organisms with some variation. Glycolysis occurs in all cells in the body to metabolize glucose to two pyruvate molecules that will enter into the tricarboxylic acid (TCA) cycle for oxidative phosphorylation (OXPHOS). OXPHOS is a multi-step process carried out in

mitochondria that requires oxygen to generate 36 ATP from a glucose molecule [49]. Glycolysis occurs in the cytosol and does not require oxygen, thus, it serves as the primary metabolic pathway to generate ATP in anaerobic or hypoxic conditions. Under normal conditions in the human body, glycolysis exclusively occurs mainly in red blood cells, which lack mitochondria, or in temporarily hypoxic tissue, such as exercising muscle [49]. Pathological states that are associated with upregulated glycolysis are certain genetic diseases, Alzheimer's disease and cancer [48, 50, 51]. Upregulation of the glycolytic pathway can occur in anaerobic conditions, termed the "Pasteur Effect" or aerobic conditions, termed the "Warburg Effect;" both are relevant to the TME and cancer metabolism.

1.1.2.1 Hypoxia and the Pasteur Effect

In 1857, Louis Pasteur discovered that fermentation in yeast was inhibited by oxygen; this was termed the "Pasteur Effect." [52] In cancer biology, the Pasteur Effect is used to describe lactate production as a result of increased glycolysis due to hypoxia within tumors. Tumor hypoxia significantly contributes to tumor aggressiveness and treatment resistance [53]. Poor patient prognosis and survival and increased incidence of metastases correlates significantly with tumor hypoxia in HNSCC [54], sarcoma [55], cervical cancer [56, 57], and breast cancer [58] among many others [59]. As mentioned previously, high lactate also correlates significantly with poor patient prognosis and OS

[20-22, 24, 60]. In some instances, when the tumor is also hypoxic, this lactate accumulation can be a direct result of the Pasteur Effect.

Features of tumor physiology that affect oxygen transport (hypoxia) can be summarized in "seven points of regulation," as described by Dewhirst *et al.* [61]. Compared to normal tissues, these points are 1). The steep longitudinal oxygen gradients within the tumor; 2). Increased intravascular gradients; 3). Shunt flow in the vascular structure to evade the tumor tissue; 4). Lower vascular density; 5). Inefficient and unorganized vascular orientation and structure; 6). Imbalance between oxygen consumption and delivery rates; 7). slower blood flow due to increased blood viscosity from intravascular hypoxia [61]. While these effects develop gradually, temporal oxygen fluctuations can occur in matter of minutes [62, 63]. Instabilities in tumor oxygenation have been found in a number of tumor types [62, 63]. Different regions of the solid tumors experience different types of hypoxia: chronic or acute (also termed "cycling" or "fluctuant").

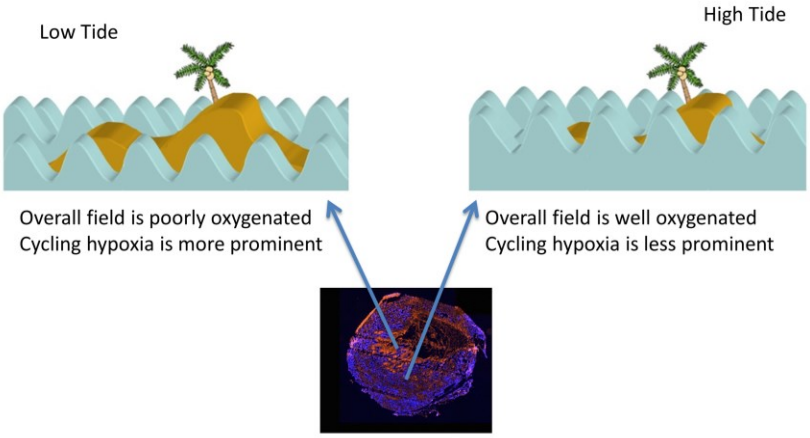

Figure 3: "Tides" of oxygen during cycling hypoxia. Microregions of tissue experience varying severity of hypoxia due to temporal fluctuations in pO_2 levels. "Low tide" is an analogy describing lack of oxygen surrounding a region of tumor tissue when pO_2 is low (left). In regions of the tumor in which pO_2 is higher, microregions experience adequate oxygenation. Adapted from [64].

A useful analogy to discuss tumor hypoxia is an island experiencing the tidal cycles of the ocean [64]. Tumor tissue that is chronically hypoxic is like the center of the island that the tides will never reach. As described by Dewhirst [64] and illustrated in Figure 2, oxygen will not reach certain areas of tumor tissue that are too far from vessels [45]. However, as red cell flux and perfusion change, there are areas within the tumor that are like the outer perimeter of the island: the "tides" of oxygen can be high or low. At "high tide," the tumor tissue will experience a relatively increased exposure to available oxygen, and at "low tide," the tissue will again be starved of oxygen [64]. The kinetics of cycling hypoxia have been measured *in vivo* in R3230Ac rat mammary carcinoma, FSA rat fibrosarcoma and 9L glioma tumors [62]. Much inter- and intratumor

heterogeneity was found in the patterns of oxygen flux in these tumors; however, R3230Ac and FSA tumors showed a greater spatial relatedness of oxygen fluctuation than 9L tumors [62, 63]. The time course of hypoxic "tides" can last as short as a couple hours to as long as a couple days [64]. What is currently unknown is whether cycling hypoxia and chronic hypoxia are distinct pathophysiologic entities and if the consequences of each are markedly different. Current cancer research is investigating the metabolic and genomic differences in cycling v. chronic hypoxic areas of tumors [61, 65]. It seems intuitive that with acute and chronic changes in oxygen transport that the substrate/metabolite concentrations would also be directly affected by this. The differences in metabolites in tumor areas of cycling v. chronic hypoxia have not been tested, but, as different imaging modalities are invented, this is a possible future direction in cancer metabolism research.

1.1.2.2 The Warburg Effect

The discovery by Otto Warburg of aerobic glycolysis resulting in increased lactate production within tumors led to a re-evaluation of the potential role and significance of lactate in cancer studies [15-17, 34, 35]. This 'metabolic switch' from normal metabolism (glycolysis followed by mitochondrial oxidative phosphorylation) to aerobic glycolysis is termed the "Warburg Effect" and has been the topic of many extensive reviews [46, 48, 66-69]. Originally implicated by Warburg as a cause of this tumor phenotype was "irreversible injuring of respiration" [16]. Since then, a niche in

cancer research has focused on mitochondria within tumors that contribute to or determine the metabolic phenotype through mtDNA alterations/mutations, TCA cycle enzyme regulation and/or redox signaling [67].

Functional mitochondria are needed for cancer progression. In ρ° cancer cells, which lack mtDNA, growth rates are slow and tumor formation in mouse models is delayed [70, 71]. One of the causes of decreased respiration in cancer cells is the propensity to acquire defects in the mitochondrial genome [70], leading to insufficient ATP production to satisfy the proliferative demand thereby instilling a need for a glycolytic shift. Notably, cancer cells experience high oxidative stress [70]. The electron transport chain is one of the primary sources of reactive oxygen species (ROS) generation via the metabolism of molecular oxygen [12, 49]. Other endogenous sources include peroxisomes and cytochrome P450 [72]. In addition to endogenous sources of ROS, there are exogenous sources which include UV light, pathogens, and inflammatory cytokines [12, 72].

Treatment-induced ROS is relevant to cancer research. For example, cyclophosphamide, radiotherapy and hyperthermia have been shown to increase oxidative stress in the TME: cyclophosphamide treatment elicited an infiltration of macrophages while radiotherapy enhanced ROS via HIF-1 activation, and hyperthermia indirectly activated NADPH oxidase [73-75]. Oxidative stress contributes greatly to membrane, lipid and protein damage; mutations; loss of organelle function and genomic

instability, which all contribute to cancer progression [72]. Tumor cells demonstrate increased proliferation and aberrant metabolism, both of which contribute to increases in ROS; ROS also contribute to the aberrant metabolic phenotype of cancer cells.

Eliciting DNA damage and increasing genomic instability is one of the primary ways ROS contribute to cancer progression. Many signaling pathways are activated or interact with ROS. Though the detailed mechanisms are still unclear, ROS have been found to activate Mitogen Activated Protein Kinase (MAPK) [76]. MAPKs are serine/threonine kinases that regulate phosphorylation of a wide variety of transcription factors that influence motility, proliferation, apoptosis and metabolism [77]. One MAPK family member, the extracellular signal-related kinase (ERK) [78], is important to cell proliferation signaling, which is closely associated with the resulting metabolic profile of a cell. Another transcription factor associated with cell proliferation and transformation is NF-KB, also known to respond ROS [79]. The final contribution of ROS to cancer metabolism that will be mentioned is stabilization of hypoxia-inducible factor-1 (HIF-1), a transcription factor that greatly contributes to both the Pasteur and Warburg effect (Section 1.1.2.3).

The signal transduction pathways described above are by no means a comprehensive view of all the factors that influence propagation of the Warburg Effect. Notably, PI3K / Akt, mTOR and AMPK signaling, microRNAs, p53 interactions, and

glutamine metabolism all influence the progression and maintenance of the Warburg Effect [69, 70, 80].

1.1.2.3 HIF and c-Myc regulation of metabolism

A consequence of tumor hypoxia and a necessary adaptation for mammalian cells to survive in hypoxic conditions is the increase in hypoxia-inducible factor-1 (HIF-1) expression. HIF-1 is a heterodimeric transcription factor consisting of α and β subunits. Much of the biological activity of HIF-1 is attributed to the expression of the α subunit, which is regulated by a degradation pathway in response to oxygen availability. Under normal aerobic conditions, proline residues in the oxygen-dependent degradation (ODD) domain are hydroxylated by prolyl hydroxylases for recognition by the VHL complex for subsequent degradation [81]. This is one of the major mechanisms of HIF-1α regulation, but other environmental influences can increase HIF-1α expression.

Hypoxia inducible factors (HIFs) are considered one group of master regulators of tumor metabolism [82-84]. HIF-1 and HIF-2 play an integral role in the survival and proliferation of hypoxic cells. HIF-1α null cells will experience significant suppression of metabolism (lactate production, acidosis) and ATP generation in hypoxic conditions compared to HIF-1α WT cells [85]. This illustrates the dependence of mammalian cells on HIF-1α expression and activity for growth in hypoxia. Hypoxia regulates over 200 genes [86] and HIF-1α has over 40 target genes [87, 88]. Notably, glycolytic genes are

upregulated by HIF-1α: phosphoglycerate kinase 1 (PGK-1), glyceraldehyde-3-phosphate dehydrogenase (GAPDH), triose phosphate isomerase (TPI), glucose transporters GLUT1 and GLUT4, lactate dehydrogenase A (LDHA), aldolase A and C, enolase 1, hexokinase 1 and 3, phosphofructokinase and pyruvate dehydrogenase kinase 1 (PDK-1) [84, 85, 87, 89]. Thus, HIF-1α expression and function is inherently linked to the Pasteur Effect in tumors. Additional oncogenic regulation that HIF-1α induces is upregulation of vascular endothelial growth factor (VEGF), and insulin-like growth factor 2 (IGF2), which promotes tumor angiogenesis and tumor cell survival, respectively [87, 90]. Many of the signaling pathways that lead to lactate accumulation in the Pasteur Effect are also activated in the Warburg Effect; one of the main distinctions between the two phenotypes is the absence or presence of adequate oxygen, respectively. Besides hypoxia, reactive oxygen species (ROS) and certain substrates, such as succinate, can stabilize HIF-1α [73, 91-94]

The proto-oncogene c-Myc also influences tumor metabolism, and crosstalk between c-Myc and HIF signaling has been documented [43, 95]. One area of convergence between the signaling of these two oncogenic factors is the glycolytic pathway; all the glycolytic genes mentioned above in relation to HIF-1α signaling are also upregulated by c-Myc [43]. However, where HIF-1α acts exclusively to upregulate glycolysis, c-Myc also promotes mitochondrial biogenesis [43, 96, 97]. Due to this divergent metabolic regulation and because HIF-1α inhibits cell cycle progression while

c-Myc promotes it, HIF-1α and c-Myc can be described as acting antagonistically [98, 99]. There are other HIFs active besides HIF-1α though, and c-Myc activity has been found to be transcriptionally enhanced by HIF-2α to increase hypoxic cell proliferation [100]. In this way, HIFs and c-Myc can work in concert to enhance a glycolytic phenotype, which leads to increased lactate in tumors.

1.1.2.4 Spatial distribution of lactate in tumors

As mentioned previously, the TME is a result of a compilation of dynamic processes, and solid tumors show pronounced intra- and inter-tumoral heterogeneity [101-103]. Likewise, lactate production and utilization may be constantly changing in the tumor. Frozen biopsy sections provide a snapshot of the metabolic profile. A limitation to using frozen sections is the lack of temporal information; however, bioluminescent techniques measuring lactate accumulation in frozen tissue can provide spatial information on lactate accumulation. In rat mammary R3230Ac tumors, lactate has been found to be associated with hypoxia, demonstrating the Pasteur Effect. This is illustrated in Figure 4 with lactate (green) overlapping hypoxic (yellow) and necrotic ("n") tumor regions [104]. In other cancer types such as FSA rat fibrosarcoma, there is evidence of lactate (green) accumulating in aerobic (no yellow) and viable ("v") regions of the tumor as well (Figure 4) [104], which is similar to the Warburg Effect. Likewise, lactate accumulation was consistently correlated with low glucose concentrations in FSA

tumors, but this correlation can also vary considerably in other tumor types [104]. These findings are consistent with the known heterogeneity of cancer.

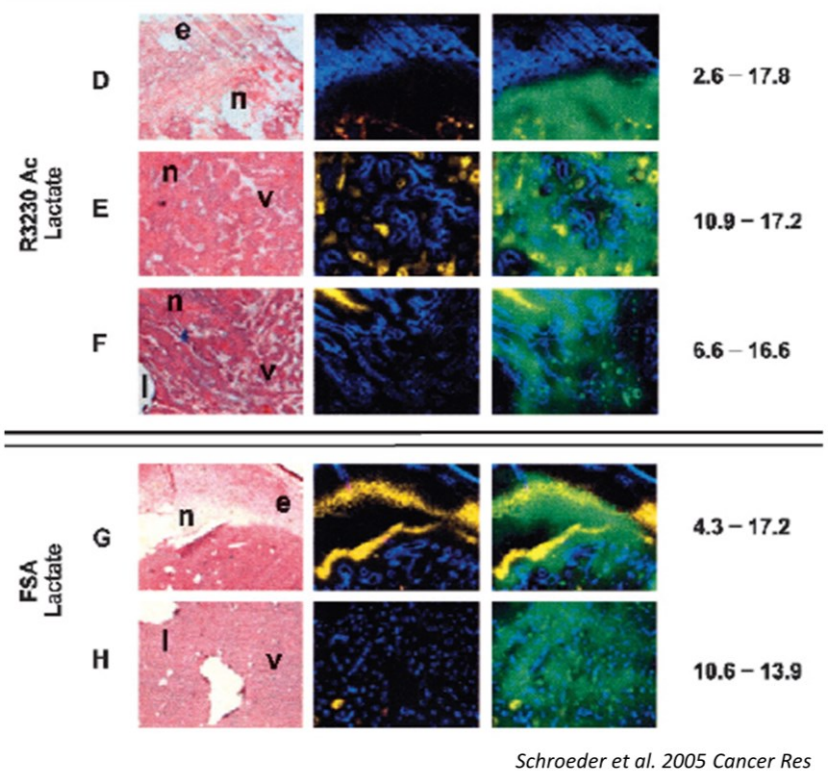

Figure 4: Spatial distribution of lactate in rat tumors. Lactate (green) accumulates in hypoxic (yellow), necrotic (n) and viable (v) tumor regions of rat tumors, R3230 Ac (top) and FSA (bottom). The tumor edge is indicated (e). Ranges of lactate measurements in microregions of represented tumor slices are indicated on the right. Reprinted from [104] with permission.

To address the limitation of the bioluminescence technique, other lactate imaging is available. Both magnetic resonance spectroscopic imaging (MRSI) and dynamic contrast-enhanced (DCE) MRI techniques can measure lactate non-invasively. The

advantages using these techniques are the ability to measure lactate *in vivo* and to gather temporal information on changes in the metabolite. Some recent efforts have been made in improving MRSI measurements of lactate levels in the brain, with encouraging results of more accurate detection [105]. MRSI also has been used in cancer studies in glioma patients [106] and in mouse models of breast and prostate cancer, both of which concluded that increased lactate detection correlated with tumor aggressiveness [107, 108]. Serganova *et al.* investigated the metabolic phenotype of different mouse mammary tumors using this technique and reported it to have a "greater dynamic range than [^{18}F]FDG-PET and may be a more sensitive measure with which to evaluate the aggressive and metastatic potential of primary breast tumors." [107] Future possibilities of pairing FDG-PET imaging with lactate MRSI include a more comprehensive view of the metabolic profile of individual tumors, which may improve tailored treatment regimens; this is discussed in Section 9: Conclusions and Future Directions.

1.2 Lactate Metabolism

Lactic acid is a three-carbon carboxylic acid with D and L isomers, L being the physiologically relevant form. Lactate is the conjugate base of lactic acid, which has a pKa of 3.86 [49]; thus, the molecule exists in ionic form in the human body. The physiological relevance of lactate to human health was first discovered in the mid-1800s by two individuals. Johann Joseph Scherer discovered lactic acid in human blood

postmortem following shock, and Carl Folwarczny discovered lactic acid in the blood of a living patient [109]. About a century later, Meyerhof and Hill independently embarked on lactate research, both utilizing frog muscle for their studies, and they were jointly awarded the 1922 Nobel Prize for Physiology or Medicine for discovering the distinction between aerobic and anaerobic metabolism [110-112]. This distinction between these two pathways is relevant to tumor physiology, as described in section 1.1.2.1-2.

There are five requisite conditions for lactate oxidation: 1) Lactate must enter the cell; 2) The movement of lactate in (and out) of the cell requires a membrane-bound monocarboxylate transporter, such as MCT1; 3) Lactate dehydrogenase (LDH) is required to convert lactate to pyruvate before it can enter into the tricarboxylic acid (TCA) cycle; 4) An adequate concentration of oxygen is required– lactate cannot be used for energy production anaerobically; 5) Healthy, functional mitochondria are required to carry out TCA cycle and the electron transport chain (ETC). Beyond this, there are other regulatory influences on lactate metabolism: 1) pyruvate dehydrogenase complex (PDC) regulation by phosphorylation via pyruvate dehydrogenase kinase (PDK;) 2) PDK inhibitors/phosphatases determine if pyruvate is converted to acetyl-coA for the first step of TCA cycle; 3) regulation of glycolysis via phosphofructokinase (PFK) and other glycolytic enzymes or intermediaries will contribute to overall cell metabolism. Other factors to mention that contribute to the trafficking of lactate into the cell or to particular

metabolic pathways are pH, the ratios of ATP/ADP, AMP/cAMP, NAD+/NADH, AMPK and inorganic phosphate (Pi) levels [113, 114].

1.2.1 Lactate Consumption in Normal Tissue

Studies on direct utilization of lactate in normal cells can provide a window into the potential metabolic processes in cancer cells, therefore, we will briefly explore lactate metabolism in normal tissue. Lactate movement and metabolism as participating in a cell-to-cell shuttle system was first intimated by the work of Carl and Gerty Cori with their discovery of the Cori cycle, a cycle in which lactate picked up from the bloodstream by the liver undergoes gluconeogenesis [115]. Later, in 1984, Brooks initiated the new wave of lactate shuttle research [116]. The basic observations of lactate transport and utilization were first studied in muscle. From here, as Gladden summarizes [117], the lactate shuttle theory that has grown to include the cell-to-cell lactate shuttle within muscle, intracellular lactate shuttle [118-120], the astrocyte-neuron lactate shuttle [32, 121-123], a lactate-alanine shuttle [124, 125], a peroxisomal lactate shuttle [126] and the spermatogenic lactate shuttles [127]. Organ systems most relevant to lactate utilization are liver, brain and cardiac and skeletal muscle. Below, lactate consumption in skeletal muscle and brain are briefly described.

1.2.1.1 Lactate Utilization in Muscle

Muscle cells have the ability to produce and export lactate as well as import and directly utilize lactate. During exercise, myocytes, which normally participate in oxidative phosphorylation, will begin to undergo glycolysis as the energy demand increases and oxygen supply decreases. Cells will export the accumulated intracellular lactate concentrations. Lactate will filter into the bloodstream and enter the liver, primarily, to undergo the Cori Cycle for gluconeogenesis [114, 115]. What is of more interest is the ability of myocytes to directly consume lactate.

Myocytes are efficient in their ATP generation, utilizing glucose, lactate, fatty acids and ketone bodies as energy sources. Briefly, the muscle-lactate shuttle occurs when lactate generated and excreted by exercising muscle is taken up by nearby resting muscle via bloodstream delivery or directly. Of the lactate generated during exercise, 55-75% will be oxidized by muscle [128]. Muscle cells express both MCT1 and MCT4, though the expression pattern and regulation in tissue is isoform-specific. Expression of MCT1 (K_m ~3.5mM for lactate) is significantly higher in heart [129] and oxidative muscle fibers compared to glycolytic muscle fibers, and strongly correlates with lactate uptake [130] while MCT4 (K_m ~ 34mM for lactate) expression is seen primarily in glycolytic muscle [129]. Lactate accounts for up to 40% of oxidative substrate utilized by the heart at rest and this portion climbs to 60% with work [131]. Experiments in rabbits show that oxidative myocytes take up and oxidize lactate at 2.5mM, while glycolytic myocytes use

lactate for gluconeogenesis and will not take it up until the concentration reaches 4mM [132]. Other studies have shown that lactate transport capacity in slow twitch muscle fibers (oxidative) is nearly twice that of fast twitch fibers (glycolytic) [133].

1.2.1.2 Lactate Utilization in Brain

Though glucose was thought of as the primary energy substrate of normal, healthy brain tissue, recent studies have found that brain tissue is an avid consumer of lactate, with the capability to take up lactate from the bloodstream after exercise [134] as well as direct consumption by neurons from lactate produced by astrocytes. Neurons account for about 90-95% of brain energy consumption as compared to glial cells, and there is evidence that lactate is a preferential substrate to glucose by neurons [135]. Lactate and glucose administered in equimolar concentrations *in vitro* are utilized for neuronal oxidative metabolism, 90% (direct lactate) and 10% (glucose-derived pyruvate) respectively [32]. In a metabolic model within the brain, astrocytes, which express MCT1 and MCT4, undergo aerobic glycolysis, exporting a considerable amount of lactate into the extracellular space. The lactate is then taken up to be used as an energy source by neighboring neurons via the lactate transporter, MCT2 (K_m for lactate ~ 0.7mM) [136] expressed on the surface [137].

Not all lactate is of equal energetic value. Studies in the early 2000s have shown that neurons in culture have a kinetic preference for extracellular lactate over

intracellular lactate (or pyruvate) generated via glycolysis from previously acquired glucose [138]. This supports a two-compartmental theory of lactate utilization. To support the assertion that lactate is being used as an energy substrate and not merely shuttled back out of the cell, NMR studies in neurons have shown the output of labeled TCA cycle intermediates and amino acids following administration of ^{13}C-lactate [125]. Further evidence for lactate as a preferential substrate for brain comes from *in vivo* studies with NMR, showing decreased utilization of glucose after raising plasma lactate levels [139, 140].

1.2.2 Lactate Utilization in Tumors

Though a majority of studies on lactate in relation to cancer have predominantly focused on its presence and accumulation, a number of studies have found that tumor cells have the ability to take up lactate and utilize it for energetic purposes as well as amino acid formation. Lactate uptake is not to be confused with its metabolism to generate ATP, as it is possible that the cell can take up lactate that may then generate alanine and glutamate. Lactate uptake occurs *in vitro* in cervical cancer SiHa cells [141] and breast cancer MDA-MB-231 cells in a pH-dependent manner [142]. If lactate uptake in tumor tissue is similar to muscle, areas with increased blood flow would show greater uptake [143].While muscle and brain tissue may be able to make use of lactate as an efficient substrate, the microenvironment of a tumor often does not have adequate oxygenation or an efficient and functional vascular network. Therefore,

tumor utilization of lactate is dependent upon oxygen availability, lactate concentrations, presence of healthy mitochondria and appropriate MCT subtype expression for lactate uptake [116, 144].

In 1991, metabolic studies were conducted on EMT6/Ro multicellular spheroids. A benefit to this method is that the spheroid mimics tumor micro-areas *in vivo*. Since the cells are not grown in a monolayer, they are exposed to varying degrees of oxygenation and nutrient availability based on their spatial distribution. Metabolic data on glucose and lactate levels were measured after spheroids were subjected to progressively increasing concentrations of lactate under conditions of 20% O_2 and 5% O_2. Cells showed lactate consumption at the highest lactate concentration (20mM) tested in both oxygenation states [145]. Other experiments in this same study showed a depressed cell growth rate when exposed to high lactate as compared to glucose, but yet, the viable rim of the spheroids showed high metabolic activity and O_2 consumption in the presence of high lactate concentrations [145]. Likewise, studies conducted in the 1970s found that three strains of Ehrlich ascites tumor cells oxidized exogenous ^{14}C-labeled lactate resulting in incorporation of ^{14}C in amino acids, acetate and CO_2 to varying proportions among the strains [146].

About one third of a series of 29 rat hepatomas were shown to utilize lactate based on calculations of arteriovenous substrate differences. The production or utilization of lactate was dependent on arterial lactate concentration and not arterial

glucose concentration or glucose utilization [25, 26]. These results showed that tumor utilization of lactate occurred when the arterial lactate concentrations rose above 2-3mM [26]. The 'metabolic fate' of the lactate removed from the arterial blood was not investigated in this particular study, and the mechanisms underlying this observation were not fully understood at the time.

Later studies with glioma cell lines *in vitro* and rat gliomas *in vivo* showed that exogenous lactate was a major source for oxidative metabolism in spite of net lactate production from aerobic glycolysis [31, 147]. *In vitro* studies were conducted using NMR with [3-^{13}C] L-lactate and [1-^{13}C] D-glucose in C6 glioma cells. Cells were incubated with either 5.5mM of labeled glucose, 11mM of labeled lactate or a combination of 5.5mM of labeled glucose with 11mM of unlabeled lactate for 4 hours before NMR samples were collected. Accounting for the fact that [1-^{13}C]D-glucose metabolizes to one mole of unlabeled lactate and one mole of [3-^{13}C]L-lactate, they found there was a high yield of glucose conversion to lactate [31]. From the NMR spectrum, peaks corresponding to 3C alanine and 4C glutamate were also seen; the former indicating [3-^{13}C] L-lactate conversion to alanine, and the latter indicating [3-^{13}C] L-lactate entering the TCA cycle to produce glutamate. Comparing the results from the dishes with lone labeled substrates, they found a "high yield of ^{13}C incorporation into glutamate when starting from [3-^{13}C]L-lactate" [31]. Additionally, their findings suggest that "lactate was a better precursor for alanine and glutamate than glucose" [31]. From these results, we can

conclude that certain tumors have the ability to utilize the lactate they take up for either energetic metabolism, as indicated by the labeled glutamate metabolite, or for amino acid formation, as indicated by the labeled alanine metabolite.

Based on observations that lactate production and utilization can occur simultaneously and/or shift from net lactate production to net lactate uptake based on the external lactate concentrations [31, 145], a two-compartmental theory was proposed. Briefly, it described two separate metabolic pools of both lactate and pyruvate within the cell; one pool of lactate being a result of cytosolic glycolysis that is separate from oxidative metabolism, and the other pool being the imported exogenous lactate to be used for oxidative phosphorylation [30, 31]. Using NMR, results from a 2001 study in perfused rat hearts support the idea of lactate compartmentalization. Glycolytically-derived lactate efflux can occur simultaneously with exogenous labeled lactate uptake, demonstrating that these metabolic pathways function separately [148].

These studies beg the question of what effects lactate utilization will have on tumor survival, aggressiveness and clinical profile. If accumulation of lactate correlates with increased metastasis and poor disease-free and overall survival [19-22, 24, 28, 33, 42], does the ability of the tumor to utilize lactate contribute to its survival, furthering cancer progression? Or does the ability to utilize lactate reduce the accumulation of lactate, and, in turn, lessen the negative effect of a hostile tumor environment? Does the ability to utilize lactate indicate a less aggressive tumor that

shows a more 'normal' metabolic ability, namely, using available oxygen as opposed to undergoing the 'Warburg effect?' Or will the increased oxygen consumption necessary for lactate oxidation ultimately lead to a more hypoxic tumor with increased reactive oxygen species? Of course, lactate may not be utilized for oxidation or energetic purposes; it may contribute to amino acid production through transamination reactions. In this case, will it serve to promote tumor survival, providing the tumor with the building blocks of protein synthesis? These are important questions in the field of cancer metabolism; ones that strongly encourage more research on the intricacies of tumor metabolism.

1.2.3 Lactate Uptake Rates

Many of the K_m values cited for MCT subtype 1 and 4 are relatively consistent among the literature. Determination of K_m values for lactate uptake can be found in studies conducted with *Xenopus laevis* oocytes. *In vitro*, oocytes expressing MCT1 showed a rate of 828 ± 79 (pmol/10 min) for uptake of 5mM lactate [149]. In a separate study, MCT4-expressing oocytes took up lactate at a rate of 323 ± 25 (pmol/10 min per oocyte) when incubated with 1mM lactate, which is still higher than oocytes without MCT4 expression (60 ± 3 pmol/10 min) [150]. When comparing one MCT subtype to another, many studies use their K_m or V_{max} values as a basis for comparison. As stated above, MCT1 as well as MCT2 both have a K_m for lactate lower than MCT4, illustrating that subtype 1 and 2 have a greater affinity for lactate than MCT4 [136];

however, the affinity for lactate in MCT4 can be increased (and the K_m decreased) by exposure to lower pH values. When *X.laevis* oocytes were incubated in a pH of 7, 6 and 5 the MCT4 K_m value for lactate dropped from 34 ± 5 mM to 10 ± 2 mM to 1.4 ± 0.5 mM, respectively [150].

Besides oocytes, lactate metabolism rates have also recently been studied in C6 glioma cells. Using ^{13}C and ^{2}H NMR, Rodrigues *et al*. were able to track lactate molecules in a "recycling" process through the plasma membrane via MCT1 [151, 152]. Rates of net 3-^{13}C lactate consumption were calculated to be 0.119 ± 0.012 μmol/mg protein/hr and a time constant of 0.227 ± 0.031/hr for lactate extrusion. A calculated lactate extrusion flux for intracellular lactate concentrations of ~ 5mM would amount to 1.135 ± 0.155 μmol/mg protein/hr. To compare lactate equilibration to lactate uptake through MCT1, these flux rates indicate that lactate equilibration is "approximately 10 times faster than net lactate uptake"[151]. Lactate recycling also occurs in the presence of physiologic glucose concentrations, and the recycling rate is faster than either glucose or lactate metabolism [151, 152]. In accordance with our lab's findings and published collaborators' results [86], this study also indicates that lactate production from glycolysis is inhibited in conditions of high lactate and hypoxia [151].

1.2.4 Lactosis versus Acidosis

Lactate and acidity are concepts that are often assumed as a singular phenomenon. Though the molecule is often referred to as "lactic acid," lactate exists

primarily in ionic form within the body at physiological pH, with over 99% of it being dissociated from the proton [117]. Upon transport, the proton and lactate anion are associated as they cross the cell membrane by MCTs [143]. Though MCTs have the ability to contribute to pH regulation, there are other transporters on the cell surface that specialize in pH regulation, such as the vacuolar proton pump (V-ATPase), sodium-proton exchangers (NHE1) and bicarbonate transporters (BCT). Many of these pH-regulatory transporters undergo expression or regulatory changes with malignant transformation, contributing to enhanced growth signaling, motility, and multi-drug resistance [153]. Low extracellular pH (pH_e) within the tumor cannot be primarily attributed to lactate or the ionic transport of MCTs. Table 3 provides a summary of the relevance of pH regulators to the tumor microenvironment, including their basic functions, expression in tumors, influences on cell migration and downstream targets and a brief reference to potential inhibitors.

Table 3: Cellular pH regulators

*pH regulator **	*Function/ mechanism*	*Expression in tumors*	*Cell migration*	*Associated/ regulated molecules*	*Inhibitors*
Na^+/H^+ exchanger: NHEs (1)	Regulates pH_e and pH_i: expels H^+ from cytosol, promotes cell polarity [154], necessary for cell proliferation and stable cell volume [153]	Anti-apoptotic activity [153]	↑ invasiveness of breast carcinoma cells [154, 155], required for migration, accumulates on leading edge of lamellipodium [154, 156] → tumor cell pseudopodia	MMP activity dependent on NHE1 activity [154]. Ras-mediated ERK, G protein-coupled receptors, PKC, RhoA and integrin receptors regulate NHE1 activity [153].	**i) Amiloride and derivatives ii) guamidine and derivatives**
Bicarbonate transporters: BCTs: i) *SLC4* = Na^+-HCO_3^- cotransporters (NBCs 1-4), Cl-/HCO_3^- exchangers (NCBE) and anion exchangers (AE1-4) ii) *SLC26*	Regulates pH_i and cell volume, ↑ in NHE1-deficient cells [154, 157]		NBC has less influence on cell migration compared to NHE1, but will contribute to migration during acute intracellular acid load [157]	Coexpression with CA9 for AE1-3 increases AE-mediated bicarbonate transport [158]	
Carbonic anhydrases: CAs (9 and 12)	Extracellular production of HCO_3^- is transported into cytosol. H^+ ions remain at cell surface, ↓ pH_e [154]	CA 9 ↑ in solid tumors, ↑ tumor cell growth [154]		CA 9 regulated by HIF-1 [154]	
Monocarboxylate transporters: *SLC16A* = MCTs (1 and 4)	Facilitated passive H^+ transport with monocarboxylates	***Refer to Table 2***	MCT4 colocalized with β1 integrin at focal adhesions, expressed on leading edge of migrating cells [154] [159]	CD147 chaperone, MCT4 regulated by HIF-1	**i) Aromatic monocarboxylates ii) Anion transport inhibitors iii) Bioflavenoids [153]**
V-ATPases	**H^+ pump, cytoplasmic pH homeostasis, endocytosis, intracellular transport [153]**	**↑ in multidrug resistant cells [153]**	**c subunit interacts with β1 integrin [153]**	**E subunit interacts with mSos-1 → Ras and Rac-1 signaling [153]**	

Glycolysis-generated lactate itself is not inherently a source of acidity; acidification can occur without glycolysis. Two different studies were conducted comparing LDH-competent verses LDH- deficient cell lines [160] and glycolysis-competent verses glycolysis-impaired *ras94*$^{-}$ and *7ras3*$^{-}$ cell lines [161] in both *in vitro* and *in vivo* systems. The non-lactate producing cells from both studies showed acidification of the culture media and tumor. The drop in pH_e tended to be greater in the LDH-competent cells than the LDH-deficient cells although this finding was not statistically significant; however, the LDH-deficient cells showed a significantly greater fraction of their $^{14}CO_2$ production from ^{14}C alanine rather than from ^{14}C glucose [160]. *In vivo*, the pH_e of the tumor tissue was similar for both LDH-competent (7.03 ± 0.03) and LDH-deficient (7.03 ± 0.05) tumors, despite the wide disparity in lactate content (1877 ± 135 verses 488 ± 91 μg/g wet weight, respectively) [160]. Studies with the glycolysis-impaired *ras94*$^{-}$ and *7ras3*$^{-}$ cells showed similar results to the LDH-deficient cells in regards to media acidification. The H_3O^+/lactate ratio was significantly higher in the glycolysis-impaired cell lines, indicating that there was a source of acidity besides lactate. *In vivo* studies with tumors of these cell lines showed a mean interstitial pH that was not significantly different between the glycolysis-competent verses glycolysis-impaired. After measuring metabolites in the tumor interstitial fluid of parental and glycolysis-impaired tumors, it was found that lactate levels were 28% lower in the

glycolysis-impaired tumors, though CO_2 and pH levels were comparable to the parental tumors [161].

Implicated in the increased acidification of the abovementioned studies was increased levels of CO_2 [161], as hydrated CO_2 generates bicarbonate (HCO_3^-) and H^+ [162]. Briefly, a recent review highlights three sources of CO_2 that can lead to acidification of the extracellular milieu. CO_2 can be generated from the TCA cycle since one carbon atom that passes through will generate one molecule of CO_2. The pentose phosphate shunt is another pathway that generates CO_2. Finally, as indicated at the beginning of this paragraph, titration of bicarbonate with protons can lead to increased CO_2 [162]. This discussion is expanded and detailed in review by Swietach *et al*. [162]. Carbonic anhydrase (CA) catalyzes this reaction; there are 14 mammalian isoforms. Certain CA isoforms, such as 9 and 12, are increased in many cancers and are HIF-1α-regulated [163]. Bicarbonate transport has been found to be increased through CA colocalization and interaction with some bicarbonate transporters [164, 165], which is partially regulated by protein kinase C (PKC) [166]. Additionally, when a sodium-bicarbonate cotransporter (NBC) was expressed together with MCT1 in *Xenopus* oocytes, the transport of lactate and H^+ by MCT1 increased almost twofold, suggesting that the buffering capability of NBC reduced H^+ intracellular accumulation, which would normally hinder MCT1 activity [151]. It is clear that no one transporter is responsible for

cellular pH regulation, and not only can many different transporters fulfill the same function, they can also assist or enhance the activity of other transporters.

Though lactate accumulates within tumors via the Pasteur Effect, the cellular response to hypoxia is not the same as with lactosis or acidosis. Both hypoxia and accumulated lactate show correlation to more aggressive cancers, poor patient prognosis and disease-free and overall survival [54, 167, 168]. However, in studies that carefully controlled for conditions of hypoxia, (non-lactate) acidosis, lactosis and lactic acidosis, the range of cell responses was intriguing. A strong lactic acidosis genomic response has been found to not only negatively correlate with a hypoxic response score, but the lactic acidosis response additionally predicts a favorable prognosis in a series of clinical breast cancer trials [86]. Found within the same data set, the cellular response to high lactic acidosis was upregulation of genes associated with aerobic metabolism, including factors involved in TCA cycle and electron transport, while the response for low lactic acidosis showed an upregulation of genes associated with matrix metalloproteinases (MMP) [86] that are implicated in many aggressive cancers that are also induced by HIF [169].

1.3 The monocarboxylate transporter (MCT) family

Proton-coupled monocarboxylate transporters are 12-span transmembrane proteins with N-terminus and C-terminus in the cytosolic domain. While there are 14 members/subtypes of MCTs coded by the *SLC16A* gene family, not all

these are currently characterized [136]. MCTs account for 70-90% of muscle lactate transport [133]. While it could be said that the distinguishing common feature among members of this family was the transport of monocarboxylates (lactate, pyruvate, butyrate, acetate, propionate), it has been found that certain subtypes have the ability to transport a wider range of substrates such as ketone bodies, some aromatic amino acids and even some pharmacological agents, such as γ-hydroxybutyrate (GHB) and statins, among others [170, 171]. Other members, MCT6, MCT8 and MCT10, will transport substrates such as diuretics, thyroid hormones T3 and T4, and aromatic amino acids, respectively [136, 170].

Of the characterized family members of *SLC16A*, MCT1 is reported to have the most ubiquitous tissue expression [136]. Other subtypes show tissue-specific expression. Expression and regulation of MCT1, MCT2, MCT3 and MCT4 have been reported in a wide variety of cancers [172-180]. For brevity and clarity, we will be addressing the subtypes of proton-coupled MCTs best characterized in human tissue, 1-4, largely focusing on MCT1 and MCT4 with only passing mention of MCT2 and MCT3 when relevant.

Sodium-coupled MCTs (SMCTs) of the *SLC5A* gene family were discovered in the early-mid 2000's, namely *SLC5A8* [181, 182] and *SLC5A12* [183]. SMCTs transport similar substrates as many of the *SLC16A* MCT family members; however, they show differences in patterns of tissue distribution and their potential

roles in cancer or cancer progression [170, 184]. *SLC5A* members will be mentioned when relevant, but the focus for a portion of my dissertation will be on *SLC16A* MCTs, particularly subtypes 1 (*SLC16A1*) and 4 (*SLC16A3*).

1.3.1 MCT1 and MCT4 expression and regulation

The characteristics of these two transporters are being covered together since they share some common traits. It is known that the function of both transporters is dependent upon interactions with other proteins, such as the chaperone CD147 [136]. Many studies have shown the tight association of CD147 with MCT1 and MCT4 with coimmunoprecipitation, and immunohistochemical techniques have shown co-expression on the plasma and mitochondrial membranes [185-188]. MCT1, MCT3 and MCT4 depend on association with the mature, glycosylated form of CD147 in order for these MCTs to be expressed and functional on either plasma or mitochondrial membranes [188, 189]. Conversely, it appears that CD147 maturation is affected by MCT expression. In MCT1 knock-down experiments in Caco-2 cells, accumulation of the immature, core-glycosylated form and disappearance of the mature glycosylated form occurred with no difference in the mRNA [188]. In other experiments, abrogation of fully glycosylated of CD147 was observed and the core-glycosylated form was restricted to the endoplasmic reticulum when MCT4 siRNA was added to MDA-MB-231 cells [176].

There is seemingly contradictory evidence in the literature supporting both upregulation and absence of regulation of MCT1 expression by exogenous and hypoxia. Studies on rat and human muscle cells, have shown that MCT1 mRNA is upregulated in response to 10mM lactate exposure for 1 or 6 hr *in vitro* [119] or in response to the increase of local lactate in exercising muscle, *in vivo* [190]. The increase in MCT1 mRNA also corresponds to significant increases in PGC-1α mRNA [119]; PGC-1α signaling is important to muscle metabolism, promoting oxidation [191]. Total and mitochondrial protein levels of MCT1 and CD147 have been shown to increase significantly with exposure to exogenous lactate, while MCT4 expression remains unchanged [119]. *In vivo* exercise studies found that while MCT1 and MCT4 will increase after training, the increase of MCT1 correlates with citrate synthase activity, indicating an active TCA cycle [190]. MCT4 did not show the same correlation, indicating that MCT1 regulation can be important to the ability of the muscle cell to directly consume lactate to be used in TCA cycle/oxidative phosphorylation while MCT4 regulation is more likely to correspond to lactate-efflux from the more glycolytic myocyte. This begs the question of whether cancer cells also have the ability to consume lactate or if the upregulation of MCT1 is more likely an adaptation to higher concentrations of intracellular lactate generated from increased glycolysis in cancer cells.

In a separate study conducted in a number of cancer cell lines (MDA-MB-231, MCF7, HeLa, SiHa, p53-WT HCT116 and p53 -/- HCT116), it was found that MCT1

mRNA regulation did not change in response to 10mM lactate exposure for 24-96 hrs. However, loss of p53 correlated with MCT1 mRNA upregulation after exposure to hypoxia for 24-96 hr, and MCT1 mRNA stability was dependent upon not only p53 expression, but also NF-κB expression [192]. It is important to note that the experiments carried out by Boidot *et al*. [192] consisted of considerably longer exposure times to lactate than experiments conducted by Hashimoto *et al.* [119]; the differences are 24-96-hr-exposures vs. 1-6-hr-exposures, respectively.

Lactate is not the only substrate that can upregulate MCT1 expression. Butyrate, a short chain fatty acid synthesized by bacterial fermentation in the colon, has been shown to stimulate MCT1 promoter activity [193]. Hormones act to regulate the expression of MCT1: both testosterone [194] and thyroid stimulating hormone (TSH) [195] will stimulate tissue protein expression of MCT1. The metabolite milieu is affected by the expression and function of MCTs. Inhibition of MCT1 and MCT2 via siRNA showed significant decrease in malignant glioma cell viability and lactate efflux (i.e. glycolysis) *in vitro*; these effects were increased when both were inhibited simultaneously [196]. MCT1 overexpression in rat β-cells has been shown to increase pyruvate oxidation, and when co-overexpressed with LDHA, islet cells will additionally increase lactate oxidation [197]. A recent study in cultured astrocytes found that basal lactate uptake was decreased with MCT1 silencing but not with MCT4 silencing. The effect was more profound than CD147 silencing, which decreased basal lactate influx

and efflux and glutamate-activated lactate release. The results from this study indicate the possibility of an uncharacterized MCT subtype or an unidentified transporter functioning within astrocytes [198].

1.3.2 MCTs and cancer

MCT expression in cancer is summarized in Table 4. Colorectal cancer provides intriguing information of MCT expression in cancer. MCT1 is expressed in normal colonic epithelium to facilitate the transport of butyrate, the primary energy source for these cells [199]. Butyrate has been shown to be important in proliferation, apoptosis and differentiation, with declining levels indicative of colon cancer progression [200]. Since butyrate is imperative for differentiation of colon cells [201, 202] as well as breast cells [203], it makes sense that low levels of this substrate would contribute to carcinogenic transition or progression. Butyrate unavailability may be due to microenvironmental levels as well as a decreased ability of the cells to take up the substrate. The loss or silencing of MCT1 has been shown to correlate with the deregulation of butyrate-responsive genes involved in differentiation and apoptosis [179, 204], transition from normalcy to malignancy in colonic epithelium [205] along with a simultaneous increase in GLUT-1 expression [173, 205], supporting the hypothesis that the primary energy source for cancerous colon cells switches from butyrate to glucose. SLC5A8, termed SMCT1, is also responsible for mediating uptake of

butyrate [184] and has been shown to act as a tumor suppressor in colon epithelium, with its silencing via aberrant correlating to neoplastic transformation of colon cells [206]. An opposing finding on MCT expression in colon tissue indicates that there is an increase in MCT1, MCT2 and MCT4 in colorectal carcinoma compared to normal colonic epithelium [172]. Expression patterns of MCT1 within a separate study showed that both membrane and cytoplasmic MCT1 expression was seen in both normal colonic tissue as well as in colonic tumor cells and tumor-associated fibroblasts [173]. Studies mentioned used immunohistochemical analysis to assess MCT1 abundance; no conclusion can be drawn about the discrepancy between results. Further studies are needed to elucidate MCT expression and its implications in colorectal cancer.

Table 4: MCT1 and MCT4 expression in solid tumors

Type of cancer	MCT1 expression	MCT4 expression
Cervical	↑ from pre-invasive to invasive [180]	↑ from pre-invasive to invasive [180]
Head & Neck	(+) (unpublished data)	(+) (unpublished data)
Colorectal	(+) in tumor cells in samples tested [173], ↑ in tumor cells compared to normal epithelium [172] (-) or loss from normalcy to malignancy [205]	Weak (+) in tumor cells [173], ↑ in tumor cells compared to normal epithelium [172]
Melanoma	(+) [207]	(+) [207]
Breast	↓ in MDA-MB-231 and some clinical samples by hypermethylation of CGI upstream [203] ↑ in basal-like breast carcinoma [208]	↑ in MDA-MB-231, metastatic breast cancer [176]
Brain	+ in gliomas, silencing leads to cell death [196]	
Lung	+ in tumor cells, - in normal [209], cytoplasmic accumulation in alveolar soft part sarcoma [210]	+ in tumor cells, - in normal [209]
Pancreatic	+ [175]	+ [175]
Neuroendocrine	↑ in neuroblastoma [211]	

Differential expression of MCT1 has been seen in clinical breast samples with hypermethylation of a CpG island (CGI) in the 5' upstream region of MCT1 accounting for silencing, similar to the expression seen in the MDA-MB-231 cell line [203]. After analysis of tumor tissue from 249 breast carcinoma cases compared to normal breast tissue, it was found that MCT1 was significantly upregulated in basal-like breast carcinoma. Upregulation of both MCT1 and CD147 were associated with poor prognostic variables [208]. In accordance with these findings, it was also reported that

breast cancer patients harboring p53 mutations in hypoxic tumors showed a significant increase in MCT1 expression and significantly lowered overall survival rates [192].

In lung cancer, MCT1, MCT2 and MCT4 expression are found among tumor cells while very weak expression was seen in stroma, and no MCT expression was found in normal lung tissue [209]. Though MCT signaling pathways are not completely known, MCT2 expression/regulation has been linked to IGF-1 [212] and PI3k/Akt or mTor pathways [213], which may be relevant to other subtypes as well. Interestingly, current research on SMCT1 shows a more consistent expression pattern in different cancers compared to MCT1; SMCT1 is reputedly silenced in thyroid, stomach, brain, breast, pancreas and kidney cancers [184]. Perhaps this indicates that the SMCTs may have an unambiguous expression pattern in cancers compared to proton-coupled MCTs; further research on the expression and function of SMCT and MCT subtypes in cancer is warranted to elucidate these possibilities.

1.3.2.1 Inhibition of MCT1 as a potential therapeutic option in cancer treatment

Rationale behind MCT inhibition is multifactorial. Inhibition of MCTs will have a direct effect on monocarboxylate transport and pH. It has been shown that MCT1 inhibition decreases intracellular pH, resulting in cell death [141, 153, 211, 214]. Since MCT1 is bidirectional, inhibition of this transporter may also cause the extracellular environment to become more acidic. While this effect is usually associated with a more aggressive phenotype, the increase in acid allows for more lactate uptake [142] and may

have additional aid in treatment if candidate drugs require lower extracellular pH to enhance their uptake [215].

Another hypothesis regarding potential efficacy of MCT1 inhibition as a cancer treatment is in relation to the proposed "metabolic symbiont" model between hypoxic and aerobic cells within the tumor microenvironment. Briefly, this model states that aerobic cells, which have the ability to consume lactate, can confer a survival advantage to the hypoxic tumor cells by allowing glucose to reach the hypoxic cells farther from vessels. By inhibiting MCT1, lactate is no longer available to the aerobic cells, forcing them to take up the glucose. This starves the more treatment-resistant hypoxic cells [141]. Inhibition of MCT1 has been found to decrease tumor growth rate [141] and elicit cell death via apoptosis and necrosis when silenced in conjunction with MCT2 [196].

Finally, inhibition of MCTs may suppress cell migration. Silencing of MCT4 via siRNA has been shown to reduce transwell migration of MDA-MB-231 cells by as much as 85% [176]. More recent studies by Philp's group have illustrated the coimmunoprecipitation and colocalization of MCT4 and β1-integrin in the leading edge lamellapodia of migrating cells [159]. Both CD147 and MCT4 interact closely with β-1-integrin; these findings paired with the dependency of CD147 expression on MCT4 expression [176], indicate that MCT4 may be exerting more of an influence on focal adhesion- and integrin-associated cell migration than previously imagined.

There are several small molecules that inhibit MCT function. The efficiency of inhibition of MCT4 function tested under conditions of 30mM lactate has been evaluated for the following inhibitors: α-cyano-4-hydroxycinnamate (CHC or CINN) (Ki ~27μM), phloretin (Ki ~1.4μM), 5-nitro-2-(3-phenylpropylamino)benzoate, 3-isobutyl-1-methylxanthine and p-chloromercuribenzene sulphonate (pCMBS) (Ki ‹1.0μM). pCMBS inhibits MCT1 via reaction with CD147 as opposed to direct MCT1 interaction [216, 217]. There are some variations of efficiency of functional inhibition of the different inhibitors based on the subtype. Of these CHC, pCMBS and phloretin are well established MCT1 inhibitors. Treatment with these drugs reduces lactate influx by up to ~80% in normal hepatocytes in a dose-dependent manner, starting at concentrations of 5mM. Similar effects have been shown with 4,4′-dibenzamidostilbene-2,2′-disulfonate (DBDS) and 4,4′-diisothiocyanostilbene-2,2′-disulfonate (DIDS) [218] and with the tumor cell line Ehrlich-Lettre, though with some variation [219, 220]. CHC is supposedly a specific MCT1 inhibitor [216]; however, studies have shown that CHC will disrupt activity of the anion exchanger AE1 and that CHC is a more potent inhibitor of the mitochondrial pyruvate carrier (MPC) than of MCT1 [136, 221]. Concentrations of CHC as low as 1μM have been found to inhibit the MPC, while at least 50μM are needed to inhibit MCTs [136, 221-223]. A recent MCT1-specific inhibitor, AR-C117977, has been found to have immunosuppressive properties that will significantly prolong skin graft and heart allograft survival in mice [224]. Some of these inhibitors can be used as broad spectrum

pH regulator inhibitors, and likewise, will inhibit lactate and proton efflux via MCTs. Inhibitors that are more MCT-specific hold promise in facilitating tumor metabolism manipulation as well as potentially acting as an immunosuppressor.

When considering MCTs as a target for therapy, it is imperative to evaluate toxicity to normal tissue. MCT inhibitors have the potential for altering metabolism, inflammatory response, intracellular pH, and angiogenic response on a broad spectrum. Local delivery may be required to prevent deleterious whole-body effects. Systemic delivery of an MCT inhibitor, and specifically MCT1, could affect almost every organ of the body with the most drastic effects on cardiac and skeletal muscle. Possible side effects in skeletal muscle include muscle fatigue and inability to tolerate moderate- to high-intensity exercise due to the build-up of intracellular lactate as well as hydrogen ions [225]. In the worst case scenario, the side effects of MCT inhibition in the heart may lead to exercise intolerance or other more severe cardiac toxicities [217, 225]. Since MCT1 is one of the transporters that will take up butyrate, it is possible that with MCT1 inhibition there may prevent or reduce proper differentiation or cell proliferation in the colon.

1.4 The epithelial to mesenchymal transition (EMT) in cancer and connections to tumor metabolism

The epithelial to mesenchymal transition is described here due to the potential relevance of lactate to this process. Experiments evaluating the connection between lactate and EMT are not included in the body of this dissertation but are included in Appendix E.

Epithelium is the tissue that lines body cavities and forms lumens and glands. Epithelial cells are polarized and firmly attached to the basement membrane unless part of a stratified epithelial structure [12]. Mesenchymal cells (also called mesenchymal stem cells (MSC)) retain multipotency, meaning they have the ability to differentiate into many different types of cells [226]. Morphologically, mesenchymal cells are typically longer and thinner than epithelial cells and have some cell processes. It has been found that MSC reside in almost all post-natal organs and tissues [227]. Cellular markers for epithelial and mesenchymal cells are provided (Table 5). The epithelial-mesenchymal transition (EMT) describes the process of an epithelial cell acquiring the phenotype of a mesenchymal cell. Contrarily, the mesenchymal-epithelial transition (MET) describes the process of a mesenchymal cell acquiring an epithelial phenotype. Normally, these processes are tightly regulated and balanced, each occurring at specific times in specialized tissues (e.g., MET occurring during development. The three primary contexts in which EMT occurs are in embryonic development, fibrosis and cancer [228] (Table 5).

Table 5: Markers of epithelial and mesenchymal cells

Cell phenotype	Markers
Epithelial	E-cadherin, Cytokeratin, ZO-1, Laminin-1, Entactin, MUC-1, Syndecan, Desmoplakin, α1 (IV) collagen, miR200
Mesenchymal	N-cadherin, Vimentin, Snail, Slug, Fibronectin, Twist, Goosecoid, LEF-1, α-SMA, FOXC2, β-catenin, SIP1, FSP-1, α5β1 integrin, miR21, miR10b

Cellular plasticity has been receiving more attention in cancer research recently, after several findings of EMT or MET events in tumor cells [229, 230]. Signaling pathways for EMT initiation and maintenance in cancer are in the beginning stages of discovery. It is known that factors of the tumor microenvironment, such as oxygen concentration, can influence EMT or MET [231, 232]. As mentioned in Section 1.1.2 of the Introduction, tumor hypoxia is a common occurrence in many types of solid tumors [63, 233] that correlates with poor patient prognosis and survival [54, 167], increased metastatic potential [55, 56] and can lead to treatment resistance [168]. EMT contributes to this aggressive phenotype. In order for metastases to occur, tumor cells must disengage from their cell-to-cell contacts and deregulate polarity in order to gain the ability to invade the BM and neighboring tissue. EMT signaling has been found to contribute to migratory, invasive and metastatic phenotypes in cancer cells [229, 230, 234, 235] that can be ablated with siRNA techniques [236, 237]. Lactate is another factor associated with poor patient prognosis and survival and an increased incidence of

metastases [19-22, 24, 60]. Lactate may be another TME-associated factor that influences EMT.

1.4.1 The potential importance of lactate signaling in EMT

There are three types of EMT [228] (Table 6). The first connection between lactate signaling and EMT is in wound-healing . EMTs are associated with fibrosis in several organs, and inflammation can initiate EMT events through cytokine signaling [228, 238-240]. Lactate is known to play an integral role in wound-healing by increasing inflammatory-like signaling and facilitating angiogenesis [241]. Some common pathways involved in lactate signaling are also involved in EMT. TGF-β is one of the primary cytokines to be upregulated in inflammation [242] and wound healing [241]. In wound-healing , high lactate concentrations stimulate TGF-β, leading a significant increase in this cytokine [241].TGF-β also plays a role in EMT signaling: Snail (an important EMT initiator) is required for TGF- β involvement to induce EMT via activating the PI3K/Akt pathway [243] and/or NF-KB [244]. NF-KB activation occurs in a time-dependent and dose-dependent manner in trabecular meshwork cells within five minutes after addition of exogenous lactate [245]. Additionally, lactate uptake via MCT1 in HUVEC cells activates NF-KB through IL-8 signaling, which facilitates tumor angiogenesis [246]. From these findings, we can see that TGF-β and NF-KB signaling are two potential points of convergence of lactate signaling and EMT signaling, also

indicating the potential for crosstalk between lactate-relevant TME and EMT signaling pathways (Table 6).

Few studies focus on the relationship between lactate and EMT, but there are some hints to suggest that nutrient balance may influence differentiation and/or EMT initiation and maintenance [247-249]. Additional evidence of the relevance of lactate to EMT signaling comes from exon-array transcriptional analyses conducted in MCF7 cells exposed to 10mM L-lactate for 48 hr [247]. In this study, >4,000 genes were differentially regulated in response to exogenous lactate. Gene set enrichment analysis showed >3,000 genes were associated with "stemness:" >1,000 genes similar to embryonic stem cell profiles and >2,000 genes similar to neural stem cells [247]. Lactate has also been found to induce genetic regulation in mesenchymal stem cells, mainly in genes associated with cell cycle, cell adhesion and communication, transcription factor, cytokine, apoptosis and oxidative metabolism; however, lactate did not induce any changes in cell surface epitope expression [250]. In sheep thyroid cells, lactate utilization was found to be associated with the degree of differentiation [248].

The studies summarized indicate a promising avenue of research in the link between EMT and lactate metabolism and/or nutrient balance. Recognizing the connections between lactate signaling and EMT signaling led me to question the possibility of lactate inducing EMT. In my dissertation, I will present brief preliminary evidence suggesting exogenous sodium lactate can elicit cell morphology changes,

regulate expression of Snail-1 and mildly increase the formation of mammospheres in breast cancer cells in tissue culture.

Table 6: Potential relevance of lactate to different EMT subtypes

Subtype of EMT	Description	Relevance of lactate
1: Implantation / Embryonic gastrulation	Epiblast forms primary mesenchyme through EMT. (Secondary epithelium derived from primary mesenchyme through MET.) [228]	Mouse embryo post-implantation: >90% of glucose converted to lactate. Addition of 24mM of exogenous lactate inhibited glucose and pyruvate metabolism in embryos. [251] 25mM lactate cannot support first cleavage division of mouse embryo [252].
2: Inflammation / Fibrosis	Inflammatory cells and resident fibroblasts secrete growth signals and chemokines → partial EMT. Destruction of basement membrane → full EMT [228]. Slug is upregulated during wound healing [253].	Lactate increased in wound-healing context. Signals to increase VEGF, TGF-β1, and collagen deposition and decrease IGF-1 [241].
3: Cancer	Loss of epithelial markers and adhesion molecules leads to resistance to cell death and an increased migratory phenotype [254, 255].	High lactate correlates with poor patient prognosis and survival [20, 22, 24, 33, 60]; high lactate correlates with metastatic disease [20-22, 24, 60].

1.5 Objective

What has become more apparent in last few decades of metabolism research is that lactate is more than merely a byproduct of glycolysis. It has the ability to influence angiogenesis, expression of surface molecules, genetic response, ATP generation, and cell migration. My dissertation work shows that:

1. Lactate accumulation can be measured in LABC biopsies. Lactate concentrations are higher than what is seen in most normal tissues, but are lower than lactate concentrations previously reported clinical trials in other cancer types. .
2. Lactate metabolism occurs in all cell lines tested, generating the metabolites alanine and glutamate.
3. Lactate can serve dually as fuel or a toxin, depending upon the concentration, duration of exposure and/or additional insults.
4. MCT1 and MCT4 have the potential to serve as biomarkers for cycling hypoxia in tumors.

2. Methods

2.1 Lactate and CHC

Sodium L-lactate ($C_3H_5NaO_3$) was purchased from Sigma-Aldrich (St. Louis, MO, USA) and added to 50mL of media to make up 80mM or 40mM stock solutions. Stock solutions were used within 3 weeks after preparation. Sodium L-lactate-3-^{13}C solution (45-55% w/w in H2O) and 99 atom % ^{13}C and α-cyano-4-hydroxy-cinnamic acid (CHC) were acquired from Sigma-Aldrich. CHC was solubilized in sterile DMSO to yield 1M and 100mM stock solutions. From these stock solutions, CHC was added to cell media to yield 5mM and 0.1mM for drug treatments.

2.2 Cell Culture

Cells were maintained in 37°C, 5% CO_2, 20% O_2 in a Forma Scientific (Marietta, OH) incubator. All cell lines were acquired through Duke University's Cell Culture Facility and from ATCC (Manassas, VA), except HMEC, which were acquired from Clonetics (Switzerland). Cell lines used were: HMEC (human mammary epithelial cells), MCF7 cells (ER^+, PR^+, $Her2^-$, invasive ductal carcinoma, luminal), MDA MB 231 cells (ER^-, PR^-, $Her2^-$, adenocarcinoma, basal), HepG2 cells (hepatocellular carcinoma) and WRL-68 cells (normal liver). Other cell lines included in limited studies were: R3230Ac (rat mammary carcinoma), CCD1112Sk (normal foreskin cells), BJ (normal foreskin cells) and SNU-182 (hepatocellular carcinoma) cells. HMEC cells were cultured in MEBM media

from Lonza/Clonetics (Switzerland) with added supplements ("MEGM media", Single®Quots®: 2mL BPE, 0.5mL hEGF, 0.5mL insulin, 0.5mL hydrocortisone, 0.5mL GA-1000). MCF7 cells were cultured in MEM media from Gibco (Invitrogen, Carlsbad, CA), supplemented with 10% fetal bovine serum (FBS: Gemini, West Sacramento, CA), 1% sodium pyruvate (Gibco), 0.1mM of non-essential amino acids (Gibco) and 1% antibiotic/antimycotic (Gibco). MDA MB 231 cells were cultured in high glucose DMEM (Gibco) +10% FBS + 1% antibiotic/antimycotic. T47D cells were cultured in RPMI 1640 media (Gibco) with 10% FBS, 1% sodium pyruvate (Gibco) and 1% antibiotic/antimycotic (Gibco). WRL-68 and HepG2 cells were cultured in MEM (Gibco) +10% FBS + 1% antibiotic/antimycotic with 1% sodium pyruvate (Gibco) and 0.1mM of non-essential amino acids (Gibco).

2.3 Protein extractions and concentration assay

2.3.1 Total Protein (RIPA buffer)

Cells were grown to 70-90% confluency in 10cm dishes. On ice, cells were washed twice with cold 1x PBS and all adherent cells were scraped off after the addition of complete RadioImmuno Precipitation Assay (RIPA) lysis buffer (150mM sodium chloride, 50mM Tris-HCl (pH 7.4), 1mM EDTA, 10% NP-40, 0.1% protease inhibitor, 0.5% sodium fluoride, 0.5% sodium vanadid, 0.5% PMSF (phenylmethanesulphonylfluoride), and 2.5% sodium deoxychlorate). For protein analysis in RIPA buffer, cells were collected in 1.5ml Eppendorf tubes, incubated on ice

for 15 minutes and then centrifuged at 15,000 RPMs in a microfuge for 10 minutes in 4°C. The pellet was discarded, and the supernatant was frozen and stored at -80°C.

2.3.2 Total Protein (Triton X lysis buffer)

For analysis of total protein in Triton X lysis buffer, cells were scraped with 1X DPBS and centrifuged at 8,000 RPM for 1 minute. DPBS was decanted, and Triton X lysis buffer (1M Tris (pH 7.5), 5M NaCl, 100mM EDTA, 100mM EGTA, 10% Triton X 100 dissolved in diH_2O with 1:100 protease cocktail added) was used to resuspend cells. Cells were vortexed, then were placed on a rocker for 45 minutes in the cold room for solubilization. After 45 minutes, cells were spun at 12,000 RPM for 10 minutes. The supernatant was collected and frozen at -80°C.

2.3.3 Protein concentration assay

Following protein extraction, samples were diluted in DI water, and 5 μL of the diluted sample was pipetted into a 96-well plate. BSA standards were serially diluted (initial concentration: 1.47 mg/mL, range: 1 – 1:16) and included in the assay. The Bio-Rad DC™ Protein Assay (Bio-Rad) was used to determine protein concentration following the manufacturer's instructions. The absorbance was measured at 750 nm using a microplate reader. A standard curve was generated to calculate the total protein in the samples.

2.4 Western Blots

2.4.1 MCT blots

For MCT1 and MCT4 Western blots, 15-50ug per sample were loaded onto 12% SDS-PAGE gels (Bio-Rad, Hercules, CA) and were separated by SDS-PAGE at 120 volts. The gel was transferred to a polyvinylidene fluoride **(**PDVF) membrane (Bio-Rad) and then blocked either for one hour or overnight at 4°C in non-fat, dry milk reconstituted in TBST (4g dry milk/100mL TBST). MCT1 rabbit anti-human IgG primary antibody (Millipore, Billerica, MA) was used, diluted 1:1000 in TBST and incubated in 4°C overnight. The membrane was washed three times for 10 minutes in TBST + 0.01% Tween. The secondary goat anti-rabbit IgG horseradish peroxidase-linked antibody (Jackson ImmunoResearch Labs, West Grove, PA) was diluted 1:2000 in TBST and incubated in room temperature for one hour. The membrane was washed three more times before incubating for 5 minutes with SuperSignal® West Pico Luminol/Enhancer Solution (Pierce, Rockford, IL). Kodak film (Rochester, NY) was used to capture the luminescent protein bands, and the film was developed on the Kodak processor with Spectra-2 developer (Merry X-Ray Corp, Mentor, OH) for x-ray film processing. Pan-actin controls were run in accordance for quantification.

2.4.1.1 MCT1/4 expression regulation

A549 and HT1080 cells were incubated in DMEM with 10% FBS and 1% antibiotic/antimycotic (10,000 units of penicillin (base), 10,000 μg of streptomycin (base), and 25 μg of amphotericin B/ml utilizing penicillin G (sodium salt), streptomycin sulfate, and amphotericin B as Fungizone® Antimycotic in 0.85% saline) in hypoxic

(0.5% O2, 5% CO2, 94.5% N2) and normoxic conditions for 0- 48 hrs. Cell culture media were acquired from Gibco (Invitrogen, Carlsbad, CA). The same cell lines were incubated with high lactate media: glucose-free, pyruvate-free DMEM with 10% FBS, 20mM lactate and 1% antibiotic/antimycotic for the same time course. MCT1/4 expression levels were assessed by Western blot to compare their regulation under each condition.

2.4.2 Snail, Slug and Twist Western blots

To prepare total cell lysate, cell pellets were washed with HBSS (Gibco) and pelleted into a 1.5 ml eppendorf tube. The pellet was lysed with a solution of 25mM Tris pH 7.5, 1% SDS, 1mM EDTA containing 1mM PMSF and Halt Protease / Phosphatase Inhibitors (Pierce). Benzonase (Sigma) was added to the samples to increase protein purity and reduce viscosity. Samples were incubated on ice for 15 to 20 minutes. Samples were centrifuged at 21000xG for 15 minutes at 4°C. Supernatants were removed and stored at -80°C. Total protein was determined by the BCA Protocol (Pierce).

Preparation of cytosolic lysates: Cytosol lysis buffer was made with the following: 10mM Hepes (7.6 pH), 10mM KCl, 1.5mM $MgCl_2$, 0.5% NP40, Protease/Phosphatase Inhibitors (Halt-Pierce), and 1mM PMSF.

Cell pellets were washed twice with 5mL HBSS, then transferred to 1.5ml Eppendorf tube and pelleted again. Next, 500 to 750 μL of cytosol lysis buffer was

added, and samples were incubated on ice for 10 minutes. Samples were centrifuged at 15000xG, and the cytosolic fraction was removed. The pellet was washed twice with cytosol lysis buffer, after which, the nuclear extraction was executed.

Preparation of nuclear lysates: The pellet was lysed with 50 to 150ul of 25mM Tris pH 7.5, 1% SDS, 1mM EDTA containing 1mM PMSF and Halt Protease / Phosphatase Inhibitors (Pierce). Benzonase (Sigma) was added to the samples and incubated on ice for 15 to 20 minutes. Samples were centrifuged at 21000xG for 15 minutes at 4°C. Supernatants were removed and stored at -80°C. Total protein was determined.

Gel Electrophoresis: Fifty to 100 µg of sample was mixed with reducing gel loading buffer and boiled for 5 minutes. Samples were loaded into a 10% Bis-Tris Nupage Gel (Invitrogen). Gel running buffer was MOPS-SDS. Gels were electrophoresed at 150V constant voltage until loading dye reached the bottom.

Western Transfer: Electrophoresed gels were incubated in cold western transfer buffer (Tris-Glycine plus 10% Methanol) for 5 to 10 minutes at 4°C. Proteins were transferred to 0.22 micron nitrocellulose membranes (GE Water & Process Technologies) at 100V constant voltage with an ice pack for 40 minutes. The transferred nitrocellulose was incubated in Blocking Buffer (Rockland) for 30 minutes at RT in black incubation boxes.

Detection: Anti-Snail-1(Cell Signaling), anti-Slug (from the Garcia-Blanco lab) and anti-Twist (Abcam) antibodies were added directly to blocked nitrocellulose and incubated overnight at 4°C. The following day the blots were washed 3 times with TBS/Tween 20.

Blocking buffer was added again and the fluorescently-labeled secondary detection antibodies for the Odyssey were added (diluted 1:5000 in 1:1 Odyssey Blocking Buffer (LI-COR Biosceinces) to TBS + 0.1 to 0.2% Tween20 + 0.01% SDS). This was incubated for 40 minutes at RT. Blots are washed 3 times with TBS/Tween 20 followed by 3 washes with PBS. Blots were imaged on an Odyssey scanner (LI-COR System).

2.5 Human LABC and HNSCC samples

2.5.1 Sample Storage

LABC human biopsies were acquired from clinician Kimberly Blackwell, MD with IRB approval. These samples were snap frozen in liquid nitrogen, stored at -80°C and transported on dry ice. The head and neck tumor samples were collected and stored similarly. Normal frozen breast tissue was acquired from Duke Comprehensive Center Shared Resource for Tissue and Blood Procurement. All samples were stored at -80°C until sectioning.

2.5.2 Cryosectioning

Cryosectioning of human LABC biopsies, normal breast samples and HNSCC samples was performed at -30°C. Sections for immunohistochemistry were cut at 10 microns and mounted on Superfrost Plus Micro Slides (VWR, West Chester, PA). Sctions for metabolite bioluminescence were cut at 20 microns and mounted on 22x40 micro cover glass (VWR) coverslips.

2.5.3 Immunohistochemistry on LABC biopsies

Routine H&E staining was carried out at room temperature. All tissue sections were fixed in 4% PFA for one hour. Following fixation, sections were incubated in hematoxylin (VWR, West Chester, PA, USA) for four minutes and subsequently rinsed for four minutes under slowly running tap water. Slides were then incubated in eosin (VWR, West Chester, PA, USA) for one minute. For dehydrating the sections, slides were dipped three times in 70%, 80%, 90% and 95% ethanol. Slides were then incubated in 100% ethanol for five minutes to extract any residual water. Finally, specimens were incubated in Fisher Brand Citrisolv™ (Fisher Scientific, Fair Lawn, NJ, USA) for five minutes before being mounted with Richard-Allan Scientific Cytoseal ™ XYL mounting media (Thermo Fisher Scientific, Waltham, MA, USA). Brightfield images of the H&E slides were imaged under 10x magnification. These images were then stitched together in Adobe Photoshop (Adobe Systems Inc., San Jose, CA, USA) and used for co-registration. A serial set of H&E slides were submitted to a pathologist at Duke University for analysis of percent invasive cancer in each sample.

Microvessel density (MVD) was assessed by CD31 immunofluorescence (IF) staining of frozen tissues. The frozen sections were fixed with ice cold 100% acetone for 20 minutes, then was washed three times with PBS + 0.2% Tween (Bio-Rad, Hercules, CA, USA) ("PBST") for 3-5 minutes. To block nonspecific binding of the primary antibody, the tissue was exposed to 10% donkey serum (Sigma-Aldrich, St. Lois, MO,

USA) for 30 minutes at room temperature before adding the primary antibody, mouse anti-human CD31 (BD Pharmigen, San Jose, CA, USA), diluted 1:100 in 10% donkey serum, for one hour at room temperature in the dark. The section was washed again with PBST, and the secondary antibody, DyLight 488 AffiniPure donkey anti-mouse IgG (Jackson ImmunoResearch, West Grove, PA, USA), was diluted 1:1000 in PBS and placed on the tissue for one hour at room temperature, in the dark. Slides were imaged on a Leica SP5 confocal microscope (Leica Microsystems, Buffalo Grove, IL, USA). Discrete microvessels were identified by positive CD31 staining; these were counted and summed for the entire section. Three separate tissue sections for each patient sample were measured for MVD, and these results were averaged for the final measurement per patient sample.

The proliferating capillaries index (PC index) was also assessed with IF staining, using the same procedure as MVD staining and imaging except mouse anti-human CD 105 (BD Pharmigen, San Jose, CA, USA) primary antibody was used in the procedure instead of anti-human CD31.

2.5.4 LABC genomics

Genomic analysis on 37 LABC biopsies was performed using Affymetrix U133 Plus 2.0 GeneChip arrays. All tissue specimens used for gene expression analysis were verified by a pathologist to have ≥60% invasive cancer before RNA harvesting. Detailed methods are provided in a previous publication [256]. Of the 23 patients with specimens

represented in the lactate analysis, 20 patients had matched genomic analysis. In order to retain statistical power in the analysis of a small sample set, specific pathways were chosen for analysis, which contained a total of 80 genes (Appendix A). Networks of interest included the full metabolic pathway of glycolysis and some TCA cycle genes, genes corresponding to cytoskeletal rearrangement, epithelial-mesenchymal transition (EMT), ion and nutrient transport, and cell death, oncogenic and inflammatory signaling. The rationale for choosing these networks was based on pathways known to be involved in lactate accumulation (glycolysis) and utilization (TCA cycle / OXPHOS) [86], as well as previous reports in breast cancer cells that lactate regulated metabolism, EMT, and tumor-promoting factors [86, 247]. Serum biomarkers found to be significantly correlated to patient treatment response to combined hyperthermia and neoadjuvant chemotherapy were also included in the analysis [257].

2.5.5 Data analysis and statistics for LABC samples

The samples were de-identified prior to cryosectioning and staining/bioluminescence, then retroactively linked to patient clinical data by a third party, following an approved IRB protocol. Four samples represented duplicate biopsies from the same patients. The remaining samples represented one biopsy per patient. Therefore, the total number of patients represented in the lactate bioluminescence data set is 23 (Table 8). Two samples could not be matched to patient information due to mislabeled specimens that did not reflect the actual tissue bank number. This reduced the number of total specimens

analyzed for correlations of lactate concentrations with clinical parameters from 23 to 21. There were 5 samples with incomplete clinical records. Nine of the samples studies (representing 8 patients) had parallel DCE-MRI data (Table 9).

The overall distribution of lactate concentrations was described by the median and interquartile range. Two methods were used to analyze whether lactate levels were correlated to clinical parameters (TMN, ER/PR/Her2 status etc: 1. The frequencies of clinical parameters were compared between subgroups of patients, split at the median value (high v. low lactate group). 2. The median, mean and standard deviation of lactate concentrations were compared for each clinical subgroup (i.e. ER+ v. ER-, etc.).

Four biopsies found to contain no invasive cancer. We termed these "benign breast tissue," and assigned them a sample name of "bb#." As seen in Table 9, one of these specimens ("bb2") was unmatched to clinical data. Similarly, specimen "LABC5" is missing matched clinical data (Table 9). While both of the unmatched specimens could not be analyzed for clinical parameters, they could be measured for lactate and % invasive cancer, so they were included in this analysis. To determine if lactate concentrations were significantly different based on the percent invasive cancer seen in the biopsy, a Pearson's Correlation Coefficient Test was conducted to compare lactate concentrations to percent invasive cancer.

To evaluate whether lactate levels or pO2 was significantly correlated to patient treatment response, ER/PR/Her2 status and inflammatory breast cancer status an

Asymptotic Wilcox Mann-Whitney Rank Sum Test was conducted. A Kendall's Tau Coefficient Test was conducted to evaluate concordant or discordant relationships between gene/pathway (Table 18) and lactate concentrations. To determine if either lactate or pO_2 levels predicted patient outcome, a Log Rank Test was used. All statistical tests were conducted and analyzed by Dr. Kouros Owzar, a biostatistician at Duke University.

2.6 Immunofluorescence in cells and tissue

2.6.1 Preparation of Coverslips for Staining

Round coverslips (18mm, VWR) were treated with a 1:10 dilution of hydrochloric acid in DI water for 5 minutes at room temperature. Coverslips were then rinsed twice with 70% ethanol. Excess ethanol was removed before placing coverslips in tissue culture hoods for 1-4 hr with UV light on, until coverslips dried. The dish of coverslips was then covered with foil to prevent contamination.

2.6.2 Membrane Expression of MCT1/4

Single cell suspensions were plated on round, glass coverslips for IHC for visualization of MCT1/4 actin signal. Coverslips were placed at the bottom of twelve well dishes and sterilized by exposure to ultraviolet (UV) light for 30 minutes prior to plating. Cell lines were seeded at 60,000-100,000 cells per well 24 hours in advance to staining. They were incubated under normal conditions (37°C, 5%CO_2, 20% O_2) in DMEM supplemented with 10% FBS and 1% antibiotic-antimycotic (10,000 units of

penicillin (base), 10,000 μg of streptomycin (base), and 25 μg of amphotericin B/ml utilizing penicillin G (sodium salt), streptomycin sulfate, and amphotericin B as Fungizone® Antimycotic in 0.85% saline). Cell culture media were acquired from Gibco (Invitrogen, Carlsbad, CA). After 24 hours, media was removed and cells were fixed with ice cold methanol for five minutes. Cells were washed with 1X calcium- and magnesium-free PBS and then blocked with 4% goat or donkey serum for 1 hour at room temperature. Rabbit anti-human MCT1 and anti-human MCT4 primary polyclonal antibodies (Millipore, Billerica, MA) were diluted 1:300 in the blocking serum. Coverslips were incubated with the primary antibody for one hour at room temperature. After washings, the secondary antibody (goat anti-rabbit IgG conjugated with Alexa 594, diluted 1:5000 in PBS) was placed on the coverslips for 45 minutes at room temperature. Prolong Gold antifade reagent with DAPI (Invitrogen, Carlsbad, CA) was used to mount the coverslips on glass slides. DAPI is a fluorescent stain that binds to DNA, which allows the nucleus to be visualized after excitation with UV light. Slides were allowed to solidify 1-8 hr before imaging. The slides were stored in the dark in 4°C until imaged.

2.6.3 Immunohistochemistry for MCT1 and MCT4 on tissue samples

Human locally advanced breast cancer (LABC) samples and head and neck tumor samples were thawed at room temperature and then fixed in 4% formalin for 30 minutes. They were washed in 1X calcium- and magnesium-free PBS, permeabilized with 0.1% Triton 100X for one minute before blocking with 10% goat serum for one hour

at room temperature. The same primary and secondary antibodies were used as in the coverslip staining. The primary rabbit anti-human MCT1 (or anti-human MCT4) antibody (Millipore, Billerica, MA) was diluted 1:200 in 10% serum and slides were incubated overnight at 4°C. The following day, samples were left to warm at room temperature with the primary for 30 minutes before following through with subsequent washing steps and incubation with the secondary antibody (diluted 1:5000) for one hour at room temperature. The samples were mounted with Prolong Gold antifade reagent with DAPI (Invitrogen, Carlsbad, CA). Slides were stored in the dark overnight at room temperature to allow the mounting media to solidify before imaging the following day.

2.6.4 Confocal Microscopy

All coverslip staining and EF5 immunohistochemistry were imaged using the Leica SP5 inverted confocal microscope (Leica, Wetzlar, Germany). Images were captured at 40X and 100 X oil immersion magnifications within 1-7 days after staining. Images are visualized and evaluated with Leica LAS AF software. Laser intensity for DAPI/UV (405) was set at 4%-14% while the red (594) and green (488) channel lasers were kept at 29% intensity.

2.7 Bioluminescence

For bioluminescence imaging, 20-μm-thick frozen sections were transferred onto glass coverslips. The sections were allowed to freeze-dry at -80°C. All reactions were carried out in a custom-fit black box, using a temperature-stabilized reaction chamber at

25°C and a fluorescence microscope with a cooled 16-bit CCD camera with photon counting capability, and image-capture software (Andor, South Windsor, CT). Three images were taken: two brightfields (before and after the enzymatic reaction) and one during the reaction. Sections were brought into contact with reaction solutions for either glucose or lactate, which were prepared following earlier published protocols [258, 259]. Light emission from the enzymatic activity of the luciferase reporter was detected through the bottom of the coverslip. Photon flux was integrated at an overall magnification level of x50, over a time interval of 30 seconds after an incubation time of 10 seconds [104]. Images were calibrated using appropriate standards, consisting of 20 μm thick cryostat sections in optimum cutting temperature embedding medium (Sakura Finetek, Torrance, CA) with known concentrations of the metabolites added. The measuring procedures were identical for standards and tumor sections. ImageJ (Rasband, W.S., ImageJ, U. S. National Institutes of Health, Bethesda, Maryland) was used for image analysis with image histograms acquired from selected regions of interest. Percentiles of pixel intensity distribution were determined from the histograms, using the 5th percentile of the intensity range as the minimum value, 50% as the median representative value for the area, and the 95th percentile as the maximum value. The bright-field images were used to evaluate rough structures like tissue edges and necrosis. Corresponding H&E slides were co-registered to identify distinct tumor

regions: tumor edge, vital non-necrotic tumor, and perinecrotic tissue areas. Three slides from each tumor (n=3) were imaged to acquire an average for regions of interest [104].

2.8 NMR for 13C-lactate *in vitro*

^{13}C-NMR was used to investigate pathways of lactate metabolism in all cell lines used. Cells were exposed to high lactate (10mM) in normoxic conditions for an appropriate time course, 4.5 and 24 hours. Tissue culture dishes (15cm diameter) were plated at cell densities between 2-3x10^6 cells. After allowing 24 hours for cells to attach, or after achieving 80% confluency, cells were washed twice with 1x DPBS and then treated with either high glucose DMEM (untreated control), no glucose (and no pyruvate) DMEM + 10mM ^{12}C (unlabeled) lactate (unlabeled control) or 10mM ^{13}C-lactate (Isotec, Sigma-Aldrich). At the end of the incubation period, 1mL of media was collected and immediately frozen at -80°C. These samples were used to acquire 1H, 13C and 2D spectra of extruded metabolites. Cells were washed twice with DPBS. For metabolite extraction, 1mL of 0.9M perchloric acid, diluted 1:10 in dH_2O, was added to each dish, and cells were harvested by scraping. The samples were centrifuged at 12,000 RPM for 10 minutes to pellet cell debris and precipitate. Supernatant was transferred to a fresh tube, and this was used for NMR on cell extracts.

For NMR readings, 600uL total volume was used. For cell extracts, 450uL of the perchloric acid cell extract, 100uL DPBS and 50uL D_2O were added to the NMR tube. For

media samples, 550uL media and 50uL D_2O were mixed. Tubes were capped and placed in the 500MHz magnet. Tony Ribeiro, PhD, provided extensive assistance and supervision of NMR data acquisition.

^{13}C-NMR spectra was acquired at 125.7 MHz with a Varian 500 MHz spectrometer equipped with a 5mm broad-brand probe, available for use at the Duke Comprehensive Cancer Center. Specifications were: a 45° flip angle, 0.8s interpulse delay, and a 1.334 s acquisition time. All proton spectra were run at 500MHz. 2D Heteronuclear Multiple Quantum Correlation (HMQC) spectra include carbon coupling and decoupling and represent intersections of peaks from proton and carbon spectra. Vnmrj software (Varian, Inc., Palo Alto, CA, USA) was used to analyze and plot 1H, 13C and HMQC spectra. Control runs of known concentrations of glutamate, lactate, and alanine were included to assess peak shape and ppm position. For data analysis, ratios obtained from peak heights of the different metabolites within a spectrum were compared.

2.9 Cell survival assays

2.9.1 Clonogenic Survival Assays

2.9.1.1 Clonogenic Survival Assay Protocol 1

Cells were plated on Falcon 6-well plates, at densities optimized to acquire visible colonies 7-14 days after treatment. Three control groups were included: “control media” (DMEM +10% FBS + 1% antibiotic/antimycotic), “nutrient depletion group”

(glucose-free, pyruvate-free DMEM +10% FBS + 1% antibiotic/antimycotic), and "0mM lactate, 5mM glucose group" (glucose-free, pyruvate-free DMEM +10% FBS + 1% antibiotic/antimycotic with 45% D-glucose added (Sigma-Aldrich)). These groups are represented in figures as "CNTRL," "0mM lactate, no glucose," and "0mM lactate, 5mM glucose," respectively. Five other lactate concentrations were included: 5, 10, 20, 40, and 80mM. Sodium L-lactate was acquired from Sigma-Aldrich (St. Louis, MO). The powder was weighed and added to glucose-free, pyruvate-free DMEM +10% FBS + 1% antibiotic/antimycotic to acquire desired concentrations. When cells were treated, total volume of each well was equal to 3mL. For the lactate concentrations with additional 5mM glucose added, 6uL of 45% D-glucose was added to 3mL of media in each well during treatment times.

Experiments were plated in triplicate and conducted between 3-8 times on separate occasions. All lactate and glucose treatment groups were plated on the same day, however each time point was not necessarily plated on the same day. Cells were incubated 18-24 hours after plating to allow attachment, then washed with 1x DPBS and treated. Treatment media remained on the cells for either 18 hr, 48 hr or 1 week. After treatment, cells were washed with 1x DPBS and replaced with fresh culture media. When colonies became visible by eye (after 7-14 days in culture), plates were removed and stained for counting.

Staining clonogenics: Media was removed and the plates were washed with 1x DPBS. Cells were then fixed for 10 minutes at room temperature with fixation solution (10% Methanol, 10% acetic acid and 80% DI H_2O), then stained for 10-30 minutes at room temperature with Crystal Violet (Sigma-Aldrich, St. Louis, MO), diluted with ethanol and DI H_2O to 4% for the working solution and washed in cold water. Plates were allowed to dry overnight on the bench top before being counted the following day either by hand (for very small, compact colonies [HepG2] or for faintly stained colonies [MDA-MB-231]) over a light box or with Oxford Optronix (Abingdon, Oxfordshire, UK) ColCount™ colony counter. When counting by hand, colonies were subsequently observed under the microscope to confirm >50 cells per colony as a positive count. On the ColCount™, separate files were made for each cell line with specified settings to assess colony shape, center, edge detection and OD for counting. These settings were not changed between plates so as not to induce bias. Data analysis and plotting of clonogenic survival was done in Microsoft Excel. Colony counts were normalized to the control wells to acquire a relative measure of surviving fraction. All control wells were assigned a surviving fraction of 1.

2.9.1.2 Clonogenic Survival Assay Protocol 2

Cells were plated to six-well plates and were allowed to grow and recover from trypsinization for 48 h, until approximately 70% confluent. At this point, media was

removed and lactate treatment was performed for 24 h (0, 10, 20, or 40 mM lactate in the preferred cell media). After 24 h, the treated cells were trypsinized and combined with the treatment media, which contained any floating cells. Cells were centrifuged at approximately 1200 g for 5 min. Media containing the lactate was aspirated off and cells were resuspended in fresh media, appropriate to the cell line. Cells were counted with a hemocytometer and re-plated at a low density (100-1500 cells per well, dependent upon cell line). Cells were then incubated for 7-14 days, then colonies were stained as previously described. Surviving fraction was defined as number of colonies counted per cells plated. Normalized surviving fraction was defined as the surviving fraction of a group divided by the average surviving fraction of untreated cells.

2.9.2 Apoptosis/Cell Death Assays: Annexin V / 7-AAD staining

All cell lines were assessed for apoptosis after 24-hour lactate exposure. Cells were plated in 6-well plates at between 200,000-450,000 cells per well, depending on cell type. After 18-24 hours, cells were washed with 1X DPBS and treated with media ± glucose and ± lactate. For lactate-treated groups, all treatment media for control and experimental groups were prepared as previously stated for clonogenics. MCF7 cells and R3230Ac cells were also exposed to high (5mM) or low (0.1mM) CHC concentrations to assess cell survival and death with high lactate and the presence or absence of glucose (Table 7).

Table 7: Conditions for cell survival experiments with CHC treatment

Group	Glucose	[Lactate]	CHC
Control	+	0mM	0mM
Vehicle control	+	0mM	DMSO (high)
CHC	+	0mM	5mM
			0.1mM
CHCNG	-	0mM	5mM
			0.1mM
40Lact	+	40mM	0mM
40LactNG	-	40mM	0mM
CHC40L	+	40mM	5mM
			0.1mM
CHC40LNG	-	40mM	5mM
			0.1mM

After 24 hours of treatment, cells were harvested and washed in the same manner as indicated in the propidium iodide staining. Cells were then suspended in 1mL of 1X Annexin Binding Buffer (BD Pharmigen, San Diego, CA) to yield approximately 10^6 cells/mL. 100uL of the cell suspension was added to a 96-well plate (BD Pharmigen, San Diego, CA). 5 µL of PE-labeled Annexin V (BD Pharmigen, San Diego, CA) and 5 µL 7-AAD (BD Pharmigen, San Diego, CA) were added to each experimental well. Samples were incubated in the dark for 15 minutes and tapped gently to mix. 100uL of Annexin Binding Buffer was added to the wells immediately before analysis by flow cytometry on the Guava Cytosoft platform (Millipore, Billerica,

MA). Separate control samples for PE and 7-AAD were used to adjust the histogram settings for each cell line. These settings were used for all experiments within the same cell line. After data was acquired, FlowJo software (Tree Star, Ashland, OR) was used to plot data and set quadrants. Once quadrant coordinates were set, these settings were applied to all samples within the same cell line for comparison. Additional samples were run by Duke University's Flow Cytometer Facility, a Shared Resource of Duke University Cancer Institute.

2.9.3 Cell Cycle/Propidium Iodide staining

Cells were plated on either $10cm^2$ or $6cm^2$ plates for these experiments and allowed to attach and grow to 70-80% confluency before treatment. Four control plates were included: a positive control for detecting subG1 fraction, a no stain negative control, a no treatment (HG DMEM) control and a "nutrient depletion" control that did not have any glucose or lactate. This final group was denoted as "0mM lactate, no glucose," and it was included to determine if any differences seen in cell cycle regulation was due to added lactate or to glucose deprivation. Experimental groups included: 5mM lactate with no glucose, 10mM lactate with no glucose, 20mM lactate with no glucose, 5mM lactate + 5mM glucose, and 10mM lactate + 5mM glucose. Treatments lasted for either 18 or 48 hours, after which cells collected immediately.

All media within the dishes were transferred to separate 15mL Falcon (York, North Yorkshire) centrifuge tubes. Plates were then washed with 2mL of sterile 1x

DPBS, which was also collected in the tubes after washing. Cells were harvested using 0.25% trypsin + EDTA (Gibco). Once cells were detached, they were collected in the respective tube. Plates were washed a final time with 1mL of 1x DPBS to collect any residual cells on the plate. This was added to the tube before centrifugation for 4 minutes at 5,000 rpm in 4°C. Supernatant was removed before resuspending the cell pellet in 2mL of sterile 1x DPBS + 1% FBS. Cells were centrifuged again at the same settings. Supernatant was disposed and cells were resuspended in 0.5mL of sterile 1x DPBS. 5mL of ice cold 80% ethanol was added to the cells and vortexed. The tubes were then wrapped in aluminum foil before being placed in the -20°C for analysis 20 minutes – 1 week later.

Sample preparation for flow cytometry was carried out on ice and in the dark. First, tubes were centrifuged for 4 minutes at 5,000 rpm in 4°C. Supernatant was removed, then the cell pellet was resuspended in 1x DPBS and transferred to 5mL polystyrene round-bottom tubes (BD Falcon™, Bedford, MA). RNAse A (Invitrogen, Carlsbad, CA) was added to all tubes. Next, propidium iodide (Sigma-Aldrich, St. Louis, MO) was added to all tubes except the "no stain" control. All sample data for cell cycle and subG1 fraction were analyzed with BD Calibur Flow Cytometer (GMI, Ramsey, MN) by either Thusitha Dissanayake or Mike Cook, PhD in the Duke Cancer Institute Shared Flow Cytometry Facility. 10,000 events were acquired and the percentage of cells in each cell cycle phase was graphed using Microsoft Excel.

2.9.4 Assessment of Cell Survival after Detachment

Experiments were plated on $10cm^2$ plates. At two particular time points (dependent upon cell line, either 12, 24, 48 or 72 hours), detached cells were collected and centrifuged. These cells were then washed, resuspended and counted, using Trypan Blue (Sigma-Aldrich, St. Louis, MO) to assess cell survival. Dead and live cells were noted for each count. The resuspended cells were then plated in new six-well plates with fresh media. Cells were allowed to grow for 5-14 days and imaged on days 5/6 and 7/8. After the allotted amount of days, cells were collected for counting with Trypan Blue or for assessment of colony formation by Crystal Violet staining, as previously described in the clonogenic assays. Plating densities and doubling times were considered in the calculation of the level of cell detachment relative to the control.

2.10 Statistics

Results were preliminarily analyzed by StatView with an One-Way ANOVA and post-hoc tests (particularly Bonferroni/Dunn). Analysis of statistics for clonogenic assays (protocol 1) were performed by a biostatistician, Lan Lan, PhD. Kouros Owzar, PhD, performed statistical analysis on LABC biopsies, which included: 1. Log rank tests for comparing pO_2 and lactate levels in LABC biopsies to patient outcome, 2. Pearson's Correlation Coefficient for correlations between lactate levels and invasive cancer and

biological parameters (e.g., MVD), 3. Kendall Tau Tests for comparing genomic data to lactate levels in LABC.

3 Lactate levels in Locally Advanced Breast Cancer (LABC)

3.1 Introduction

The primary emphasis of the work done in this thesis is on breast cancer. To establish the clinically relevant boundaries of lactate concentrations to study *in vitro*, I measured lactate concentrations in core biopsies obtained from patients with LABC, prior to therapy.

Locally advanced breast cancer (LABC) comprises about 5-10% of all newly diagnosed breast carcinomas in the U.S. The diagnosis of LABC includes all stage III and a subdivision of stage IIb breast cancers [260]. LABC is a highly heterogeneous disease but common features in clinical presentation and tumor biology include: a large primary breast tumor (typically >5 cm, T3), nonmetastatic T3 and T4 tumors, tumors with chest wall involvement, extensive regional lymph node involvement and/or inflammatory carcinoma [261-263]. LABC has a notoriously poor prognosis, with three and five year disease-free survival (DFS) of 65% and 55%, respectively, even with combined therapy [264].

A phase I/II clinical trial involving neoadjuvant paclitaxel, liposomal doxorubicin and hyperthermia was conducted at Duke University between 2000-2004. Several reports have been published related to this trial. First a number of ancillary studies were conducted on these patients, including oxygen electrode measurements of hypoxia.

Combined chemotherapy and hyperthermia treatment significantly improved oxygenation of eight out of eleven hypoxic LABC tumors [265]. The improvement in oxygenation was associated with better response to therapy. Genomic analysis of biopsies acquired prior to surgery revealed gene signatures for: 1) positive lymph nodes at the time of surgery, 2) inflammatory breast cancer and 3) presence of tumor hypoxia. Further, serum cytokines were analyzed in these patients prior to treatment. Significantly increased levels of MMP-9, IL-6 and IL-8 were found in the serum of patients who responded to therapy [257].

Perfusion measurements were also performed on a subset of these patients, using dynamic contrast enhanced MRI (DCE-MRI). A morpho-physiological tumor score (MPTS) derived from DCE-MRI parameters was also highly correlated with response to therapy [266].

What is now evident is the substantial influence the tumor microenvironment has on the tumor phenotype, and the metabolic milieu is one facet of the tumor microenvironment. Since the initial discovery of altered tumor metabolism by Warburg in the 1920s [16, 17, 34], there has been increasing interest in the causes and consequences of the highly glycolytic cancer metabolism. A common feature of many solid tumors is an increase in lactate production [34, 36]. Lactate concentrations do not typically rise above 2mM in healthy, resting individuals [267]. Normal tissues that display higher concentrations of lactate, like exercising skeletal muscle (up to 25mM)

[267], have adapted methods of coping with or utilizing the high lactate, such as the Cori Cycle [49, 268, 269] . Lactate accumulation in normal tissue often serves a specialized purpose, such as mimicking inflammatory signaling in wound-healing to promote collagen remodeling [241]. Intriguingly, many of the molecules that lactate can regulate in certain contexts (wound-healing) are also relevant to tumor physiology, including VEGF and TGF-β [241].

High lactate concentration has been found to be prognostically significant in many different solid tumors including head and neck [21, 22], cervical [19, 20], colorectal [24], lung [33] and brain cancers [27, 28, 41, 42]. In a number of these clinical studies, lactate concentrations were analyzed utilizing bioluminescence techniques on frozen tumor sections [19-22, 24]. In every solid tumor type tested, high lactate concentrations were associated with higher TMN stage, significantly reduced overall survival and a greater incidence of metastases [19-22, 24]. To date, lactate levels have not been reported for LABC.

As cancer research has progressed, it has become more evident that tissue architecture and the tumor microenvironment play an integral role in cancer initiation and progression. As discussed in Section 1.1.2, lactate is a common component of the tumor milieu that is implicated in tumor progression. To date, a number of studies have assessed lactate in a number of human solid tumors (Table 2). In all known cases, lactate accumulation correlated with poor patient prognostic indicators and poor DFS and OS;

more aggressive tumors have often shown increased lactate levels. To date, no studies have illustrated spatial distribution of lactate or measured the range of lactate concentrations within breast tumor biopsies.

Bioluminescence techniques have been previously established to measure metabolites in tissue [104, 258, 259, 270]. This technique captures the heterogeneity of the metabolic profile of tumors upon the time of extraction and freezing. While it provides a snapshot, much information can be gleaned from the specimen: correlation of metabolites 1. with other metabolites, 2. with tumor necrosis, 3. with tissue architecture, and 4. with biomarkers of interest. Provided patient information is available, the metabolic profile of the tumor can be correlated to prognosis, DFS, OS, blood/plasma biomarkers, and other measurements. A summation of many of the findings from using quantitative bioluminescence on tumor tissue has been provided in Section 1.1.

3.2 Results

3.2.1 Patient clinical parameters

Table 8: Clinical characteristics of LABC patients

Characteristic	*Number of Patients*
Patients	
Total patients in lactate analysis study	23
Matched lactate values to clinical data	21
Extensive clinical information available	20
Clinical Stage	
IIb	9
IIIa	5
IIIb	6
Clinical Response	
Complete	6
Partial	7
Stable Disease	7
Pathological Response	
Complete	1
Partial	12
Stable Disease	7
TMN	
2	5
3	9
4	6
Tumor Size	
2-5cm	6
>5cm	12
Nodal involvement	
Node+	12
Node-	5
Outcome	
Alive	15
Dead	6
Relapse	

Yes	5
No	15
Distant Metastases	
Yes	6
No	14
ER status	
ER+	10
ER-	10
PR status	
PR+	15
PR-	5
Her2 status	
Her2+	3
Her2-	17
Triple Negative	
Yes	2
No	18

Of the twenty patients with clinical information, nine had stage IIb tumors, five had stage IIIa and six had stage IIIb tumors (Table 8). After therapy, six patients had a clinical complete response (cCR), seven patients had a clinical partial response (cPR), and seven patients had clinical stable disease (cSD). Of these same patients, one was found to have a pathologic complete response (pCR), twelve had a pathologic partial response (pPR), and seven demonstrated pathologic stable disease (pSD) (Table 8). Other clinical parameters of the patient population include a TMN score of 2, 3, or 4 demonstrated in five, nine and six patients, respectively, six patients with a primary tumor 2-5cm and twelve patients with a primary tumor >5cm. Twelve patients had lymph node involvement and five patients showed no lymph node involvement. Node

involvement on three patients was not available. There was a relatively equal distribution ER status in the high and low lactate groups and two patients with triple negative tumors. At a median follow-up of 53.5 months, the majority of patients were alive and without metastases (Table 9).

Table 9: Comparison of patient clinical parameters and specimen lactate concentrations in the low (Lo [L]) vs. high (Hi [L]) lactate groups

Grp	Sample #	% Inv ca	Inflam Br Ca	Outcome	DCE-MRI Pattern	MPTS	TMN	Dist Mets.	Node	ER	PR	Her2	Relapse	Age	[L] 5P Min	[L] 25P	[L] 50P Med.	[L] 75P	[L] 95P Max
Lo [L]	bb1	0	n	alive			2	n	2	n	p	n	n	39	0.0	0.0	0.8	1.5	2.6
	LABC1	70	n	alive	CP	0	2	n	1	n	p	n	n	62	0.0	0.0	0.6	1.3	2.5
	bb3	0	n	alive			3	n	1	n	p	n	n	54	0.6	1.7	2.5	3.9	4.8
	LABC2	30	n	alive			3	n	1	p	p	n	n	62	0.3	1.5	2.6	3.5	5.2
	LABC3	70	n	alive	CP	1	3	n	1	p	n	p	n	55	0.6	1.8	2.9	3.8	5.4
	LABC4	95	n	alive			4	y	1	p	p	n	n	32	0.4	1.8	3.3	3.7	5.4
	LABC6	80	y	dead			4	y	?	p	p	n	n	63	1.1	2.5	3.8	4.9	7.0
	LABC7	75	y	dead			4	y	0	n	n	p	y	58	1.2	2.7	4.0	5.2	7.2
	LABC8	75	n	alive			3	n	0	p	p	n	n	55	1.4	2.9	4.2	5.3	7.5
	LABC9	70	n	alive	CF	2	3	n	0	p	p	p	n	43	1.4	3.0	4.2	5.5	7.7
	LABC710(d)	65	n (d)	alive (d)	CP (d)	0 (d)	2 (d)	n (d)	1 (d)	n (d)	P (d)	n (d)	n (d)	62 (d)	1.7	3.1	4.3	5.3	7.1
	bb4	0	n	alive	CP	1	2	n	1	n	p	n	n	35	0.7	2.5	4.4	5.5	7.8
Hi [L]	LABC11	70	y	dead			4	y	2	*n*	*n*	*n*	y	75	1.6	3.1	4.5	5.7	7.8
	LABC12	75	y	dead	CF	5	4	y	1	p	n	n	?	66	0.9	2.6	4.5	5.1	7.2
	LABC13	80	n	alive	CP	3	2	n	1	p	p	n	n	44	1.5	3.2	4.6	5.7	7.8
	LABC14	60	n	alive			?	?	?	?	?	?	?	?	1.5	3.3	5.0	6.3	8.9
	LABC15	95	n	alive			3	n	?	n	p	n	n	35	1.0	2.9	5.1	5.7	8.6
	LABC16	80	n	dead			3	n	0	*n*	*n*	*n*	y	32	1.6	3.1	5.2	6.0	8.2
	LABC17	80	n	alive	CF	4	3	n	0	n	p	n	y	49	2.0	3.7	5.2	6.6	8.9
	LABC18	80	n	dead	CP	2	2	n	1	p	p	n	n	27	1.8	3.8	5.6	7.0	9.4
	LABC19	75	y	alive	CF	6	4	y	?	n	p	n	n	52	2.9	4.9	6.6	8.1	10.9
	LABC20	80	n	alive			3	n	1	p	p	n	n	43	3.3	5.3	7.2	8.8	12.3
	LABC21(d)	90	n (d)	alive (d)			3 (d)	n (d)	?	n (d)	p (d)	n (d)	n (d)	35 (d)	4.0	6.0	8.0	9.4	12.2

Specimens are named based on presence of benign breast tissue (bb) or presence of invasive cancer (LABC). Duplicate specimens are indicated (d). Measured lactate concentrations (µmol/g of tissue) are displayed in the last five columns. These values correspond to the lactate concentration range ([L]) seen in microregions in each specimen: fifth percentile/minimum (5P),twenty-fifth percentile (25P), fiftieth percentile/median (50P), seventy-fifth percentile (75P) and ninety-fifth percentile/maximum (95P). Samples are arranged in ascending order of median lactate concentrations. High and low lactate groups were determined based on median lactate concentrations >4.4 µmol/g.

3.2.2 Lactate accumulation occurs in LABC biopsies, but higher lactate concentrations do not significantly correlate with greater % invasive cancer

Tumor and stroma areas of the H&E section were identified (Figure 5A&C) and particular areas of lactate accumulation were assessed after co-registration of the H&E image with the lactate bioluminescence image (Figure 5B&D). Lactate accumulation co-localized primarily to the stroma in 17% of the specimens (Table 10, Figure 5). Thirty percent of the specimens showed a relatively even lactate distribution between the stroma and tumor bearing regions of the section, while the majority of samples (53%) demonstrated lactate accumulation in regions containing tumor (Table 10). Two specimens showed relatively high lactate signal at the tumor-stromal interface. Biopsies displaying no invasive cancer were not included in the assessment.

Table 10: Lactate distribution in LABC biopsies

Region of biopsy	% of samples showing lactate accumulation primarily in given region
Stroma	17% (n = 3)
Even	30% (n = 5)
Tumor	53% (n = 9)

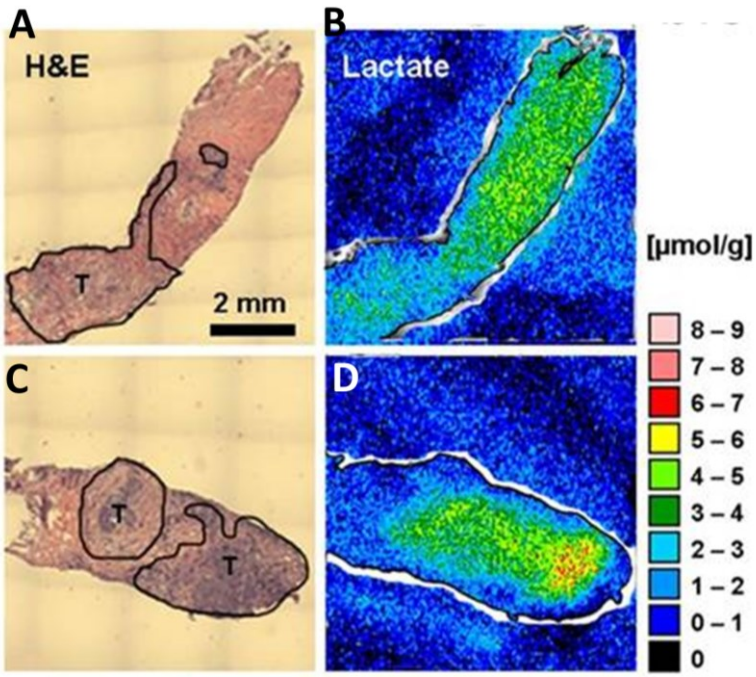

Figure 5: Representative images of the lactate distribution in LABC biopsies. Tumor regions ("T") are indicated in H&E (A&C) sections of LABC biopsies. Lactate bioluminescence (B&D) shows lactate accumulation in the stroma (B) and tumor (D) region of LABC biopsies. For each sample, lactate measurements are n=3-4 sections.

All specimens showed some lactate accumulation. The minimum lactate accumulation found in certain microregions of an individual sample was 0 µmol/g, and the maximum lactate concentration was 12.3 µmol/g (Table 9). The median of all biopsies was 4.4 µmol/g. Within individual specimens the median lactate concentrations ranged from 0.5-8.0 µmol/g of tissue ("[L] 50P Med." Table 9). To determine if higher lactate concentrations correlated with greater percent invasive cancer found in the biopsy, a Pearson's correlation coefficient test was used. Higher lactate concentrations in

the LABC biopsy did not significantly correlate with the percent invasive cancer seen in the biopsy (correlation coefficient = 0.505).

3.2.3 Lactate levels show intratumoral heterogeneity

Patient specimens were divided into high and low lactate groups using a median lactate concentration cut-off of 4.4 μmol/g. The differences in the ranges of mean lactate concentrations for each percentile (95^{th} "maximum," 75^{th}, 50^{th} "median," 25^{th} and 5^{th} "minimum") were statistically significant when low (specimens: n=13, patients: n=12) and high (specimens: n=12, patients n=11, Table 9) lactate group measurements were compared (ANOVA, $p=0.0002$ for 5^{th} percentile, $p<0.0001$ for all other percentiles). This suggests that there is less heterogeneity within a single biopsy than there is between biopsies.

The two specimens that represented second biopsy site from the same patient fell into the same high or low lactate group as the first biopsy site. Specimens LABC1 and LABC10 (Figure 6) are biopsies from the same patient and are in the low lactate group, while specimens LABC15 and LABC21 (Figure 6) are from another patient and are in the high lactate group (second site indicated by "d" in Table 9). The median lactate concentrations measured in LABC1 and LABC10 were 0.6 and 4.3 μmol/g (Student's T-test, $p<0.05$), and the median lactate concentrations measured in LABC15 and LABC21 were 5.1 and 8.0 μmol/g, respectively (Table 9, Figure 6). From these dual biopsy sites

from one tumor, the intra-tumor metabolic heterogeneity is illustrated, indicating that lactate levels can vary significantly among different areas of the same tumor.

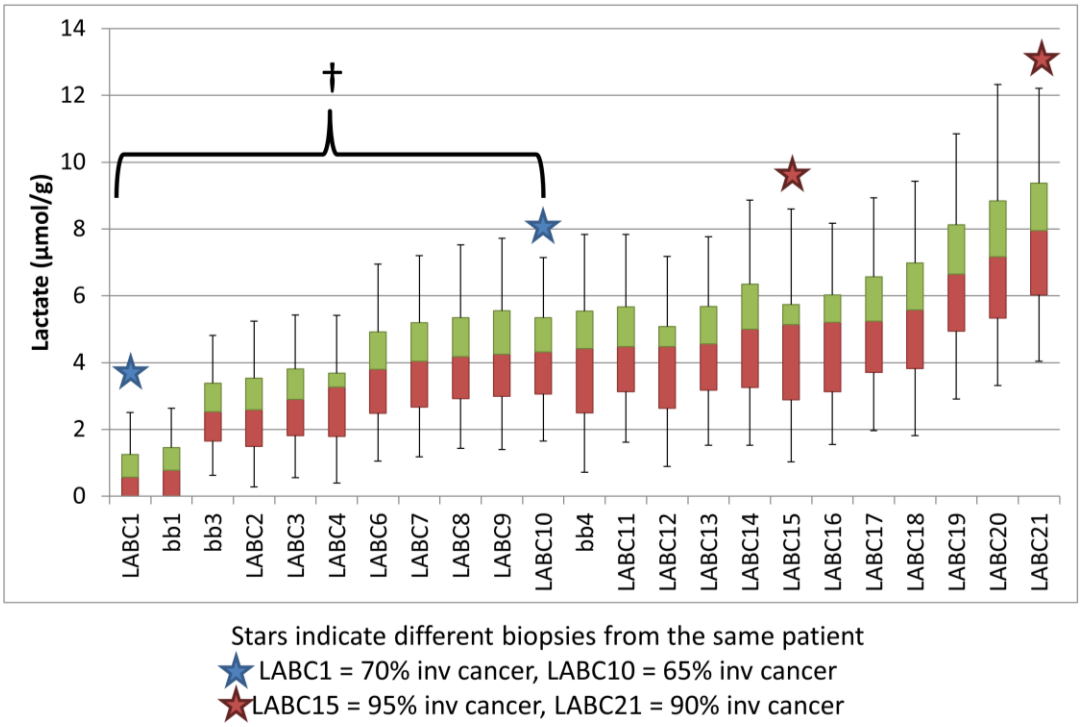

Figure 6: Waterfall chart of lactate concentrations in each individual LABC biopsy with accompanying clinical information. Biopsies with invasive cancer are denoted as "LABC," but biopsies without invasive cancer are marked as "bb." The median concentration is represented by the middle line of the boxplot. Ranges of the 25th and 75th percentile concentrations are represented by the black and gray portions of the box, respectively. Error bars indicate 95% confidence intervals. †$p<0.05$

Initial evaluation of lactate levels measured in LABC biopsies and patient clinical parameters was attempted; however, the sample set (25 biopsies, 21 patients) was too small to derive any statistical significance. Mean lactate concentration ranges for each

individual clinical and biological parameter are given in Appendix A. Due to the small sample set, correlation between lactate accumulation and regulation of certain genomic pathways could not be reliably analyzed. Prospective pathways that were of interest are provided in Appendix A.

In summary, all LABC biopsies tested by metabolite bioluminescence demonstrated lactate accumulation. The range of lactate concentrations within microregions of these specimens was 0 – 12.3 μmol/g of tissue, which are lower than what has previously been documented in other solid tumors [19-22, 24, 60]. Implications of this finding are discussed below.

3.3 Discussion

The implications of lactate accumulation within solid tumors are beginning to be brought to light with increasing research on cancer metabolism, but the complete picture is still hazy. Since the beginning of the 20th century, we have known that lactate accumulation is a common feature to solid tumors, which undergo a metabolic switch to prefer glycolysis [16, 17, 34]. This is regulated by genetics, biochemistry, mitochondrial defects and environmental factors [46, 48, 271]. Lactate accumulation due to hypoxia (the Pasteur Effect) and HIF -1α upregulation gains much additional attention. While this phenomenon is certainly pertinent to many hypoxic tumors, lactate accumulation still occurs in aerobic conditions due to the Warburg Effect. Our study did not show a

relationship between pO_2 levels and lactate concentrations in LABC biopsies; however, without statistical power to make definitive statements, future study into this relationship is warranted, especially given the occurrence of hypoxia in a number of these same tumors [265]. With further analysis, it may be determined if lactate accumulation in LABC is primarily due to the Pasteur Effect or the Warburg Effect.

A number of clinical studies in different types of solid tumors have found that higher lactate accumulation significantly correlates with poor patient survival and increased metastases [19-22, 24, 33]. High lactate has been suggested to be a useful tool for classification of aggressive rectal adenocarcinomas [24] and a surrogate marker for prostate cancer aggressiveness [108]. Unfortunately, patient survival in relation to lactate concentrations could not be assessed in this study.

From the samples with more than one biopsy site, we determined that lactate accumulation was highly heterogeneous. The lack of correlation between lactate concentration and percent invasive cancer in the biopsy may be due to high intratumoral lactate heterogeneity or could indicate that the metabolic profile of LABC may be considerably different from other solid tumors. Furthermore, breast core needle biopsies are small samples (11-16 gauge needle = 0.3-1.7 mm diameter) compared to the size of the tumor (mean LABC tumor size for sample set = 7cm). The lactate levels found in this study may not always accurately reflect the dominant tumor metabolic profile. In order

to more fully investigate lactate metabolism in LABC, different sampling methods may be required.

The lactate median cut-off value in the LABC specimens (4.4 μmol/g) is substantially lower than lactate median cut-off values in previous studies of human tumors: 10 μmol/g in cervical cancer specimens [20] and ~7 μmol/g in head and neck cancer [22]. Given these ranges, it is possible that high lactate accumulation is not a characteristic of LABC; however, this conclusion will require further exploration with a larger sample set and/or larger biopsy samples. *In vivo* studies in rat hepatomas [272, 273] and *in vitro* studies in glioma cells [30, 31] have shown that lactate can be utilized as a metabolic substrate. If LABCs have the same ability to utilize lactate, this may be another reason why lower lactate concentrations overall were demonstrated in these biopsies.

As tumor metabolism manipulation gains favor as a potential therapeutic option, it will be important to monitor tumor metabolites. [18F]-2-fluoro-2-deoxy-D-glucose (FDG)-positron emission tomography (PET) is already used in the clinic to monitor breast cancer (including LABC) progression and has been proven to predict patient response to chemotherapy [274-276]. FDG is a glucose analog that is used to acquire metabolic information about the tumor, particularly glycolysis, since FDG is taken up by glycolytic cells but cannot progress fully through the glycolytic pathway [277].Given the highly glycolytic phenotype of tumors, lactate levels may mirror cellular proliferation

[66, 278, 279]; however, if the tumor avidly consumes lactate, lactate levels would not reflect tumor cell proliferation. This question may be of value to clinicians: a solid tumor with the ability to consume lactate may be more treatment-resistant than one unable to consume lactate, as postulated by the metabolic symbiont model [141]. Lactate-consumption markers (Section 6) or comparisons of glycolytic flux and lactate utilization may be helpful to address this. Currently, very few noninvasive methods for lactate measurements *in vivo* are available. Notably, lactate magnetic resonance spectroscopic imaging (MSRI) is one method of obtaining lactate concentrations *in vivo*. This method has recently been used to assess lactate concentrations in gliomas [280]. Using hyperpolarized pyruvate to determine lactate concentrations in tumors is another noninvasive method of lactate detection [281]. Using this method, metabolic flux of the pyruvate-to-lactate conversion has been measured in T47D breast cancer cells [282]. Additionally, this method has been used to correlate increases in lactate concentrations to cancer detection and grading in the transgenic adenocarcinoma of mouse prostate (TRAMP) model [283].

In a recent study by Serganova *et al*., two murine breast cancer cell lines and tumors (67NR and 4T1) were measured for FDG uptake and lactate accumulation with FDG-PET and MRSI, respectively [107]. There was no significant difference in FDG accumulation between the two tumors. However, 4T1 tumors (the more aggressive breast cancer of the two lines) showed significantly higher lactate accumulation earlier

after implantation than 67NR [107]. This is one demonstration of the importance of metabolically profiling tumors. Combining FDG-PET and lactate imaging (MRSI) has the potential to give a more complete picture of tumor metabolism *in vivo*, which can be used to tailor treatment options for patients. In the case of LABC, combining FDG-PET and lactate MRSI may help determine if LABC has the potential to utilize lactate, resulting in the lower lactate concentrations seen in this study.

In conclusion, this study defined the expectations of the range of lactate concentrations and the spatial distribution of lactate in LABC biopsies. A more rigorous study in a larger sample set is needed to determine the value an implications of lactate accumulation or utilization in LABC.

4. Lactate uptake and catabolism occurs *in vitro* in cancer cells and normal cells

4.1 Introduction

In order for lactate to be metabolized, it must first enter the cell though membrane-bound, proton-coupled MCTs (see Section 1.3). Once inside a mammalian cell, lactate can participate in a finite but impressive number of biochemical pathways (Figure 7). Each of these pathways requires that lactate is converted to pyruvate first. Lactate shuttles exist between organ systems and include one of the most well-known routes of lactate metabolism: the Cori Cycle. Section 1.2 gives an overview of lactate metabolism in the body. However, the Cori Cycle and gluconeogenesis are not available pathways in a tumor. The most straight-forward pathways available in tumor metabolism in which lactate may participate are: (glutamate generation) lactate $\rightleftharpoons$ pyruvate $\rightarrow\rightarrow$ TCA cycle partial completion $\rightarrow$ α –ketoglutarate $\rightarrow$ glutamate and 2. (alanine generation) lactate $\rightleftharpoons$ pyruvate + glutamate $\rightleftharpoons$ alanine + α-ketoglutarate (Figure 8).

Modified and cropped from wikipedia.org

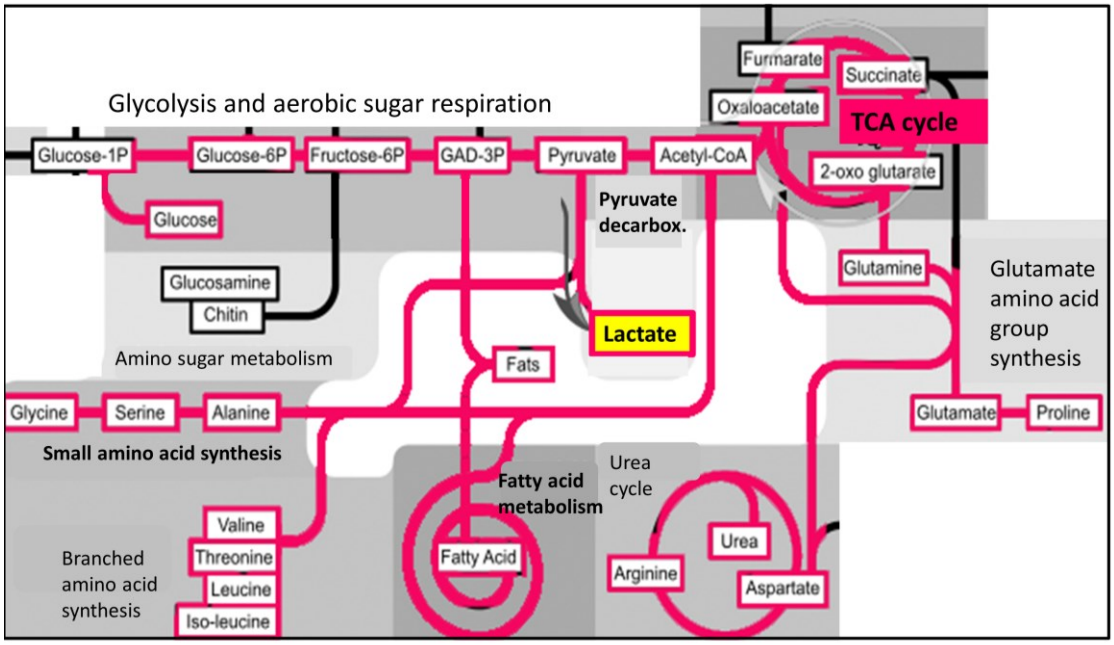

Figure 7: Metabolic pathways in which lactate (yellow) participates are marked in pink.

A useful tool for detecting metabolites and determining their structure is nuclear magnetic resonance (NMR) spectroscopy, which takes advantage of the magnetic properties of atomic nuclei. Electromagnetic radiation is absorbed by nuclei (e.g., ^{1}H or ^{13}C) when placed in a magnetic field. The chemical shift refers to the resonant frequency of a nucleus relative to a standard. The position (ppm), number and shape of the chemical shifts are indicative to the structure of a particular molecule. These characteristics can be interrogated experimentally by "spiking" a solution with a known molecule of interest to reliably describe that molecule. An important aspect of the nuclei

that allows obtainment of chemical shifts is the spin. Both ^{1}H and ^{13}C have a spin of ½, while ^{12}C has a spin of 0, meaning ^{12}C is NMR inactive and cannot be evaluated by NMR spectroscopy. Evaluation of many organic molecules will require labeling with an NMR active isotope, such as ^{13}C (^{13}C 1.1% natural occurrence [284]), for increased clarity and detection.

NMR spectroscopy is often employed for metabolic studies. Lactate accumulation in MCF7 cells and xenografts has been previously assessed via NMR techniques [285]. These studies found that multi-drug resistant MCF7 cells had increased lactate accumulation compared to WT MCF7 cells. Additionally, NMR studies showed that breast tumor tissue had higher levels of lactate, succinate and phosphocholine compared to normal breast tissue [286]. However, lactate uptake (as opposed to production) in breast cancer cells has not been studied previously by NMR spectroscopy. As summarized in Section 1.2.2, NMR studies have been employed to measure lactate uptake and metabolism in hepatomas *in vivo* [272, 273] and gliomas *in vitro* [30, 31, 147]. These studies found that common metabolites generated from labeled lactate were alanine and glutamate. These results can be explained by the biochemical pathways available to lactate (Figure 7, Figure 8). However, lactate metabolism can converge with glutamine metabolism, either as a product of glutaminolysis or, theoretically, as a substrate for glutamine synthesis [287-289]. This will be discussed at more length in Section 4.3.

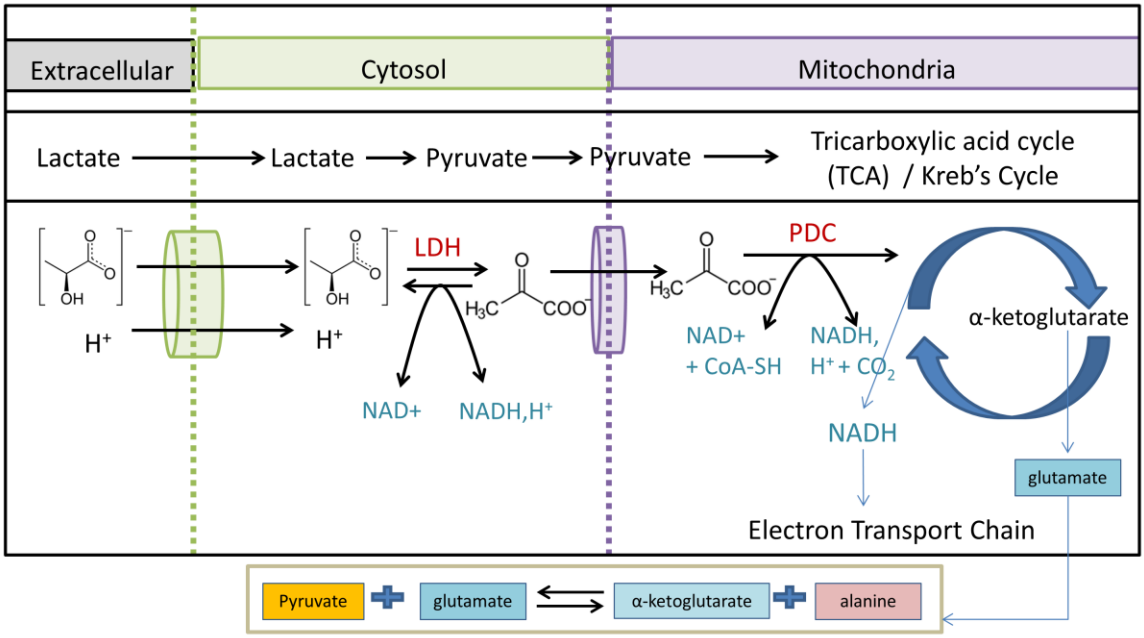

Figure 8: Lactate uptake and intracellular metabolism. Lactate enters the cell through a MCT (green cylinder) and is converted to pyruvate before being transported into the mitochondria via the MPC (purple cylinder). Pyruvate can complete oxidative phosphorylation or generate glutamate from α-ketoglutarate after partial completion of the Kreb's Cycle. Alanine can be generated from the reversible reaction of pyruvate + glutamate → α-ketoglutarate + alanine.

We sought to characterize lactate metabolism in cancer and normal cells, focusing mostly on breast cell lines. The important questions we intended to answer were: 1. Do cancer cells and normal cells take up lactate? 2. What metabolites are generated from lactate uptake? 3. Are there differences in lactate uptake or metabolism in cancer cells vs. normal cells? 4. Does treatment with CHC effectively block lactate uptake and/or export?

Our expectations for lactate metabolism varied dependent upon the cell type in question. We hypothesized that both normal liver and liver cancer cell lines would take up and metabolize lactate. For breast cell lines, we hypothesized MDA-MB-231 cells would not take up or metabolize much because it lacked MCT1 expression. We hypothesized some lactate metabolism in both MCF7 cells and normal breast cells but hypothesized that the relative rates of lactate metabolism or metabolites generated would be different. We anticipated that treatment with CHC would prevent lactate uptake in these cell lines.

4.2 Results

4.2.1 MCT1 expression in breast cell lines

Before investigating lactate uptake, we first tested the expression of monocarboxylate transporter 1 (MCT1). Western blot analysis of total MCT1 protein expression was conducted on breast cell lines (HMEC, MCF7, and MDA-MB-231). MCT1 protein was detected in all cell lines tested except MDA-MB-231 cells (Figure 9), in agreement with previous reports [203]. In a manuscript currently in press [290], we showed that R3230Ac tumor tissue contained MCT1 protein. We did not seek to confirm the expression of MCT subtypes in breast lines since this had been previously reported by another group [291]. Briefly, it was found that HMEC and MCF7 but not MDA-MB-231 cells expressed MCT1 on the plasma membrane, and MCT4 and MCT2 were localized to the mitochondrial membrane as well as showing expression on the plasma

membrane of all cell lines tested [291]. Section 6.2 includes immunofluorescent images of MCT1 and MCT4 membrane expression on cells grown on coverslips.

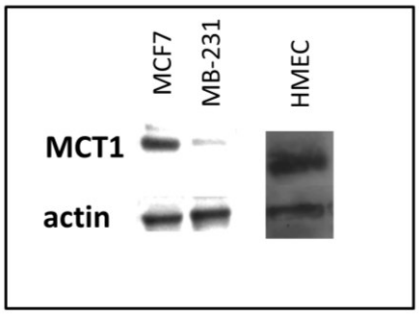

Figure 9: Representative Western blot showing MCT1 expression in total protein samples from MCF7, MDA-MB-231 and HMEC cells. MCF7 and HMEC show MCT1 expression, but MDA-MB-231 showed very little to no MCT1 expression.

4.2.2 Preliminary lactate consumption experiments *in vitro* show greater lactate uptake in MCF7 cells compared to MDA-MB-231

Prior to utilizing NMR technology to measure lactate uptake, we used a commercially available device called the Lactate Pro™ meter that was designed to measure blood lactate levels of human patients to measure lactate in cell media. The accuracy of the meter for measuring lactate in media samples was validated using standards of known lactate concentrations (SEM: ±0.38mM). Cells were treated with 20mM of sodium lactate. This was supplemented in glucose-free DMEM for 5 days. Cells were counted on Day 0 and Day 5. Lactate measurements were taken from the cell

media at 0, 1, 2, 4, 8, 12 and 24 hr and subsequent days (2-5). A media control (a cell culture dish without any cells) was included.

Results were evaluated by assessing relative rates of lactate uptake in two ways: 1. Employing a linear regression model, which did not account for cell numbers, and 2. Comparing an estimated lactate consumption "rate" of each cell line by dividing the total lactate consumed over the 5-day period by the final cell count on the last day. A significant batch effect was controlled for in the model. Scatterplots display the raw measurements from each cell line (Figure 10). Visually, it is apparent that the lactate in the media of MCF7 cells drops at a faster rate (steeper slope) than the lactate in the media of MDA-MB-231 cells (Figure 10). The model found significant interaction terms between time and cell line ($p<0.0001$), indicating different relative rates of lactate consumption for MCF7 (rate coefficient = 4.0092) and MDA-MB-231 cells (rate coefficient = 0.7088).

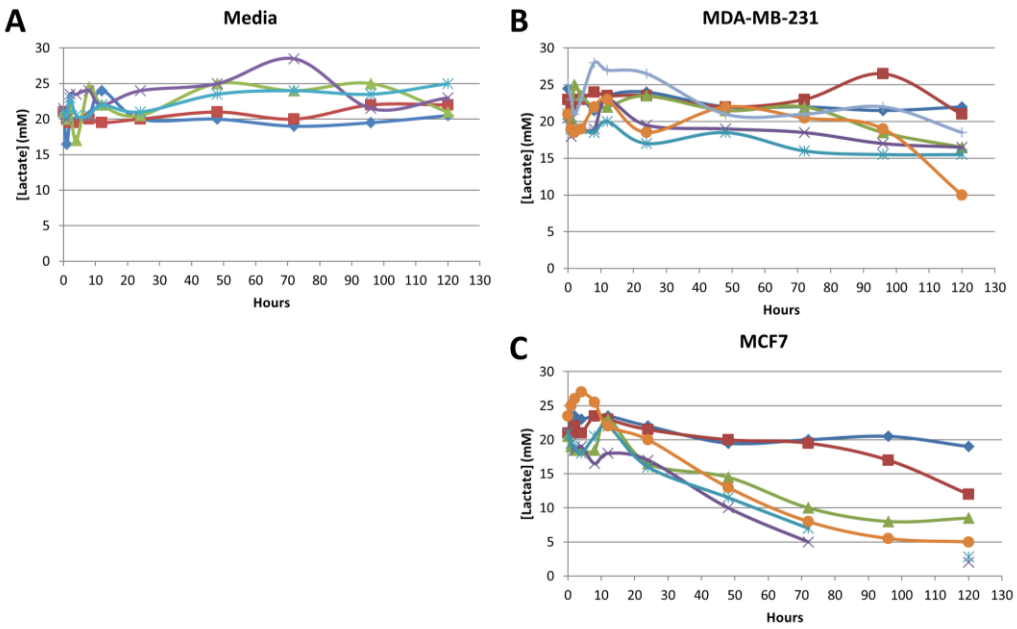

Figure 10: Lactate concentration measurements over five days showed a greater decline in the cell media of MCF7 cells than in the cell media of MDA-MB-231 cells. Lines in the plots represent individual experiments. Samples were taken from cell media of a cell-free plate (Media, A), MDA-MB-231 (B) and MCF7 cells (C) over a period of 5 days (n=5). Rate coefficients of lactate consumption as determined by a linear regression model are significantly different for MCF7 compared to MDA-MB-231 cells.

Though the linear regression results were promising, this model did not account for cell number because cell counts were only conducted at two time points. For this reason, we evaluated the total decrease in the lactate from Day 0 to Day 5. The media control showed a small variation in measurements as expected (Figure 11). The media from MCF7 cells showed a significantly greater mean decrease (18.3mM) in lactate than MDA-MB-231 cells (5.5mM, p=0.0006, Figure 11). When normalized to the final cell number at Day 5, the results recapitulated the results of the linear regression model:

MCF7 cells showed a significantly higher relative rate ($2.4x10^{-5}$ mM lactate / cell) of lactate consumption compared with MDA-MB-231 cells ($4.4x10^{-6}$ mM lactate / cell, $p<0.05$, Student's T-test, Figure 11). Thus MCF7 cells take up lactate more readily and at a higher rate than MDA-MB-231 cells. This was expected because MCT1 expression is minimal to absent in MDA-MB-231 cells [203] (Figure 9).

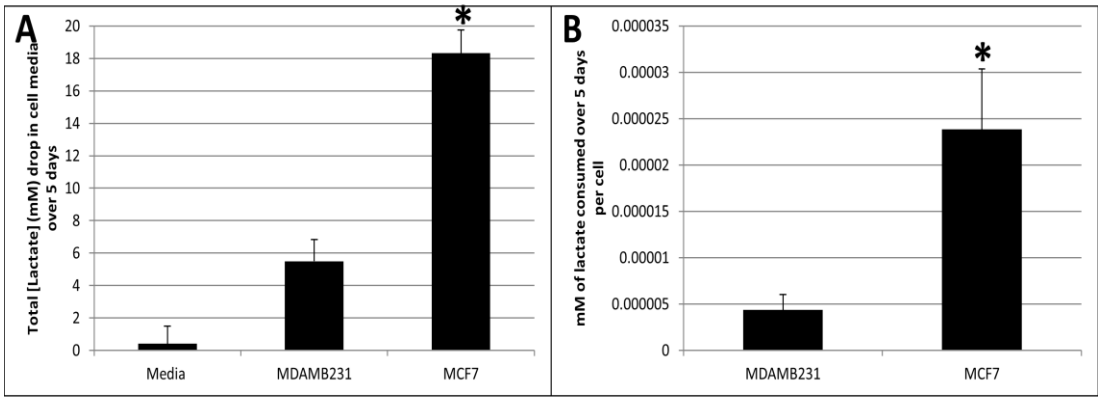

Figure 11: MCF7 cells show a significantly different relative rate of lactate consumption compared to MDA-MB-231 cells. Total drop in lactate concentration (mM) in the cell media of MCF7 and MDA-MB-231 cells after 5 days of 20mM lactate exposure. Mean lactate concentration decrease in the media of MCF7 cells was 18.3mM, significantly greater than the mean decrease in lactate concentration in the media of MDA-MB-231 cells (5.5mM, *$p = 0.0006$, $n = 5$) (A). Relative rates of lactate consumption for breast cancer cell lines reported as mM of lactate consumed per cell show significantly more lactate is consumed by MCF7 cells compared to MDA-MB-231 cells (*$p < 0.05$, $n = 5$) (B).

4.2.3 ^{13}C NMR *in vitro*

We next sought to determine the fate of lactate following uptake. To do this, we investigated lactate-generated metabolites with 13C NMR. The cell lines used in these studies included different cancer types as well as several normal cell lines (Table 11).

Table 11: Cell lines used for *in vitro* ^{13}C-lactate metabolism experiments

Cell line name	Description
BJ	Human newborn foreskin, fibroblast
CCD 1112Sk	Human normal foreskin, fibroblast
HepG2	Human hepatocellular carcinoma
HMEC	Human mammary epithelial cells, primary
HUVEC	Human umbilical vein endothelial cells
MCF-7	Human mammary adenocarcinoma, ER+ PR+
MDA-MB-231	Human mammary adenocarcinoma, triple -, metastatic
MEF	Mouse embryonic fibroblasts
SNU-182	Human hepatocellular carcinoma
WRL-68	Human normal liver, embryonic source (some sources state a HeLa contaminant)
R3230Ac	Rat mammary carcinoma

Before collecting and analyzing cell samples, we made standards of known ^{13}C-labeled metabolites in order to identify the corresponding peaks on ^{1}H and/or ^{13}C spectra. Included in these controls were lactate, pyruvate, alanine and glutamate (Figure 12). This was used as a reference to identify anticipated metabolites to be generated from labeled lactate. We expected that lactate would be taken up by most cell lines; however, we anticipated that normal cells and cancer cells would metabolize lactate differently, with either different metabolic end products or different relative rates or amount of lactate conversion.

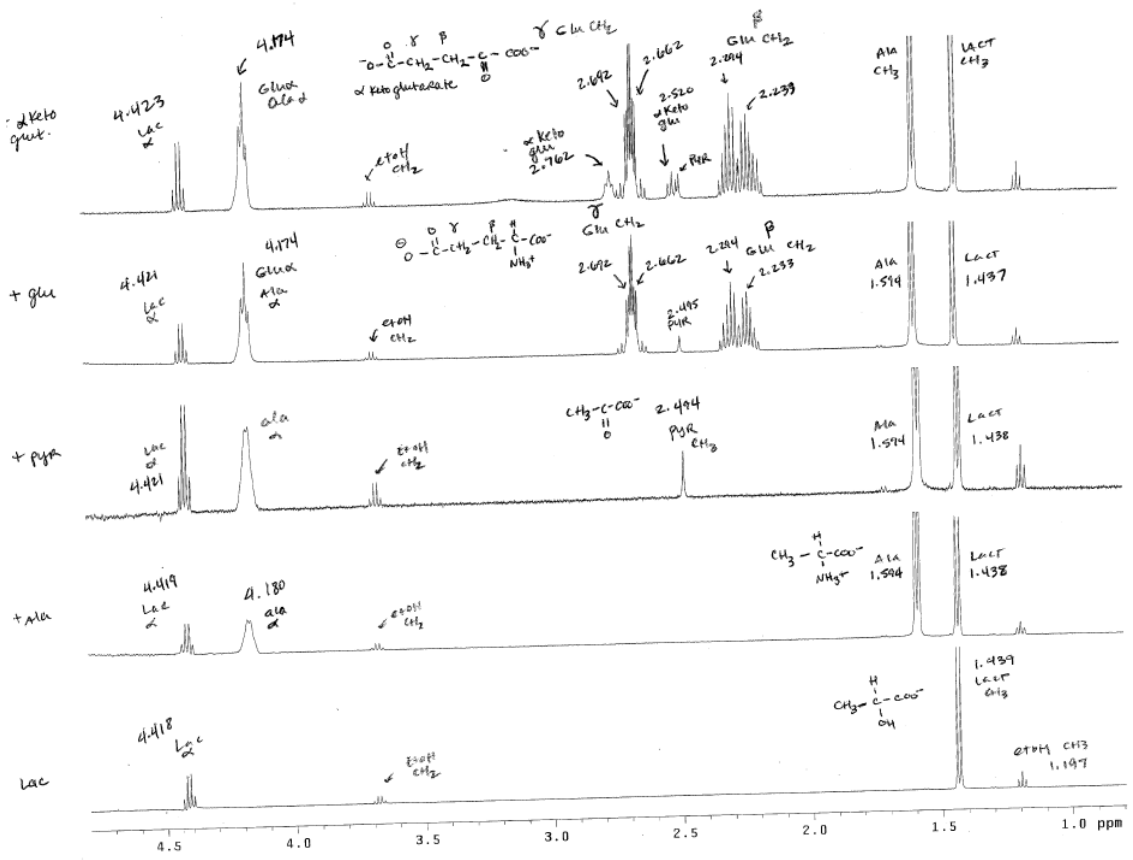

Figure 12: ^{1}H NMR plots of known metabolites to acquire chemical shifts. Starting from the bottom, the spiked metabolites are lactate, alanine, pyruvate, glutamate, and α-ketoglutarate.

One dimensional ("1D") plots consist of the ^{1}H or ^{13}C spectra alone, with the position of the chemical shifts in ppm indicated on the bottom scale. Peak height corresponds to the relative amount of a metabolite. Heteronuclear multiple quantum correlation (HMQC) acquisition generates "2D plots" of the metabolites, with the proton spectrum as the vertical scale and the carbon spectrum as the horizontal scale. The metabolite peaks are represented as a series of concentric circles that intersect at the

corresponding ^{1}H and ^{13}C chemical shifts. Reading 2D plots is much like reading mathematical coordinates on a coordinate plane. A useful analogy to keep in mind when reading peaks on NMR plots is the visualization of mountains: 1D plots are like visualizing mountains (i.e. peaks) from the side (as if viewing on land) while 2D plots are like visualizing mountains from the top (as if viewing from a helicopter). While peak height in the 1D plot corresponds to the relative amount of a metabolite, the amount of concentric circles in the 2D plot corresponds to the amount of the metabolite with each circle being roughly equivalent to an exponential increase in the metabolite.

Using NMR is especially powerful at identifying metabolites due to the information it provides about chemical shift and molecule structure. However, quantifying exact metabolite concentrations requires additional analysis. By comparing metabolite peak heights to internal standards, it is possible to derive relative metabolite amounts, which can be reported as fold increases or decreases in metabolites.

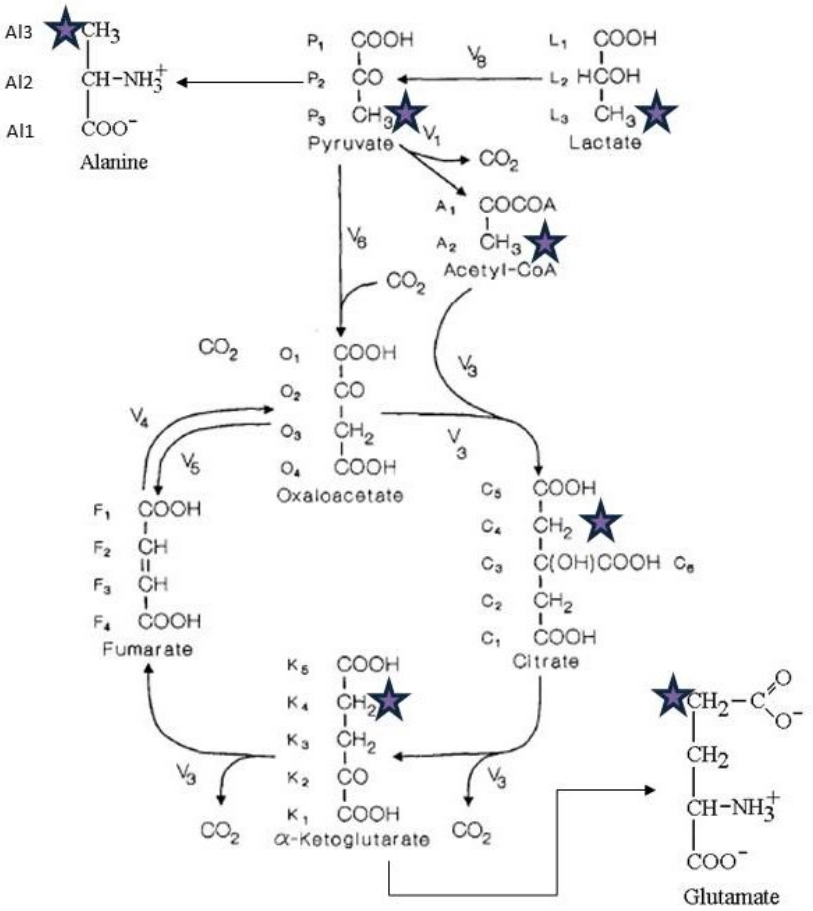

Figure 13: Biochemical pathways of labeled lactate generate labeled metabolites. A ^{13}C enrichment label is represented by the stars. 3-^{13}C-lactate can generate 3-^{13}C-pyruvate, 3-^{13}C-alanine, 4-^{13}C-citrate, 4-^{13}C-α-ketoglutarate and 4-^{13}C-glutamate. Modified with permission from [292].

Identification of metabolites by peak ppm shifts was determined by control spectra that included known metabolite spikes (Figure 12) or from the available literature [293]. The pathway from 3-^{13}C-lactate to labeled metabolite generation through anticipated biochemical pathways was modified from Di Donato *et al*. [292] (Figure 13).

Table 12 outlines the approximate anticipated location of each metabolite peak on the decoupled 2D $^{1}H/^{13}C$ spectrum. These reference ranges are liable to shift in different solutions; these differences will be addressed throughout the dissertation when relevant.

Table 12: Chemical shifts for anticipated metabolites generated from 3-^{13}C-lactate

Metabolite	^{1}H	^{13}C
Methyl-lactate 3C	1.4	19
2C lactate	4.4	52
Methyl-pyruvate 3C	2.5	27-28 [293]
2C pyruvate	unknown	206 [294]
Methyl-alanine 3C	1.6	17
2C alanine	4.2	unknown
4C glutamate	2.7	32-34 [30]
3C glutamate	2.3	27-28
2C glutamate	4.2	53
α-ketoglutarate	2.5	unknown
α-ketoglutarate	2.7	unknown

4.2.3.1 All cell lines tested take up ^{13}C-lactate

Cells were exposed to 10mM 3-^{13}C -L-lactate for different time periods in the context of available glucose or glucose deprivation (indicated by +G or –G in Figures). After exposure, cell media and cell extract was collected for NMR spectroscopy analysis. We acquired ^{1}H and ^{13}C spectra and generated 2D plots from HMQC acquisition. For a majority of the HMQC results, generally using a decoupler. ^{13}C-methyl-lactate peaks ("L") resonated at ~1.3 and 1.5 ppm (coupled) in the ^{1}H spectra and at ~19 ppm in the ^{13}C

spectra (decoupled). Unless otherwise specified, all plots shown are derived from cell extracts of cells exposed to 10mM lactate.

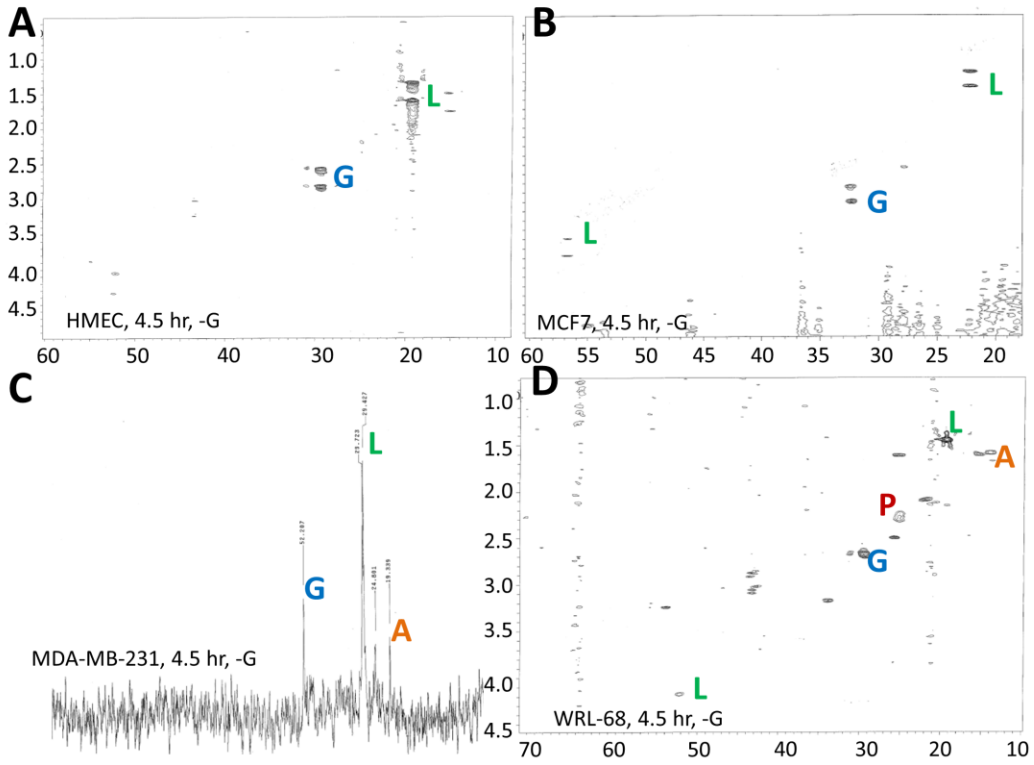

Figure 14: HMQC and ^{13}C NMR plots of metabolites generated from labeled lactate. HMQC (A, B, D) or ^{13}C (C) NMR plots of cell extracts treated for 4.5 hr with 10mM ^{13}C-lactate showing ^{13}C-lactate (L) uptake and ^{13}C-glutamate (G), ^{13}C-alanine (A), and ^{13}C-pyruvate (P) generation in HMEC (A), MCF7 (B), MDA-MB-231 (C) and WRL-68 cells (D)

All cell lines tested took up some lactate, indicated by the labeled peaks (^{1}H and/or ^{13}C plots) or concentric circles (2D plots) present in the cell extracts after 4.5 hr (Figure 14, Figure 15) or 24 hr (Figure 16). Simply by visual comparison, it is evident that some cell lines (MCF7, MDA-MB-231, HepG2, WRL-68, Figure 14, Figure 16) showed

larger lactate peaks (or circles) in the plots of cell extract than other cell lines (SNU-182, CCD1112sk, Figure 15). This could indicate a number of possibilities, including that the former cells lines took up relatively more lactate than the latter ones or that the former cell lines metabolized lactate (and excreted metabolites from lactate) more slowly than the latter ones. All of the cell lines tested took up lactate regardless of cell lineage or type.

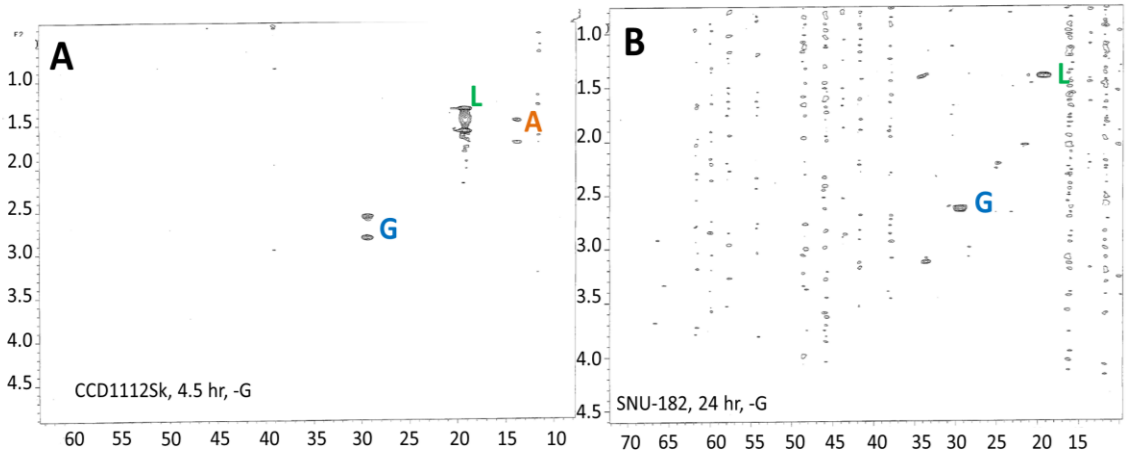

Figure 15: HMQC NMR plots of cell extracts of CCD1112Sk and SNU-182 cells. CCD1112sk (A) and SNU-182 (B) cells treated for 4.5 hr (A) or 24 hr (B) with 10mM ^{13}C-lactate showing ^{13}C-lactate (L) uptake and ^{13}C-glutamate (G), and ^{13}C-alanine (A) generation

4.2.3.2 Most cell lines show common lactate-derived metabolites

In addition to taking up lactate, all cell lines tested show evidence of ^{13}C-labeled glutamate ("G", Figure 14, Figure 15, and Figure 16), indicating that the labeled lactate partially completed the TCA cycle. The labeled glutamate is present in all breast cell

lines as early as 4.5 hr (Figure 14) and remains there after 24 hr (Figure 16). After 4.5 hr, MDA-MB-231 cells and WRl-68 cells showed evidence of labeled alanine ("A", Figure 14) as well.

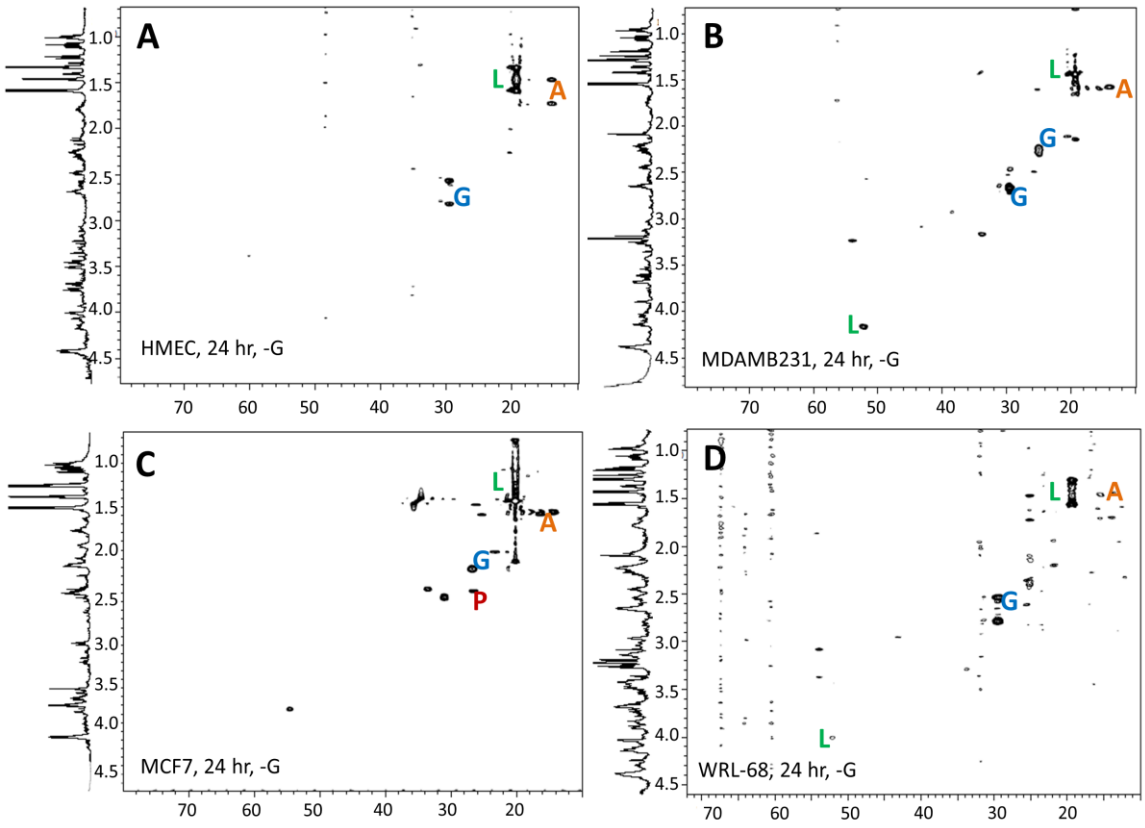

Figure 16: HMQC NMR plots of cell extracts of HMEC, MDA-MB-231, MCF7 and WRL-68 cells. Each cell line was treated for 24 hr with 10mM ^{13}C-lactate. Cell extracts revealed ^{13}C-lactate (L) uptake and ^{13}C-glutamate (G), ^{13}C-alanine (A), and ^{13}C-pyruvate (P) generation in HMEC (A), MDA-MB-231 (B), MCF7 (C) and WRL-68 cells (D)

After 24 hr exposure to 10mM ^{13}C-lactate in glucose-deprived conditions, all three human breast cell lines tested (normal and cancer) and WRL-68 cells displayed peaks corresponding to lactate (methyl group, ~1.4, 19 ppm, "L") (Figure 16). This

uptake occurred even in MDA-MB-231 cells, which do not express MCT1 (Figure 9), but do express MCT4 and MCT2 [142, 291], suggesting that other MCT subtypes are likely responsible for lactate uptake. Each breast line also showed evidence of lactate metabolism to labeled alanine (1.6, 17 ppm, "A") and glutamate (2.7, 32 ppm, "G" and 2.3, 27-28 ppm, "G"). From this, we can deduce that ^{13}C-lactate has been taken up and progressed at least partially through the TCA cycle, generating glutamate from α-ketoglutarate. Furthermore, some of the labeled glutamate and/or pyruvate was converted to form labeled alanine in the breast cell lines. WRL-68 cells showed evidence of labeled lactate and glutamate after 24 hr exposure (Figure 16), but the alanine peak seen at 4.5 hr is barely present (Figure 14), suggesting that either the conversion to alanine is relatively inefficient in this line or that the labeled alanine was converted to some other downstream metabolites that are not detectable with this method.

To confirm that the metabolite peaks were the same for each breast cell line, the 2D spectra were plotted on the same scale and the images were overlaid in Photoshop. As seen in Figure 17, though there are relative size differences in the peaks, lactate, alanine and glutamate peaks overlap in each cell line. Together this shows that lactate can be used as an oxidative substrate and that exogenous lactate is metabolically active in both breast cancer and normal breast epithelial cells. While the 2D spectrum of the HMEC cell extract is fairly sparse, MCF7 and MDA-MB-231 spectra from cell extract show some additional metabolite species (Figure 17).

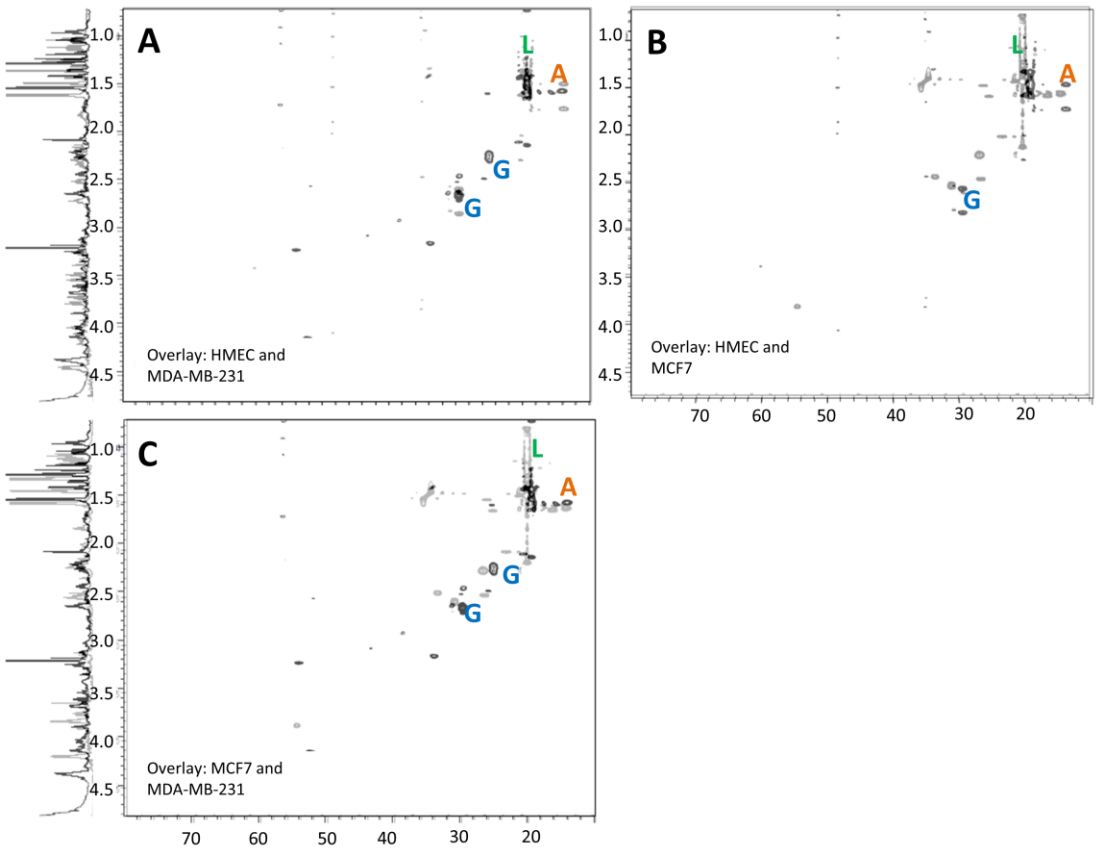

Figure 17: Overlaid HMQC NMR plots of breast cell extracts. HMQC NMR plots from breast cells treated for 24 hr with 10mM ^{13}C-lactate were overlaid to identify common metabolites generated from labeled lactate in HMEC and MDAMB231 cells (A), HMEC and MCF7 cells (B) and MDAMB231 and MCF7 cells (C).

4.2.3.3 HepG2 and MEF cells convert ^{13}C-lactate to produce a diverse metabolic profile

Of the cell lines tested, HepG2 and MEF cells show the most diverse ^{13}C-lactate-generated metabolic species. After an incubation period of 24 hr (no glucose) with ^{13}C-lactate, both cell lines show evidence of alanine, glutamate and pyruvate generation. Peaks corresponding to all the carbons of the labeled lactate and glutamate species are present (Figure 18). The large circles indicate relatively higher concentrations of each

metabolite than were seen in the other cell lines tested. For the breast cell lines, the peak corresponding to lactate is larger in the HMQC plots (Figure 16) than it is in HepG2 or MEF cells (Figure 18), indicating that HepG2 and MEF cells utilize more lactate than the breast cell lines. Furthermore, there are a number of unknown species that carry the 13C label in HepG2 and MEF cell extracts (Figure 18, "?"). Identification of these metabolites was attempted through literature searches, but these species have not been verified experimentally. The most likely candidates for the unknown species are: 1. α-ketoglutarate, 2. citrate, 3. other TCA cycle intermediates 4. glutamine and 5.acetate.

Because α-ketoglutarate is the precursor to glutamate, it is likely that α-ketoglutarate species will be seen in the cell extract. From our α-ketoglutarate spiking experiment (Figure 12), we know α-ketoglutarate peaks appear at 2.5 and 2.7 ppm in the 1H spectra (Table 12). These peaks overlap with pyruvate and glutamate peaks in the ^{1}H spectra. To confidently identify α-ketoglutarate in the HMQC plots, one would need to know the positions of the peaks in the ^{13}C spectra. Citrate and other TCA cycle intermediates may also be labeled due to the necessity of their formation prior to labeled glutamate generation. Glutamine is another possibility for the identity of the unknown peaks. Convergence of glutaminolysis /glutamine generation biochemical pathways and lactate metabolic pathways has been demonstrated [287-289]. Additionally, several studies have shown ^{13}C-glutamine generation in response to a ^{13}C-lactate treatment or infusion [30, 31]. Yet there is another possible metabolic species that may be present in

the HepG2 and MEF cell extracts: acetate. Both the HepG2 and MEF HMQC plots show numerous peaks around 23 ppm (^{13}C) and 2 ppm (^{1}H) (Figure 18). The peak for ^{13}C-acetate appears at 23 ppm in the ^{13}C spectra [295]. Spiking a solution with ^{13}C-acetate to acquire the 1H plot could validate the identification of these peaks as acetate.

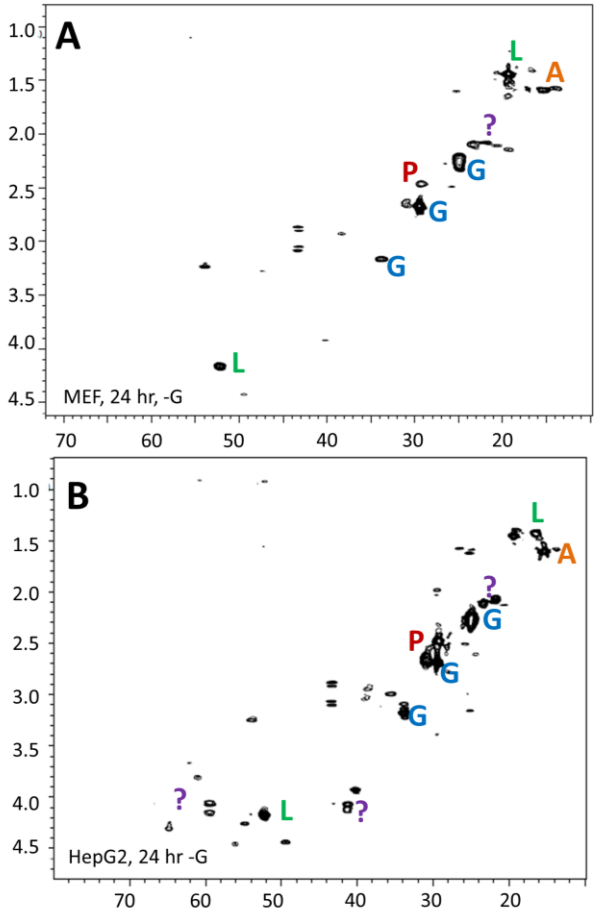

Figure 18: HMQC NMR plots of HepG2 and MEF cell extracts. After 24 hr treatment with 10mM lactate cell extracts showed ^{13}C-lactate (L) uptake and ^{13}C-glutamate (G), ^{13}C-alanine (A), ^{13}C-pyruvate (P) and unknown ^{13}C metabolite species generation in MEF (A) and HepG2 cells (B)

From visual comparisons of HMQC plots from all the cell lines tested, it is easy to recognize the differences in lactate uptake and utilization in cells of different tissue types and disease states. Because the majority of the NMR spectra are plotted on the same scale and have the same amount of D_2O in the sample, relative comparisons between metabolite levels can be made but molar concentrations cannot be derived from these data.

4.2.3.4 Cell lines transport lactate-generated metabolites out of the cell

After observing evidence of lactate uptake and catabolism in the cell extracts, the cell culture media was tested for labeled lactate and metabolites. If labeled metabolites were found in the media, this would indicate that these metabolites were transported out of the cell after formation from the labeled lactate. For each of these experiments, 40mM ^{13}C-lactate (no glucose) was added to cells for 24 hr. After that incubation period, cell media and cell extracts were collected.

In fact, breast cancer cell lines and normal cells (HUVEC) show lactate-generated metabolites in the cell media after 24 hr (Figure 19). The relative rates of lactate metabolism among the cell lines can be determined by comparing the relative peak heights in the ^{13}C spectra. Lactate peaks were observed in the cell extract of R3230Ac cells after 4 and 12 hr. After 24 hr, R3230Ac cells showed no lactate peaks in the cell extract, but the culture media showed the largest lactate ("3") and alanine ("4") peaks in the cells lines tested (Figure 19). Each of the other cell lines (MCF7, MDA-MB-231 and

HUVEC) showed lactate peaks in the cell extract at the same time point; however, there was still evidence of labeled metabolite extrusion into the media, as indicated by alanine ("4") and glutamate ("1,2") peaks in the media (Figure 19). This indicates that R3230 Ac cells take up and metabolize lactate (in the context of glucose deprivation) relatively faster than the human breast cancer cells or HUVEC cells (Figure 19). The spectra of media and cell extracts also indicate that some of the labeled lactate goes unutilized. This is possibly in accordance with previous studies showing futile lactate cycling through the plasma membrane of glioma cells [296]. Alternatively, with such a high extracellular lactate concentration, much of the lactate may not get taken up after 24 hr.

Finally, by comparing the metabolite generation of each cell line, it can be deduced which metabolic pathway of lactate catabolism is favored in each cell type. The labeled metabolite peaks in MDA-MB-231 cell extract and media are noticeably smaller than the other cell lines (Figure 19), suggesting that MDA-MB-231 utilize relatively lactate less than the other cell lines. This result confirms the lower relative lactate consumption rate of MDA-MB-231 cells compared to MCF7 cells, discussed in Section 4.2.2 (Figure 10).

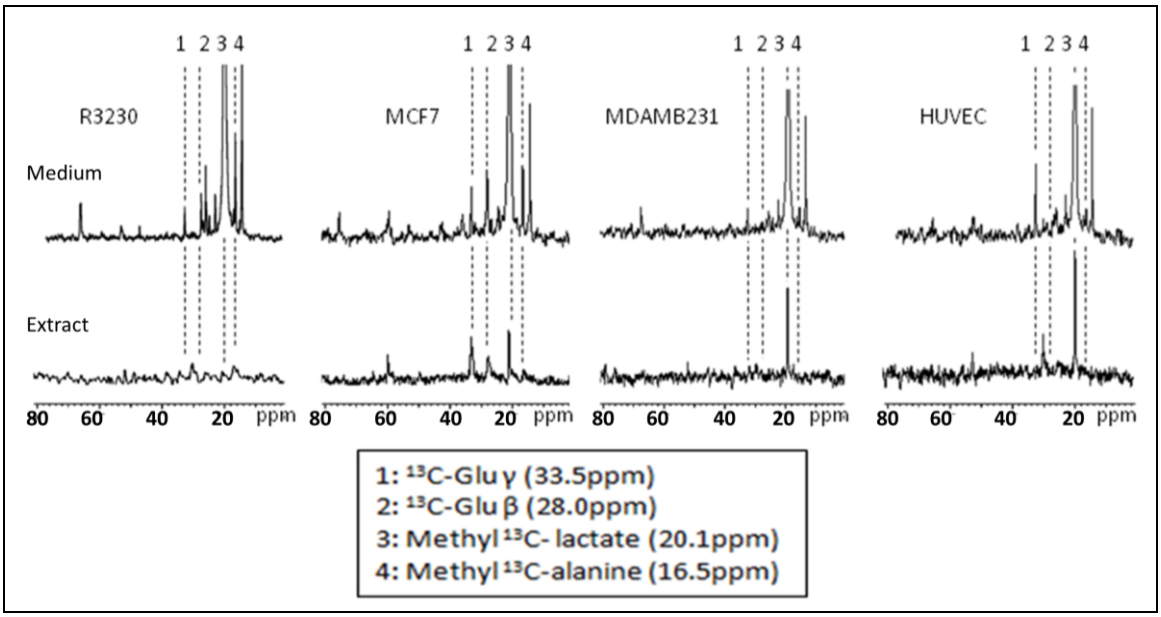

Figure 19: ^{13}C-labeled metabolites generated from lactate catabolism are transported out of the cell. Labeled metabolites (^{13}C-glutamate "1, 2", ^{13}C-lactate "3", and ^{13}C-alanine "4") were observed in the cell culture media after 24 hr incubation with ^{13}C-lactate. Each cell line shows different relative rates and amount of lactate utilization. Studies conducted in collaboration with and Figure made by Dr. Thies Schroeder.

4.2.4 CHC does not effectively inhibit lactate uptake in HUVEC cells but does inhibit uptake in R3230Ac rat mammary carcinoma for lactate concentrations ≤20mM

A majority of the metabolic experiments with MCT1 inhibition were conducted in R3230Ac cells, to match additional *in vivo* experiments described in a recent manuscript. HUVEC cells were also included as part of a collaborative project [297]. Two concentrations of CHC (0.1mM "low" and 5mm "high") were used for ^{13}C-lactate NMR experiments. The concentrations chosen were based on previous studies and the

available literature on other targets of CHC. Sonveaux *et al*. used a 5mM concentration of CHC in their studies [141, 297]; however, commentary from other experts criticized the use of such a high concentration [221]. It has been shown that ~1000-fold less drug is needed to inhibit the mitochondrial pyruvate carrier (MPC), thus potentially substantially influencing the metabolism of the cell regardless of MCT1 activity [136, 222, 223]. Figure 20 shows the expected biochemical pathways of ^{13}C-lactate metabolism with low and high CHC concentrations.

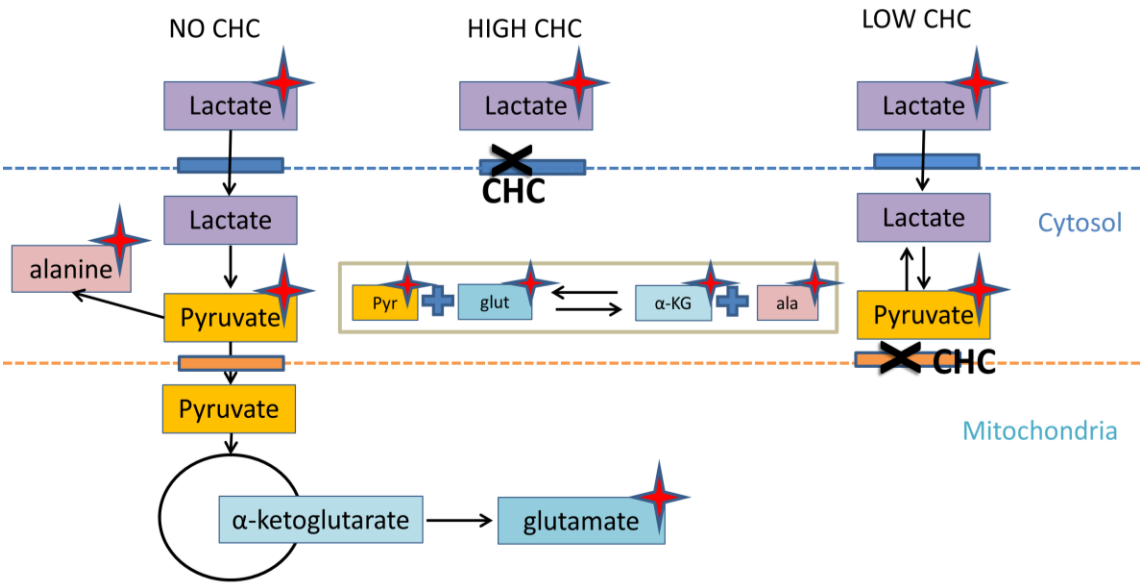

Figure 20: Expected ^{13}C-lactate metabolism with high (5mM) and low (0.1mM) CHC treatments. Labeled lactate metabolism in the absence of CHC will show generation of labeled alanine and glutamate. High CHC will prevent lactate uptake via MCT1-inhibition; low CHC will prevent lactate catabolism to alanine and glutamate via MPC-inhibition. Stars indicate ^{13}C enrichment.

To test whether CHC would prevent lactate uptake in a normal human cell line, HUVEC cells were treated for 6 hr with 5mM CHC and 10mM ^{13}C-lactate. Theoretically, 5mM of CHC should prevent lactate uptake via MCT1 inhibition. 1D ^{13}C plots show a ^{13}C-lactate peak despite CHC treatment (Figure 21). Thus, at least in HUVEC cells, lactate can still enter the cell even though CHC is present. This suggests other subtypes of MCTs that are or may be expressed in the cell transport lactate just as readily as MCT or that CHC is an ineffective MCT1 inhibitor. More detailed experiments on the CHC-MCT1 interaction are needed to describe the sensitivity and specificity of CHC for MCT1 inhibition.

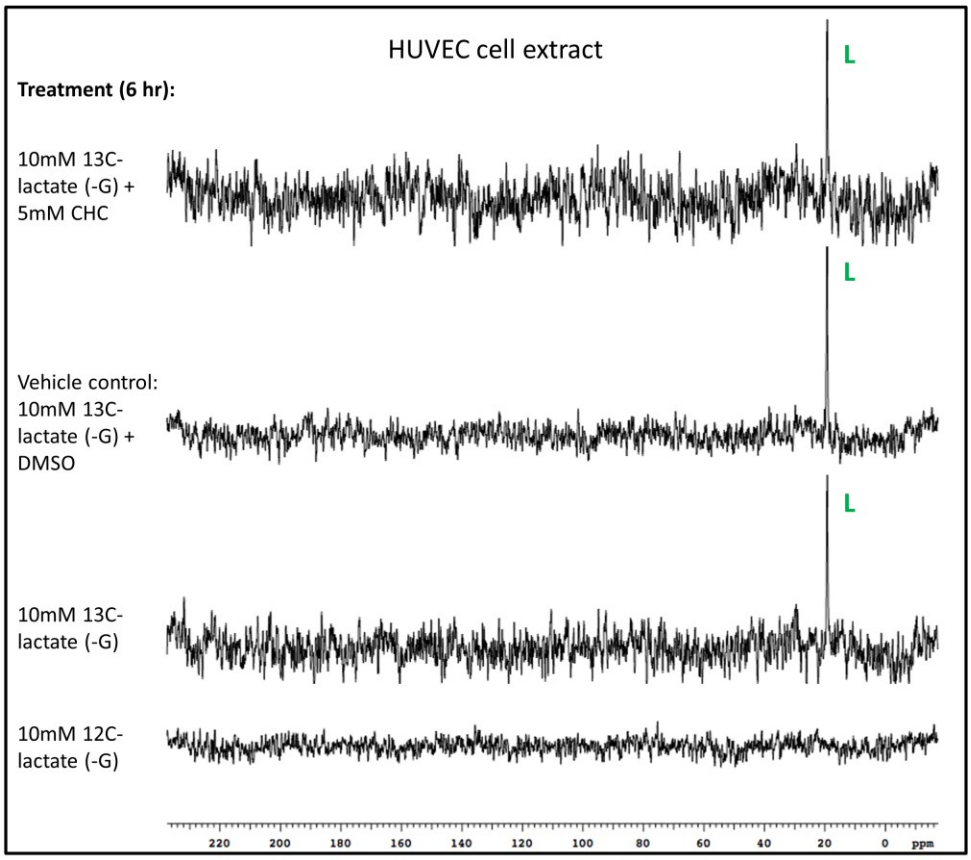

Figure 21: 5mM CHC does not prevent lactate uptake in HUVEC cells. 1D ^{13}C NMR plots of HUVEC cell extracts after 6 hr treatment with 10mM ^{12}C-lactate (bottom), 10mM ^{13}C-lactate (second from bottom), 10mM ^{13}C-lactate + DMSO (second from top), and 10mM ^{13}C-lactate + 5mM CHC (top). ^{13}C-lactate (L) is present in all 13C-lactate treatments despite the presence of CHC, a putative MCT1 inhibitor.

To test whether CHC would prevent lactate uptake in a breast cancer cell line, R3230 Ac cells were treated for 4 and 24 hr with 5mM CHC ("high CHC") and 0.1mM CHC ("low CHC") and 20mM ^{13}C-lactate. After both the 4 hr and 24 hr treatment period with 20mM ^{13}C-lactate and high or low CHC, no ^{13}C-lactate was found in the cell extracts (Figure 22). Endogenous lactate (likely formed from glutamine metabolism) was present

in the cell extracts of R3230Ac cells treated with high and low CHC after 4 hr and 24 hr. Endogenous alanine was formed from the endogenous lactate, as indicated by the peak at ~1.5 ppm after 24 hr. The fact that endogenous lactate remained in the cell extract may imply that the CHC is preventing some endogenous lactate from leaving the cell. Unfortunately, the presence of endogenous lactate formation can interfere with the detection of ^{13}C-metabolites, as the peaks corresponding to the metabolite structures may overlap.

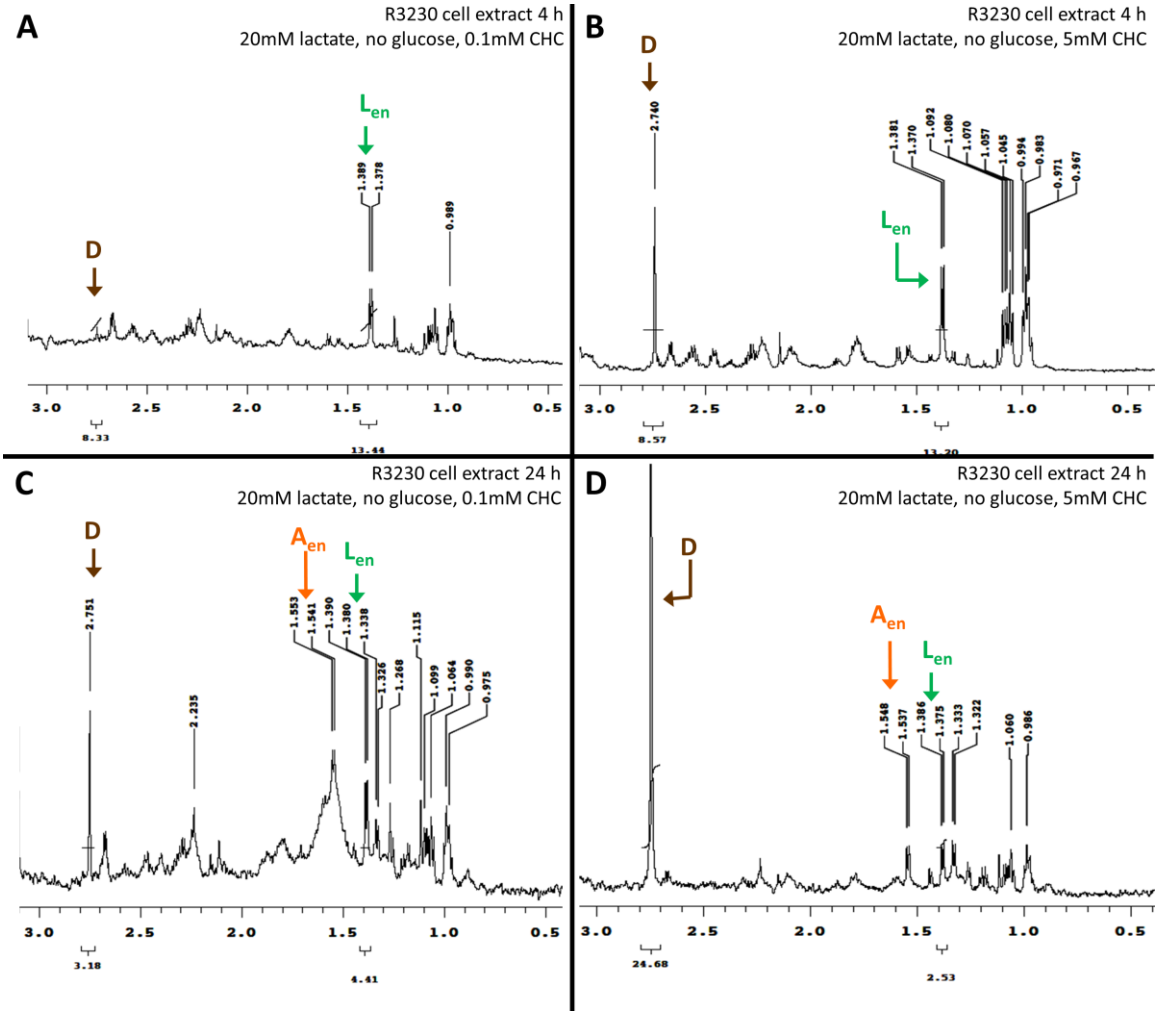

Figure 22: R3230Ac cells treated with 20mM ^{13}C-lactate + Low (0.1mM) or high (5mM) CHC treatment show no intracellular labeled metabolites in ^{1}H NMR spectra of the cell extract. Cell extracts from R3230 Ac cells treated for 4hrs (A&B) or 24hrs (C&D) with 0.1mM CHC (A&C) or 5mM CHC (B&D) and 20mM of ^{13}C-lactate. Metabolites in the cell extract included endogenous lactate (L_{en}) and endogenous alanine (A_{en}). DMSO is indicated by D.

When comparing the cell media from each experiment, ^{13}C-lactate was found in each condition at very similar relative concentrations, indicated by peak heights of the same size (Figure 23). CHC effectively prevented uptake of a majority of the exogenous

^{13}C- lactate at concentrations of 20mM (Figure 23). Endogenous lactate was also found in the cell media (Figure 23), implying that treatment with CHC does not completely prevent lactate transportation out of the cell.

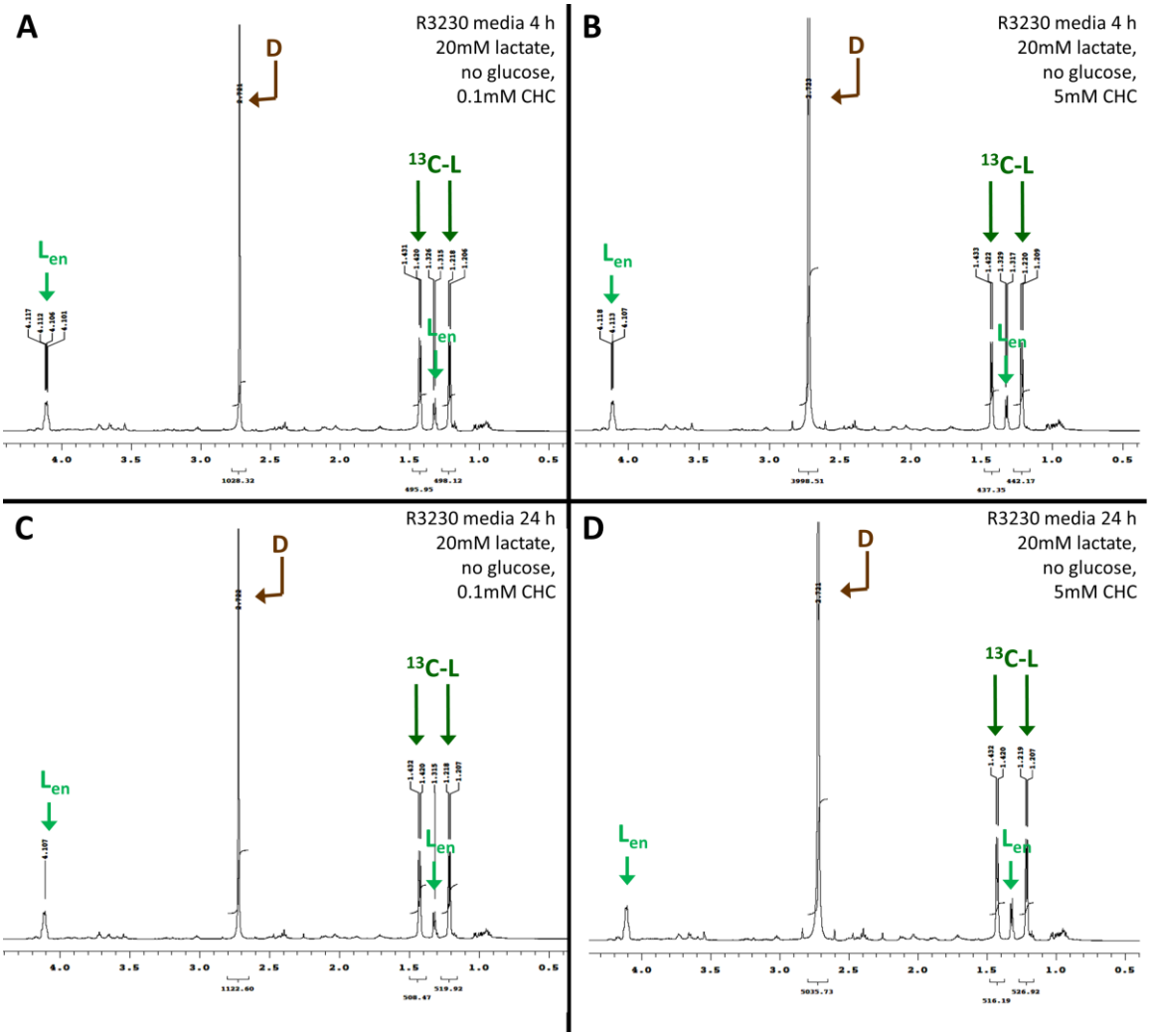

Figure 23: R3230Ac cells treated with 20mM ^{13}C-lactate + Low (0.1mM) or high (5mM) CHC treatment show abundant ^{13}C-lactate and endogenous lactate in the ^{1}H NMR spectra of the cell media. Cell media from R3230 Ac cells treated for 4hrs (A&B) or 24hrs (C&D) with 0.1mM CHC (A&C) or 5mM CHC (B&D) and 20mM of ^{13}C-lactate. Metabolites in the cell media included ^{13}C-lactate (^{13}C-L) and endogenous lactate (Len). DMSO is indicated by D.

4.3 Discussion

All cell lines tested showed some uptake of lactate and generation of alanine and/or glutamate. Based on these studies, lactate conversion appears to correlate with specific cell lines rather than tissue of origin. HepG2 and MEF cells showed the greatest utilization of lactate and most diverse metabolic species formed from the exogenous labeled lactate. Interestingly, both MEF cells and HepG2 cells share the phenotypic attributes of high motility and migration that are associated with invasive potential [298, 299]. Following this thought, there are three important facts to note: 1. MEF cells are from an embryonic source [300], 2. Embryonic cells are almost synonymous with "stem cells," [301] and 3. A highly migratory phenotype is characteristic of stem cells and CSCs [302, 303]. A 2011 study that interrogated the transcriptional response to exogenous sodium lactate (10mM) in MCF7 cells showed that the "lactate-specific gene profile was most similar to neural stem cells…" but the "genes commonly upregulated by both lactate and ketones were most similar to embryonic stem cells."[247] This same study also showed that exogenous lactate significantly increased embryonic stem cell colony formation and colony size in culture. This suggests that if cancer cells acquire stem-like characteristics, they may be more likely to metabolize lactate. Conversely, these data also suggest that characterizing a tumor's lactate metabolism may help to identify more stem-like or metastatic-prone tumors. Experiments investigating lactate induction of EMT markers are presented in Appendix E.

A portion of my NMR results are included in a recent manuscript [290]. The next three paragraphs will be devoted to summarizing the findings of this study, as it directly relates to the NMR results in my individual exploration and provides more information and context on our findings of the role of lactate in tumor metabolism. This joint study included work by Dr. Thies Schroeder, Dr. Rachel Richardson and Dr. Hong Yuan to assess lactate uptake and metabolism in rat mammary carcinoma R3230 Ac *in vitro* and *in vivo*.

To summarize our results with ^{13}C-lactate NMR, we found that *in vitro*, R3230 cells take up lactate in a concentration-dependent manner after 4 hr of treatment [290]. Lactate metabolism in R3230 Ac cells produced the same metabolites (alanine and glutamate) seen in the cell lines tested in my studies, previous reports [31, 32, 147] and *in vivo* experiments previously published [272, 273]. Similar to the results seen in the breast and liver cell lines, there was evidence of generation of these metabolites as early as 4 hr after lactate addition. The ^{13}C NMR time course conducted in R3230 Ac cells showed lactate metabolism over a 24 hr period, with the lactate peak diminishing in the cell extract samples and metabolite peaks increasing during this time course. By 24 hr, there was no evidence of lactate in the cell extract; the metabolite peaks were small in the cell extract but large in the cell media. This indicated that lactate was metabolized and alanine and glutamate were excreted to the cell media [290].

Lactate uptake *in vivo* was investigated, and kinetics of glucose and lactate uptake, retention, and clearance were measured using a novel scintillation probe following i.v. administration of either ^{14}C-glucose or ^{14}C-lactate. A pharmacokinetic model was formed from the data to determine rate constants for glucose and lactate uptake by the tumor and SQ tissue. Methods for these experiments are provided in the 2013 publication. The results from this animal model are summarized briefly. For the plasma curves, lactate was cleared much faster compared to glucose. The rate constant for the transfer of lactate from blood compartment into the tumor was much higher than glucose (0.238 vs. 0.038), indicating much faster uptake of lactate than glucose, which was also consistent with the plasma curves [290].

Taken together, the kinetic results clearly showed: 1. lactate uptake occurred in a rat mammary carcinoma *in vivo*; 2. Lactate uptake was faster in tumor tissue than subcutaneous tissue; and 3. Tumor tissue took up lactate faster than it took up glucose. Previous studies have shown that lactate uptake occurs in hepatoma [273] and sarcoma [272], and that lactate acts as preferred substrate in gliomas [31, 147].

For lactate to act as an energetic substrate, it needs to be converted to pyruvate, enter the mitochondria and go through oxidative phosphorylation. Through use of labeled lactate, it has been previously found that lactate completes the course of oxidative phosphorylation, as shown by generation of labeled CO_2 [273, 304]. Labeled

CO2 production was not measured in this study; however, there was a strong indication of the use of labeled lactate as a substrate to enter the TCA cycle: the appearance of labeled glutamate in the cell extracts and media of all cell lines tested. The most straight-forward pathway for ^{13}C-glutamate formation is: ^{13}C-L-lactate $\rightleftharpoons$ ^{13}C-pyruvate $\rightarrow\rightarrow$ TCA cycle partial completion $\rightarrow$ ^{13}C- α –ketoglutarate $\rightarrow$ ^{13}C-glutamate. We also identified alanine peaks after adminstration of ^{13}C-L-lactate. Labeled alanine formation occurs through: ^{13}C-L-lactate $\rightleftharpoons$ ^{13}C-pyruvate + glutamate $\rightleftharpoons$ ^{13}C-alanine + α-ketoglutarate. Alanine and glutamate (whether labeled or endogenous) can participate in the reaction catalyzed by alanine aminotransferase (α -ketoglutarate + alanine $\rightleftharpoons$glutamate + pyruvate). While this seems to only shift the balance of lactate catabolites, this reaction may serve to temporarily alleviate nitrogen stress in the cell by transferring it to glutamate.

It is also important to mention the convergence of lactate metabolism and glutamine metabolism. For all of our experiments, glutamine was included in the cell culture media. Glutamine is a major source of energy for some cancer cell lines, like HeLa [288]. Previous studies have shown that up to 13% of glutamine is converted to lactate *in vitro* in human fibroblasts [289]. Other metabolites generated from glutamine included glutamate, citrate, pyruvate, malate and aspartate; the relative amount of generation each metabolite was dependent upon cell confluency [289]. Because glutamine can be converted to lactate, the results of our lactate assays may not

accurately reflect the total amount of lactate that is converted in cells. Exogenous lactate has been shown to be metabolized in C6 glioma cells in the presence of glucose and glycolytically-derived lactate *in vitro* [30, 31]; therefore; it is reasonable to assume that glutamine-derived lactate can also be metabolized. Relatively little literature covering lactate conversion to glutamine is available. It is undetermined if ^{13}C-glutamine could be produced from ^{13}C-lactate, but this can be investigated experimentally with ^{13}C NMR.

Therapeutically targeting lactate metabolism in tumor cells has been proposed [18, 141, 297, 305] and is currently being evaluated in Phase I/II clinical trials [306]. Previously, inhibition of MCT1, specifically with CHC, was used to block lactate uptake in more oxidative cells, thereby starving their more hypoxic neighbors of glucose [141]. While these results are encouraging, it is well documented that CHC does not only inhibit lactate transport. MCTs transport many monocarboxylates. Though each subtype has a different affinity for particular monocarboxylates, the most widely-expressed and well-characterized subtypes (MCT1, 2 and 4) are capable of transporting lactate, pyruvate, butyrate and ketone bodies [136]. Inhibiting the transporter will theoretically prevent trafficking of each of these monocarboxylates. This study showed that the competitive MCT1 inhibitor CHC inhibited lactate transport at concentrations of lactate ≤20mM. In the joint study, it was found that lactate uptake occurred at high lactate concentrations (40mM) even with CHC treatment [290]. Interestingly, Diers *et al*. recently reported that 0.5mM CHC treatment prevented pyruvate uptake and inhibition

of mitochondrial respiration in breast cancer cells [307]. Inhibition of pyruvate uptake and mitochondrial respiration are consistent with previous reports indicating CHC inhibits the mitochondrial pyruvate carrier (MPC) [222]. The most likely explanation of the absence of labeled catabolites from our NMR studies in the conditions of 40mM lactate + CHC is consistent with CHC inhibition of the mitochondrial pyruvate carrier (MPC) [222, 223]. The labeled metabolites cannot enter the TCA cycle without first entering the mitochondria. Without labeled glutamate, labeled alanine cannot be generated, as the alanine transaminase reaction requires glutamate. This explanation requires that CHC is taken up in cells, and there are contradictory reports about CHC uptake by cells. Previous studies have shown that CHC enters isolated cells and organs [223, 308], while some more recent reports indicate that CHC added to media will not be taken up by cells unless a permeabilizing agent is used [309, 310]. For our study, we dissolved CHC in DMSO, which would allow CHC transport into cells.

MCT1 has been found to be localized to the plasma membrane of MCF7 and HMEC cells [291] but has not been found in MDA-MB-231 cells [203, 291]. Additionally, it has been reported that MCT1 does not localize to the mitochondrial membrane but that MCT2 and MCT4 do [291]. More detailed studies with this compound and lactate supplementation could elucidate the mechanisms of inhibition of lactate catabolism by plasma membrane MCT1 inhibition vs. mitochondrial membrane MPC, MCT2 or MCT4.

In summary, we have found that 1. Lactate is taken up and utilized *in vitro* in every cell line tested regardless of tissue of origin, disease state or MCT1 expression; 2. Common metabolites generated from lactate are alanine, pyruvate and glutamate; 3. Diversity of metabolite generation from lactate is cell line dependent. In collaboration with others, we have found that R3230 Ac tumors consume lactate *in vivo*, producing the same metabolites as cultured cell lines [290]. When comparing the pharmokinetics of lactate and glucose *in vivo*, lactate showed faster clearance from the plasma and higher uptake in the tumor than glucose. Finally, the competitive MCT1 inhibitor, CHC, was found to prevent lactate uptake in R3230Ac cancer cells at lactate concentrations ≤20mM.

5. Cell Viability after Lactate Exposure

5.1 Introduction

A common viewpoint of the influence of lactate on the tumor microenvironment can be described in an analogy that our lab has affectionately referred to as "the creosote effect." A characteristic of the desert-faring creosote bush is the ubiquitous "dead zone" surrounding the plant. Previously, it was believed this was due to a water-soluble inhibitor that the plant secreted into the soil, preventing the growth of other plants. Similarly, lactate was often touted as merely a waste product that elicited a "dead zone," without its actions being distinguished from the noxious effects of extracellular acidity and/or hypoxia [46, 271, 311-313]. Few studies have directly investigated the effects of lactate on cellular survival [152, 314, 315]. This work focused on the clonogenic assay to analyze long-term reproductive capacity and Annexin V / 7-AAD staining for short-term apoptotic vs. necrotic responses in cells treated with lactate.

Clonogenic assays assess the ability of a cell to survive treatment and subsequently form colonies. In 1981, Seymour and Mothersill studied the effect of lactate treatment prior to irradiation on the clonogenic survival of the Chinese hamster ovary cell line CHO-K1 [152]. Results suggest that there is a different biological response to chronic lactate treatment ("prolonged incubation") vs. acute lactate exposure ("short treatments"). Specifically, chronic lactate exposure sensitized CHO-K1 cells to

irradiation while acute lactate exposure elicited a radioprotective effect [152]. This indicates that different exposure times to lactate can have significantly different biological consequences. Additionally, in particular conditions, the cellular response to exogenous lactate may be the exact opposite of the creosote effect.

However, Chinese hamster ovary cells are not tumor cells. The direct effects of lactate on tumor cell viability were not studied until the 2000s; still, most of these studies did not solely focus on lactate concentration. In 2009, Grotius *et al.* tested whether 20 hr treatment with high lactate (20mM) and acidic conditions (pH 6.4) prior to irradiation sensitized or protected colorectal and HNSCC cell lines to radiation [314]. Each cell line tested demonstrated a different response to lactate, acidosis and irradiation, alone or combined. One colorectal carcinoma cell line showed no significant decrease in clonogenic surviving fraction with addition of any or all of the insults, while another showed significant and dramatic decrease in clonogenic survival and a significant increase in radiosensitivity after lactic acidosis treatment [314]. This study is one example of the heterogeneous responses to lactate that different tumor lines can exhibit. We hypothesized that increasing lactate concentrations and duration of exposure would significantly affect cell viability and responses.

Cell viability, proliferation and/or death cannot be discussed without the mention of the cell cycle. The cell cycle has distinct phases: G1, S (synthesis), G2 and M (mitosis). G0 is a non-proliferative phase that cells enter into usually from G1 typically

in response to noxious or threatening stimuli [316]. Terms for cells in G0 include quiescent, referring to cellular dormancy, or senescent, referring to the inability to re-enter the cell cycle after sustaining irreconcilable damage. G1 is the growth phase and can be influenced by environmental factors such as oxygenation, nutrient availability and presence of toxins. For this reason, we questioned whether the presence of lactate would induce changes in the cell cycle.

Finally, we hypothesized that treatment with the commercially available MCT1-inhibitor, α-cyano-4-hydroxycinnamic acid (CHC), would decrease cell survival in the presence of lactate and glucose-deprivation, the rationale being that CHC inhibition of MCT1 would prevent lactate entry into the cell and thereby prevent utilization of lactate as an energy substrate. After observing that CHC ineffectively blocked lactate uptake when extracellular lactate concentrations reached 40mM (Section 4), if "lactate detoxification" (via catabolism in the mitochondria) was necessary to cell survival, we would expect that CHC treatment in conjunction with 40mM of lactate would elicit cell death (in – or + glucose conditions) via inhibition of the MPC. An introduction to CHC is provided in Section 1.3.1, and CHC has been suggested to be a potential therapeutic option [18, 211] based on previous studies showing CHC treatment can delay tumor growth to an extent similar to siMCT1 [141]. The leading hypotheses on the mechanisms of decreased tumor cell survival after MCT1 inhibition under high lactate conditions are 1. the metabolic symbiont model, in which hypoxic cells are starved of glucose when

lactate-oxidizing cells are treated with drug [141]; and 2. decreased intracellular pH after lactate and drug treatment, which leads to cell death [211]. In order to probe further into the effects of CHC on cell survival in high lactate conditions, Annexin V / 7-AAD staining was conducted in two breast cancer cell lines in conditions of high lactate (+/- glucose). We expected that glucose deprivation combined with the highest lactate concentration and highest CHC concentration would yield the most cell death.

5.2 Results

5.2.1 High pathophysiologic lactate levels and prolonged lactate exposure significantly decrease clonogenicity and increase cell death

We hypothesized that cellular responses to pathophysiologic lactate levels were dynamic, serving as a fuel at lower concentrations and then acting as a poison at higher concentrations. The first experiments assessed cell survival after sodium lactate treatment using clonogenic assays. It is important to note that a relatively small fraction (~5-20%) of the plated cells in Protocol 1 (Section 2.9.1.1) detached from the plate (Appendix B). Many steps in this protocol discard the media, which includes any detached cells. There is the false notion that these cells will not form colonies. Because the initial clonogenic assays were completed when the potential importance of this observation was realized, the first approach to address the issue of cell detachment was to collect detached cells in a separate experiment, count the cells and assess their viability with the Trypan Blue Exclusion assay. The Figures for these "detachment

assays" are provided in Appendix B and will not be discussed in this Results section. To address the potential detachment artifact, a different protocol was used that incorporated detached cells into the clonogenic assay (Section 2.9.1.2). Results of both clonogenic assays are presented.

These experiments had three objectives: 1. What was the critical concentration to elicit statistical decrease in cell survival?; 2. How quickly would lactate effect cell survival?; and 3. Could availability of glucose "rescue" cells from lactate toxicity predicted to be seen in the lactate treated glucose (-) groups? Five concentrations of lactate (0-80mM) in glucose-available and glucose-deprived conditions, and three time points (18 and 48 hr and 1 week) were chosen to investigate the effects of "acute" versus "chronic" lactate exposure. The rationale for including very high concentrations of lactate in these experiments were based on unpublished data indicating that some microregions of tumors reach lactate concentrations ≥70mM. Additionally, the concentrations of 40 and 80mM lactate were included in order to test the upper limits of the capabilities of cell survival.

To compare long-term clonogenic response to acute cell death responses, we conducted flow cytometry on these same cell lines with Annexin V and 7-aminoactinomycin D (7-AAD) to assess apoptosis and membrane integrity, respectively.

5.2.1.1 Breast cancer cell lines MCF7 and MDA-MB-231 showed clonogenic decline after lactate exposure

5.2.1.1.1 Protocol 1:

Clonogenicity of MCF7 was significantly decreased by increasing lactate concentrations, with a significant reduction of colony formation occurred at lactate concentrations ≥20mM ($p<0.05$ compared to 0mM lactate). After 18 hr exposure to lactate (no glucose), MCF7 colony formation was ~2% lower at 20mM, 19% lower at 40mM and 26% lower at 80mM compared to the untreated control (Figure 24A). For MDA-MB-231 cells, clonogenicity compared to the control was 12% lower at 10mM, 30% lower at 20mM, 25% lower at 40mM and 43% lower at 80mM (Figure 24C). After 48 hr lactate exposure (no glucose), the colony formation at 20mM, 40mM and 80mM lactate-treated MCF7 cells were 16%, 43% and 66% lower compared to the no treatment group (Figure 24A). For MDA-MB-231 cells, the clonogenicity of 10mM, 20mM, 40mM and 80mM lactate-treated MDA-MB-231 cells were 22%, 33%, 55% and 83% lower, compared to the no treatment group (Figure 24C). Finally, after 1 week lactate exposure (no glucose), the clonogenicity of 20mM, 40mM and 80mM lactate treated MCF7 cells were 57%, 71% and 92% lower, respectively, than the clonogenicity of the no treatment group (Figure 24A). The colony formation of 10mM, 20mM, 40mM and 80mM lactate-treated MDA-MB-231 cells were 42%, 57%, 73% and 97% lower, than the no treatment group after 1 week exposure (Figure 24C). The glucose-deprived breast cancer cells responded

in a similar manner to lactate as cells treated with glucose in the media (Figure 24B, D). In the statistical analysis, there was no significant difference in clonogenic response for breast cancer cells with or without glucose. In the combined statistical analysis, colony formation was significantly decreased for both breast cancer cell lines with lactate concentrations ≥10mM (Table 13).

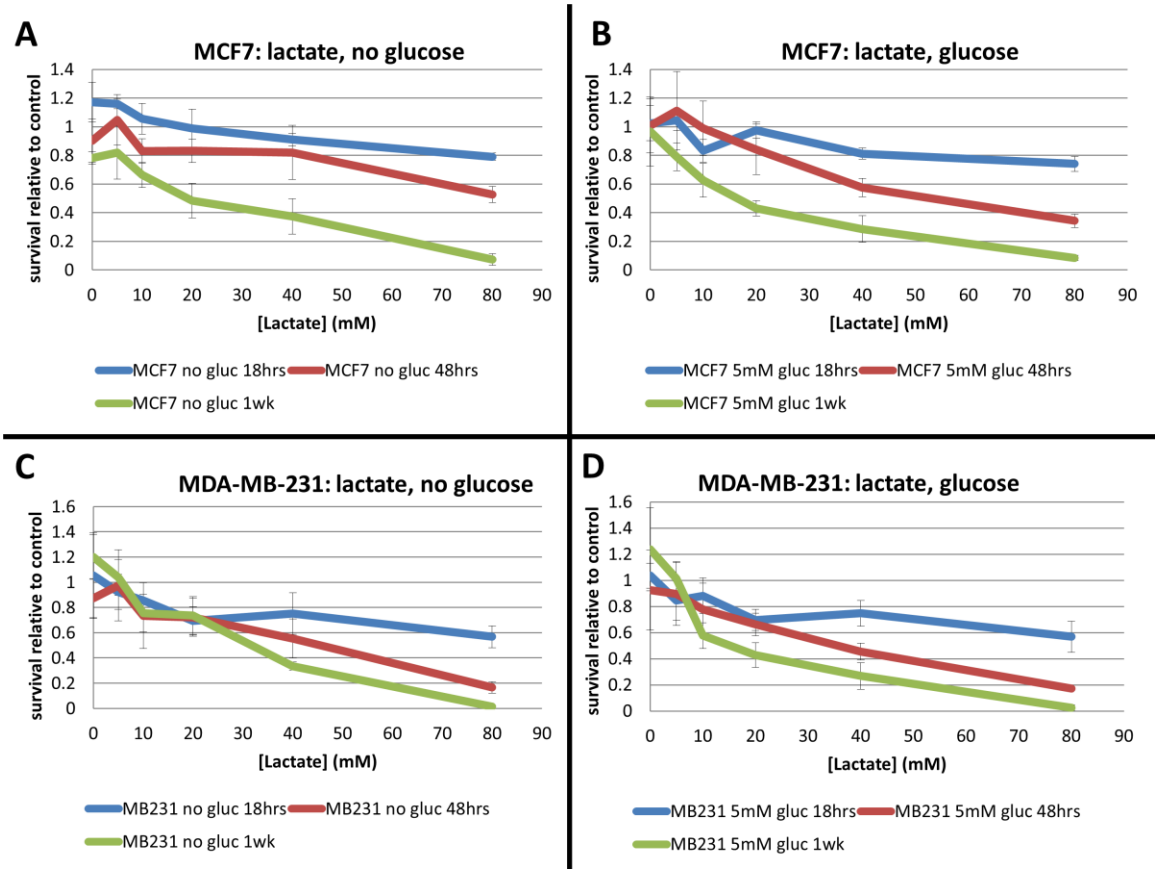

Figure 24: Lactate treatment significantly decreased colony forming abilities of breast cancer cell lines (protocol 1). Clonogenic survival assays using protocol 1 showed a significant decrease in the colony-forming abilities of MCF7 (A, B) and MDA-MB-231 (C, D) cells with increasing lactate concentrations and duration of lactate exposure in glucose-deprived (A, C) and glucose-available (B, D) conditions. All results are reported after normalizing to the untreated control. Detached cells were excluded from these assays, per clonogenic survival assay protocol 1.

Table 13: Statistical analysis of lactate concentrations that significantly decrease clonogenic survival of breast cancer cells

	No glucose	5mM glucose	Combined analysis
[Lactate] (mM)	≥20mM	≥10mM	≥10mM
p value	<0.01	<0.01	<0.01

No significant difference was found in how MCF7 and MDA-MB-231 cells respond to lactate (table 16), indicating that these breast cancer cell lines show a similar clonogenic response to lactate treatment. Comparing the 18 hr, 48 hr and 1 wk clonogenic results, we found that duration of lactate exposure significantly decreased the clonogenicity of both breast cancer cell lines as exposure time increased (MCF7: $p<0.0001$, MDA-MB-231: $p= 0.0255$, Table 14). Different from MCF7 cells, clonogenic responses at 18 hr in MDA-MB-231 cells were significantly worse after 48 hr or 1 week (Table 14), but there was no statistical significance found between 48 hr and 1 week exposure to lactate.

Table 14: Increased duration of lactate exposure significantly decreases clonogenic survival of breast cancer cell lines

Cell line	18hr v. 48hr	48hr v. 1 wk	18hr v. 1 wk	TIME
MCF7	p = 0.0066	p < 0.0001	p < 0.0001	p < 0.0001
MDA-MB-231	p = 0.03	NS	p = 0.012	p = 0.0255

5.2.1.1.2 Protocol 2:

To address potential cellular detachment during the assay, clonogenic assays that included the detached cells in the seeding of plates after the lactate treatment were also performed (Section 2.9.1.2). Using this procedure, normal mammary (HMEC) cells could be included because the treated plates are allowed to grow to 70-90% confluency before treatment. HMEC cells grown at low densities struggle to proliferate, while HMEC cells plated at higher densities grow much better. Two different seeding densities (100 and 500 cells per well) were used for the HMEC clonogenic assay. The relative clonogenic survival of HMEC cells in response to 24 hr lactate exposure was higher in the 500-cell seeding density than in the 100-cell seeding density (Figure 25A, B). At 10mM and 20mM lactate, HMEC cells show 82% and 77% relative survival at a seeding density of 100 and show 87% and 92% relative survival at a seeding density of 500 (Figure 25), indicating that lactate is more toxic to cells when the cell density is low. This makes sense because, at lower cell densities, an individual cell will be exposed to

relatively more lactate than it would be if there were numerous other neighboring cells to cope with the lactate also. At 40mM lactate, both densities show a significant decrease of relative HMEC survival: 47% and 68% relative survival at 100-cell and 500-cell densities, respectively (Figure 25A, B). Results were analyzed by a One-Way ANOVA. In both the 100-cell density and 500-cell density, the effect of lactate treatment on HMEC clonogenicity was significantly different from the untreated control ($p = 0.022$ for the 100-cell density and $p = 0.015$ for the 500-cell density).

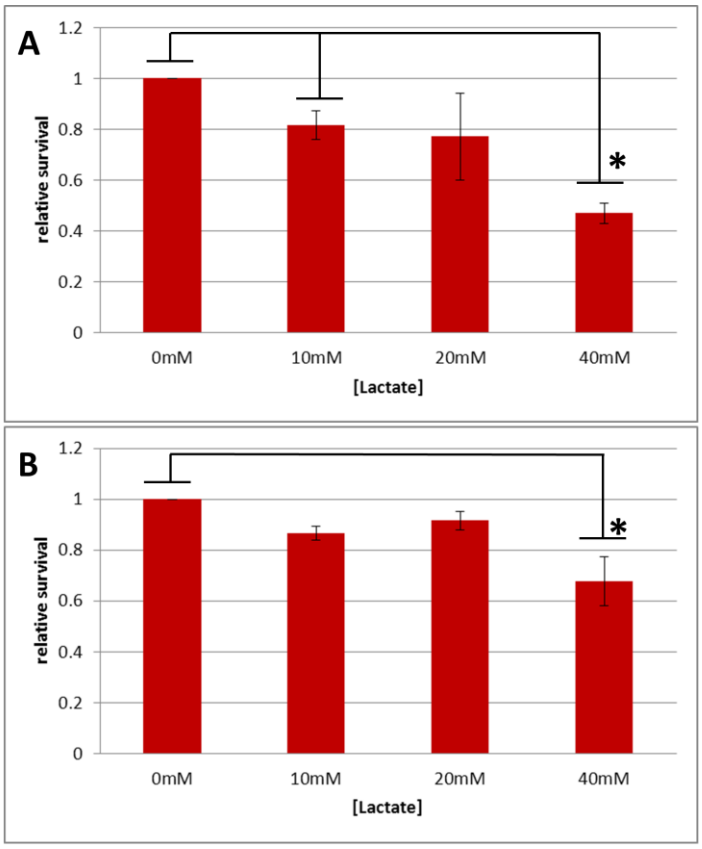

Figure 25: High lactate treatment for 24 hr significantly decreased colony formation of HMEC cells. HMEC cells seeded at a density of 100 (A) or 500 (B) show a significant decrease in clonogenic survival (protocol 2) with 24 hr treatment with 40mM lactate (One-Way ANOVA, $p<0.05$) in the presence of glucose. Detached cells included.

Two different seeding densities (500 and 1500 cells per well) also were used for the MCF7 clonogenic assay. The relative clonogenic survival of MCF7 cells in response to 24 hr lactate exposure followed a similar pattern regardless of seeding density (Figure 26A, B). The largest initial decline in colony-forming ability was seen in the 10mM lactate –treated group (73% and 77% in the 500- and 1500-seeding densities, respectively). At 20mM and 40mM lactate, MCF7 cells show 102% and 87% relative survival at a seeding density of 500 and show 97% and 81% relative survival at a seeding density of 1500 (Figure 26), indicating that the reproductive capabilities of the MCF7 cells are as capable as the untreated cells at 20mM of lactate. A lactate concentration of 10mM is the most clonogenically toxic concentration measured. The reason for the demonstrated toxicity at 10mM of lactate but not 20mM or 40mM of lactate is unclear. It is possible that 10mM lactate is not a high enough concentration to adequately feed the MCF7 cells, which were shown to be lactate-consumers (Section 4.2.2), resulting in decreased colony formation.

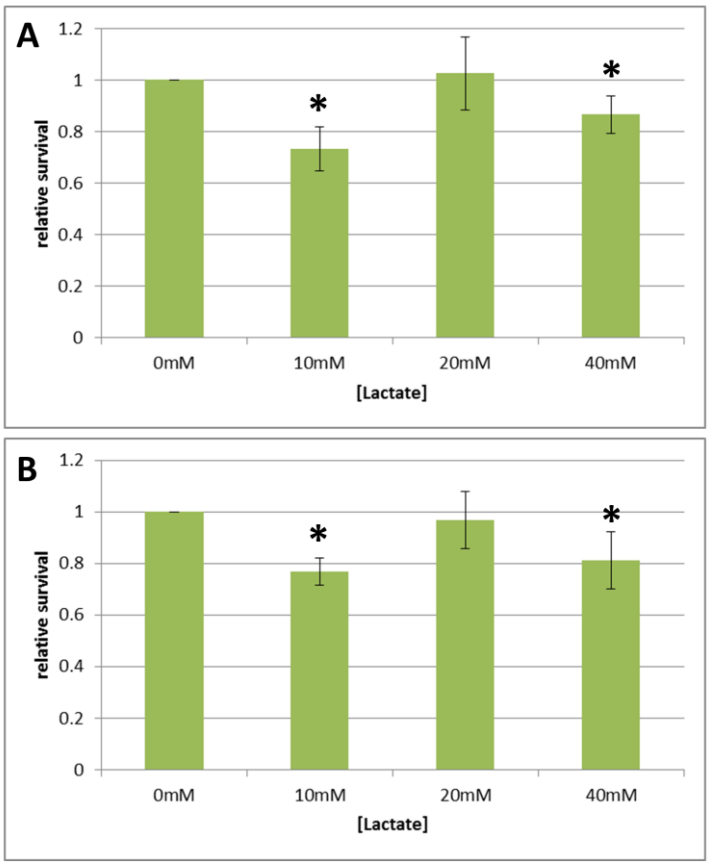

Figure 26: Lactate treatment of 10mM and 40mM for 24 hr showed significantly decreased colony formation of MCF7 cells. MCF7 cells seeded at a density of 500 (A) or 1500 (B) show a significant decrease in clonogenic survival (protocol 2) at lactate concentrations of 10mM and 40mM (One-Way ANOVA, *$p<0.05$) in the presence of glucose. Detached cells included.

Two different seeding densities (200, Figure 27A, C, and 1000 cells per well, Figure 27B, D) also were used for MDA-MB-231 and R3230Ac clonogenic assays. The relative colony formation of MDA-MB-231 and R3230Ac cells in response to 24 hr lactate exposure was not significantly different from the untreated control (Figure 27A-D). In

fact, there a trend for increased colony formation in R3230Ac cells with 10mM of lactate when seeded at the lower density (Figure 27C).

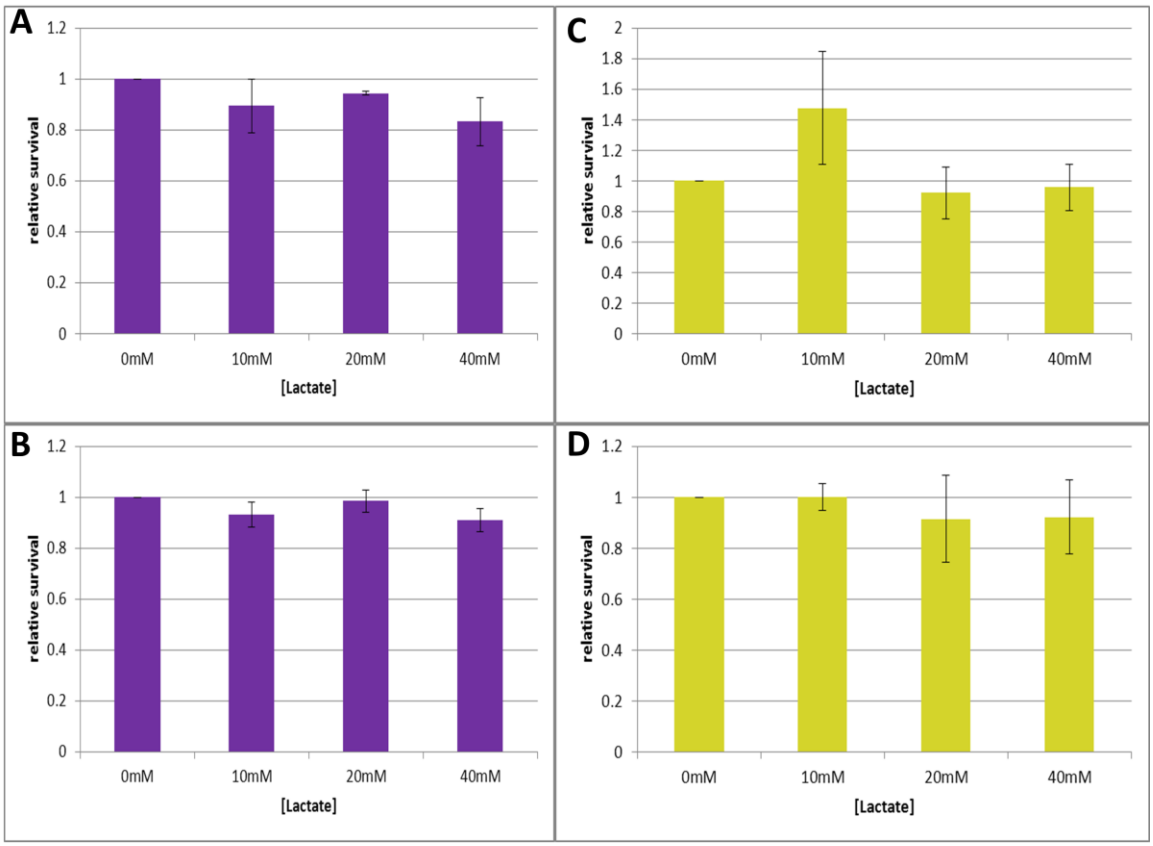

Figure 27: Lactate treatment for 24 hr did not significantly influence the colony-forming abilities of MDA-MB-231 or R3230Ac cells. MDA-MB-231 (A, B) and R3230Ac (C, D) cells seeded at a density of 200 (A, C) or 1000 (B, D) do not show significant changes in clonogenic survival (protocol 2) in response to 24 hr exogenous lactate treatment in the presence of glucose. Detached cells included.

5.2.1.2 Glucose-deprived breast cancer cell lines MCF7 and MDA-MB-231 but not normal breast cells (HMEC) or R3230Ac cells showed a significant increase in cell death after 24 hr exposure to very high lactate levels (≥40mM)

Annexin V staining in conjunction with 7-aminoactinomycin D (7-AAD) was used to evaluate cell toxicity after lactate treatment. The Annexin V assay is a common measurement of apoptosis events; the binding of Annexin V is used as a probe to detect phosphatidlyserine on the cell surface. 7-AAD intercalates in DNA and does not pass through healthy and intact cell membranes. Its use in assays is to assess membrane integrity. Breast cell lines were treated with different lactate concentrations (± glucose) and stained for Annexin V and 7-AAD to assess apoptosis and membrane integrity, respectively (Figure 28, Figure 29). To compare cancer cell survival to normal cell survival, human mammary epithelial cells (HMEC) were included in the assays.

We first tested cell survival with exogenous lactate in the presence of glucose (Figure 28). We found no significant changes in any acute cell death responses in any of the cell lines tested after 24 hr exposure to exogenous lactate + glucose (Figure 28). Interestingly, HMEC cells did not show an increase in cell death responses to any lactate concentration tested; in fact, cell death responses show a trend of suppression as lactate concentrations increase (Figure 28E).

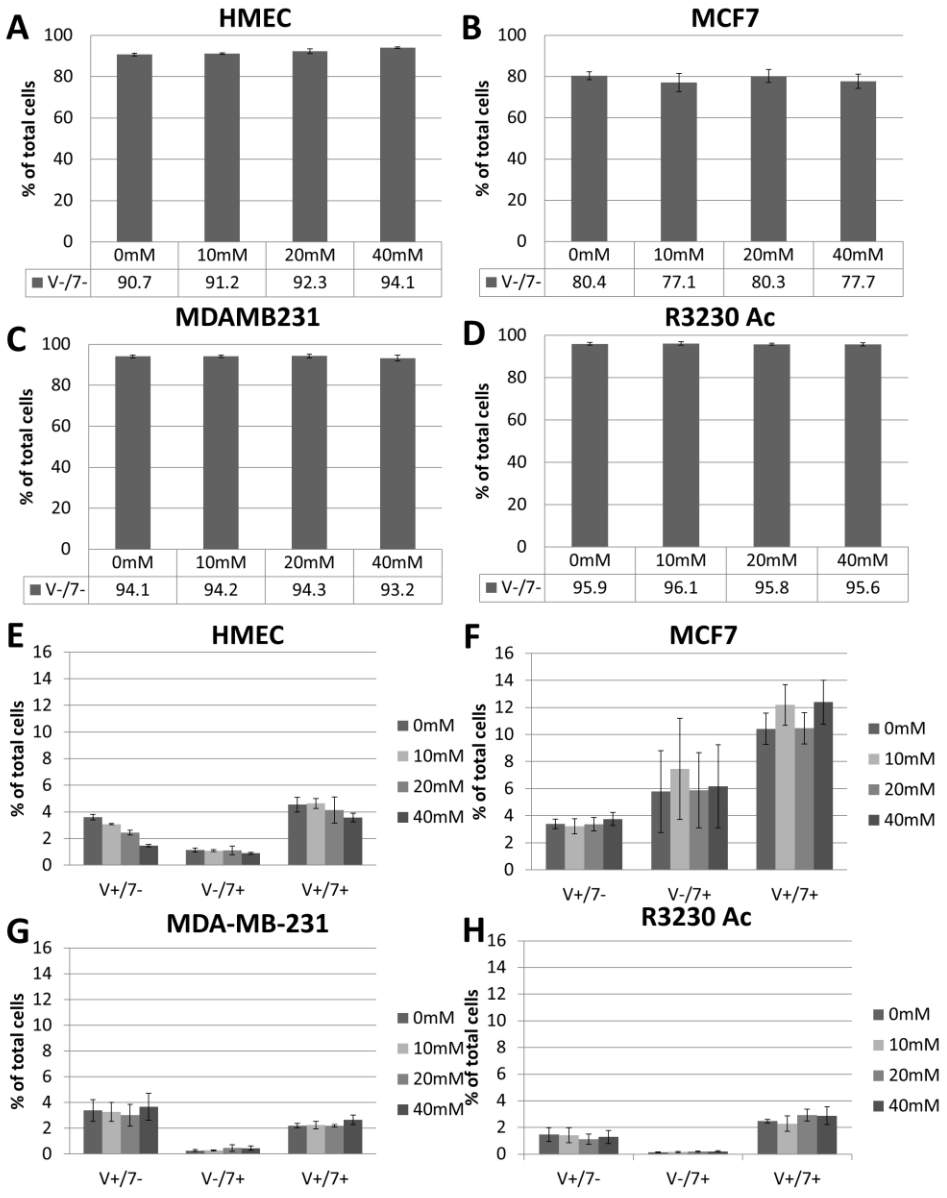

Figure 28: Cell viability as measured by Annexin V / 7-AAD labeling (n=3) in lactate-treated (+glucose) breast cell lines. HMEC (A), MCF7 (B), MDA-MB-231 (C), and R3230Ac (D) cells show no significant changes after 24 hr exposure to exogenous lactate (0-40mM) in the context of available glucose. No significant changes in cell death responses (Annexin V+ / 7-AAD-, Annexin V- / 7-AAD+, or Annexin V+ / 7-AAD+) were observed in HMEC (E), MCF7 (F), MDA-MB-231 (G) or R3230Ac cells (H) after 24 hr exposure to exogenous lactate (0-40mM) in the context of available glucose.

We then tested the effects of exogenous lactate on cell viability in conjunction with glucose deprivation because previous studies showed that lactate accumulated in tumor regions where very little to no glucose was available [104]. Measurements of live cell populations (Annexin V - / 7-AAD - cells), early apoptosis events (Annexin V + / 7-AAD - cells) or complete loss of membrane integrity (Annexin V - / 7-AAD + cells) did not show significant differences in all glucose-deprived cell lines tested after lactate treatment (Figure 29). At 40mM, the percentage of Annexin V + / 7-AAD + cells was significantly increased for both breast cancer cell lines, with 17% of MDA-MB-231 cells and 34% of MCF7 cells showing positive staining for both markers (Figure 29F, G). The cell death responses to the lactate-treated glucose (+) groups were not significantly different from the matched lactate-treated glucose (-) groups except for 40mM lactate group in the breast cancer cell lines (Figure 28, Figure 29). HMEC and R3230Ac cells were tolerant to all lactate concentrations even with glucose-deprivation (Figure 28, Figure 29).

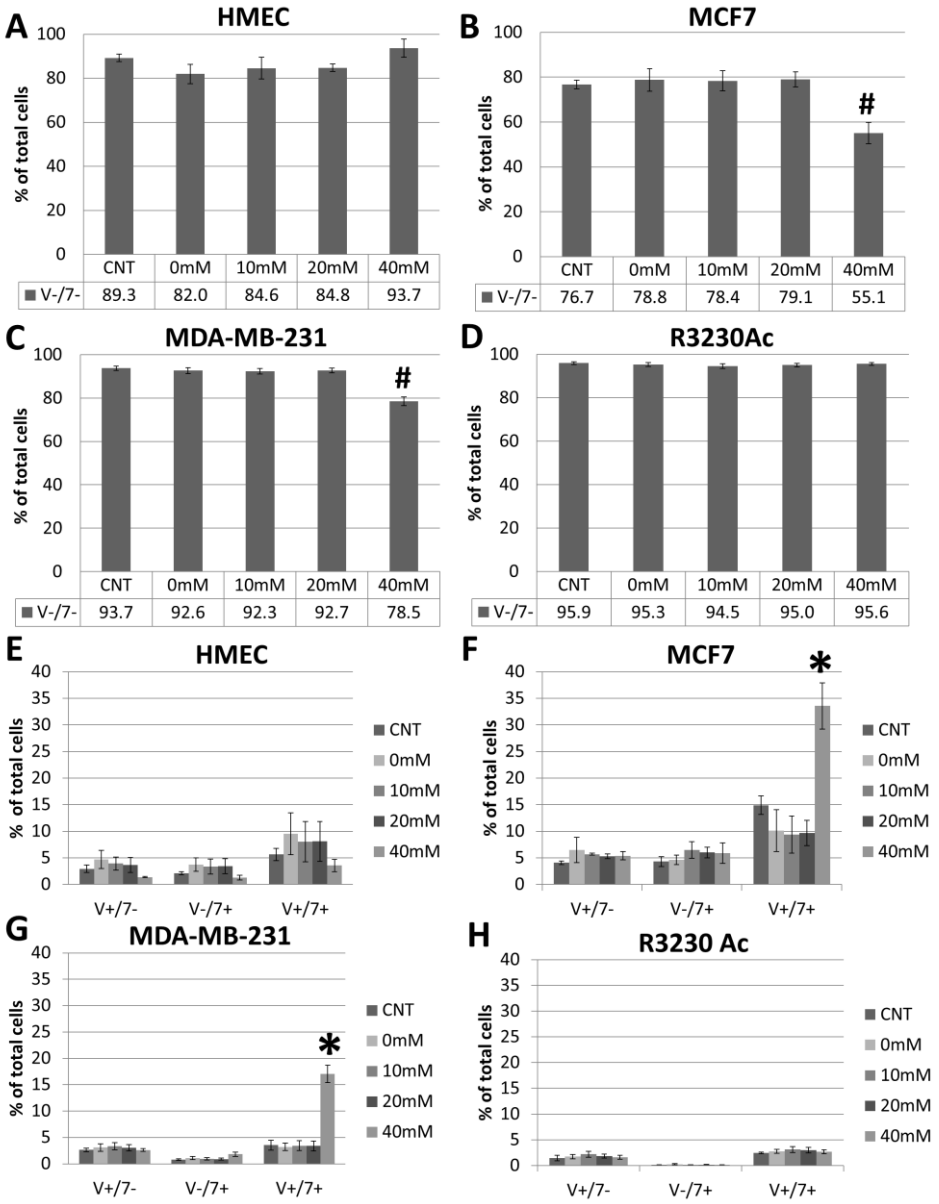

Figure 29: Cell viability as measured by Annexin V / 7-AAD labeling (n=3) in lactate-treated (-glucose) breast cell lines HMEC (A) and R3230Ac (D) cells show no loss of cell viability with 24 hr lactate treatment. MCF7 (B) and MDA-MB-231 (C) showed a significant decrease in live cells after 24 hr exposure 40mM lactate (no glucose). There were no cell death responses in HMEC (E) and R3230Ac cells (H) after 24 hr exposure to exogenous lactate (0-40mM, no glucose). The percentage of Annexin V+ / 7-AAD+ MCF7 (F) and MDA-MB-231 (G) cells increased significantly with 24 hr 40mM lactate treatment in the absence of glucose. CNT = complete media (including glucose), no lactate. # $p < 0.001$, * $p < 0.05$ One-Way ANOVA

5.2.1.3 Normal liver cells WRL-68 showed clonogenic decline after lactate exposure; hepatocellular carcinoma cells HepG2 showed a varied clonogenic response to lactate exposure

Clonogenicity was also examined in liver cells after lactate exposure. Studies included a cell line that was indicated to be normal embryonic liver, WRL-68, as a control for the hepatocellular carcinoma line, HepG2. The same concentrations and time points were used as in the breast cancer cell clonogenic assays. All of the clonogenic assays conducted in the liver cell lines followed protocol 1.

Colony formation of WRL-68 was significantly decreased by increasing lactate concentrations; according to the combined statistics, significant reduction of clonogenicity occurred at lactate concentrations ≥10mM ($p<0.05$ compared to 0mM lactate, Table 13). After 18 hr exposure to lactate, clonogenicity compared to the control was 8% lower at 10mM and 20mM, 16% lower at 40mM and 49% lower at 80mM (Figure 30A). After 48 hr lactate exposure, the colony formation of 10mM, 20mM, 40mM and 80mM lactate treated WRL-68 cells were 29%, 31%, 33% and 79% lower, respectively, than the clonogenicity of the no treatment group (Figure 30A). Finally, after 1 week lactate exposure, the clonogenicity of 10mM, 20mM, 40mM and 80mM lactate treated WRL-68 cells were 25%, 52%, 75% and 96% lower than the no treatment group (Figure 30A). The glucose-deprived WRL-68 cells responded in a similar manner to lactate (Figure 30B). In the statistical analysis, there was no significant difference in clonogenic

response to lactate treatment between the +glucose or –glucose WRL-68 cells but the effect of duration of exposure was significant (Table 15).

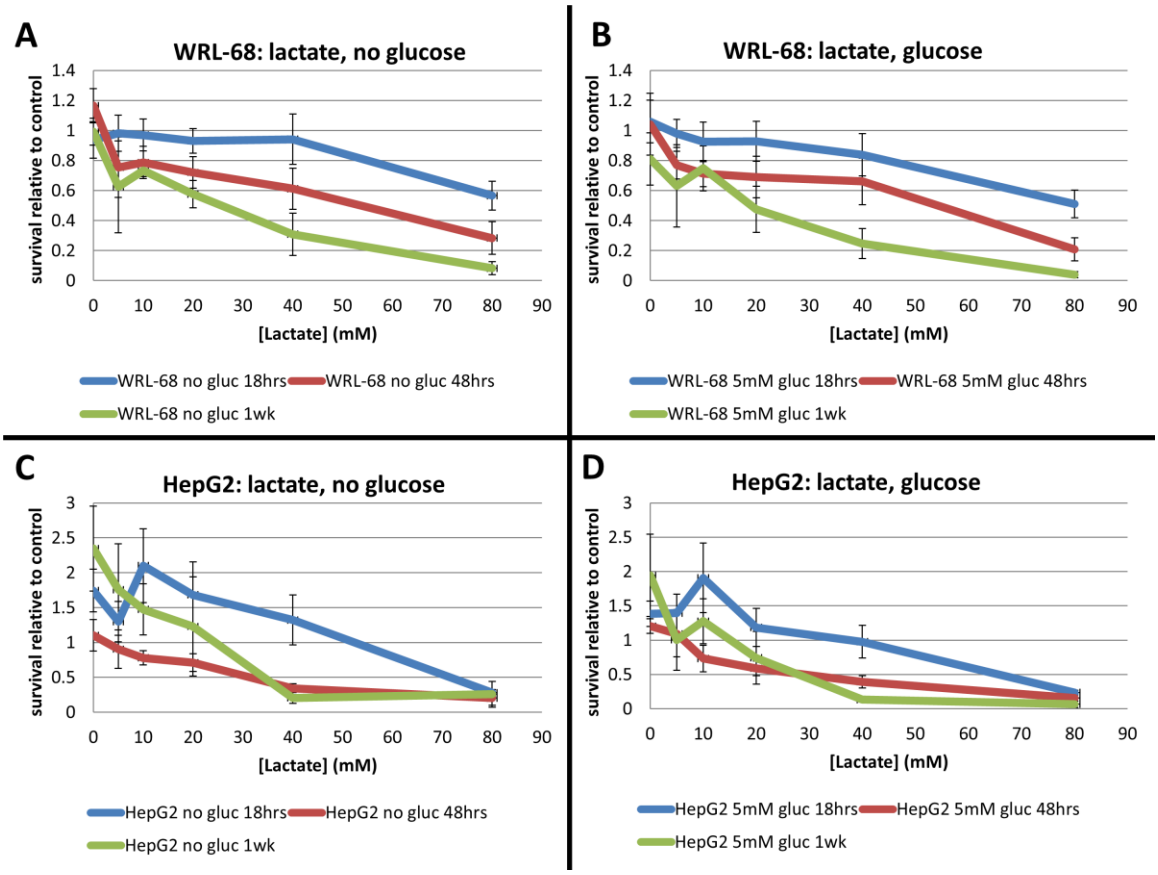

Figure 30: Lactate treatment significantly decreased colony forming abilities of WRL-68 cells, but HepG2 cells showed a variable response to lactate treatment (protocol 1). Clonogenic survival (protocol 1) decreases in WRL-68 (A, B) increasing lactate concentrations and duration of lactate exposure in glucose-deprived (A) and glucose-available (B) conditions. HepG2 cells (C, D) show decreasing clonogenic survival with 48 hr exposure but show highly variable responses at different lactate concentrations and exposure times.

HepG2 cells showed a much different response to exogenous lactate than any of the other cell lines. MCF7, MDA-MB-231 and WRL-68 cells all showed a general

downward trend of colony formation with increasing lactate concentrations and duration of exposure (Figure 24, Figure 30A, B). HepG2 cells showed an increase in colony formation relative to the no treatment group after 18 hr lactate treatment with concentrations ≤20mM (Figure 30C). At 40mM lactate, HepG2 cells showed close to equal clonogenic survival to the no treatment control (Figure 30C). Only when concentrations reached 80mM was a great reduction (76% reduction) in clonogenic survival evident (Figure 30C). After 48 hr of lactate treatment, lactate-treated groups <5mM showed a decline in clonogenic survival relative to the no treatment control (Figure 30C). The clonogenicity of 10mM, 20mM, 40mM and 80mM lactate treated HepG2 cells after 48 hr exposure were 27%, 41%, 61% and 84% lower compared to the no treatment group (Figure 30C). These numbers more closely match the other cell lines; however, after 1 week lactate exposure, the clonogenic survival showed an increase relative to the no treatment control with lactate concentrations ≤10mM (Figure 30C). After 1 week exposure to lactate concentrations of 20mM, 40mM and 80mM HepG2 clonogenic survival decreased relative to the control by 26%, 87% and 93%, respectively (Figure 30C). The glucose-deprived HepG2 cells showed a similar pattern of response to lactate treatment (Figure 30D).

Table 15: Increased duration of lactate exposure significantly influences clonogenic survival of liver cell lines

Cell line	18hr v. 48hr	48hr v. 1 wk	18hr v. 1 wk	TIME
WRL-68	p = 0.017	p = 0.027	p < 0.0001	p < 0.0001
HepG2	p = 0.001	p = 0.03	NS	p = 0.004

When comparing the responses of cell lines to each other, it was found that only HepG2 cells showed a significantly different clonogenic response to lactate treatment (Table 16). This indicates that MCF7, MDA-MB-231 and WRL-68 cells respond in a similar manner clonogenically to lactate exposure, varying slightly in their sensitivity to particular lactate concentrations and exposure times. In the combined statistics, in which all cell lines were analyzed together, all cell lines except HepG2 cells showed a significant decline in survival at lactate concentrations over 10mM (+glucose) or 20mM (-glucose) (Table 13).

Table 16: Clonogenic survival response to lactate is significantly different in HepG2 cells

1st cell line	2nd cell line	p value
MCF7	MDA-MB-231	NS
MCF7	WRL-68	NS
MCF7	**HepG2**	**p=0.0001**
MDA-MB-231	WRL-68	NS
MDA-MB-231	**HepG2**	**p<0.0001**
WRL-68	**HepG2**	**p<0.0001**

5.2.1.4 Normal liver cells (WRL-68) and liver cancer cells (HepG2) showed a significant increase in cell death and early apoptosis events (HepG2 only) after 24 hr exposure to very high lactate levels (≥40mM)

Next, lactate toxicity (± glucose) in WRL-68 and HepG2 cells was evaluated using Annexin V and 7-AAD (Figure 31). For WRL-68 cells, addition of 40mM of lactate led to a significant decrease in the percentage of live cells ($p<0.01$, Figure 31A). Treatment with 40mM lactate for 24 hr significantly increased the percentage of cells with complete loss of membrane integrity (4.5%) compared to all other treatment groups (<1.5%) ($p<0.0033$, Figure 31B).

Measurements of live cell populations (Annexin V - / 7-AAD - cells) showed a significant decrease from 78% to 18% in HepG2 cells with 24 hr 40mM lactate treatment

(p<0.0001, Figure 31C). The percentage of total HepG2 cells showing apoptosis (Annexin V + / 7-AAD - cells) was significantly increased to 48% with 40mM of lactate (p<0.0033 compared to all other groups, Figure 31D). Overall, the HepG2 cell line showed the greatest cell death response to 40mM lactate supplementation in absence of glucose.

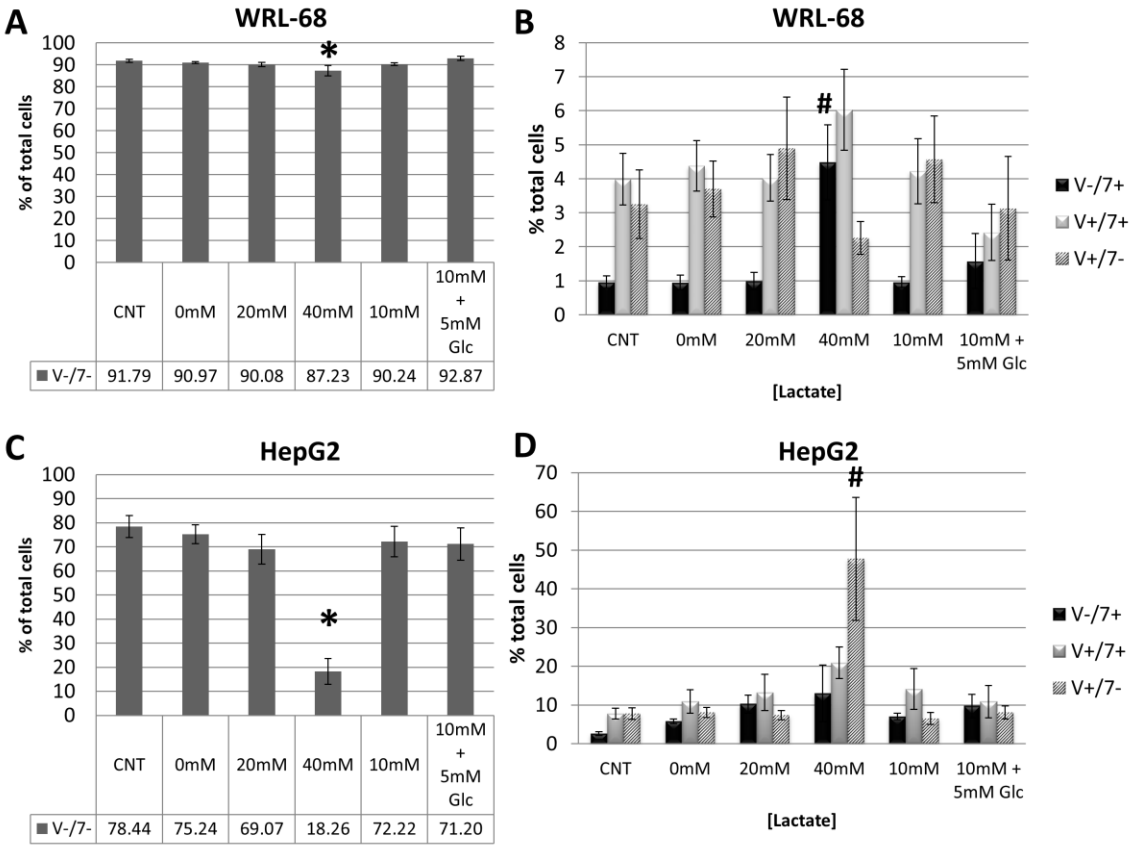

Figure 31: Cell viability and death as measured by Annexin V / 7-AAD labeling (n=3) in liver cell ines. WRL-68 (A, B) and HepG2 cells (C, D) showed a significant decrease in Annexin V- / 7-AAD- labeled cells after 24 h exposure to 40mM exogenous lactate in the context of glucose deprivation (A, C). Percentage of Annexin V- / 7-AAD+ WRL-68 cells (B) increased significantly with 24 h 40mM lactate treatment in the absence of glucose. Percentage of Annexin V+ / 7-AAD- HepG2 cells showed a significant increase with 24 h 40mM lactate treatment (-glucose) (D). CNT = complete media (including glucose), no lactate. *p < 0.01, #p < 0.0033, One-Way ANOVA.

5.2.1.5 Comparison of clonogenic assay and flow cytometry results

The results from the Annexin V/7-AAD and clonogenic assays from protocol 1 seem to contradict each other. The Annexin V/7-AAD assay showed that cells were quite tolerant to high concentrations of lactate (up to 40mM); in contrast, the clonogenic assays showed loss of clonogenic potential in MCF7, MDA-MB-231 and WRL-68 after exposure to lower lactate concentrations (10mM or 20mM). This could indicate that the cells were alive after lactate treatment but perhaps not reproductive. However, there was another possibility of mismatched results due to methodology. In the standard clonogenic assay (protocol 1), the media was replaced after various exposures and in the process, the detached cells were discarded. Cell detachment is not necessarily synonymous with cell death [317]. We suspected that lactate might induce cell detachment and that these detached cells might still retain clonogenic capacity. The second protocol we utilized for the clonogenic assays (Section 2.9.1.2) included detached cells in the seeding (results in Appendix B). Therefore, any differences seen between the clonogenic assays and Annexin V/7-AAD staining are not artifacts but distinct differences in immediate (Annexin V/7-AAD) and delayed (clonogenic assays) cell death responses to lactate.

In HMEC cells, relative clonogenic survival decreases with increased lactate, dropping to 68% survival after 24 hr exposure to 40mM of lactate concentrations (Figure 25). These assays include glucose, so the effects seen are not due to glucose deprivation.

The apoptosis assays were conducted with the presence and absence of glucose. As seen, for HMEC cells, there was no change in cell viability response with any lactate concentration (Figure 28, Figure 29). The short-term response to high lactate does not change compared to the untreated control in HMEC cells, while the long-term response to high lactate is reproductive death. Because the reduced colony formation is not due to apoptosis or necrosis, it is possible that high lactate stimulates HMEC cells to become quiescence or senescent. Senescent cells would not show evidence of colony growth in the clonogenic assay though quiescent cells might [318]. Cell cycle analysis would show evidence of if a cell was in a resting state.

5.2.3 Glucose deprivation has a greater influence on cell cycle than treatment with exogenous lactate

In the first experiments conducted to assess lactate consumption *in vitro* (Section 4.2.2), lactate was supplemented in glucose-free media. Cells were plated in parallel in high glucose DMEM to compare cell counts after the 5-day treatment period. In 20mM of lactate (with glucose deprivation), cell counts were lower for both MCF7 (~8.7×10^5) and MDA-MB-231 (~1.2×10^6) cells compared to the high glucose DMEM control (MCF7 = ~1.7×10^6, MDA-MB-231 = ~3×10^6). When cells were normalized to the high glucose control plate, MDA-MB-231 cells treated with lactate in the absence of glucose showed a cell count 60% lower than the high glucose control (Figure 32). This was a significant decrease compared to the high glucose control group (Figure 32). A complete nutrient deprivation group (no glucose, no lactate) was not included in this assay; however, in

future assays, this group was included to discern whether the growth suppression was due to exogenous lactate addition or glucose deprivation.

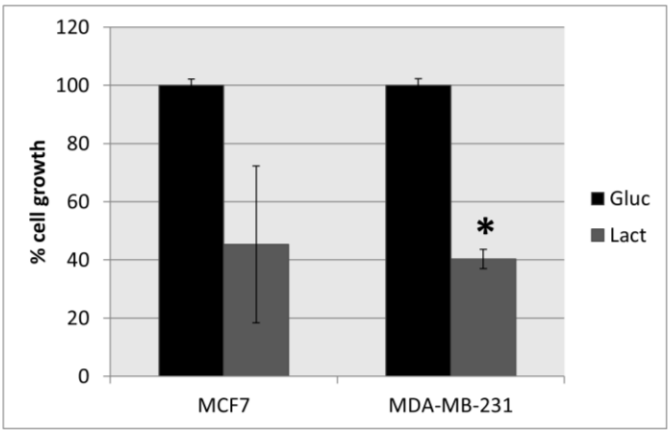

Figure 32: Five-day lactate treatment impairs breast cancer cell line growth. Treatment with 20mM of lactate in the context of glucose deprivation for 5 days decreased MCF7 cell growth and significantly decreased MDA-MB-231($p < 0.05$, One-Way ANOVA) cell growth *in vitro*, as measured by hemocytometer cell counts, compared to high glucose DMEM control.

Because the Annexin V / 7-AAD staining results showed that there were no significant cell death responses after treatment with 20mM of lactate in the context of glucose deprivation (Figure 29), we questioned if the suppression of cell proliferation in these conditions was due to cell cycle regulation by lactate. Propidium iodide staining was employed to measure changes in phases of the cell cycle after lactate treatment five cell lines (MCF7, MDA-MB-231, HMEC, HepG2 and WRL-68). Two time points were chosen (18 and 48 hr) and a range of lactate concentrations (0-20mM) was tested in the context of glucose availability (+5mM glucose) and deprivation. We assessed the

percentage of total cells in each phase with flow cytometry. A complete nutrient deprivation control ("0mM") was included in these experiments. The distribution of cells in each phase did not significantly change in any of the cancer cells or WRL-68 cells with lactate treatment for 48 hr (Figure 33).

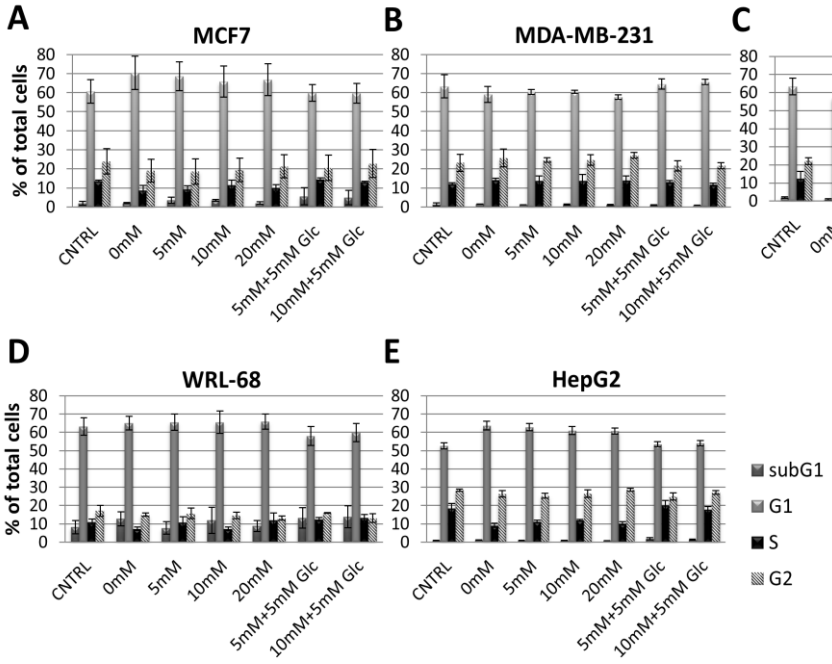

Figure 33: Cell cycle distribution of cell lines after 48 hr lactate exposure. Cell cycle distribution of MCF7 (A), MDA-MB-231 (B), HMEC (C), WRL-68 (D) and HepG2 (E) cells were measured by P.I. staining, after 48 hr treatment with lactate (0-20mM) in the context of no glucose or 5mM of glucose. There were no significant changes in cell cycle distribution except in glucose-deprived HMEC cells compared to glucose-sufficient HMEC cells (*$p < 0.05$, One-Way ANOVA). Lactate was not found to be a significant factor in cell cycle regulation. CNTRL = complete media, no lactate.

No significant changes were seen in the cell cycle distribution with any treatment group in MCF7, MDA-MB-231, WRL-68 or HepG2 cells (Figure 33). HMEC cells showed

a significant increase in the G2/M phase with glucose deprivation (Figure 33C, *$p < 0.05$); however, lactate treatment did not have a significant influence on cell cycle regulation in any of the cells. These statistics taken together show that glucose availability has a greater influence on cell cycle regulation than lactate treatment does. Lactate by itself did not elicit an effect on the cell cycle in any of the cell lines tested. This supports the idea that the growth suppression seen in Figure 32 may be an effect of glucose deprivation instead of exogenous lactate addition.

5.2.4 The effect of MCT1-inhibitor (CHC) on cell survival

At higher concentrations (5mM) typically used in cancer research, the MCT1-inhibitor, α-cyano-4-hydroxycinnamic acid (CHC)will inhibit MCT1 as well as the MPC; at lower concentrations (<200μM), CHC will still inhibit the MPC, but has little effect on the MCTs [136, 223]. For this reason, we chose to use two concentrations of CHC for investigation: 5mM (high) and 100 μM / 0.1mM (low).We hypothesized that the cells would show less cell death overall, regardless of the conditions, with the lower CHC concentration, but we anticipated that both concentrations would modify the metabolism of cells (Section 4.2.4). If both the lower and higher CHC concentration showed significant cell death when lactate was supplemented, then lactate toxicity would be due to the inability of the cell to "detoxify" the lactate via biochemical pathways (generation of alanine and glutamate, Section 4.2.4). If, however, cell death is elicited by another mechanism, we would expect that the lower CHC concentration

would not show any cell death. This would mean that lactate "detoxification" via mitochondrial metabolism is not the primary pathway of cancer cell survival (assuming the MPC is truly blocked). If only the high concentration of CHC elicits cell death, then the mechanism of "lactate toxicity" is due to some other associated factor, such as redox stress or lower pH_i. Of note, it has previously been shown that cell death is elicited by other MCT1 inhibitors via the inability of the cell to effectively regulate the lower pH_i that results from lactic acid accumulation from glycolysis [211].

The two cell lines chosen for these cell viability studies were MCF7 and R3230Ac cells. R3230Ac cells were included to compare cell death responses with the metabolic profile presented in Section 4.2. Before mentioning the results, it is important to more closely address the rationale behind choosing the conditions we tested (Table 7). We first tested the effects of the high and low CHC concentrations on cell survival without other confounding factors (lactate, glucose-deprivation) to understand the baseline toxicity of each concentration. We expected that the concentration would have a significant influence on cell death.

After this, we added glucose and lactate concentration manipulation. For these experiments, the highest lactate concentration was chosen (40mM) and glucose was either left in the media or completely absent (0mM). In a recent publication, we showed that 5mM CHC did not effectively prevent lactate uptake when extracellular lactate concentrations reached 40mM [290]. These manipulations would test if lactate was

significantly toxic to cells after inhibition of lactate extrusion. If so, this would imply that lactate catabolism may be a necessary strategy for cancer cell survival under high lactate conditions. Glucose was tested as an interacting factor. As glucose deprivation usually elicits cell stress responses, such as activation of JNK1 and increased oxidative stress [319, 320], we hypothesized that any toxic effects lactate elicited would be augmented in conditions of glucose deprivation.

CHC would also prevent extrusion of glycolytically-derived lactic acid. Indeed, our group found that both 0.1mM and 5mM CHC blocked some extrusion of endogenous lactate formed from glutamine in glucose-deprived R3230Ac cells [290]. If the cell death was due to prevention of glycolytically-derived lactate extrusion, then we would anticipate that the percent of cell death with the CHC in the context of available glucose (and no lactate) would be significantly higher than that of the CHC treatment in the absence of glucose (and lactate). The results were analyzed with One-Way ANOVA with posthoc tests and linear regression models to determine significant differences between groups.

Figure 34 shows the percent of total MCF7 and R3230Ac cells that were viable (Annexin V- / 7-AAD-) after treatment with high (5mM) or low (0.1mM) CHC concentrations with or without glucose and/or lactate. Without glucose in the media, the percentage of viable MCF7 cells dropped to 56% with high CHC ($p=0.004$ compared to control, Figure 34A). High CHC in the context of high lactate and no glucose resulted in

a mean percent of viable of 59%. This result was significantly different compared to the untreated control group ($p=0.003$, Figure 34A) and all groups with no CHC or low CHC, (except for the no glucose, no lactate low CHC group). When a linear regression model was conducted for MCF7 cells, it was found that CHC concentration and glucose availability significantly influenced cell viability ($p<0.0001$ and $p=0.001$, respectively) but the presence of high lactate showed no significant changes in cell viability.

All high CHC treatments in R3230Ac cells showed a significantly decreased percentage of live cells compared to control groups and all low CHC treatments (*$p<0.008$) and cells treated with 40mM of lactate (+ and – glucose) in the absence of CHC (†$p<0.0001$, Figure 34B). This indicates that high lactate had the least influence on cell survival in this assay. Additionally, treatment with the low CHC concentration showed no significant changes in cell survival compared to the control or vehicle treatments.

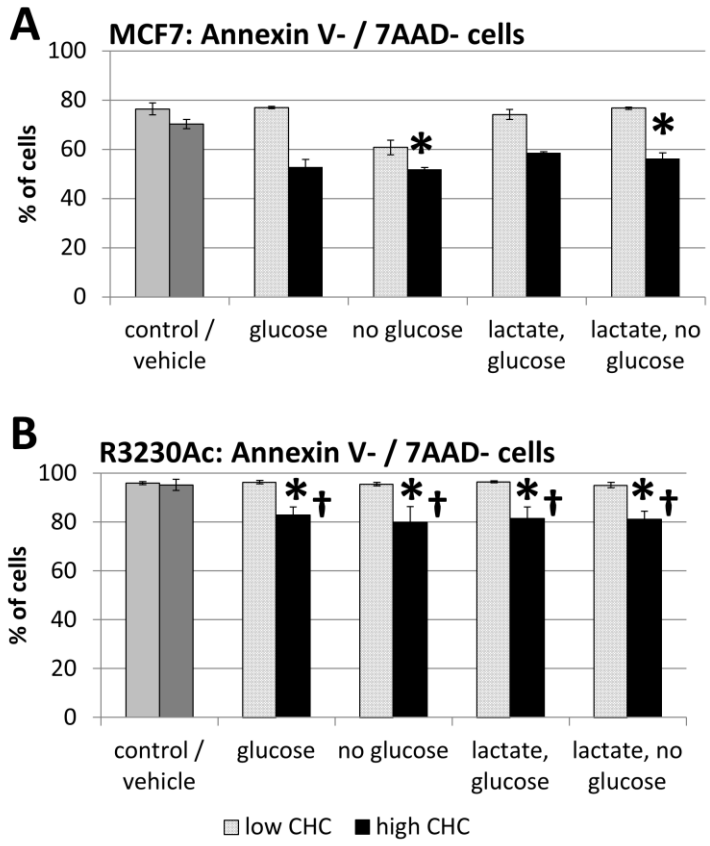

Figure 34: High CHC significantly decreases breast cancer cell viability. Percent of viable (Annexin V- / 7-AAD-) MCF7 (A) or R3230Ac (B) cells significantly decreases after 24 hr treatment with high (5mM) CHC independent of exogenous lactate (40mM) supplementation. *$p < 0.05$ high CHC compared to all other groups, †$p < 0.0001$ high CHC compared to 0mM CHC groups, One-Way ANOVA.

Also available from the data set is whether cells died via apoptosis, necrosis or both after CHC treatment. As seen in Figure 35, treatment with high CHC elicited an overall increased cell death response compared to low CHC. Nutrient deprivation elicited a significant increase in apoptosis in CHC-treated MCF7 cells (*$p < 0.05$, Figure 35A). The percentage of MCF7 cells marked for both apoptosis and loss of membrane

integrity was significantly increased with all high CHC treatments (except the high CHC –glucose, -lactate group) compared to all no or low CHC groups (*$p < 0.05$, Figure 35C). In all the statistical tests conducted, low CHC concentration was not significantly different from control; high CHC concentration showed significance compared to low CHC and no CHC. Glucose also significantly influenced cell survival. The presence or absence of lactate had no effect on cell death.

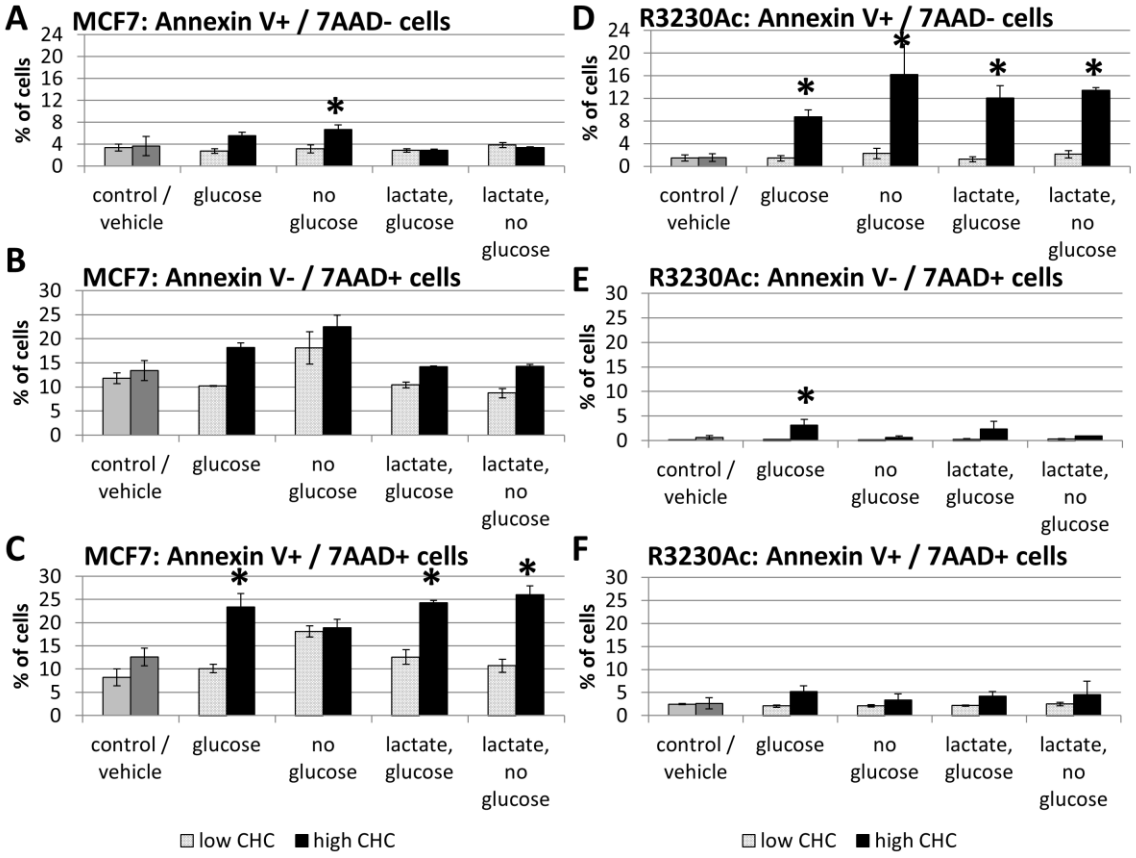

Figure 35: High CHC significantly increased cell death responses in breast cancer cell lines. Cell death responses to 24 h treatment with high (5mM) or low (0.1mM) CHC in MCF7 (A-C) or R3230Ac (D-F) cells showed that high CHC significantly increased the percent of MCF7 cells with Annexin V+ / 7-AAD+ staining (C) and the percent of R3230Ac cells undergoing apoptosis (D). *$p < 0.05$, One-Way ANOVA

The percentage of R3230Ac cells that stained positive for Annexin V only was significantly increased in all high CHC groups compared to groups with low CHC or no CHC (*$p<0.05$, Figure 35D). Only the –glucose –lactate+high CHC group showed a significantly increased percentage of R3230Ac cells with loss of membrane integrity (*$p<0.05$, Figure 35E); there were no significant changes in the percentage of R3230Ac cells marked for both cell death pathways with any treatment (Figure 35F). Taken together, these results show that R3230Ac cells primarily undergo apoptosis in response to high CHC. Glucose deprivation acts as a confounding factor, but high lactate elicits very little influence on R3230Ac cell death.

5.3 Discussion

In recent history, cell survival after lactic acid exposure has been assessed in normal keratinocytes [321] and neural precursor cells [322]. This was the first study to directly investigate cell survival after sodium lactate treatment without additional insults, such as radiation. In general, we found that relatively low lactate concentrations and shorter exposure times were better tolerated by cells than very high lactate concentrations or chronic exposure; however, sensitivity to exogenous lactate varied greatly between cell lines. Acutely, exogenous lactate was well-tolerated by all cell lines tested when glucose was present (Figure 28, Figure 31)

Additionally, we found that, in the presence of glucose, the normal breast cells and MCF7 cells showed significantly decreased clonogenicity with 24 hr lactate exposure (Figure 25, Figure 26). MDA-MB-231 and R3230Ac cells showed no significant change in colony formation with lactate treatment (+glucose) (Figure 27). What is interesting about this result is that MDA-MB-231 cells lack MCT1 expression; MCT1 silencing may render this cell line less sensitive to the presence of exogenous lactate. This mechanism could be confirmed in future studies via overexpressing MCT1 in MDA-MB-231 cells. Restoring lactate-induced growth inhibition would support the hypothesis that MCT1 is required for clonogenic sensitivity to exogenous lactate. The reason for the observed clonogenic insensitivity of R3230Ac cells to lactate treatment is not due to a lack of MCT1 since we have found evidence of abundant MCT1 expression in R3230Ac tumor tissue [290]. A likely explanation for R3230Ac clonogenic survival is the finding that R3230Ac tumors are avid lactate consumers [290]. For this tumor line, lactate seems to be more of a fuel than a poison at physiologic and pathophysiologic concentrations.

Of note, the HepG2 cell line showed a significantly different response to lactate treatment than other cell lines tested. Specifically, in the clonogenic survival showed a dramatic increase after 18 hr or 1 week exposure to exogenous lactate, but the 48 hr treatment showed a decrease in clonogenic survival. One possible reason why there was such a discrepancy in HepG2 results is cellular detachment. If the control group was

detaching from the plate, this would skew results because all the experimental groups are normalized to the control. One method of cell protection may come from resistance to anoikis [323], as suggested by the observations of cellular detachment with lactate treatment. For this to be determined, further studies are needed.

Therapeutically targeting lactate metabolism in tumor cells has been proposed [18, 141, 297, 305], and CHC has been the drug of choice for MCT1 inhibition in some studies [141, 297]. Despite the ability of 5mM CHC to inhibit lactate catabolism and extrusion at 40mM concentrations [290], we found that 40mM of exogenous lactate had no significant effect on the cell death responses of MC7 and R3230Ac cells (Figure 34, Figure 35). High CHC elicited significant cell death independent of addition of exogenous lactate, indicating another mechanism or off-target effects are responsible for cancer cell death at this concentration of CHC. These results suggest that CHC may not be the best therapeutic MCT1 inhibitor. Other MCT1 inhibitors have elicited cancer cell death via decreased pH_i with treatment [211].

Table 17 combines the results from Section 4, Section 5 and [290] to summarize the different lactate phenotypes of the breast lines tested, including the cell viability response (including CHC treatment), lactate uptake and utilization and implications of MCT1 inhibition. MCT1 inhibition has received attention in recent years [18, 141, 211, 297, 305, 306]. Our studies support the concept that it is important to first know the metabolic phenotype of the individual tumor before administering metabolic

intervention. As seen in our study, breast cancer cell line survival varies in response to exogenous lactate, with some showing sensitivity to high lactate (MCF7) while others show little to no change in viability in response to high lactate (R3230Ac, MDA-MB-231, Table 17). Given these observations, it would make sense to inhibit lactate excretion in MCF7 cells, which are sensitive to high lactate. We also showed that catabolite generation from extracellular lactate was not equal in relative rates or amounts, with MDA-MB-231 cells showing smaller peaks of alanine and glutamate compared to R3230Ac or MCF7 cells (Table 17). Inhibiting lactate uptake in aerobic R3230Ac cells may starve their hypoxic neighbors (metabolic symbiont); however, MDA-MB-231 cells may not be a good candidate for manipulation of lactate pathways, as they lack MCT1 and show little relative lactate consumption (Table 17). Given these inherent differences, it is clear that therapeutically targeting tumor metabolism would need to be tailored to particular metabolic phenotypes.

Table 17: Summary of breast cell line responses to exogenous lactate

Condition	R3230Ac	MCF7	MDA-MB-231	HMEC
Sensitivity to high lactate (cell survival)	Insensitive	Sensitive	Insensitive	Sensitive (clonogenically)
MCT1	+	+	-	+
Lactate uptake	Yes, quicker than glucose *in vivo*	Yes	Yes	Yes
Lactate catabolites produced / detected	Alanine (relatively higher *in vitro* than other breast cell lines), glutamate	Alanine, glutamate, pyruvate	Alanine (relatively less than R3230Ac and MCF7), glutamate (relatively less than R3230Ac and MCF7), pyruvate	Alanine and glutamate
Lactate catabolites extruded (24 hr)	Alanine (relatively quicker *in vitro* than other breast cell lines), glutamate	Alanine and glutamate	Alanine and glutamate (very little *in vitro* compared to R3230Ac and MCF7)	Not tested
Effects of low CHC	Inhibition of lactate uptake (≤20mM) *in vitro*. No cell death	No cell death	Not tested	Not tested
Effects of high CHC	Inhibition of lactate uptake (≤20mM) *in vitro*; incomplete inhibition of lactate uptake at 40mM lactate. Significant cell death independent of lactate addition.	Significant cell death independent of lactate addition.	Not tested	Not tested
Lactate phenotype (relative)	High lactate consumer	Average lactate consumer	Low to average lactate consumer	Low lactate consumer
Strategy	Inhibit lactate consumption in aerobic cells	Inhibit lactate extrusion	None / lactate pathways not targeted	Minimize toxicity of MCT1 inhibition
Model / assumption	Metabolic symbiont model	Cancer cell death in high lactate conditions	Insensitive to MCT1 inhibition	Not tested

6. MCT1 and MCT4 as Potential Markers of Cycling Hypoxia

6.1 Introduction

In many different solid tumors, tumor hypoxia has been shown to significantly correlate with poor patient prognosis and survival and increased incidence of metastases [54-59]. In Section 1.1.2, the causes of and differences between chronic and cycling tumor hypoxia were briefly discussed. It is important to distinguish between these two types of hypoxia because cancer cells experiencing cycling hypoxia appear to demonstrate molecular and physiological responses consistent with a more aggressive phenotype [53, 56, 101, 324]. Hypoxic cancer cells display treatment resistance for several reasons: 1. Treatment cannot be delivered; 2. decreased proliferation due to increased distance from blood vessels [61, 325, 326]; 3. Increased selection of cells that lack sensitivity to p53-mediated apoptosis; 4. Lack of oxygen present in the immediate TME renders some treatments (e.g.radiation) ineffective [45, 327]; and 5. Hypoxia upregulates genes involved in multi-drug resistance [328, 329]. Cycling hypoxia, as opposed to chronic hypoxia, has been specifically implicated in contributing to chemoresistance and radioresistance via stabilization of HIF-1α through reactive oxygen species (ROS) signaling [330-333].

Reliable biomarkers of cycling hypoxia do not currently exist. It may be possible to connect MCT subtype regulation and the different hypoxic states. It has been shown that in some cancer cells MCT subtypes are specifically expressed, with MCT1 being more abundant in cells with the potential for lactate oxidation while MCT4 is restricted to the more glycolytic cells. SiHa cervical cancer cells, which were found to be able to import and utilize lactate, express abundant MCT1 and little MCT4, while the reverse was found for the more glycolytic cell line WiDr [141]. Given that HIF-1α has been found to upregulate MCT4 mRNA and protein expression while having no effect on MCT1 expression [334], it is possible that these MCT subtypes are also specifically expressed in aerobic (more abundant MCT1) and hypoxic cells (more abundant MCT4). Previous studies conducted in non-small cell lung cancer biopsies showed that MCT1 did not colocalize with EF5, a hypoxia marker drug [141]. We hypothesized that the dual expression of MCT1 and MCT4 could be used as a biomarker for cycling hypoxia.

6.2 Results

We explored MCT1 and MCT4 regulation in a number of cell lines after exposure to different oxygenation states and exogenous lactate. We anticipated MCT4 upregulation in response to hypoxia and MCT1 upregulation in response to lactate. After examining if MCT1 and MCT4 co-expression were upregulated after exposure to cycling hypoxia, we tested human frozen tumor biopsies for expression of these two transporters.

6.2.1 MCT1 and MCT4 regulation with lactate exposure and hypoxia

6.2.1.1 Coverslip IF shows positive MCT1 expression in normoxic conditions and positive MCT4 expression in hypoxic conditions

First we established MCT1 and MCT4 baseline expression using IF on single cells grown on glass coverslips. It has been documented that many cancer cells express and show upregulation of MCT1 (Table 4) [172, 180, 208, 335], so virtually any cancer cell line could be chosen as a positive control. We chose to use SiHa cells as our MCT1 positive control. MDA-MB-231 cells have been shown to be negative for MCT1 expression due to hypermethylation [203] and were used as a negative control for MCT1. Previous reports indicate that SiHa cells express MCT1 but lack MCT4 while WiDr cells express MCT4 but lack MCT1 [141]. WiDr cells served as our MCT4 positive control, while SiHa was our negative control for MCT4. Also included was a negative staining control that omitted the primary antibody to ensure there was no background from the secondary antibody. As seen in Figure 36 and Figure 37, our coverslip IF protocol for detecting both MCT subtypes was reliable: SiHa cells showed MCT1+ and MCT4- expression (Figure 36, Figure 37), MDA-MB-231 cells showed no MCT1- expression (Figure 36), and WiDr cells showed MCT4+ expression (Figure 37).

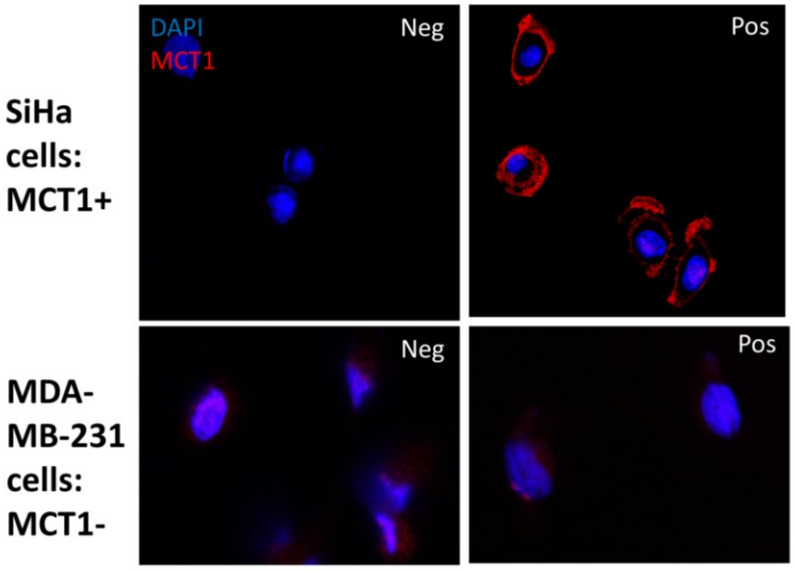

Figure 36: Coverslip IF demonstrating reliable detection of MCT1. SiHa cells (positive MCT1 control, top) but not MDA-MB-231 cells (negative control, bottom) displayed membrane expression of MCT1 (red) when grown on glass coverslips.

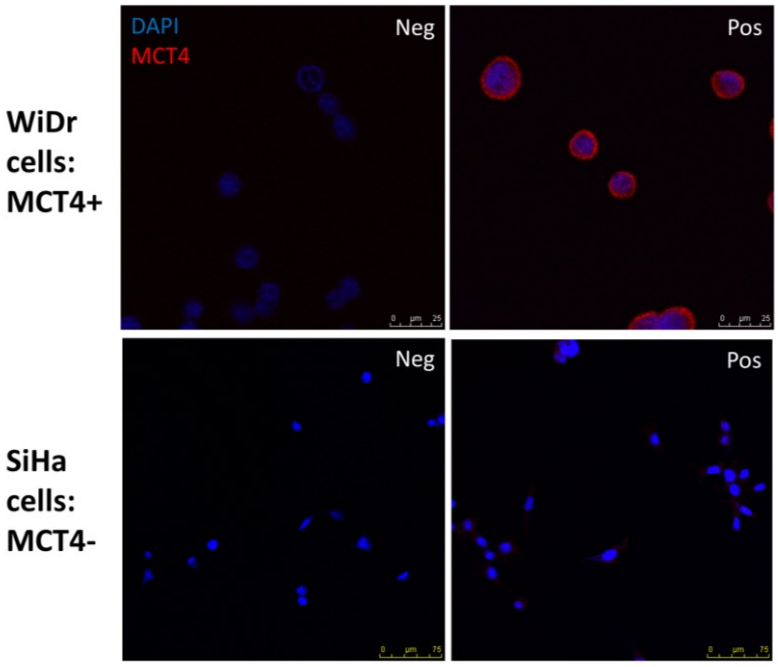

Figure 37: Coverslip IF demonstrating reliable detection of MCT4. WiDr cells (positive MCT4 control, top) but not SiHa cells (negative control, bottom) displayed membrane expression of MCT4 (red) when grown on glass coverslips.

6.2.1.2 MCT1 and MCT4 are regulated by lactate and hypoxia *in vitro*; cycling hypoxia upregulates both MCT1 and MCT4

6.2.1.2.1 MCT1 is upregulated with addition of exogenous lactate

The 'metabolic symbiont' model of lactate consumption states that lactate is consumed by MCT1-expressing, aerobic cells, allowing glucose to reach the neighboring MCT4-expressing hypoxic cells [141]. This led us to hypothesize that exogenous lactate might upregulate MCT1 expression and downregulate MCT4 expression. MCT1 total

protein expression was analyzed after exposure to 10mM of exogenous sodium lactate for different exposure times (1-48 hr).

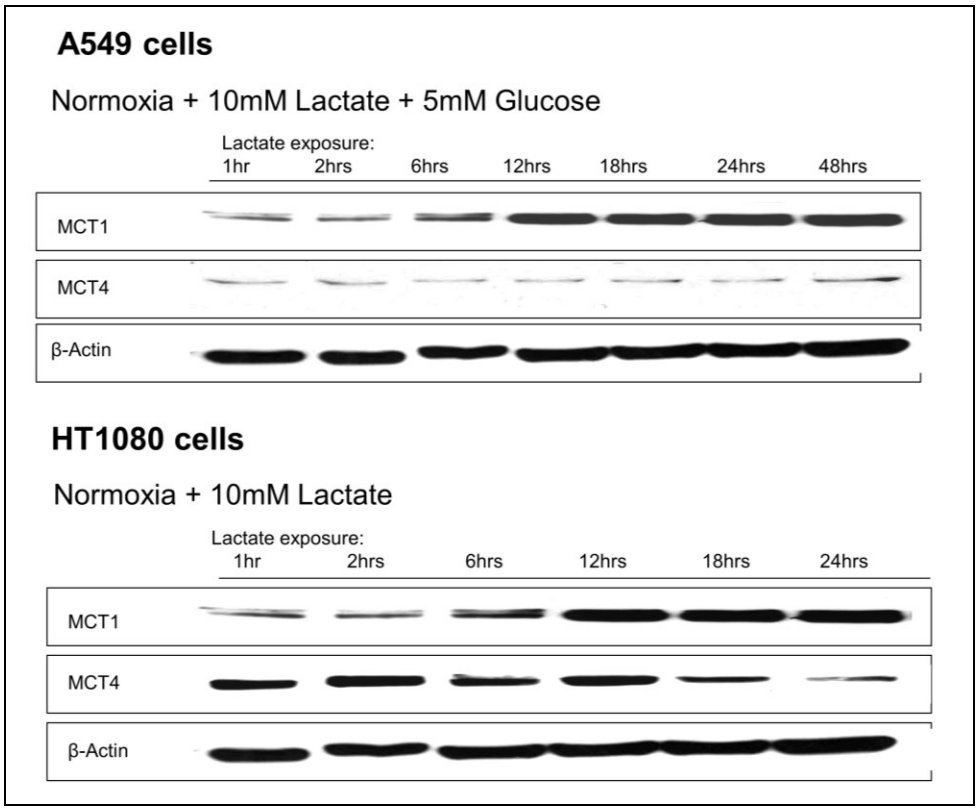

Figure 38: MCT1 expression increased after treatment with exogenous lactate. Representative Western blots of the time course of MCT1 and MCT4 expression changes in A549 (top) and HT1080 cells (bottom) after exposure to 10mM lactate. MCT1 increased in each cell line as the duration of lactate exposure increased.

Both A549 and HT1080 cells showed a time-dependent increase in MCT1 expression with 10mM lactate, with levels reaching the maximum expression ~12 hr. Additionally, MCT4 expression in HT1080 cells decreased over time after exposure to 10mM lactate (Figure 38). A549 cells did not show changes in MCT4 expression after the

lactate stimulus (Figure 38), but overall expression of MCT4 is low in this cell line (Figure 39, normoxia). The overlapping time points for similar levels of expression for both transporters in HT1080 cells is roughly between 6 and 12 hr (Figure 38).

6.2.1.2 MCT4 is upregulated and MCT1 is downregulated by chronic hypoxia; cycling hypoxia upregulates both MCT1 and MCT4

We next sought to characterize MCT1 and MCT4 expression after chronic and cycling hypoxia (0.5% O_2). In A549 cells, MCT1 expression diminished after 18 hr exposure to chronic hypoxia (Figure 39). At 24 hr, there was evidence of some recovery of MCT1 expression; however, the protein levels were still below baseline (normoxia, Figure 39). MCT4 showed an increase in expression as early as 1 hr after chronic hypoxia, and this increase in expression continued through 18 hr, at which time, the protein levels appeared to stabilize (Figure 39). Likewise, MCT1 protein levels in HT1080 cells decreased after 6 hr exposure to chronic hypoxia, and MCT4 expression increased after 2 hr in chronically hypoxic conditions (Figure 39). A549 cell showed transporter co-expression throughout the time course of exposure to chronic hypoxia, though the higher expression levels of both transporters were between 1-12 hr of chronic hypoxia exposure (Figure 39). Chronically hypoxic HT1080 cells show co-expression of MCT1 and MCT4 for a shorter time period, with the 2 hr time point showing relatively

similar protein levels of each (Figure 39). These time frames are windows of opportunity for MCT co-expression under chronic hypoxia.

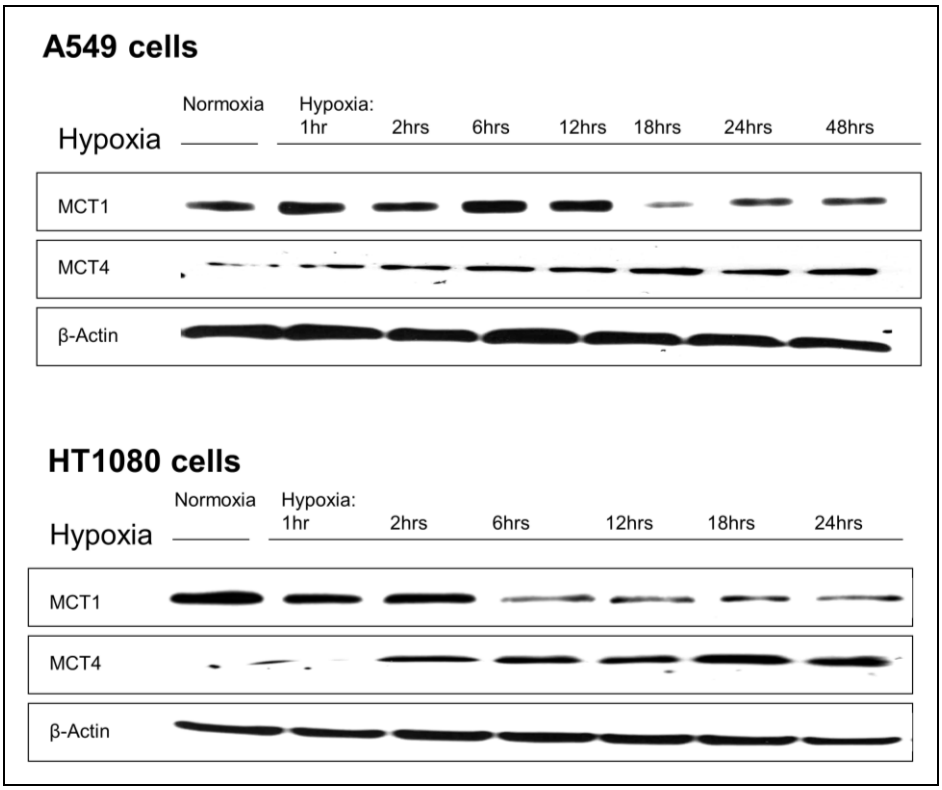

Figure 39: MCT1 expression decreased and MCT4 expression increased after exposure to chronic hypoxia. Representative Western blots of the time course of MCT1 and MCT4 expression changes in A549 (top) and HT1080 cells (bottom) after exposure to 0.5% O_2. In both cell lines, MCT1 protein expression was downregulated and MCT4 protein expression was upregulated after prolonged exposure to hypoxia.

Following the results from the chronic hypoxia experiments, we hypothesized that cycling hypoxia would result in a greater expression of both transporters and that re-oxygenation would elicit an even greater co-expression. Indeed, after 3 and 5 cycles of hypoxia, both A549 and HT1080 cells showed upregulation of total protein of both

transporters (Figure 40). When cells were re-oxygenated for 12 hr between cycles, both cell lines showed a dramatic increase in MCT1 and MCT4 protein (Figure 40). These results indicate that co-expression of these MCTs are viable markers of cycling hypoxia.

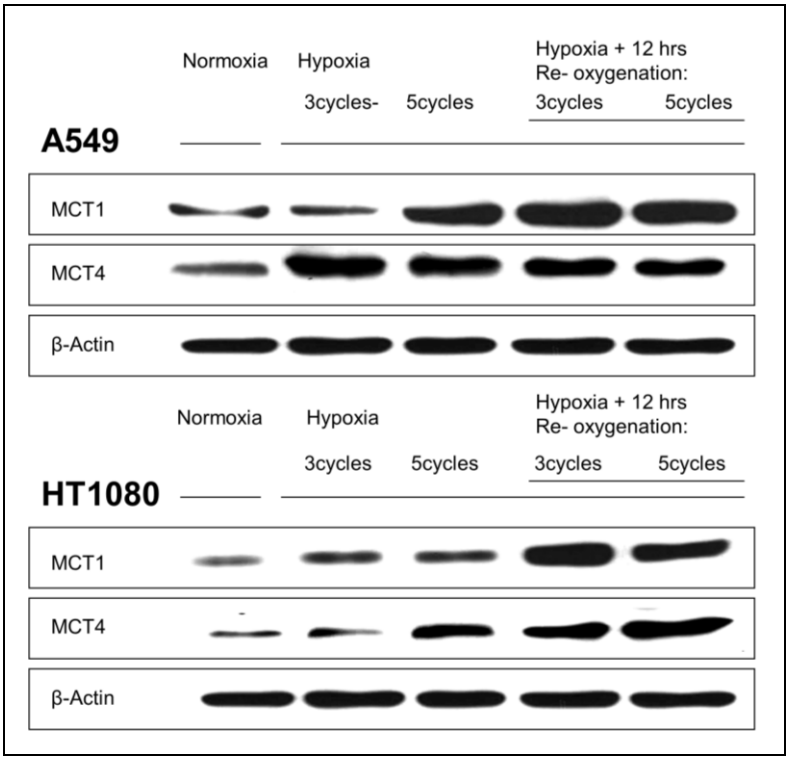

Figure 40: MCT1 and MCT4 expression increased with exposure to cycling hypoxia and re-oxygenation. Representative Western blots of MCT1 and MCT4 protein expression changes in A549 (top) and HT1080 cells (bottom) in response to cycling hypoxia. After 3-5 cycles of hypoxia and 12 hr re-oxygenation, MCT1 and MCT4 protein was upregulated in both cell lines.

6.2.2 MCT1 and MCT4 expression in human cancer biopsies

6.2.2.1 Seventy percent of LABC biopsies show positive expression of MCT1

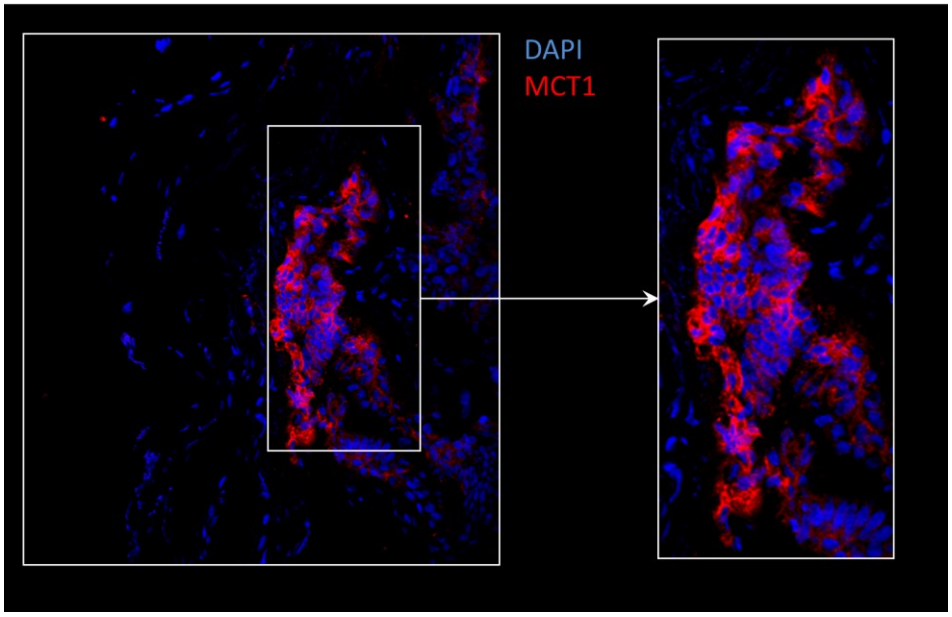

Figure 41: Seventy percent of LABC biopsies showed expression of MCT1. Representative image (n=3) of positive MCT1 (red) IF in a locally advanced breast cancer biopsy.

In Section3, we investigated lactate accumulation in LABC and correlated lactate levels to patient outcome and clinical parameters. We now performed IF on the frozen sections available to determine what percentage of samples showed expression of MCT1. Seventy percent of the 25 biopsies showed positive staining for MCT1. We found that expression of MCT1 in LABC was not uniform, with islands of MCT1 tissue expression among the negative surrounding tissue (Figure 41).

6.2.2.2 MCT1 and MCT4 expression in HNSCC

Samples from nine patients with head and neck squamous cell carcinomas were also immunostained for MCT1, MCT4 and the hypoxia marker EF5. The hypoxia marker EF5 had been infused 12 hr prior to surgery in all patients. Interpretation was challenged by substantial bleed-through of the EF5 signal (red channel) into the MCT4 signal (green channel) during confocal imaging (Figure 42). This bleed-through was not evident in MCT1 staining (Figure 43). Thus, the MCT subtype analysis on the frozen HNSCC tissue was restricted primarily to the MCT1 expression. When MCT4 results are mentioned, appropriate caveats will be reiterated.

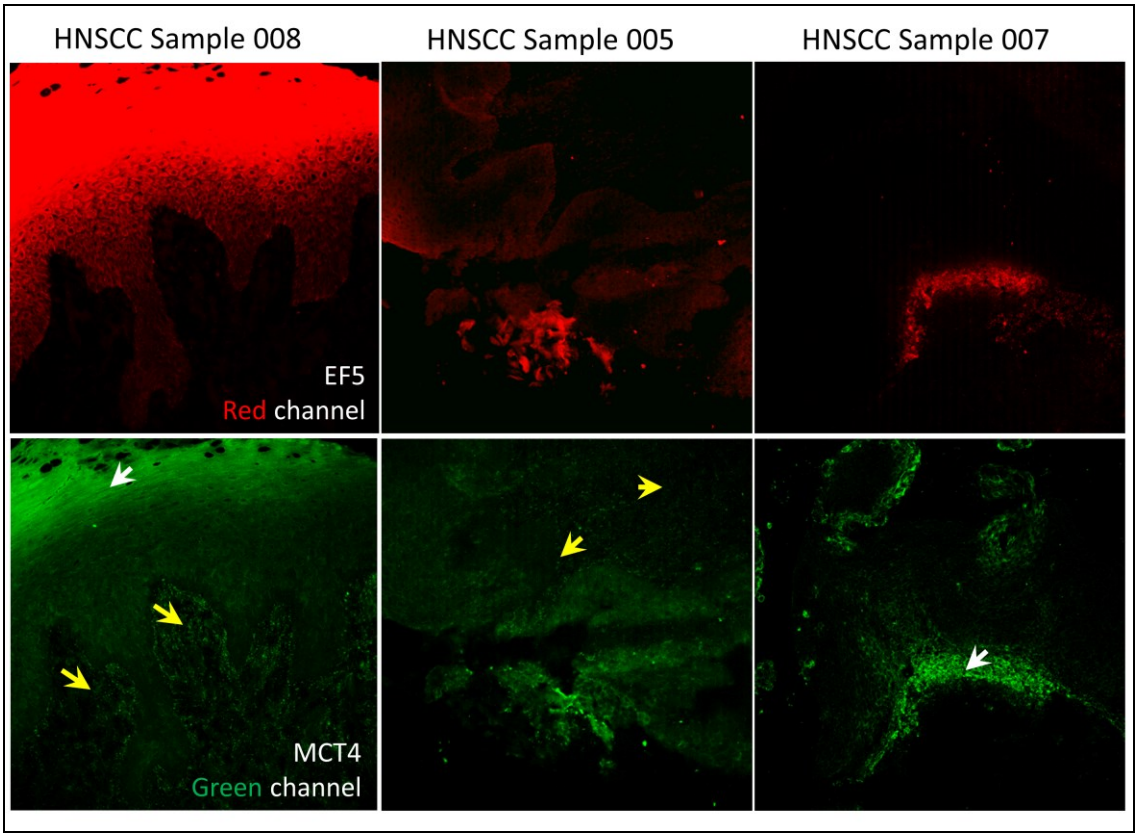

Figure 42: Demonstration of IF artifacts in head and neck patient biopsies. EF5 (red) signal bleed-through to the MCT channel (green) is marked by the white arrows. High background in the MCT channel from secondary antibody is marked by the yellow arrows.

HNSCC samples from all patients (n=9) were positive for MCT1. In normoxic regions, indicated by negative EF5 staining, there was a significantly higher percentage of MCT1 expression compared to apparent MCT4 expression (p<0.001) (mean MCT1: 94% ± 5.3; mean MCT4: 10% ± 13.5) (Figure 44). In areas of high EF5 signal, there was a significantly lower percentage of MCT1 expression compared to apparent MCT4 expression (p<0.001) (mean MCT1: 6% ± 5.3; mean MCT4: 89% ± 13.4) (Figure 44).

However, given the limitations of MCT4 signal mentioned in the previous paragraph, the inverse relationship between MCT1 and MCT4 expression cannot be confidently concluded.

Comparing the percent MCT1 staining in normoxic vs. hypoxic tumor regions, it was found that MCT1 signal was significantly higher in normoxic regions (Student's T-test, $p<0.0001$, Figure 44A). The percent MCT1-positive area in HNSCC sections correlated positively to the percent of normoxia (defined as being non-necrotic EF5-negative tissue; $r= 0.9$, $p<0.0001$, Figure 44B) and negatively to percent of hypoxia (strong EF5 signal).

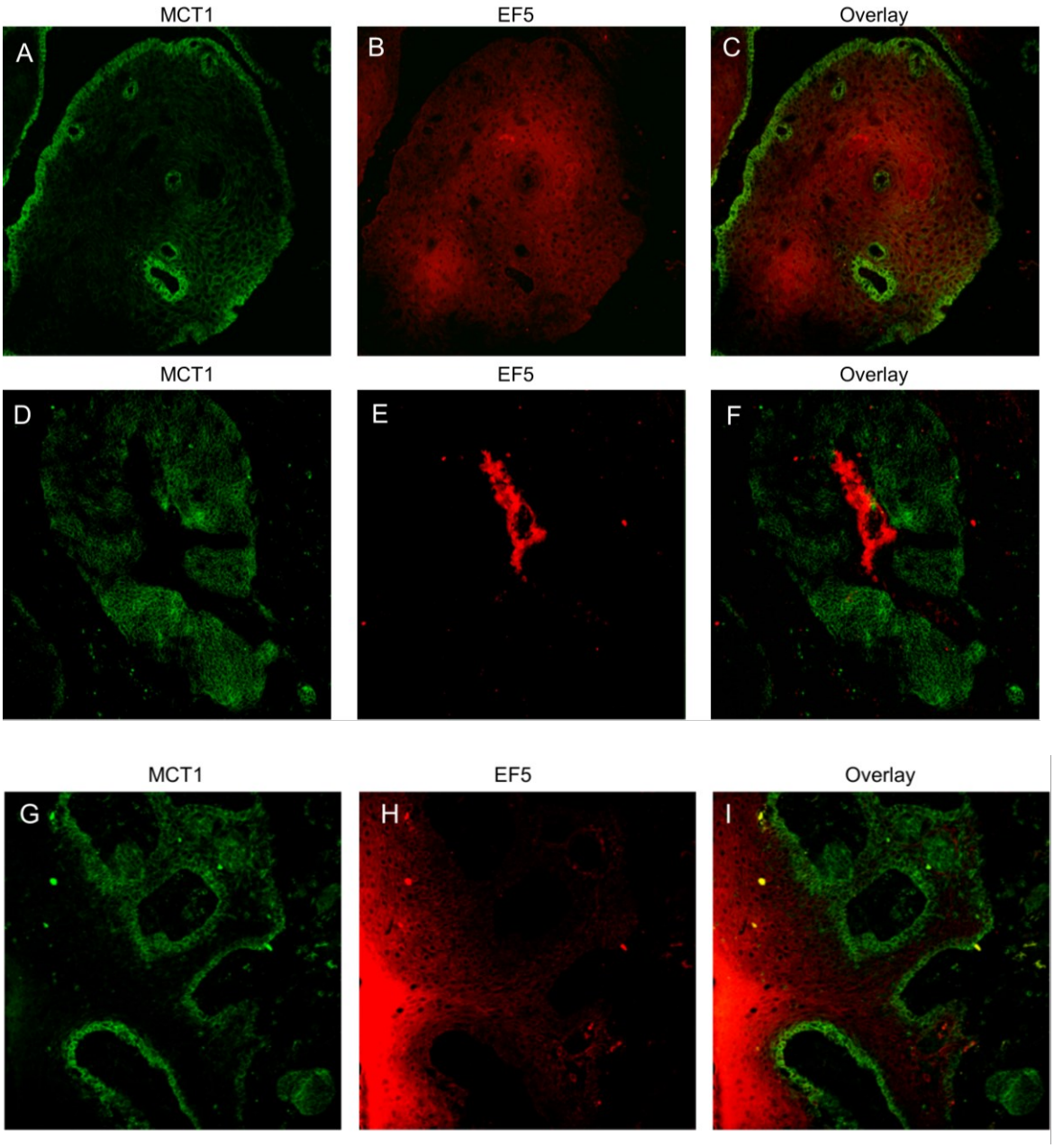

Figure 43: Representative images (n=3) demonstrating of the inverse relationship between MCT1 expression (green) and hypoxia (EF5, red) in human head and neck cancer samples.

This study demonstrated a strong inverse relationship between MCT1 expression and hypoxia in human HNSCC samples.

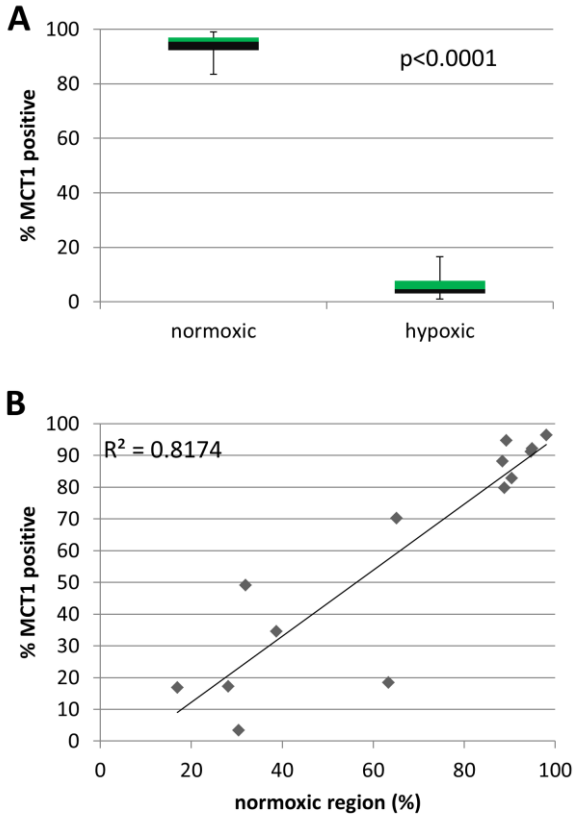

Figure 44: MCT1 expression is significantly correlated to normoxic regions of human head and neck cancer specimens. Positive MCT1 staining (n=3 per section) in HNSCC biopsies (n=9) is significantly higher in normoxic regions than in hypoxic regions ($p<0.0001$, A), and MCT1 signal is highly correlated with normoxia (negative EF5 staining) ($r=0.9$, $p<0.0001$, B).

6.3 Discussion

MCT subtypes 1 and 4 have been reported to be upregulated in cancer cells [172, 180, 208, 335]. Our investigation found evidence of expression of both transporters in a

majority of the cells tested. LABC and HNSCC human samples were positive for MCT1, as anticipated. Exposure to exogenous lactate upregulates MCT1 expression, as seen in the Western blots. These results paired with the lactate uptake shown in breast cancer cells (Section 4.2) support the possibility of lactate uptake in LABC.

Examination of the expression patterns of the two monocarboxylic transporters in relation to chronic and cycling hypoxia in cell-based experiments showed a striking difference in the oxygen-dependent expression. MCT1 was downregulated within 18 hours under chronic hypoxic conditions, whereas MCT4 upregulation was seen at 2 hours under chronic hypoxic conditions. In cycling hypoxia (5 cycles of hypoxia) MCT1 and MCT4 expression was clearly upregulated, showing an even greater increase after reoxygenation. The time delay between MCT4 upregulation after hypoxia (~2 hr) and MCT1 downregulation (~6-18 hr) provides an opportunity for transporter co-expression. These results paired with the concordant upregulation of both transporters after exposure to cycling hypoxia supports the hypothesis that MCT1 and MCT4 overlap in tumor biopsy samples could be used as markers of cycling hypoxia.

Ullah and colleagues showed that MCT4 was upregulated through a HIF-1α-dependent mechanism [334], whereas MCT1 was downregulated under hypoxic conditions in a HIF-1α independent manner. The author concluded that upregulation of MCT4 was a necessary adaptive response of hypoxic cells, allowing the accumulated lactate to be released [334]. Taking the metabolic symbiont model into consideration

[141], downregulation of MCT1 in hypoxic conditions may prevent uptake of additional lactate into the cell. This is advantageous because hypoxic cells cannot oxidize lactate for ATP production. Our group's recent findings indicate that hypoxic cells retain the ability to take up lactate after 12 hr exposure to chronic hypoxia if extracellular lactate is very high; however, the lactate is not metabolized [290]. Downregulation of MCT1 under hypoxia may prevent lactate uptake at lower concentrations.

Hypoxia in tumors is a well-established cause of resistance to radiation and chemotherapy. However, a large body of evidence suggests that molecular effects of chronic and cycling hypoxia differ considerably. Graeber *et al*. showed that multiple rounds of hypoxia selected for tumor cells that are resistant to apoptosis [53] and cycling hypoxia also selects for tumor cell mutations [101]. Mutation frequency increased with each cycle of hypoxic exposure, which could lead to tumor progression and treatment resistance [336, 337]. Studies investigating oxidative stress have shown that cycling hypoxia increased HIF-1α protein expression through molecular mechanisms that are distinct from chronic hypoxia [338]. These molecular differences between chronic and cycling hypoxia are consistent with our study, which demonstrated substantial increase in MCT4 and MCT1 under cycling hypoxia when compared to chronic hypoxia.

Cycling hypoxia has been shown to occur in murine xenograft models [339], as well as in spontaneous canine tumors [340]. Even so, there are only two published studies that directly studied whether there is fluctuating pO_2 in human tumors. It has

been shown pre-clinically that fluctuations in red cell flux are responsible for cycling hypoxia [341, 342]. Temporal changes in red cell flux have been measured in superficial human tumors, suggesting the possibility that cycling hypoxia exists. Second, a clinical study in a small number of patients with head and neck cancer demonstrated fluctuations in uptake of the hypoxia PET tracer, 18F-misonidazole over a 3-day interval [343]. Our study was able to begin to characterize expression patterns of MCT1 and MCT4 that seem to be consistent with chronic and cycling hypoxia in a unique set of human tumor specimens that were obtained from head and neck cancer patients after an EF5 infusion. All tumors tested expressed MCT1 and a portion of the tumors tested expressed MCT4. Though there were some limitations in our study, including nonspecific background in the MCT4 staining and evidence of bleed-through of the EF5 signal, these issues can be addressed in future studies with a higher quality or a more specific MCT4 antibody and more stringent attention to image settings. With these suggested modifications, this tandem staining approach may be a promising tool to assess tumor oxygenation status in human tumor biopsies. Our study showed that aerobic areas of the specimens, identified by lack of EF5 staining, strongly correlated with MCT1 expression on individual cell membranes. Additionally, hypoxic areas of the specimens, identified by presence of EF5, showed a strong negative correlation with MCT1 expression, and there was some evidence of EF5 correlation with MCT4 expression. Though we could not reliably quantify areas of potential overlap between

expression of transporters due to the methodology limitations, visually, it can be seen that there are areas where both transporters are expressed. It is these areas of potentially overlapping signal that may indicate cycling hypoxia.

In conclusion, the quantification of overlap between MCT1 and MCT4, once validated in other sample sets, may be a useful tool to estimate the amount of cycling hypoxia in a tumor sample. Further studies are needed to verify our preliminary results before assessment of the prognostic importance of this marker and future possibilities with MCT inhibition-based therapies can be adequately addressed.

7. Conclusions and Future Directions

7.1 Consequences of lactate metabolism

My work focused on mainly lactate uptake and catabolism, MCT1 and MCT4 regulation, and cell survival responses to exogenous lactate. However, there are many more aspects of lactate metabolism that were not addressed: redox status / oxidative stress, mitochondrial health and function, and pH influences (mentioned in Section 1.2.4), among others. Some of these influences will be discussed briefly.

Redox balance was not addressed in our study, but it is important to mention the possible effects of exogenous lactate uptake on cellular NAD+/NADH levels. Unpublished studies from members of our group have demonstrated that NAD+ is depleted in cancer cell lines after lactate is taken up. This makes sense, as NAD+ is a cofactor for the lactate to pyruvate conversion, resulting in NAD+ depletion and NADH accumulation. Interactions in which NAD+ participates can be separated into two broad categories: metabolic redox reactions and non-redox signaling. In redox metabolism, NAD+ is necessary for beta oxidation, glycolysis and the tricarboxylic acid (TCA) cycle. NAD+ serves as an important oxidizing agent for reduced molecules such as glucose and fatty acids. Without NAD+, these reactions come to a halt and many enzymes in the

TCA cycle, including citrate synthase, isocitrate dehydrogenase and α-ketoglutarate dehydrogenase, are inhibited by increased NADH [49].

NAD+ also acts as a signaling molecule in non-redox reactions, e.g. acting as a substrate for sirtuins. The sirtuins are a class of histone deacetylases that regulate transcription, apoptosis and cell stress responses [344]. SIRT1 regulates or interacts with a host of metabolic factors, including HIF-1 α [345]and PGC-1α [346]. NAD+ depletion can result in aberrant signaling by sirtuins in general [344]. Depletion in NAD+ also induces genotoxic stress [347] and PARP-1 induction [348, 349], which leads to cell death. If cells cannot mitigate the effects of NAD+ by some other means, it is possible that NAD+ depletion with exogenous lactate uptake and conversion to pyruvate may elicit cell stress.

Diers *et al*. compared the cellular effects of pyruvate v. lactate (+ and – glucose) metabolism in MCF7 cells, showing that 1mM lactate treatment significantly reduced the mitochondrial reserve capacity [307]. Mitochondrial reserve capacity is important to maintaining normal cell and organ functioning under conditions of oxidative stress or ischemia; depletion of the reserve capacity can eventually become lethal [350-352]. My studies used 10-40mM lactate, concentrations far greater than the 1mM lactate treatment used in the above-mentioned study. There is a very high likelihood that the reduced mitochondrial reserve capacity contributed in part to increased cell death responses at high lactate levels. Additionally, it is well-documented that many cancers, including

breast cancer, harbor mutations in mtDNA [70], have increased levels of ROS / oxidative stress [70] and lower activity of superoxide dismutase (SOD) and particularly of the mitochondrial-associated MnSOD [353]. Treatment with exogenous lactate has been documented to significantly increase superoxide anion generation in cardiac myocytes [354]. Exogenous lactate (10mM) also significantly increased ROS in endothelial cells, leading to activation of NF-KB [246]. Thus, one of the effects of exogenous lactate is to influence ROS production, exacerbating the already elevated oxidative stress in cancer cells and mutating DNA to contribute to tumor progression [355].

7.2 Tumor metabolism manipulation as a therapeutic strategy

The cellular responses to exogenous lactate must be taken into account when evaluating the potential of manipulating tumor metabolism for therapeutic purposes. It is already well-established that tumors show a higher glycolytic rate than normal tissue [14, 46, 48, 356]. One attempt at modifying tumor metabolism was the use of dichloroacetate (DCA) to stimulate oxidative phosphorylation in tumor cells via suppression of aerobic glycolysis by inhibiting the activity of PDK1 and PDK3 [357, 358]. This treatment is relevant to the manipulation of lactate biochemical pathways because by inhibiting PDK activity, there is the potential for greater utilization of lactate. In fact, DCA has been used for decades to treat congenital and acquired lactic acidosis under the premise of forcing pyruvate oxidation [359]. *Ex vivo* and *in vitro* experiments with DCA

treatment demonstrated a significant increase in apoptosis via mitochondria depolarization in GBM tissue and in cancer cell lines (lung, breast) with no toxicity to normal tissue/cells [358, 360]. Additionally, when DCA was supplemented in drinking water, A549 tumors grown in mice showed a significant decrease in size, significantly increased apoptosis (as measured by TUNEL staining) and significantly decreased proliferation of tumor cells (as measured by PCNA staining) after 12 weeks of treatment [358]. In contrast, a 2011 study found that DCA treatment did not significantly influence tumor growth, recurrence or likelihood of metastases in MDA-MB-231 xenografts in mice [361]. Researchers determined that the ineffectiveness of DCA treatment was due to hypoxia [361], illustrating the importance of taking into account all tumor microenvironmental factors when considering anti-cancer treatments.

In recent years the pharmacological inhibition of MCTs, specifically MCT1 with α-cyano-4-hydroxycinnamate (CHC), has gained attention as a potential cancer therapy [18, 141, 362]. The metabolic symbiont model describes a theory of substrate sharing between hypoxic and aerobic cells, specifically that MCT1-expressing, aerobic tumor cells may use lactate produced by their MCT4-expressing, hypoxic neighbors. It is proposed that MCT1 inhibition will force the aerobic cells to use the glycolytic pathway, thereby starving the hypoxic tumor cells of glucose [18, 141]. Part of my dissertation focused on the potential of MCT1 and MCT4 to serve as biomarkers of oxygenation status of tumors (Section 6). Our results supported *in vitro* findings from the study

mentioned above: aerobic tumor regions demonstrated significantly higher MCT1staining and hypoxic tumor regions seemed to show significantly higher MCT4 staining, although this needs confirmation with more rigorous testing. The areas corresponding to low EF5 seemed to show overlapping MCT1 and MCT4 signals, indicating potential cycling hypoxia occurring in these tumor regions. Considering the K_m values of each transporter for lactate (MCT1 = ~3.5mM, MCT4 = ~28mM) [136], the likelihood of MCT1 transporting extracellular lactate (at concentrations <28mM) inside the cell is greater than the probability of MCT4-mediated lactate uptake. This work lends greater support to the metabolic symbiont model.

In a 2008 study, treatment with CHC resulted in slower tumor growth by over 2-3 weeks in both a Lewis Lung carcinoma line (LLc) and in WiDr colorectal cancer line in mouse xenograft models. Additionally, tumors with MCT1 inhibition showed histological evidence of increased necrosis [141, 362]. While these results look promising, several issues have been raised in regard to CHC treatment. There is still the question of the mechanism of tumor growth delay. Though the proposed metabolic symbiont model suggests that slowed tumor growth is due to the lack of lactate oxidation available to aerobic tumor cells after CHC addition, this has still not been confirmed *in vivo*. It is unclear if such results are due to MCT1 inhibition primarily preventing lactate uptake or preventing lactate release. Fang *et al*. found that MCT1 inhibition by lonidamine and CHC led to a lethal decrease in intracellular pH [211]. Adding to the mechanistic

concerns, Halestrap has commented on the specificity of the MCT1 inhibitor, noting that CHC also is a potent inhibitor of the mitochondrial pyruvate carrier (MPC) [221], which carries similar substrates, such as pyruvate. There is also the concern of the systemic effect of MCT1 inhibition, as MCT1 is expressed in nearly every organ and is functionally very important to heart, brain and skeletal muscle [363]. Encouragingly, a recent study has indicated that mice receiving CHC treatment at 9.5 μM/day showed no signs of morbidity with treatment alone [362]. Should be noted that this CHC concentration is an order of magnitude lower than what has been used in some *in vitro* studies [141, 297].

Although the initial *in vivo* results of tumor growth delay with MCT1 inhibition by CHC were intriguing [141], these results were not recapitulated in a prostate cancer model which was verified to express MCT1; however, CHC treatment did significantly increase the necrotic fraction of these tumors [362]. Taken together, this does not dismiss MCT1 as a viable target for cancer therapy; it illuminates the need for further investigation. What is also coming to light are the more diverse roles of MCT1 besides metabolism, such as activating NF-KB and contributing to angiogenesis in endothelial cells [246] and its interaction with p53 [192]. Indeed, with several mechanisms of induced cell death due to MCT1 inhibition already documented [141, 211], there are a number of avenues to explore when employing MCT1 inhibition as a therapy. What

needs to be clarified for clinicians are the consequences and downstream effects of this inhibition on the tumor metabolism and systemic metabolism.

In Section 5 and [290], cell viability post-lactate treatment and post-CHC treatment was evaluated in a variety of cell lines. Dramatic differences in lactate sensitivity among cell lines were seen (Table 17). These cell lines also showed similar metabolite generation from extracellular lactate but differences in the relative rate/amount of lactate metabolism (Section 4, Table 17, [290]). These comparisons highlight the heterogeneity in cellular responses to exogenous lactate and indicate that targeting lactate metabolism in tumors is not a "one-size fits all" solution. In fact, the two breast cancer cell lines (R3230Ac and MDA-MB-231) that showed no significant changes in cell viability in response to exogenous lactate demonstrated very different lactate-consuming phenotypes and levels of MCT1 expression (Table 17). Therefore, it cannot be assumed that cells or a tumor that sustain viability in high lactate conditions also avidly utilize lactate. One reason for the dramatically different phenotypes between R3230Ac and MDA-MB-231 cells could be that MCT1 expression is high in R3230Ac cells but low in MDA-MB-231 cells; however, MCF7 cells, which express MCT1, showed a significant decrease in colony formation with 10mM and 40mM lactate. These results imply that expression of MCT1 alone does not determine the cellular response to exogenous lactate.

Many different factors influence tumor cell metabolism, including p53 status, HIF-1α expression/stabilization, and myc expression, among others [364]. In my studies, several different breast lines were included to begin characterizing differences in lactate metabolism and cellular responses to extracellular lactate among breast cell lines. HMEC cells were included to compare a normal cell response to exogenous lactate with cancer cell responses to lactate. Both MCF7 and MDA-MB-231 cells were included as breast cancer models for a number of reasons. First, we wanted to represent a luminal (MCF7) and a basal-like (MDA-MB-231) breast cancer subtype [365], as these subtypes are known to be considerably different clinically and pathologically [365-367]. Second, R3230Ac and MCF7 cells are p53 WT [368-370] while MDA-MB-231 cells are p53 null [371, 372]. p53 influences many metabolic pathways including glycolysis, oxidative phosphorylation and mTOR signaling [373]; therefore, it was important to include both WT and mutant p53 cells. Future studies may focus on more thoroughly characterizing responses to lactate in breast lines of the same classification (luminal vs. basal) or receptor status (ER^+ vs. ER^-). If a common lactate phenotype (or overall metabolic phenotype) can be assigned to a particular category, then these classifications would provide clinicians with the additional information on the best potential therapeutic strategies for targeting the metabolic pathways of that particular tumor.

In clinical studies, it has been found that lactate accumulation is an indicator of poor metastasis-free and overall patient survival [19-22, 24, 60]. A recent study

measuring lactate accumulation and spatial distribution in prostate cancer compared the aggressive, anaplastic, fast-growing Dunning R3327-AT to the parental, well-differentiated, slow-growing Dunning R3327-H in animal models [108]. Similar to the findings in human solid tumors, the more aggressive AT tumor line showed significantly more lactate accumulation and necrosis, specifically in the tumor core [108]. Not surprisingly, the same conclusion from human and animal studies emerges: lactate accumulation is a reliable indicator of tumor aggressiveness, associated with fast growth and necrosis within a solid tumor [21, 24, 60, 104, 108, 374, 375].

High lactate production is characteristic of both the Pasteur effect and the Warburg effect. Our group has previously shown that R3230Ac tumors accumulate lactate primarily in response to hypoxia (the Pasteur effect) [104]. We have shown in our recent manuscript [290] that R3230Ac tumors take up lactate in aerobic but not hypoxic tumor regions. These observations are in support of the metabolic symbiont model [141]. In comparison, results shown in Section 3 demonstrate that lactate levels did not correlate with pO_2 in LABC biopsies; this is indicative of a Warburg phenotype. As mentioned previously, LABC is quite aggressive with a poor prognosis of three and five year disease-free survival (DFS) of 65% and 55%, respectively, even with combined therapy [264]. Interestingly, R3230Ac tumors are not highly aggressive and do not readily metastasize [376]. An important question is whether there is a significant difference in tumor aggressiveness as classified by a Warburg vs. Pasteur phenotype. If

so, these classifications may also help in deciding therapeutic interventions for altering tumor metabolism.

Finally, in recent years, a new phenomenon in tumor metabolism is beginning to be characterized: stimulation of increased glycolysis in tumor-associated fibroblasts and stromal tissue by neighboring epithelial cancer cells, termed the "Reverse Warburg Effect."[377] Much like the metabolic symbiont, central to the model is the proposition that aerobic epithelial tumor cells will oxidize lactate produced by the neighboring cells. The primary differences between the two models are the type of cells that are implicated in providing the lactate and the underlying reason for increased lactate production in these cells. The metabolic symbiont focuses on tumor cells only, while the Reverse Warburg Effect implicates tumor-associated fibroblasts and stromal cells as well. The overproduction of lactate in the metabolic symbiont model is due to tumor hypoxia, while the lactate production by fibroblasts in the Reverse Warburg Effect is due to tumor cell-stimulated upregulation of myo-fibroblast markers and glycolytic enzymes in normoxic conditions [141, 377]. The Warburg-ian fibroblasts demonstrated a loss of caveolin-1 (Cav-1 $^{-/-}$), which has been associated with tumor initiation, metastases and breast tumor recurrence [378, 379]. Cav-1$^{-/-}$ stromal cells showed upregulation of two microRNAs (miR-31 and miR-34c) associated with oxidative stress and hypoxia/HIF-1α, which is hypothesized to drive autophagy/mitophagy on which epithelial cancer cells feed [380-382]. This same group has published on lactate induction of "increased

stemness" in MCF7 cells [247]. These results seem to suggest that tumors with the ability to utilize lactate are more aggressive; however, the results also beg another question: Are the implications of lactate utilization different or similar between stromal cell lactate utilization vs. cancer cell lactate utilization? This may pose yet another quandary for scientists.

Lactate accumulation and metabolism are two sides of the same coin. The unanswered questions regarding the ability of the tumor to utilize lactate are: 1. Is it an indicator of a less aggressive tumor or is the ability to consume lactate a survival advantage and are these questions mutually exclusive?; 2. Can we effectively alter and sustain the alteration of the lactate phenotype of a tumor through manipulation of metabolic pathways? Recently there has been increasing interest in targeting lactate metabolism in tumors. A greater understanding of the complex and dynamic metabolic pathways that operate in tumors provide more avenues for tailored treatments.

Appendix A

Additional Tables for Section 3

Presented in this section are the Tables showing the pathways of interest for genomic analysis and lactate median values for each clinical patient parameter.

Table 18: Genes and pathways of interest for LABC analysis

Pathway	*HUGO gene*
glycolysis	*HK1*
glycolysis	*GAPDH*
glycolysis	*PFKFB1*
glycolysis	*TPI1*
glycolysis	*GPI*
glycolysis	*ALDOA*
glycolysis	*PGK1*
glycolysis	*PGM1*
glycolysis	*ENO1*
glycolysis	*PKLR*
glycolysis	*PKM*
glycolysis	*LDHA*
glycolysis	*PDK1*

glycolysis	*PDK2*
glycolysis	*PDK3*
glycolysis	*PDK4*
glycolysis	*HIF1A*
TCA	*PDP1*
TCA	*PDHA1*
TCA	*PDHA2*
TCA	*PDHB*
TCA	*PDHX*
TCA	*CS*
TCA	*IDH1*
TCA	*IDH2*
lactate metabolism	*GPT*
lactate metabolism	*GPT2*
lactate metabolism	*LDHB*
metabolism	*SIRT1*
metabolism	*SIRT3*
EMT	*SNAI1*
EMT	*SNAI2*

EMT	*TWIST1*
EMT	*ZEB1*
EMT	*CDH2*
EMT	*GSC*
EMT	*ACTA2*
EMT	*VIM*
EMT	*FN1*
EMT	*CTNNB1*
EMT	*ALDH1A1*
MET	*CDH1*
MET	*LAMA1*
MET	*MUC1*
MET	*TJP1*
cytoskeleton	*KRT7*
cytoskeleton	*KRT8*
cytoskeleton	*KRT13*
cytoskeleton	*KRT14*
cytoskeleton	*KRT16*
cytoskeleton	*KRT17*

cytoskeleton	*KRT18*
cytoskeleton	*KRT19*
cytoskeleton	*TUBB*
cytoskeleton	*TUBB3*
cytoskeleton	*TUBA1A*
cytoskeleton	*TUBA1B*
cytoskeleton	*TUBA1C*
cytoskeleton	*LMNA*
cytoskeleton	*LMNB1*
transport	*SLC25A5*
transport	*SLC25A3*
transport	*VDAC1*
transport	*VDAC2*
transport	*SLC16A1*
transport	*SLC16A3*
cell death	*PARP1*
cell death	*CALR*
cell death	*CYCS*
cell death	*HSP90AB1*

signaling	*MMP9*
signaling	*IL8*
signaling	*IGFBP1*
signaling	*IL6*
signaling	*EGFR*
signaling	*MIF*
signaling	*MMP2*
signaling	*FASLG*
signaling	*SERPINE1*
signaling	*ARRB1*

Table 19: Mean lactate concentrations in inflammatory vs. noninflammatory LABC specimens

Mean [L] (μmol/g)	Inflammatory N=5	Noninflammatory N=16
Max	8.0	7.5
75P	5.8	5.4
Median	4.7	4.4
25P	3.2	2.9
Min	1.5	1.5

Table 20: Mean lactate concentrations in ER+ vs. ER- LABC specimens

Mean [L] (μmol/g)	ER+ N=10	ER- N=10
Max	7.5	7.4
75P	5.3	5.3
Median	4.3	4.3
25P	2.8	2.8
Min	1.3	1.4

Table 21: Mean lactate concentrations in PR+ vs. PR- LABC specimens

Mean [L] (μmol/g)	PR+ N=15	PR- N=5
Max	7.5	7.2
75P	5.4	5.2
Median	4.3	4.2
25P	2.9	2.7
Min	1.4	1.2

Table 22: Mean lactate concentrations in Her2+ vs. Her2- LABC specimens

Mean [L] (μmol/g)	Her2+ N=3	Her2- N=17
Max	6.8	7.5
75P	4.9	5.4
Median	3.7	4.4
25P	2.5	2.9
Min	1.0	1.4

Table 23: Mean lactate concentrations in LABC specimens from patients with triple negative breast cancer vs. not triple negative breast cancer

Mean [L] (μmol/g)	Triple Negative N=2	Non Triple Negative N=18
Max	8.0	7.5
75P	5.9	5.3
Median	4.8	4.3
25P	3.1	2.8
Min	1.6	1.3

Table 24: Mean lactate concentrations in LABC specimens from patients with relapse vs. no relapse

Mean [L] (μmol/g)	Relapse N=4	No Relapse N=15
Max	8.0	7.3
75P	5.9	5.2
Median	4.7	4.2
25P	3.2	2.8
Min	1.6	1.3

Table 25: Mean lactate concentrations in LABC specimens from patients with TMN staging ≥ 3 vs. TMN staging < 3

Mean [L] (μmol/g)	TMN ≥ 3 N=15	TMN < 3 N=5
Max	7.9	6.2
75P	5.7	4.4
Median	4.6	3.4
25P	3.1	2.1
Min	1.5	1.0

Table 26: Mean lactate concentrations in LABC specimens from patients with nodal involvement (+) vs. no nodal involvement (-)

Mean [L] (μmol/g)	Node+ N=12	Node- N=5
Max	6.5	7.9
75P	4.6	5.7
Median	3.6	4.6
25P	2.3	3.1
Min	1.0	1.5

Table 27: Mean lactate concentrations in LABC specimens from patients with distant metastases vs. no distant metastases

Mean [L] (μmol/g)	Distant Mets N=6	No Mets N=15
Max	7.6	7.4
75P	5.4	5.3
Median	4.4	4.2
25P	2.9	2.8
Min	1.3	1.4

Table 28: Mean lactate concentrations in LABC specimens from patients with a positive (alive) or negative (dead) outcome

Mean [L] (μmol/g)	Dead N=6	Alive N=15
Max	7.8	7.4
75P	5.6	5.3
Median	4.6	4.2
25P	3.0	2.8
Min	1.3	1.4

Table 29: Mean lactate concentrations in LABC specimens from patients with cCR, cPR or cSD

Mean [L] (μmol/g)	Clin. CR N=7 spec. (6 pts.)	Clin. PR N=7	Clin. SD N=8 spec. (7 pts.)
Max	8.3	7.3	6.8
75P	6.0	5.3	4.8
Median	4.9	4.2	3.7
25P	3.3	2.7	2.5
Min	1.8	1.2	1.2

Table 30: Mean lactate concentrations in LABC specimens from patients with pCR, pPR or pSD

Mean [L] (μmol/g)	Path. CR N=1	Path. PR N=13 spec. (12 pts.)	Path. SD N=8 spec. (7 pts.)
Max	10.9	7.3	7.2
75P	8.1	5.2	5.1
Median	6.6	4.3	4.0
25P	4.9	2.8	2.7
Min	2.9	1.3	1.3

Table 31: Mean lactate concentrations in LABC specimens from patients with IIb, IIIa or IIIb tumors

Mean [L] (μmol/g)	IIb N=11 spec. (9 pts.)	IIIa N=5	IIIb N=6
Max	8.0	6.1	7.6
75P	5.8	4.2	5.4
Median	4.7	3.2	4.4
25P	3.1	2.1	2.9
Min	1.6	1.0	1.3

Table 32: Mean lactate concentrations in LABC specimens from patient tumors displaying MPTS 4-6 vs. MPTS 0-3

Mean [L] (μmol/g)	MPTS 4-6 N=3	MPTS 0-3 N=7
Max	9.0	6.8
75P	6.6	4.9
Median	5.5	3.8
25P	3.8	2.5
Min	1.9	1.1

Table 33: Mean lactate concentrations in LABC specimens from patient tumors displaying a centrifugal (CF) vs. centripetal (CP) DCE-MRI parameters

Mean [L] (μmol/g)	CF N=4	CP N=5
Max	9.0	6.1
75P	6.6	4.3
Median	5.5	3.4
25P	3.8	2.1
Min	1.9	0.9

Appendix B

Cell Detachment after Lactate Treatment

In our initial investigation of cancer cell clonogenic survival response to exogenous lactate, we used "Protocol 1" (Sections 2.9.1.1, 5.2.1.1.1 Protocol 1:). This method can create artifacts two ways. First, because cells are plated at such a low density to start, the effects of the treatment may be augmented or exacerbated because there may not be enough cells to cope with exposure. Some cell lines require higher plating densities in order to grow appropriately (HMEC cells). If HMEC cells are plated in low densities, their growth will be much slower and irregular. The second way this method creates an artifact is through the possibility of discarding viable but detached cells. Many steps necessitate discarding media. With discarding the media, detached cells are also discarded. After 24 hr of treatment with lactate, T47D cells show the highest percentage of detachment (19%) of the breast cancer cell lines (Figure 45). In a 48 hr period, about 5% of MCF7 cells and as many as 13% of MDA-MB-231 cells may become detached (Figure 45). After 1 week of lactate treatment, T47D cells show 25% detachment at the highest lactate concentration tested (Figure 45).

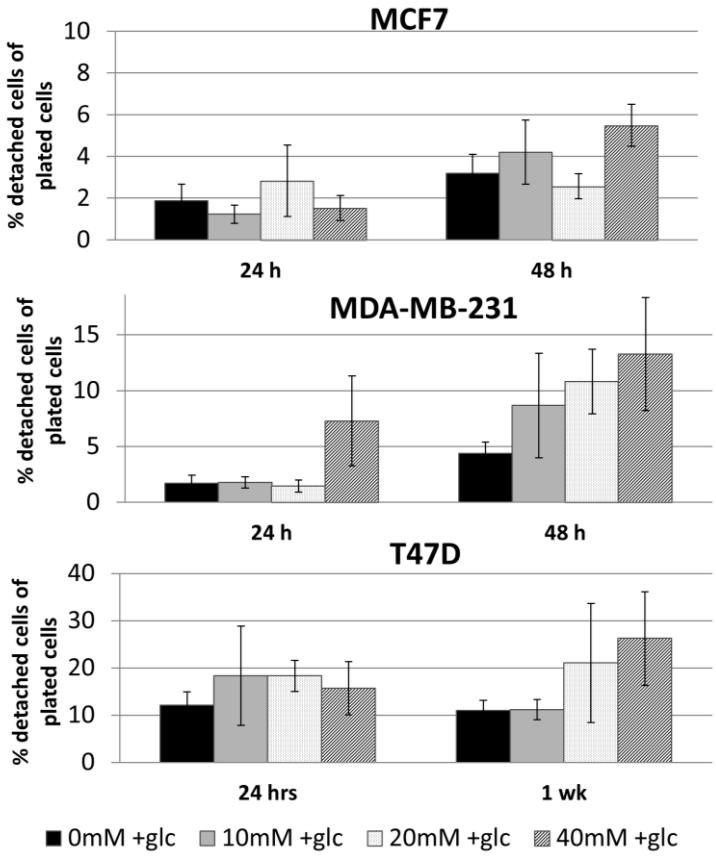

Figure 45: Breast cancer cell detachment after lactate treatment. MCF7 (top), MDA-MB-231 (middle), and T47D (bottom) cells show cellular detachment from the culture plate after treatment with 0-40mM of lactate (+glucose) for 24 h, 48 h, or 1 week.

A majority of the detached cells are viable. Detached MCF7 cells show up to 70% viability after 24 hr of lactate treatment (Figure 46). Detached T47D cells show viability between 55% – 67% after treatment with exogenous lactate for 24 hr or 1 week (Figure 46). We realized that these viable cells could possibly reattach to the culture plate at different times. By leaving them out of "Protocol 1," we were skewing our results

towards decreased clonogenic survival with treatment. For these reasons, we changed our clonogenic survival assay to "Protocol 2" (Sections 2.9.1.2, 5.2.1.1.2 Protocol 2:), which dictates treating cells when they are 70% confluent and collecting media after lactate treatment.

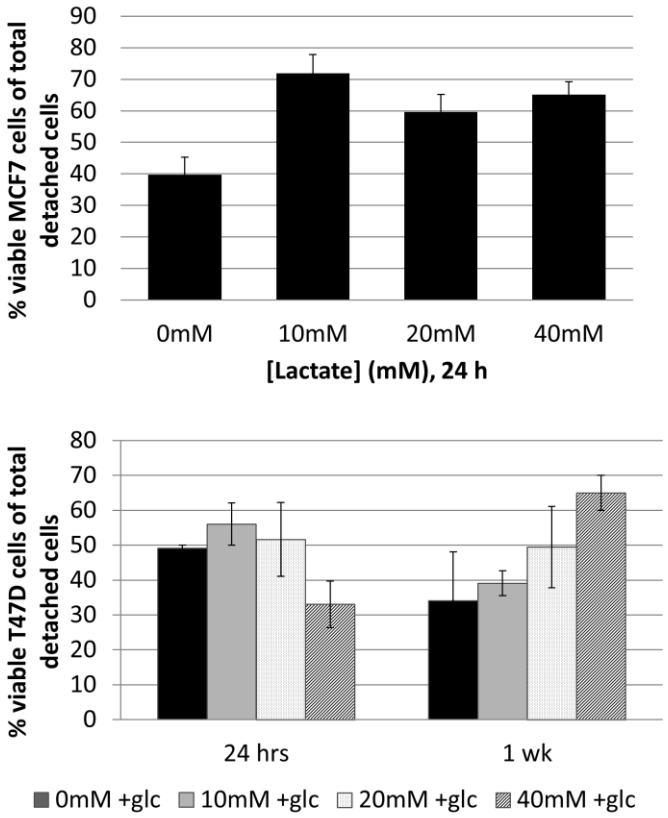

Figure 46: Viability of breast cancer cells post-detahment as assessed by the Trypan Blue Exclusion assay. A majority of MCF7 (top) and T47D (bottom) cells retain viability after detaching from the culture plate post-lactate treatment.

Appendix C

MCT1 Regulation by ERRα

ERRα is an orphan nuclear receptor with similar homology to the estrogen receptor (ER); however, the signaling pathways of ERRα versus ER are not identical, though there is theoretical cross-talk. ERRα has been reported to be upregulated in breast cancer [383, 384], critical to ER-negative tumor growth (MDA-MB-231 xenografts) [385] and to directly induce VEGF in both ER- and ER+ cell lines [386]. ERRα has been validated as a therapeutic target for breast cancer treatment [387]. Recent studies have shown that ERRα signaling can regulate metabolic response after activation by PPARγ-coactivator 1α (PGC-1α) [385]. SLC16A1 that codes for MCT1 is one of the upregulated genes after ERRα activation by PGC-1α [385]. MCT1 is a membrane and mitochondrial transporter that is involved in transport of monocarboxylates such as lactate and pyruvate [136] and has been shown to be upregulated in response to PGC-1α [388]. As discussed throughout the text, exogenous lactate influences HIF-1α and VEGF signaling and can increase MCT1 levels. ERRs act as cofactors for HIF as well as stimulating the Warburg Effect [389]. With such connections between lactate/MCT1 and ERRα, we hypothesized that MCT1 may be regulated by ERRα .We briefly investigated MCT1 regulation by estrogen –related receptor alpha (ERRα) with real time PCR.

Abbreviated Methods: Plasmids for increased and decreased ERRα activity were provided by the McDonnell lab in adenovirus vectors, previously described in Gaillard et. al [390]. The plasmids were: wild type ERRα (WT), ERRα with coactivator PGC-1α (2x9), ERRα with coactivator PGC-1α mutant (L2L3M), and ERRα knockdown (siERR). Included controls were control siRNA (siCON) and empty vector (bgal). 150,000 cells were plated in 12-well and given 24 hr to attach. Adenovirus infections were then performed in MCF7 and MDA-MB-231 cells the following day after calculation of the multiplicity of infection. After 48 hr, RNA was extracted using the Qiagen RNeasy Mini Kit (Qiagen). SYBR Green quantitative PCR was performed [385]. MCT1 primers used: sense, 5'-ATCTCCGGACCAGAAAGACA -3' and antisense, 5'-CTGGGTCATGAACTGCTCAA-3'.

Results: ERRα was induced 4 fold with ERRα-specific PGC-1α (2x9), greater than WT (~2.5 fold induction) in MCF7 cells. ERRα was not induced any more with 2x9 infection than with WT PGC-1α in MDA-MB-231 cells and very little in comparison to βgal infection. MCT1 was induced in MCF7 cells with PGC-1α infection, but 2x9 showed a less dramatic effect on induction of MCT1 than with induction of ERRα. In MDA-MB-231 cells, infection with any PGC-1α shows no MCT1 induction, perhaps even down-regulation (Figure 47).

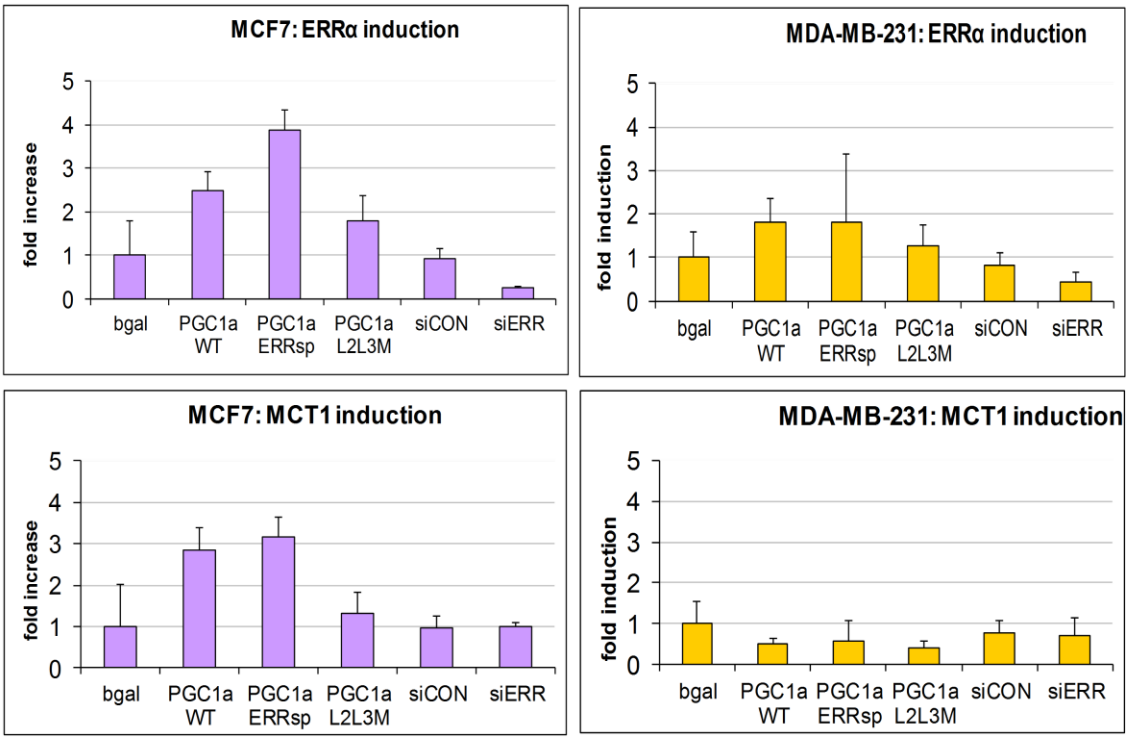

Figure 47: MCT1 regulation by ERRα. ERRα and MCT1 induction in MCF7 (top) and MDA-MB-231 cells (bottom) after transfection with ERRα-specific plasmids. MCT1 shows upregulation with ERRα/PGC-1α stimulation.

Appendix D

Proteomics and phosphoproteomics in liver cell lines reveal cytoskeletal protein regulation by lactate

Since the advent of miniaturized microarrays for gene expression analysis and profiling in the 1990s [391, 392], the "omics" approach has gained steady popularity for understanding cell and tissue response to different conditions and treatment. Besides "genomics," which is a term to describe the field of research that analyses the structure and/or function of the complete DNA set of a cell [393], there are new fields of research termed "proteomics" and "metabolomics." Where genomics studies the genome [393], proteomics studies the proteome (comprehensive set of protein changes/functions) [394] and metabolomics studies the metabolome (total set of metabolic pathways) [395]. These disciplines allow for fast, high-throughput analysis of thousands of target genes, proteins, and enzymes to understand global changes in regulation or expression and indicate potential important networks of signaling. For these reasons, the "omics" are often employed to analyze large datasets of tissue samples or cellular material to find potential signaling pathways or transcripts (PTMs, metabolites, etc.) of interest that are involved in or contribute to specific process or disease states. Though the "omics" can be a fruitful and promising exploit, there are some drawbacks to this approach: 1. These analyses are often expensive; 2. Due to the number of targets, there is often lower signal to noise (especially with samples of questionable quality or purity); and 3. If used

improperly, it can send researchers on unfocused exploration. If the "omics" are used correctly and in conjunction with other methods, they can be a very powerful tool.

Proteomics and phosphoproteomics were utilized to investigate the protein expression change and phosphorylation events in a wide variety of proteins after lactate treatment. While native protein expression is interpreted as a gain or loss of translation (and therefore function) of particular proteins of interest, phosphorylation events can result in activation or suppression of activity depending upon a protein's specific regulatory responses. Proteomics and phosphoproteomics provide a more global view of regulation of protein expression and phosphorylation events in response to exogenous lactate. We focused on the liver cell lines for proteomic and phosphoproteomic analysis after lactate treatment. Using both HepG2 and WRL-68 cells, we could get a sense of the phosphoprotein networks regulated by lactate that are relevant to cancer and then compare these with the regulation seen in a normal cell line of the same tissue type. After the observation of potentially lactate-stimulated cellular detachment in our cell viability assays (Section 5), we hypothesized that the proteomics results would support the observation of this phenomenon. The additional advantage to this approach was to possibly discover cellular responses that were currently being overlooked.

Abbreviated Methods:

All proteomic data acquisition and analysis was done through the Duke Proteomic Core Facility with extensive help from Arthur Moseley, PhD. Samples of each cell line were prepared less than one week prior to proteomic analysis. Cells were allowed to grow to ~80-90% confluency before analysis. Each cell line had two groups and was treated for 24 hr with preferred media (control) or preferred media +10mM sodium L-lactate. All media was serum-free since FBS creates considerable noise in proteomic samples. After treatment, cells were washed 3-5 times with DPBS, then scraped with 50mM ammonium bicarbonate before centrifugation at 8,000 rpm for 1 minute. The supernatant was discarded, the pellet was rinsed twice with 50mM ammonium bicarbonate, then the pellet was resuspended in 0.1% Rapigest (Waters, Milford, MA) solubilized in 50mM ammonium bicarbonate. Samples were transported to the Proteomic Facility on ice.

Phosphoproteomics: Brenna Richardson, PhD , at Duke University's Proteomic Facility, conducted the following procedures and analysis: Cells were lysed with burst sonication (3 x 10 seconds) in 0.3% ALS-1 after five 1-mL washes in 50mM ammonium bicarbonate. Samples were centrifuged at 15,000 x g to remove remaining insoluble material and 1 mg total protein was subjected to in-solution digestion according to standard protocol (http://www.genome.duke.edu/cores/proteomics/sample-preparation/documents/In-solutionDigestionProtocol_012309.pdf). Samples were then analyzed using unbiased LC-MSE (3 µg per sample) on Synapt G2 HDMS (Waters,

Milford, MA). 980ug digested protein was subjected to standard phosphopeptide enrichment protocol and run on the LTFTQ Orbitrap (Thermo Fisher Scientific, Waltham, MA). Data processing was performed with Elucidator ® (Rosetta Biosoftware, Cambridge, MA). Agglomerative Cluster Analysis with z-score and cosine correction was used to organize proteomic array data. Lactate groups were compared to control to find the significantly regulated proteins by lactate. These data were used as input for Ingenuity Pathway Analysis (Ingenuity Systems, Redwood City, CA) to detect pertinent pathways, potential mechanisms and active networks.

Results:

Lactate was found to regulate a total of 472 proteins in HepG2 cells. Of these, 145 proteins showed ≥2 fold change. Proteins related to the cytoskeleton or motility comprised ~10% of the 145 proteins regulated. When assessing proteins that changed >4 fold, this percentage rose to 20%, indicating that cytoskeletal rearrangement is occurring in response to lactate. Table 34 shows some of the most highly regulated proteins after lactate treatment; the alpha-2-chain of tubulin was found to have a 65-fold downregulation of expression after HepG2 cells were treated with exogenous lactate. This finding of cytoskeletal regulation supports our previous observation of cellular detachment after lactate treatment (Section5.2.1).

Table 34: Highly regulated proteins in HepG2 cells after 24 hr treatment with 10mM of sodium lactate

Protein	Function	Fold change
Tubulin alpha-2 chain (Alpha-tubulin 2)	major constituent of microtubules	65 ↓
Tropomyosin-1 alpha chain (Alpha-tropomyosin)	stabilizing cytoskeleton actin filaments	42 ↑
Aldo-keto reductase family 1 member C3	catalyzes the conversion of aldehydes and ketones to alcohols.	42 ↑
Actin, gamma-enteric smooth muscle	involved in various types of cell motility	22 ↑
Phosphoenolpyruvate carboxykinase, cytosolic [GTP]	main control point for the regulation of GNG, phosphophenylpyruvate → oxaloacetate	21 ↓
DNA topoisomerase I, mitochondrial precursor	relieves DNA strain that arise during duplication of mitochondrial DNA	19 ↓

Cell detachment events paired with cytoskeletal regulation following lactate treatment imply the possibility of enhanced motility or migration of cells. We briefly followed-up on the proteomic results of actin regulation post lactate treatment by using IF techniques (phalloidin staining) to observe F-actin expression in HepG2 cells and breast cancer cell lines (MCF7, MDA-MB-231). The results reported come with the caveat that the investigation was limited and illustrative; F-actin levels were not quantified. The phalloidin signal with lactate treatment (+ or – glucose) was not uniform among the cell lines tested (Figure 48). Without additional studies, not much can be gleaned from the

breast cancer cell line results (Figure 48, MCF7: A-D, MDA-MB-231: E-H), as the relative intensities do not seem to follow a cohesive pattern. MCF7 cells did show high F-actin expression with 10mM of lactate in the context of available glucose (Figure 48D), while MDA-MB-231 cells showed lower F-actin in these same conditions (Figure 48H). The phalloidin signal in HepG2 cells demonstrated some dependence on glucose availability, with increased intensity in glucose deprivation conditions (Figure 48J, K). When 10mM of lactate was added, HepG2 cells showed suppressed phalloidin signal (Figure 48L).

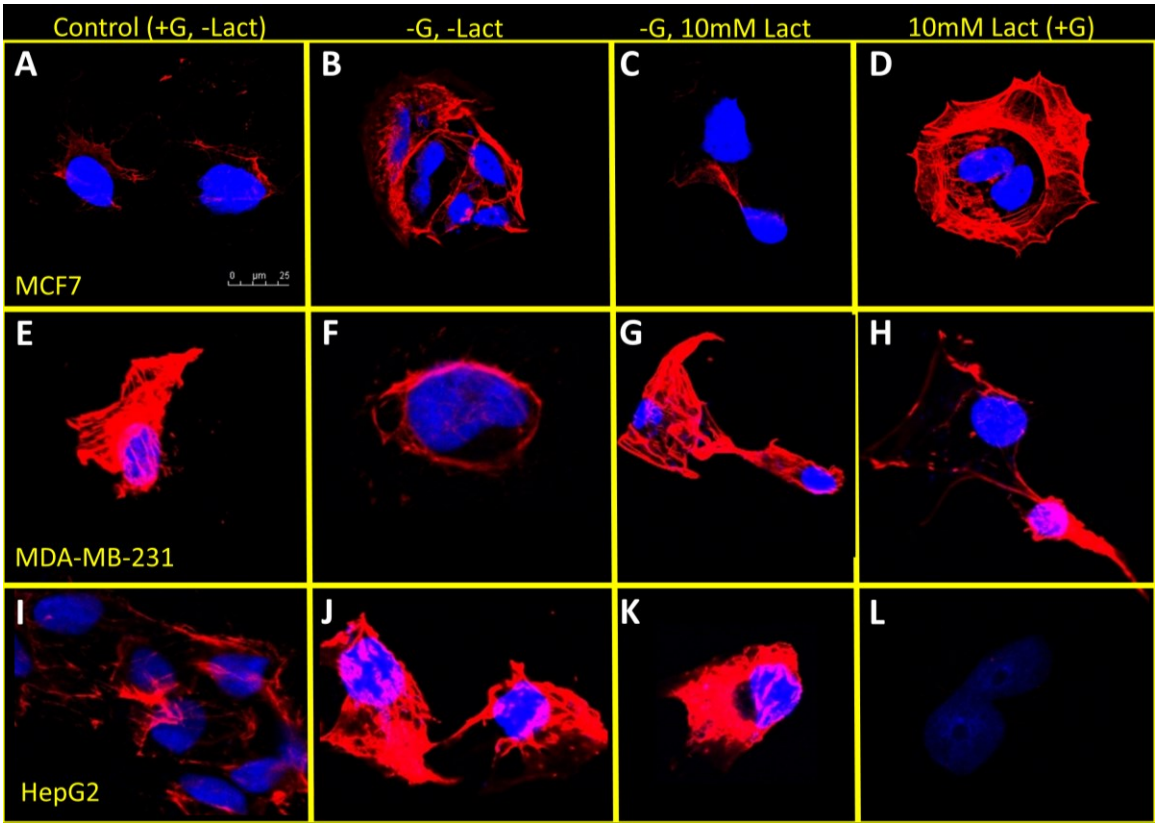

Figure 48: Representative image of F-actin changes after 24 hr lactate treatment. Phalloidin staining was conducted for detection of F-actin in MCF7 (A-D), MDA-MB-231 (E-H) and HepG2 (I-L) cells (n=2). F-actin expression varied between cell lines with 24 hr glucose deprivation ("-G") (B-C, F-G, J-K) and lactate supplementation (C-D, G-H, K-L). Lactate (+G) enhances F-actin expression in MCF7 cells but suppresses F-actin expression in HepG2 cells.

Following the proteomic evaluation, we wanted to compare phosphoprotein expression between our hepatocellular cancer cell model (HepG2) and our normal liver cell model (WRL-68). WRl-68 and HepG2 cells were exposed to 10mM lactate for 24 hr and collected for phosphoproteomic analysis. Phosphorylation is a common posttranslational modification that often relates to activation or, less frequently,

inactivation of particular protein functions [49]. One of the benefits of phosphoproteomic analysis is the potential for pinpointing pathways that respond to the presence or uptake of lactate. A total of 442 and 423 phosphoproteins were differentially regulated in WRl-68 and HepG2 cells, respectively, in response to lactate treatment. 176 of these phosphoproteins were significantly regulated in WRL-68 cells while 174 were significantly regulated in HepG2 cells. There were 63 phosphoproteins that were regulated in both cell lines in response to lactate; however, the direction and extent of regulation was not always concordant between the two cell lines. Twenty-five phosphoproteins shared common regulation between the two cell lines, but there were 38 that were regulated differently. Table 35 and Table 36 show the fold-changes of expression and p values for representative shared upregulated and downregulated phosphoproteins in the two cell lines. For both cell lines, phosphoproteins relating to the cytoskeleton or cell adhesion are highly regulated in both directions, as seen indicated by the asterisk in Table 35 and Table 36.

Table 35: Commonly upregulated phosphoproteins in HepG2 and WRL-68 cells after lactate treatment

Phosphoprotein	Fold Change HepG2	P-value HepG2	Fold Change WRL-68	P-value WRL-68
Voltage-dependent anion-selective channel protein 2	1.335	2.17E-12	1.22	3.44E-05
Integrin beta-1 *	1.411	5.87E-06	1.379	5.33E-05
ADP/ATP translocase 2	1.112	1.06E-05	1.185	3.93E-23
Cytoskeleton-associated protein 4 *	1.177	3.16E-04	1.143	0.003
Lamin-A/C	1.169	4.12E-04	1.082	5.92E-05

Table 36: Commonly downregulated phosphoproteins in HepG2 and WRL-68 cells after lactate treatment

Phosphoprotein	Fold Change HepG2	P-value HepG2	Fold change WRL	P-value WRL
High mobility group protein B2	-1.493	2.07E-35	-1.233	5.29E-05
Calumenin	-1.453	3.60E-19	-1.146	0.005
Glyceraldehyde-3-phosphate dehydrogenase	-1.865	1.10E-14	-1.235	1.40E-09
Tubulin beta chain *	-1.248	6.79E-10	-1.074	0.001
Heat shock protein HSP 90-beta	-1.137	1.15E-06	-1.158	3.37E-04
Tubulin alpha-1B chain *	-1.351	1.67E-04	-1.142	2.12E-07

It is apparent from Table 35 and Table 36 that phosphoproteins with shared regulation between the two cell lines comprised phosphoproteins related to the cytoskeleton, metabolism, ion channels and calcium signaling. Also of interest were the 63 differentially regulated phosphoproteins (Table 37). From these results, the overall message was the same: cytoskeletal, calcium signaling, and metabolic regulation. HepG2 cells showed downregulation of phosphorylation of cytokeratins 8, 18 and 19, while WRL-68 cells showed upregulation of these.

Table 37: Differentially regulated phosphoproteins in HepG2 and WRL-68 cells after lactate treatment

Phosphoprotein Description	Fold Change HepG2	P-value HepG2	Fold change WRL	P-value WRL	HepG2	WRL-68
Calreticulin	1.14	6.09E-30	-1.064	0.006	↑	↓
Endoplasmin	1.889	1.99E-17	-1.092	0.015	↑	↓
Myosin-9	-1.291	6.37E-17	1.088	1.46E-10	↓	↑
Dolichyl-diphosphooligosaccharide--protein glycosyltransferase subunit 2	-1.134	1.30E-10	1.164	2.12E-13	↓	↑
Nucleolin	1.103	1.23E-09	-1.339	2.08E-05	↑	↓
Keratin, type II cytoskeletal 8	-1.317	3.34E-07	1.14	1.89E-09	↓	↑
Keratin, type I cytoskeletal 18	-1.301	8.42E-07	1.161	6.05E-07	↓	↑
Dolichyl-diphosphooligosaccharide--protein glycosyltransferase subunit 1	-1.187	2.68E-06	1.139	1.25E-05	↓	↑
Cytochrome c	1.266	1.20E-05	-1.298	2.29E-06	↑	↓
Dolichyl-diphosphooligosaccharide--protein glycosyltransferase 48 kDa subunit	-1.382	6.15E-05	1.264	7.75E-10	↓	↑
Keratin, type I cytoskeletal 19	-1.136	0.001	1.273	8.22E-06	↓	↑
Tubulin beta-3 chain	1.565	0.002	-1.422	2.61E-05	↑	↓
X-ray repair cross-complementing protein 6	-1.578	0.003	-1.12	1.94E-06	↓	↑

Ingenuity IPA was used to analyze the phosphoproteomic data further by grouping the significantly regulated phosphoproteins into larger networks of cellular systems, phenotypes or disease states. Common pathways and processes regulated in both cell lines were "cellular assembly and organization, hair and skin development and function and cell death," as assessed and grouped by Ingenuity based on regulated phosphoproteins and predicted interacting phosphoproteins. A representative network (Figure 49) shows groups of highly regulated phosphoproteins that correspond to ion channels / solute carriers, metabolism, cytoskeletal rearrangement and calcium

signaling. In an unbiased analysis of networks of regulation related to both cell lines, β-arrestin emerged as a focal point of interaction for many proteins.

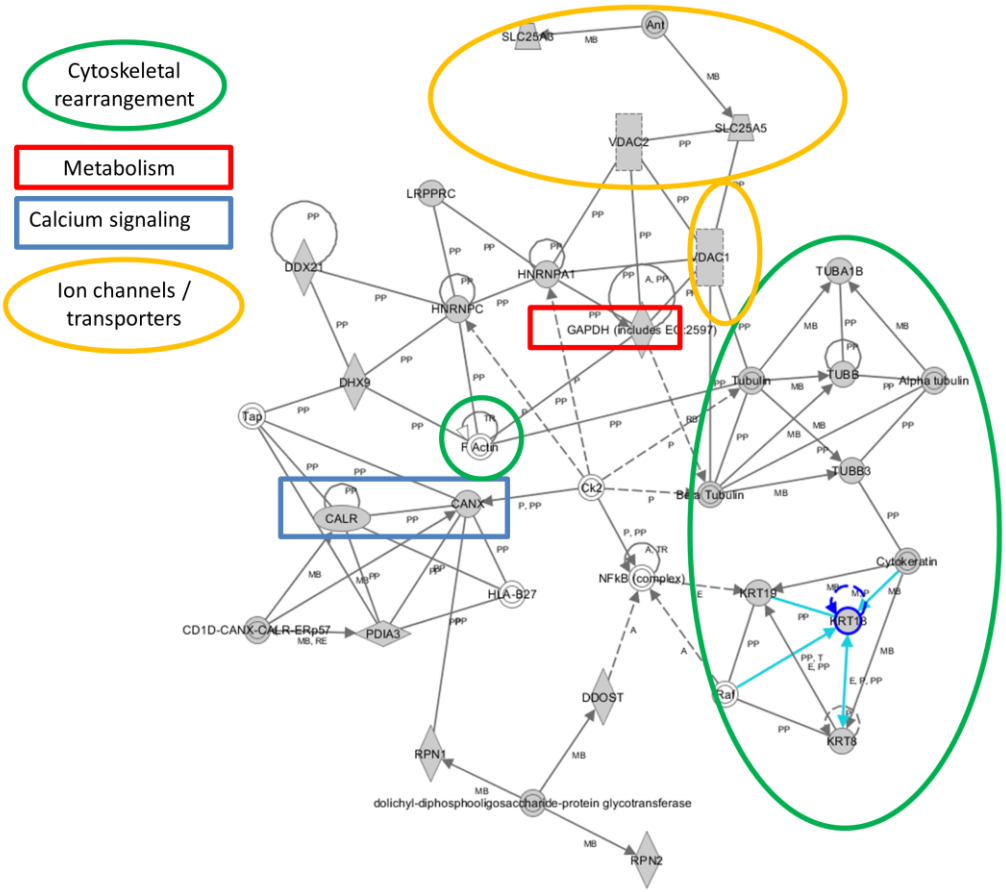

Figure 49: Network of lactate-regulated phosphoproteins common to WRL-68 and HepG2 cells. Processes affected by lactate include ion channels, solute carrier transporters, calcium signaling, metabolism and cytoskeletal rearrangement.

Appendix E

Assessment of EMT Signaling After Lactate Treatment

Few studies that have investigated the effect of lactate treatment on cell differentiation and the results are contradictory [248, 250]. Experimental findings show that lactate increases differentiation in sheep thyroid cells [248] and in leukemia cells [396], involved especially in terminal cell division. Zieker *et al*. examined the influence of lactate treatment (15mM treatment for 1 hr – 7 days) on gene expression in mesenchymal stem cells [250]. While gene expression differences were seen as early as 1 hr after treatment and accumulated up to the 7-day time point, none of the clusters of differentiation (CDs) changed significantly; however, the most highly upregulated genes included IL-6 (>4 fold increase, 3 days), HSP70 (>2 fold increase, 3 days) and HIF-1a (>2 fold increase, 3 days). That particular study concluded that lactate did not "profoundly change the phenotype of MSC."[250] However, we were interested if lactate could profoundly change the phenotype of epithelial cells to mesenchymal cells. The breast cell lines, MCF7 and T47D, were used for EMT studies. Of phenotypic changes that occur in EMT (Table 5), my exploration of possible lactate-induced EMT focused on general cell morphology, CD24 and CD44 expression, Snail expression, and mammosphere formation.

Abbreviated Methods:

Western blots for Snail, Slug and Twist are provided in Section 2.9

Staining for CD24 and CD44: Cells were plated in 6-well plates at densities of ~200,000 – 900,000 cells per well, dependent on cell line. Cells were allowed to attach for 18-30 hours then treated with preferred media (control) or 10 - 40mM lactate supplemented media (glucose deprivation groups were included in the chronic exposure experiments). After 24 hours ("Acute") or 10 days ("Chronic"), cells were collected and stained for CD24 and CD44.

After collection of media and trypsinized cells, tubes were spun at 4,400 RPM for 4 minutes to pellet. All subsequent steps were carried out on ice or in 4^0C. Cells were fixed with 2% formalin for 15 minutes. Cells were centrifuged, formalin was decanted, and then cells were washed with PBS. After pelleting cells and decanting PBS, cells were resuspended in 1-2% BSA (diluted in PBS). Then 10 μL (for every 10^6 cells) of anti-human PE-conjugated CD24 or FITC-conjugated CD44 (BD Pharmigen) were added to the tubes and allowed to incubate in the dark for 20 minutes. Cells were centrifuged and then resuspended again in 1-2% BSA. Plots and histograms were generated by Mike Cook, PhD at Duke University's Flow Facility. In plots, quadrants were defined as CD24-/CD44-, CD24+/CD44-, CD24-/CD44+ and CD24+/CD44+. To take into account $CD24^{low}$ phenotypes, histograms were generated to increase accuracy of cellular number or proportion of cells expressing low CD24.

Mammosphere assays:

Reagents: Mammocult media® and mammocult supplementary media was acquired from Stem Cell Technologies (Vancouver, BC, Canada). Heparin (4μg/mL) and hydrocortisone (0.48μg/mL) were acquired from Sigma-Aldrich. Each batch of Complete Mammocult media (45mL of Mammocult media with 5mL mammocult supplementary media , 4ug/mL of heparin and 0.48ug/mL of hydrocortisone) was made fresh each week. Ultra-low attachment 6- and 24-well plates were purchased from Corning Inc. (Corning, NY) and used for plating primary and secondary mammosphere assays, respectively.

Assay: Cells were seeded on 10cm^2 or 6-well plates (BD Falcon,Franklin Lakes, NJ) and given 24 hr to attach. Figure 50 shows the procedure to perform mammosphere formation assays. After the appropriate treatment, all detached and attached cells were collected. Cells were centrifuged, washed and re-seeded (25,000 cells/well) into the primary mammosphere formation assay. Each control and experimental group was conducted in triplicate. Each "pre" treatment group was also plated for chronic lactate exposure ("post"), in which lactate was added to the Mammocult media. Lactate was weighed out and dissolved in Mammocult media prior to filtering. Primary spheres were given either 4-5 days or 1 week to form before visual enumeration. Eight to fifteen fields of each well were counted under 5 X magnification. Only spheres with greater

than 35 cells were counted. Primary spheres were plotted as the average of 15 fields and also plotted after being normalized to the control (no treatment) group.

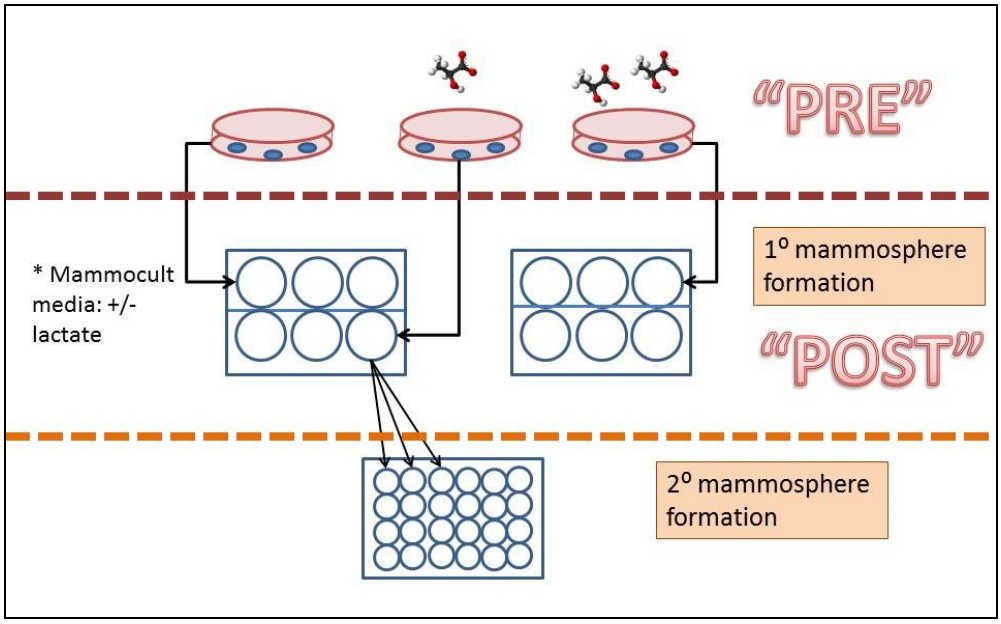

Figure 50: Schematic of mammosphere assays. "Pre" lactate treatment indicates lactate supplementation while cells were grown in monolayer; "Post" lactate treatment indicate lactate supplementation while cells were grown as primary and secondary spheres.

After visual counting, all mammospheres were collected in 15mL conical tubes and spun down. Spheres were washed and then treated with trypsin (0.25%) for 10 minutes to ensure the spheres were fully dissociated. The trypsin was quenched with complete culture media containing FBS. Cells were centrifuged, washed and resuspended in Complete Mammocult media. Ultra-low attachment 24-well plates were seeded with 5,000 cells per well. Chronic lactate treatment "post" groups were cultured

in Complete Mammocult media with 10 or 20mM of sodium lactate. Cells were given another 4-5 days (or 1 week) for secondary mammosphere formation and then spheres were totaled. In the secondary sphere assay, 8-12 fields were counted per sample. Only spheres with more than 25 cells were counted. Secondary spheres were plotted as the average of 5 fields and also as relative to the no treatment control.

Results:

CD24/44 expression does not significantly change in breast cancer cell lines with lactate treatment

One common cellular anomaly indicative of EMT is the loss of cellular adhesion [397]. For investigation of stem cell-like markers in breast cells, we chose to examine CD44 and CD24 expression in MCF7s, MDA-MB-231s and HMECs with Flow Cytometry. The expression pattern of $CD44^{high}/CD24^{low}$ has been reported to be associated with human breast stem cells, both normal and cancer [398-400]. It is also known that different types of breast cancer will display particular expression patterns of these molecules: luminal type breast cancers (MCF7) are typically $CD44^{low}/CD24^{high}$ and basal type breast cancers (MDA-MB-231) are $CD44^{high}/CD24^{low}$. Purely from these definitions, one can hypothesize that the cell line MDA-MB-231 would display more stem-cell-like behaviors, such as loss of cellular adhesion, increased invasion, and ability to form mammospheres and self-renew.

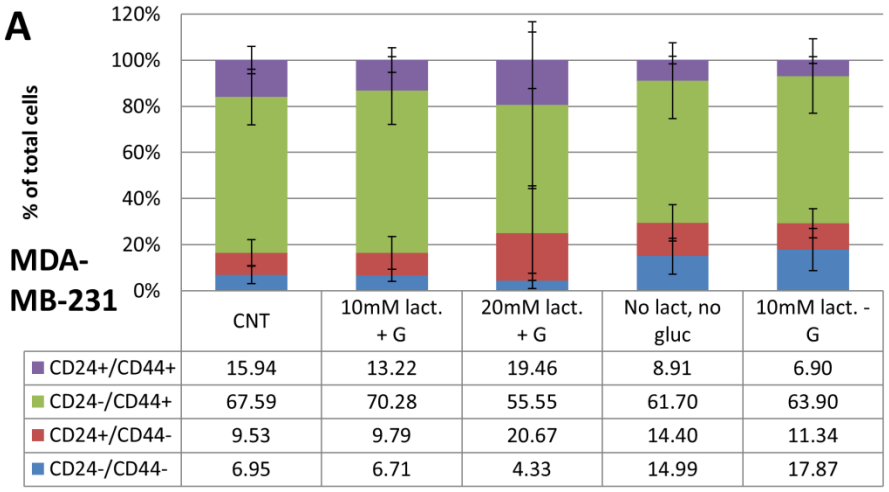

	CNT	10mM lact. + G	20mM lact. + G	No lact, no gluc	10mM lact. - G
CD24+/CD44+	15.94	13.22	19.46	8.91	6.90
CD24-/CD44+	67.59	70.28	55.55	61.70	63.90
CD24+/CD44-	9.53	9.79	20.67	14.40	11.34
CD24-/CD44-	6.95	6.71	4.33	14.99	17.87

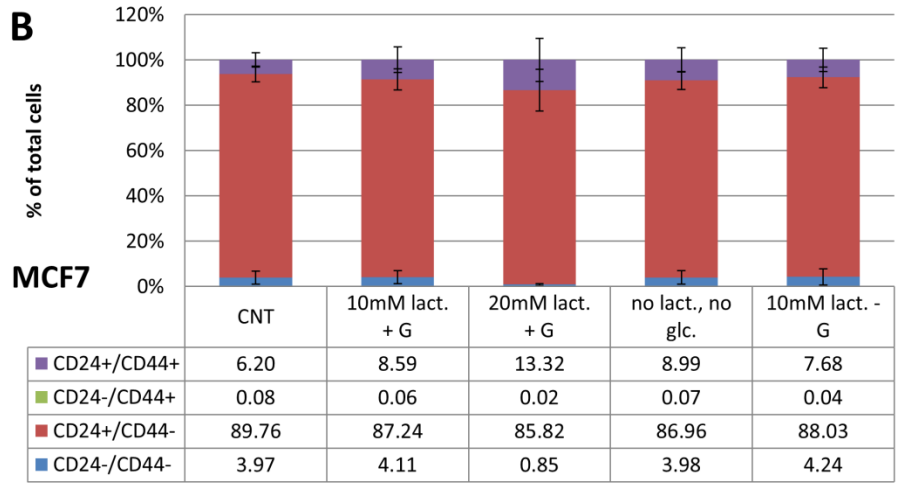

	CNT	10mM lact. + G	20mM lact. + G	no lact., no glc.	10mM lact. - G
CD24+/CD44+	6.20	8.59	13.32	8.99	7.68
CD24-/CD44+	0.08	0.06	0.02	0.07	0.04
CD24+/CD44-	89.76	87.24	85.82	86.96	88.03
CD24-/CD44-	3.97	4.11	0.85	3.98	4.24

Figure 51: Stacked bar graphs (% of cells) of CD24 and CD44 expression changes in breast cancer cell lines after 24 hr exposure to lactate. There were no significant changes in CD24 or CD44 expression after 24 hr treatment with exogenous lactate (+ or – glucose) in MDA-MB-231 (A) and MCF7 cells (B).

Neither MDA-MB-231 nor MCF7 cells showed significant changes in CD44/24 status after both acute (24 hr, Figure 51) and chronic (10 days, Figure 52) lactate treatment.

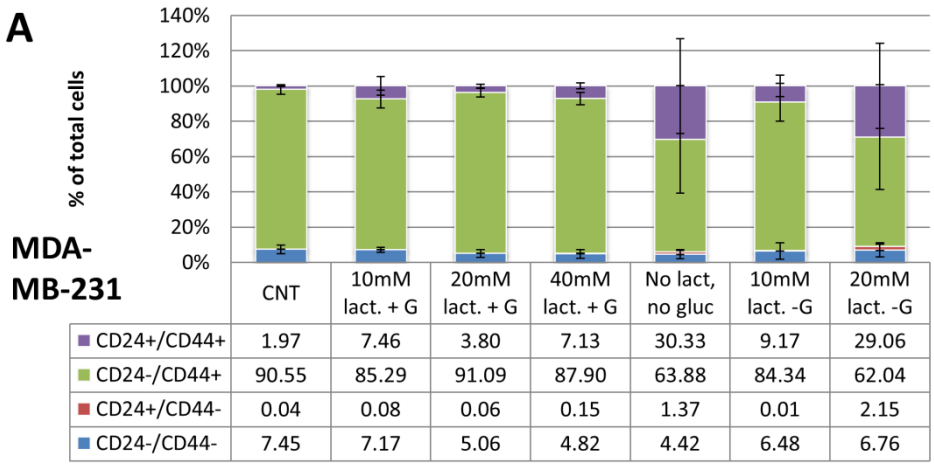

	CNT	10mM lact. + G	20mM lact. + G	40mM lact. + G	No lact, no gluc	10mM lact. -G	20mM lact. -G
CD24+/CD44+	1.97	7.46	3.80	7.13	30.33	9.17	29.06
CD24-/CD44+	90.55	85.29	91.09	87.90	63.88	84.34	62.04
CD24+/CD44-	0.04	0.08	0.06	0.15	1.37	0.01	2.15
CD24-/CD44-	7.45	7.17	5.06	4.82	4.42	6.48	6.76

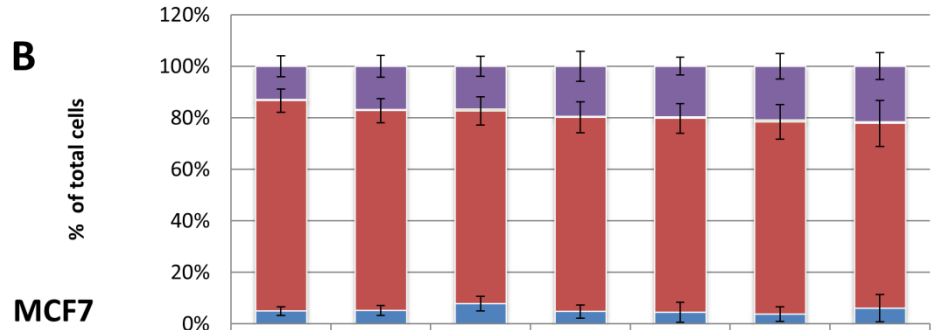

	CNT	10mM lact. + G	20mM lact. + G	40mM lact. + G	No lact, no gluc	10mM lact. -G	20mM lact. -G
CD24+/CD44+	13.03	16.96	16.70	19.51	19.77	20.99	21.57
CD24-/CD44+	0.27	0.35	0.64	0.35	0.45	0.59	0.66
CD24+/CD44-	81.65	77.49	74.80	75.33	75.27	74.65	71.69
CD24-/CD44-	4.87	5.20	7.86	4.82	4.51	3.76	6.08

Figure 52: Stacked bar graphs (% of cells) of CD24 and CD44 expression changes in breast cancer cell lines after 10 day exposure to lactate. There were no significant changes in CD24 and CD44 expression after 10 day treatment with exogenous lactate (+ or – glucose) in MDA-MB-231 (A) and MCF7 cells (B).

Regulation of Snail-1 mRNA increased in T47Ds with addition of lactate

We first used RT-PCR to investigate Snail-1 regulation in response to lactate-treatment in MCF7 and T47D cells. MCF7 cells showed high endogenous expression of

Snail-1 (Figure 53). In accordance with the high Snail-1 expression, MCF7 cells also showed global suppression of E-cadherin (Figure 53).

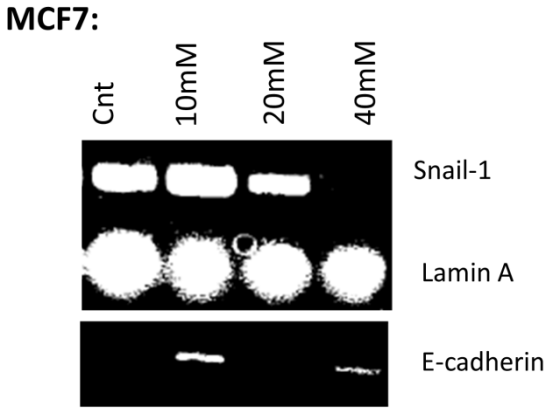

Figure 53: High endogenous Snail-1 expression in MCF7 cells. MCF7 cells exposed to lactate for 3 days (n=2) showed high endogenous Snail-1 mRNA (top) and low E-cadherin (bottom).

In T47D cells, we saw no evidence of Snail-1 mRNA in the control group (0mM lactate) and strong upregulation of Snail-1 with all lactate treatments (Figure 54A). All quantification of Snail-1 levels were first normalized against the loading control (Lamin A) before comparing lactate-treated groups to each other. As seen in Figure 54A, the Lamin A levels in each treatment group are not equal. By normalizing the Snail-1 signal to the Lamin A signal in the respective lane, this difference in the loading control was taken into account. Because the relative Snail-1 mRNA expression could not be quantified compared to an absent band in the control lane, relative upregulation of Snail-1 mRNA was quantified using the 10mM lactate treatment group. Compared to

the 10mM lactate-treated group, 20mM lactate treatment elicited a decline in mRNA expression by ~13%, but the 40mM lactate treatment group showed a 25% increase in Snail-1 mRNA (Figure 54B). Additionally, E-cadherin mRNA levels were 33% and 28% lower in the 20mM and 40mM lactate-treated groups than control (Figure 54C), corresponding with the expectations of Snail-1 upregulation coinciding with E-cadherin downregulation in the event of EMT.

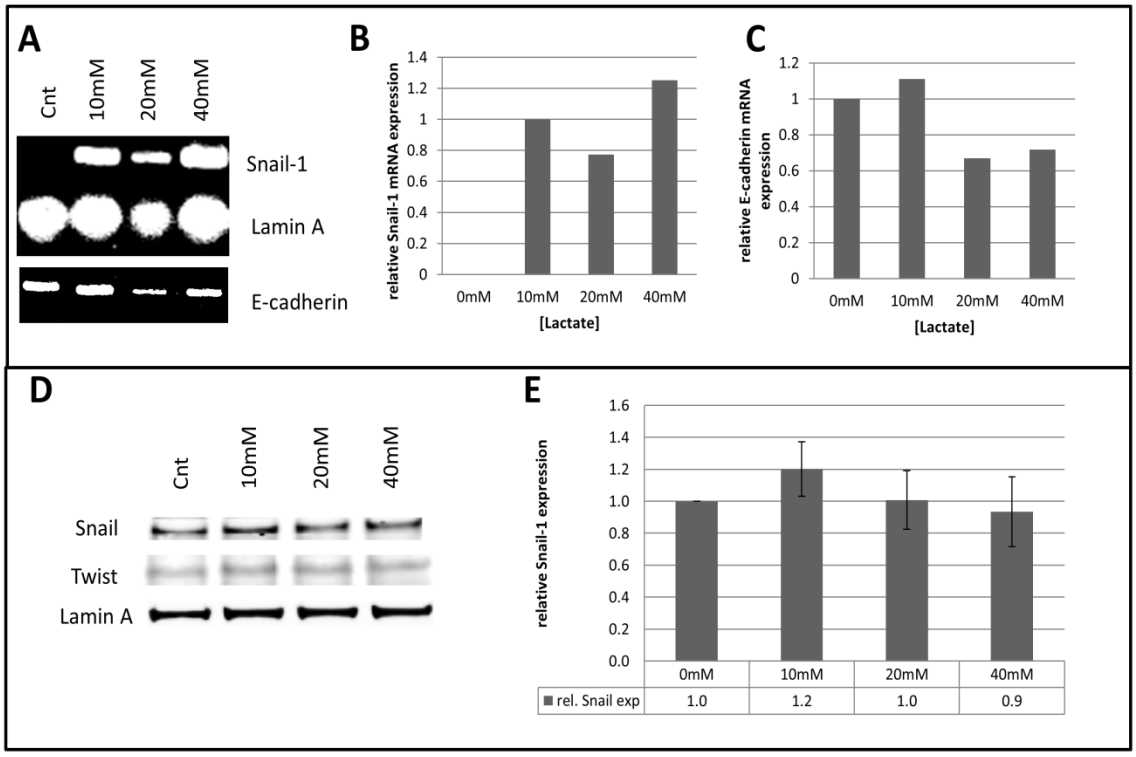

Figure 54: Snail-1 mRNA expression but not protein expression increased with 3-day lactate treatment in T47D cells. Representative images of Snail-1 mRNA (top) and protein expression (bottom) in T47D cells after lactate treatment (n=3). Increased mRNA expression of Snail-1 and decreased E-cadherin after 3-day lactate treatment (A). Quantified Snail-1 mRNA relative to 10mM lactate-treated group (B) and quantified E-cadherin mRNA (C) for results pictured in A. Representative Western blot of Snail-1 and Twist in T47D cells shows slight increase after lactate exposure (D); quantified protein expression of Snail-1 relative to the control (E).

Snail-1 protein expression in lactate-treated T47D cells was assessed with Western blot techniques, with the expectation that protein expression would match the mRNA results. In the Western blot of Snail-1 from lactate-treated T47D cells, there was no dramatic increase in band intensity visually in any of the lactate treatments (Figure 54D). A slight increase in expression is visible in the 10mM lactate group (Figure 54D). In the

20mM and 40mM treatment groups, Snail-1 protein expression was equal to and less than the untreated group (Figure 54E); these results do not reflect the increase in Snail-1 mRNA. The regulation of Snail-1 protein levels in the 40mM lactate group was inconsistent, showing downregulation compared to the control in two trials and upregulation in another; however, Snail-1 mRNA was significantly increased after lactate treatment. The literature indicates that T47D cells do not express Snail-1 protein [401], which may be one reason for the lack of Snail-1 protein expression in my studies.

T47D cells treated for three days with 10 and 40mM lactate showed increased primary mammosphere formation.

T47D cells treated for 24 hr or 10 days (Abbreviated Methods) showed no significant changes in mammosphere formation. To simplify the experimental model, experiments testing 3-day lactate exposure refer to T47D cells treated in monolayer. Results are reported as mean number of mammospheres per 15 fields or mean number of mammospheres per well for the secondary mammosphere assays. Figure 55 shows a representative independent experiment from this series. A significant increase in primary mammosphere formation was seen with lactate treatments of 10mM and 40mM compared to the untreated control group (Figure 55A); however, there was no significant increase in secondary mammosphere formation (Figure 55B).

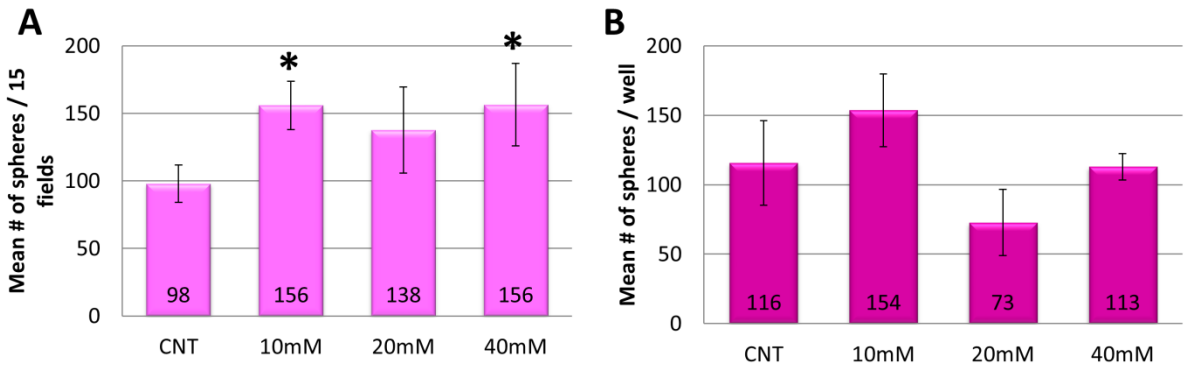

Figure 55: Primary mammosphere formation was significantly increased with 3-day 10mM and 40mM lactate treatments in T47D cells. Representative independent experiments of primary (A) and secondary (B) mammosphere formation in T47D cells after 3-day treatment with exogenous lactate. 10mM and 40mM lactate significantly increase primary mammosphere formation (*$p<0.05$, One-Way ANOVA, A). No significant changes were seen in secondary mammosphere formation after lactate treatment (B).

References

1. Jemal, A., et al., *Global cancer statistics.* CA Cancer J Clin. **61**(2): p. 69-90.

2. Ferlay, J., et al., *Estimates of worldwide burden of cancer in 2008: GLOBOCAN 2008.* Int J Cancer. **127**(12): p. 2893-917.

3. *The Global Burden of Disease: 2004 Update* 2008, World Health Organization: Geneva.

4. AmericanCancerSociety. *Cancer Facts & Figures 2012*. 2012; Available from: http://www.cancer.org/acs/groups/content/@epidemiologysurveilance/documents/document/acspc-031941.pdf.

5. Bray, F., et al., *Global cancer transitions according to the Human Development Index (2008-2030): a population-based study.* Lancet Oncol. **13**(8): p. 790-801.

6. Howlader N, et al. *SEER Cancer Statistics Review, 1975-2009 (Vintage 2009 Populations)*. 2012; Available from: http://seer.cancer.gov/csr/1975_2009_pops09/.

7. Ravdin, P.M., et al., *The decrease in breast-cancer incidence in 2003 in the United States.* N Engl J Med, 2007. **356**(16): p. 1670-4.

8. DeSantis, C., et al., *Breast cancer incidence rates in U.S. women are no longer declining.* Cancer Epidemiol Biomarkers Prev. **20**(5): p. 733-9.

9. Finkel, T., M. Serrano, and M.A. Blasco, *The common biology of cancer and ageing.* Nature, 2007. **448**(7155): p. 767-74.

10. AmericanCancerSociety, *The Global Economic Cost of Cancer*, AmericanCancerSociety, Editor 2010.

11. Tzu, S., *The Art of War by Sun Tzu - Special Edition*2005: El Paso Norte Press.

12. Kumar, V., A.K. Abbas, and N. Fausto, *Robbins and Cotran Pathological Basis of Disease*. 7th ed2005, Philadelphia, PA: Elsevier Saunders.

13. Hanahan, D. and R.A. Weinberg, *The hallmarks of cancer.* Cell, 2000. **100**(1): p. 57-70.

14. Hanahan, D. and R.A. Weinberg, *Hallmarks of cancer: the next generation.* Cell. **144**(5): p. 646-74.
15. Warburg, O.H., F. Dickens, and Kaiser-Wilhelm-Institut fuÌˆr Biologie., *The Metabolism of tumours : investigations from the Kaiser Wilhelm Institute for Biology, Berlin-Dahlem*1930, London: Constable. xxviii, 327 p., 5 leaves of plates.
16. Warburg, O., *On the origin of cancer cells.* Science, 1956. **123**(3191): p. 309-14.
17. Warburg, O., *On respiratory impairment in cancer cells.* Science, 1956. **124**(3215): p. 269-70.
18. Kennedy, K.M. and M.W. Dewhirst, *Tumor metabolism of lactate: the influence and therapeutic potential for MCT and CD147 regulation.* Future Oncol, 2010. **6**(1): p. 127-48.
19. Schwickert, G., et al., *Correlation of high lactate levels in human cervical cancer with incidence of metastasis.* Cancer Res, 1995. **55**(21): p. 4757-9.
20. Walenta, S., et al., *High lactate levels predict likelihood of metastases, tumor recurrence, and restricted patient survival in human cervical cancers.* Cancer Res, 2000. **60**(4): p. 916-21.
21. Walenta, S., et al., *Correlation of high lactate levels in head and neck tumors with incidence of metastasis.* Am J Pathol, 1997. **150**(2): p. 409-15.
22. Brizel, D.M., et al., *Elevated tumor lactate concentrations predict for an increased risk of metastases in head-and-neck cancer.* Int J Radiat Oncol Biol Phys, 2001. **51**(2): p. 349-53.
23. Le, Q.T., et al., *In vivo 1H magnetic resonance spectroscopy of lactate in patients with stage IV head and neck squamous cell carcinoma.* Int J Radiat Oncol Biol Phys, 2008. **71**(4): p. 1151-7.
24. Walenta, S., et al., *Metabolic classification of human rectal adenocarcinomas: a novel guideline for clinical oncologists?* J Cancer Res Clin Oncol, 2003. **129**(6): p. 321-6.
25. Sauer, L.A. and R.T. Dauchy, *Ketone body, glucose, lactic acid, and amino acid utilization by tumors in vivo in fasted rats.* Cancer Res, 1983. **43**(8): p. 3497-503.

26. Sauer, L.A., J.W. Stayman, 3rd, and R.T. Dauchy, *Amino acid, glucose, and lactic acid utilization in vivo by rat tumors.* Cancer Res, 1982. **42**(10): p. 4090-7.

27. Paschen, W., *Regional quantitative determination of lactate in brain sections. A bioluminescent approach.* J Cereb Blood Flow Metab, 1985. **5**(4): p. 609-12.

28. Paschen, W., et al., *Lactate and pH in the brain: association and dissociation in different pathophysiological states.* J Neurochem, 1987. **48**(1): p. 154-9.

29. Semenza, G.L., *Regulation of metabolism by hypoxia-inducible factor 1.* Cold Spring Harb Symp Quant Biol. **76**: p. 347-53.

30. Bouzier, A.K., et al., *Compartmentation of lactate and glucose metabolism in C6 glioma cells. A 13c and 1H NMR study.* J Biol Chem, 1998. **273**(42): p. 27162-9.

31. Bouzier, A.K., et al., *Glucose and lactate metabolism in C6 glioma cells: evidence for the preferential utilization of lactate for cell oxidative metabolism.* Dev Neurosci, 1998. **20**(4-5): p. 331-8.

32. Bouzier-Sore, A.K., et al., *Lactate is a preferential oxidative energy substrate over glucose for neurons in culture.* J Cereb Blood Flow Metab, 2003. **23**(11): p. 1298-306.

33. Yokota, H., et al., *Lactate, choline, and creatine levels measured by vitro 1H-MRS as prognostic parameters in patients with non-small-cell lung cancer.* J Magn Reson Imaging, 2007. **25**(5): p. 992-9.

34. Warburg, O., *The metabolism of tumors.* Arnold Constable, 1930. **London, UK**.

35. Warburg, O.H. and Kaiser-Wilhelm-Institut fuÌˆr Biologie., *Ãœber den Stoffwechsel der Tumoren : Arbeiten aus dem Kaiser Wilheim-Institut fÃ¼r Biologie, Berlin-Dahlem*1926, Berlin: Julius Springer. 263 p.

36. Waterhouse, C., *Lactate metabolism in patients with cancer.* Cancer, 1974. **33**(1): p. 66-71.

37. Holroyde, C.P., et al., *Lactate metabolism in patients with metastatic colorectal cancer.* Cancer Res, 1979. **39**(12): p. 4900-4.

38. Paschen, W., et al., *Regional quantitative determination of brain glucose in tissue sections: a bioluminescent approach.* J Cereb Blood Flow Metab, 1985. **5**(3): p. 465-8.

39. Mueller-Klieser, W., et al., *Comparative imaging of structure and metabolites in tumours.* Int J Radiat Biol, 1991. **60**(1-2): p. 147-59.

40. Tamulevicius, P. and C. Streffer, *Metabolic imaging in tumours by means of bioluminescence.* Br J Cancer, 1995. **72**(5): p. 1102-12.

41. Fulham, M.J., et al., *Mapping of brain tumor metabolites with proton MR spectroscopic imaging: clinical relevance.* Radiology, 1992. **185**(3): p. 675-86.

42. Hossmann, K.A., et al., *Regional metabolism of experimental brain tumors.* Acta Neuropathol, 1986. **69**(1-2): p. 139-47.

43. Gordan, J.D., C.B. Thompson, and M.C. Simon, *HIF and c-Myc: sibling rivals for control of cancer cell metabolism and proliferation.* Cancer Cell, 2007. **12**(2): p. 108-13.

44. Jones, R.G. and C.B. Thompson, *Tumor suppressors and cell metabolism: a recipe for cancer growth.* Genes Dev, 2009. **23**(5): p. 537-48.

45. Vaupel, P., *Tumor microenvironmental physiology and its implications for radiation oncology.* Semin Radiat Oncol, 2004. **14**(3): p. 198-206.

46. Gatenby, R.A. and R.J. Gillies, *Why do cancers have high aerobic glycolysis?* Nat Rev Cancer, 2004. **4**(11): p. 891-9.

47. Gillies, R.J. and R.A. Gatenby, *Adaptive landscapes and emergent phenotypes: why do cancers have high glycolysis?* J Bioenerg Biomembr, 2007. **39**(3): p. 251-7.

48. Gillies, R.J., I. Robey, and R.A. Gatenby, *Causes and consequences of increased glucose metabolism of cancers.* J Nucl Med, 2008. **49 Suppl 2**: p. 24S-42S.

49. Garrett, R.H. and C.M. Grisham, *Biochemistry*. Second ed1999: Saunders College Publishing.

50. Bonda, D.J., et al., *The sirtuin pathway in ageing and Alzheimer disease: mechanistic and therapeutic considerations.* Lancet Neurol. **10**(3): p. 275-9.

51. Etiemble, J., et al., *Erythrocytic pyruvate kinase deficiency and hemolytic anemia inherited as a dominant trait.* Am J Hematol, 1984. **17**(3): p. 251-60.

52. Racker, E., *History of the Pasteur effect and its pathobiology.* Mol Cell Biochem, 1974. **5**(1-2): p. 17-23.

53. Graeber, T.G., et al., *Hypoxia-mediated selection of cells with diminished apoptotic potential in solid tumours.* Nature, 1996. **379**(6560): p. 88-91.

54. Brizel, D.M., et al., *Tumor hypoxia adversely affects the prognosis of carcinoma of the head and neck.* Int J Radiat Oncol Biol Phys, 1997. **38**(2): p. 285-9.

55. Brizel, D.M., et al., *Tumor oxygenation predicts for the likelihood of distant metastases in human soft tissue sarcoma.* Cancer Res, 1996. **56**(5): p. 941-3.

56. Cairns, R.A. and R.P. Hill, *Acute hypoxia enhances spontaneous lymph node metastasis in an orthotopic murine model of human cervical carcinoma.* Cancer Res, 2004. **64**(6): p. 2054-61.

57. Hockel, M., et al., *Tumor hypoxia in pelvic recurrences of cervical cancer.* Int J Cancer, 1998. **79**(4): p. 365-9.

58. Vaupel, P., S. Briest, and M. Hockel, *Hypoxia in breast cancer: pathogenesis, characterization and biological/therapeutic implications.* Wien Med Wochenschr, 2002. **152**(13-14): p. 334-42.

59. Vaupel, P. and A. Mayer, *Hypoxia in cancer: significance and impact on clinical outcome.* Cancer Metastasis Rev, 2007. **26**(2): p. 225-39.

60. Walenta, S., T. Schroeder, and W. Mueller-Klieser, *Lactate in solid malignant tumors: potential basis of a metabolic classification in clinical oncology.* Curr Med Chem, 2004. **11**(16): p. 2195-204.

61. Dewhirst, M.W., Y. Cao, and B. Moeller, *Cycling hypoxia and free radicals regulate angiogenesis and radiotherapy response.* Nat Rev Cancer, 2008. **8**(6): p. 425-37.

62. Cardenas-Navia, L.I., et al., *Comparison of fluctuations of oxygen tension in FSA, 9L, and R3230AC tumors in rats.* Adv Exp Med Biol, 2003. **510**: p. 7-12.

63. Cardenas-Navia, L.I., et al., *The pervasive presence of fluctuating oxygenation in tumors.* Cancer Res, 2008. **68**(14): p. 5812-9.

64. Dewhirst, M.W., *Relationships between cycling hypoxia, HIF-1, angiogenesis and oxidative stress.* Radiat Res, 2009. **172**(6): p. 653-65.

65. Bristow, R.G. and R.P. Hill, *Hypoxia and metabolism. Hypoxia, DNA repair and genetic instability.* Nat Rev Cancer, 2008. **8**(3): p. 180-92.

66. Lunt, S.Y. and M.G. Vander Heiden, *Aerobic glycolysis: meeting the metabolic requirements of cell proliferation.* Annu Rev Cell Dev Biol. **27**: p. 441-64.

67. Kim, J.W. and C.V. Dang, *Cancer's molecular sweet tooth and the Warburg effect.* Cancer Res, 2006. **66**(18): p. 8927-30.

68. Bensinger, S.J. and H.R. Christofk, *New aspects of the Warburg effect in cancer cell biology.* Semin Cell Dev Biol, 2012. **23**(4): p. 352-61.

69. Vander Heiden, M.G., L.C. Cantley, and C.B. Thompson, *Understanding the Warburg effect: the metabolic requirements of cell proliferation.* Science, 2009. **324**(5930): p. 1029-33.

70. Wallace, D.C., *Mitochondria and cancer.* Nat Rev Cancer, 2012. **12**(10): p. 685-98.

71. Magda, D., et al., *mtDNA depletion confers specific gene expression profiles in human cells grown in culture and in xenograft.* BMC Genomics, 2008. **9**: p. 521.

72. Waris, G. and H. Ahsan, *Reactive oxygen species: role in the development of cancer and various chronic conditions.* J Carcinog, 2006. **5**: p. 14.

73. Moon, E.J., et al., *NADPH oxidase-mediated reactive oxygen species production activates hypoxia-inducible factor-1 (HIF-1) via the ERK pathway after hyperthermia treatment.* Proc Natl Acad Sci U S A. **107**(47): p. 20477-82.

74. Viola, R.J., et al., *In vivo bioluminescence imaging monitoring of hypoxia-inducible factor 1alpha, a promoter that protects cells, in response to chemotherapy.* AJR Am J Roentgenol, 2008. **191**(6): p. 1779-84.

75. Moeller, B.J., et al., *Radiation activates HIF-1 to regulate vascular radiosensitivity in tumors: role of reoxygenation, free radicals, and stress granules.* Cancer Cell, 2004. **5**(5): p. 429-41.

76. Torres, M. and H.J. Forman, *Redox signaling and the MAP kinase pathways.* Biofactors, 2003. **17**(1-4): p. 287-96.

77. Seger, R. and E.G. Krebs, *The MAPK signaling cascade.* Faseb J, 1995. **9**(9): p. 726-35.

78. Kohno, M. and J. Pouyssegur, *Targeting the ERK signaling pathway in cancer therapy.* Ann Med, 2006. **38**(3): p. 200-11.

79. Sen, C.K. and L. Packer, *Antioxidant and redox regulation of gene transcription.* Faseb J, 1996. **10**(7): p. 709-20.

80. Upadhyay, M., et al., *The Warburg effect: Insights from the past decade.* Pharmacol Ther, 2012.

81. Maxwell, P.H., et al., *The tumour suppressor protein VHL targets hypoxia-inducible factors for oxygen-dependent proteolysis.* Nature, 1999. **399**(6733): p. 271-5.

82. Gordan, J.D. and M.C. Simon, *Hypoxia-inducible factors: central regulators of the tumor phenotype.* Curr Opin Genet Dev, 2007. **17**(1): p. 71-7.

83. Hagg, M. and S. Wennstrom, *Activation of hypoxia-induced transcription in normoxia.* Exp Cell Res, 2005. **306**(1): p. 180-91.

84. Marin-Hernandez, A., et al., *HIF-1alpha modulates energy metabolism in cancer cells by inducing over-expression of specific glycolytic isoforms.* Mini Rev Med Chem, 2009. **9**(9): p. 1084-101.

85. Seagroves, T.N., et al., *Transcription factor HIF-1 is a necessary mediator of the pasteur effect in mammalian cells.* Mol Cell Biol, 2001. **21**(10): p. 3436-44.

86. Chen, J.L., et al., *The genomic analysis of lactic acidosis and acidosis response in human cancers.* PLoS Genet, 2008. **4**(12): p. e1000293.

87. Semenza, G.L., *HIF-1 and tumor progression: pathophysiology and therapeutics.* Trends Mol Med, 2002. **8**(4 Suppl): p. S62-7.

88. Semenza, G.L., *Oxygen sensing, homeostasis, and disease.* N Engl J Med, 2011. **365**(6): p. 537-47.

89. Kim, J.W., et al., *HIF-1-mediated expression of pyruvate dehydrogenase kinase: a metabolic switch required for cellular adaptation to hypoxia.* Cell Metab, 2006. **3**(3): p. 177-85.

90. Kung, A.L., et al., *Suppression of tumor growth through disruption of hypoxia-inducible transcription.* Nat Med, 2000. **6**(12): p. 1335-40.

91. Selak, M.A., et al., *Succinate links TCA cycle dysfunction to oncogenesis by inhibiting HIF-alpha prolyl hydroxylase.* Cancer Cell, 2005. **7**(1): p. 77-85.

92. Goyal, P., et al., *Upregulation of NAD(P)H oxidase 1 in hypoxia activates hypoxia-inducible factor 1 via increase in reactive oxygen species.* Free Radic Biol Med, 2004. **36**(10): p. 1279-88.

93. Chandel, N.S., et al., *Reactive oxygen species generated at mitochondrial complex III stabilize hypoxia-inducible factor-1alpha during hypoxia: a mechanism of O2 sensing.* J Biol Chem, 2000. **275**(33): p. 25130-8.

94. Mansfield, K.D., et al., *Mitochondrial dysfunction resulting from loss of cytochrome c impairs cellular oxygen sensing and hypoxic HIF-alpha activation.* Cell Metab, 2005. **1**(6): p. 393-9.

95. Dang, C.V., et al., *The interplay between MYC and HIF in cancer.* Nat Rev Cancer, 2008. **8**(1): p. 51-6.

96. Li, F., et al., *Myc stimulates nuclearly encoded mitochondrial genes and mitochondrial biogenesis.* Mol Cell Biol, 2005. **25**(14): p. 6225-34.

97. O'Connell, B.C., et al., *A large scale genetic analysis of c-Myc-regulated gene expression patterns.* J Biol Chem, 2003. **278**(14): p. 12563-73.

98. Adhikary, S. and M. Eilers, *Transcriptional regulation and transformation by Myc proteins.* Nat Rev Mol Cell Biol, 2005. **6**(8): p. 635-45.

99. Koshiji, M., et al., *HIF-1alpha induces cell cycle arrest by functionally counteracting Myc.* Embo J, 2004. **23**(9): p. 1949-56.

100. Gordan, J.D., et al., *HIF-2alpha promotes hypoxic cell proliferation by enhancing c-myc transcriptional activity.* Cancer Cell, 2007. **11**(4): p. 335-47.

101. Reynolds, T.Y., S. Rockwell, and P.M. Glazer, *Genetic instability induced by the tumor microenvironment.* Cancer Res, 1996. **56**(24): p. 5754-7.

102. Fukumura, D. and R.K. Jain, *Tumor microenvironment abnormalities: causes, consequences, and strategies to normalize.* J Cell Biochem, 2007. **101**(4): p. 937-49.

103. Fidler, I.J., *Tumor heterogeneity and the biology of cancer invasion and metastasis.* Cancer Res, 1978. **38**(9): p. 2651-60.

104. Schroeder, T., et al., *Spatial heterogeneity and oxygen dependence of glucose consumption in R3230Ac and fibrosarcomas of the Fischer 344 rat.* Cancer Res, 2005. **65**(12): p. 5163-71.

105. Corrigan, N.M., et al., *Improving 1H MRSI measurement of cerebral lactate for clinical applications.* Psychiatry Res. **182**(1): p. 40-7.

106. Park, I., et al., *Implementation of 3 T lactate-edited 3D 1H MR spectroscopic imaging with flyback echo-planar readout for gliomas patients.* Ann Biomed Eng. **39**(1): p. 193-204.

107. Serganova, I., et al., *Metabolic imaging: a link between lactate dehydrogenase A, lactate, and tumor phenotype.* Clin Cancer Res. **17**(19): p. 6250-61.

108. Yaligar, J., et al., *Lactate MRSI and DCE MRI as surrogate markers of prostate tumor aggressiveness.* NMR Biomed. **25**(1): p. 113-22.

109. Kompanje, E.J., et al., *The first demonstration of lactic acid in human blood in shock by Johann Joseph Scherer (1814-1869) in January 1843.* Intensive Care Med, 2007. **33**(11): p. 1967-71.

110. Bassett, D.R., Jr., *Scientific contributions of A. V. Hill: exercise physiology pioneer.* J Appl Physiol, 2002. **93**(5): p. 1567-82.

111. Meyerhof, O., Arch. ges. Physiol. , 1920. **185**(11).

112. Raju, T.N., *The Nobel chronicles. 1922: Archibald Vivian Hill (1886-1977), Otto Fritz Meyerhof (1884-1951).* Lancet, 1998. **352**(9137): p. 1396.

113. Bergeron, R., et al., *Effect of AMPK activation on muscle glucose metabolism in conscious rats.* Am J Physiol, 1999. **276**(5 Pt 1): p. E938-44.

114. Garrett R.H., G.C.M., *Biochemistry*. 3 ed2004: Brooks Cole.

115. Cori, C., *Mammalian carbohydrate metabolism.* Physiological Reviews, 1931. **11**(2): p. 143-275.

116. Brooks, G.A., *Intra- and extra-cellular lactate shuttles.* Med Sci Sports Exerc, 2000. **32**(4): p. 790-9.

117. Gladden, L.B., *Lactate metabolism: a new paradigm for the third millennium.* J Physiol, 2004. **558**(Pt 1): p. 5-30.

118. Hashimoto, T., et al., *Evidence for the mitochondrial lactate oxidation complex in rat neurons: demonstration of an essential component of brain lactate shuttles.* PLoS ONE, 2008. **3**(8): p. e2915.

119. Hashimoto, T., et al., *Lactate sensitive transcription factor network in L6 cells: activation of MCT1 and mitochondrial biogenesis.* Faseb J, 2007. **21**(10): p. 2602-12.

120. Gladden, L.B., *Lactic acid: New roles in a new millennium.* Proc Natl Acad Sci U S A, 2001. **98**(2): p. 395-7.

121. Pellerin, L., et al., *Evidence supporting the existence of an activity-dependent astrocyte-neuron lactate shuttle.* Dev Neurosci, 1998. **20**(4-5): p. 291-9.

122. Pellerin, L., et al., *Expression of monocarboxylate transporter mRNAs in mouse brain: support for a distinct role of lactate as an energy substrate for the neonatal vs. adult brain.* Proc Natl Acad Sci U S A, 1998. **95**(7): p. 3990-5.

123. Pellerin, L., *Lactate as a pivotal element in neuron-glia metabolic cooperation.* Neurochem Int, 2003. **43**(4-5): p. 331-8.

124. Zwingmann, C., et al., *NMR spectroscopic study on the metabolic fate of [3-(13)C]alanine in astrocytes, neurons, and cocultures: implications for glia-neuron interactions in neurotransmitter metabolism.* Glia, 2000. **32**(3): p. 286-303.

125. Waagepetersen, H.S., et al., *A possible role of alanine for ammonia transfer between astrocytes and glutamatergic neurons.* J Neurochem, 2000. **75**(2): p. 471-9.

126. McClelland, G.B., et al., *Peroxisomal membrane monocarboxylate transporters: evidence for a redox shuttle system?* Biochem Biophys Res Commun, 2003. **304**(1): p. 130-5.

127. Storey, B.T. and F.J. Kayne, *Energy metabolism of spermatozoa. VI. Direct intramitochondrial lactate oxidation by rabbit sperm mitochondria.* Biol Reprod, 1977. **16**(4): p. 549-56.

128. Gaesser, G.A. and G.A. Brooks, *Metabolic bases of excess post-exercise oxygen consumption: a review.* Med Sci Sports Exerc, 1984. **16**(1): p. 29-43.

129. Bonen, A., *The expression of lactate transporters (MCT1 and MCT4) in heart and muscle.* Eur J Appl Physiol, 2001. **86**(1): p. 6-11.

130. McCullagh, K.J., et al., *Role of the lactate transporter (MCT1) in skeletal muscles.* Am J Physiol, 1996. **271**(1 Pt 1): p. E143-50.

131. Stanley, W.C., *Myocardial lactate metabolism during exercise.* Med Sci Sports Exerc, 1991. **23**(8): p. 920-4.

132. Pagliassotti, M.J. and C.M. Donovan, *Role of cell type in net lactate removal by skeletal muscle.* Am J Physiol, 1990. **258**(4 Pt 1): p. E635-42.

133. Poortmans, J.R., *Principles of exercise biochemistry*. 3 ed, ed. J.R. Poortmans2003: Karger Publishers. 306.

134. Ide, K., et al., *Lactate, glucose and O2 uptake in human brain during recovery from maximal exercise.* J Physiol, 2000. **522 Pt 1**: p. 159-64.

135. Pellerin, L. and P.J. Magistretti, *Neuroenergetics: calling upon astrocytes to satisfy hungry neurons.* Neuroscientist, 2004. **10**(1): p. 53-62.

136. Halestrap, A.P. and D. Meredith, *The SLC16 gene family-from monocarboxylate transporters (MCTs) to aromatic amino acid transporters and beyond.* Pflugers Arch, 2004. **447**(5): p. 619-28.

137. Pellerin, L., et al., *Cellular and subcellular distribution of monocarboxylate transporters in cultured brain cells and in the adult brain.* J Neurosci Res, 2005. **79**(1-2): p. 55-64.

138. Itoh, Y., et al., *Dichloroacetate effects on glucose and lactate oxidation by neurons and astroglia in vitro and on glucose utilization by brain in vivo.* Proc Natl Acad Sci U S A, 2003. **100**(8): p. 4879-84.

139. Smith, D., et al., *Lactate: a preferred fuel for human brain metabolism in vivo.* J Cereb Blood Flow Metab, 2003. **23**(6): p. 658-64.

140. Bouzier, A.K., et al., *The metabolism of [3-(13)C]lactate in the rat brain is specific of a pyruvate carboxylase-deprived compartment.* J Neurochem, 2000. **75**(2): p. 480-6.

141. Sonveaux, P., et al., *Targeting lactate-fueled respiration selectively kills hypoxic tumor cells in mice.* J Clin Invest, 2008. **118**(12): p. 3930-42.

142. Wang, Q. and M.E. Morris, *The role of monocarboxylate transporter 2 and 4 in the transport of gamma-hydroxybutyric acid in mammalian cells.* Drug Metab Dispos, 2007. **35**(8): p. 1393-9.

143. Gladden, L.B., *Muscle as a consumer of lactate.* Med Sci Sports Exerc, 2000. **32**(4): p. 764-71.

144. Gladden, L.B., *A lactatic perspective on metabolism.* Med Sci Sports Exerc, 2008. **40**(3): p. 477-85.

145. Bourrat-Floeck, B., K. Groebe, and W. Mueller-Klieser, *Biological response of multicellular EMT6 spheroids to exogenous lactate.* Int J Cancer, 1991. **47**(5): p. 792-9.

146. Katz, J., et al., *Lactate and pyruvate metabolism and reducing equivalent transfer in Ehrlich ascites tumor.* Cancer Res, 1974. **34**(4): p. 872-7.

147. Bouzier-Sore, A.K., P. Canioni, and M. Merle, *Effect of exogenous lactate on rat glioma metabolism.* J Neurosci Res, 2001. **65**(6): p. 543-8.

148. Chatham, J.C., C. Des Rosiers, and J.R. Forder, *Evidence of separate pathways for lactate uptake and release by the perfused rat heart.* Am J Physiol Endocrinol Metab, 2001. **281**(4): p. E794-802.

149. Broer, S., et al., *Characterization of the monocarboxylate transporter 1 expressed in Xenopus laevis oocytes by changes in cytosolic pH.* Biochem J, 1998. **333 (Pt 1)**: p. 167-74.

150. Dimmer, K.S., et al., *The low-affinity monocarboxylate transporter MCT4 is adapted to the export of lactate in highly glycolytic cells.* Biochem J, 2000. **350 Pt 1**: p. 219-27.

151. Becker, H.M., S. Broer, and J.W. Deitmer, *Facilitated lactate transport by MCT1 when coexpressed with the sodium bicarbonate cotransporter (NBC) in Xenopus oocytes.* Biophys J, 2004. **86**(1 Pt 1): p. 235-47.

152. Seymour, C.B. and C. Mothersill, *The effect of lactate on the radiation response of CHO-K1 cells in culture.* Int J Radiat Biol Relat Stud Phys Chem Med, 1981. **40**(3): p. 283-91.

153. Izumi, H., et al., *Cellular pH regulators: potentially promising molecular targets for cancer chemotherapy.* Cancer Treat Rev, 2003. **29**(6): p. 541-9.

154. Stock, C. and A. Schwab, *Protons make tumor cells move like clockwork.* Pflugers Arch, 2009. **458**(5): p. 981-92.

155. Reshkin, S.J., et al., *Phosphoinositide 3-kinase is involved in the tumor-specific activation of human breast cancer cell Na(+)/H(+) exchange, motility, and invasion induced by serum deprivation.* J Biol Chem, 2000. **275**(8): p. 5361-9.

156. Stock, C., et al., *pH nanoenvironment at the surface of single melanoma cells.* Cell Physiol Biochem, 2007. **20**(5): p. 679-86.

157. Schwab, A., et al., *Functional role of Na+-HCO3- cotransport in migration of transformed renal epithelial cells.* J Physiol, 2005. **568**(Pt 2): p. 445-58.

158. Morgan, P.E., et al., *Interactions of transmembrane carbonic anhydrase, CAIX, with bicarbonate transporters.* Am J Physiol Cell Physiol, 2007. **293**(2): p. C738-48.

159. Gallagher, S.M., J.J. Castorino, and N.J. Philp, *Interaction of monocarboxylate transporter 4 with beta1-integrin and its role in cell migration.* Am J Physiol Cell Physiol, 2009. **296**(3): p. C414-21.

160. Yamagata, M., et al., *The contribution of lactic acid to acidification of tumours: studies of variant cells lacking lactate dehydrogenase.* Br J Cancer, 1998. **77**(11): p. 1726-31.

161. Helmlinger, G., et al., *Acid production in glycolysis-impaired tumors provides new insights into tumor metabolism.* Clin Cancer Res, 2002. **8**(4): p. 1284-91.

162. Swietach, P., R.D. Vaughan-Jones, and A.L. Harris, *Regulation of tumor pH and the role of carbonic anhydrase 9.* Cancer Metastasis Rev, 2007. **26**(2): p. 299-310.

163. Wykoff, C.C., et al., *Hypoxia-inducible expression of tumor-associated carbonic anhydrases.* Cancer Res, 2000. **60**(24): p. 7075-83.

164. Vince, J.W., U. Carlsson, and R.A. Reithmeier, *Localization of the Cl-/HCO3- anion exchanger binding site to the amino-terminal region of carbonic anhydrase II.* Biochemistry, 2000. **39**(44): p. 13344-9.

165. Vince, J.W. and R.A. Reithmeier, *Identification of the carbonic anhydrase II binding site in the Cl(-)/HCO(3)(-) anion exchanger AE1.* Biochemistry, 2000. **39**(18): p. 5527-33.

166. Alvarez, B.V., G.L. Vilas, and J.R. Casey, *Metabolon disruption: a mechanism that regulates bicarbonate transport.* Embo J, 2005. **24**(14): p. 2499-511.

167. Moon, E.J., et al., *The potential role of intrinsic hypoxia markers as prognostic variables in cancer.* Antioxid Redox Signal, 2007. **9**(8): p. 1237-94.

168. Rofstad, E.K., et al., *Hypoxia-induced treatment failure in advanced squamous cell carcinoma of the uterine cervix is primarily due to hypoxia-induced radiation resistance rather than hypoxia-induced metastasis.* Br J Cancer, 2000. **83**(3): p. 354-9.

169. Petrella, B.L., J. Lohi, and C.E. Brinckerhoff, *Identification of membrane type-1 matrix metalloproteinase as a target of hypoxia-inducible factor-2 alpha in von Hippel-Lindau renal cell carcinoma.* Oncogene, 2005. **24**(6): p. 1043-52.

170. Morris, M.E. and M.A. Felmlee, *Overview of the proton-coupled MCT (SLC16A) family of transporters: characterization, function and role in the transport of the drug of abuse gamma-hydroxybutyric acid.* Aaps J, 2008. **10**(2): p. 311-21.

171. Bhattacharya, I. and K.M. Boje, *Potential gamma-hydroxybutyric acid (GHB) drug interactions through blood-brain barrier transport inhibition: a pharmacokinetic simulation-based evaluation.* J Pharmacokinet Pharmacodyn, 2006. **33**(5): p. 657-81.

172. Pinheiro, C., et al., *Increased expression of monocarboxylate transporters 1, 2, and 4 in colorectal carcinomas.* Virchows Arch, 2008. **452**(2): p. 139-46.

173. Koukourakis, M.I., et al., *Comparison of metabolic pathways between cancer cells and stromal cells in colorectal carcinomas: a metabolic survival role for tumor-associated stroma.* Cancer Res, 2006. **66**(2): p. 632-7.

174. Lin, R.Y., et al., *Human monocarboxylate transporter 2 (MCT2) is a high affinity pyruvate transporter.* J Biol Chem, 1998. **273**(44): p. 28959-65.

175. Schneiderhan, W., et al., *CD147 Silencing Inhibits Lactate Transport and Reduces Malignant Potential of pancreatic cancer cells in in-vivo and in-vitro Models.* Gut, 2009.

176. Gallagher, S.M., et al., *Monocarboxylate transporter 4 regulates maturation and trafficking of CD147 to the plasma membrane in the metastatic breast cancer cell line MDA-MB-231.* Cancer Res, 2007. **67**(9): p. 4182-9.

177. Chan, M.M., et al., *Gene expression profiling of NMU-induced rat mammary tumors: cross species comparison with human breast cancer.* Carcinogenesis, 2005. **26**(8): p. 1343-53.

178. Dai, Z., et al., *Global methylation profiling of lung cancer identifies novel methylated genes.* Neoplasia, 2001. **3**(4): p. 314-23.

179. Daly, K., et al., *The importance of colonic butyrate transport to the regulation of genes associated with colonic tissue homoeostasis.* Biochem Soc Trans, 2005. **33**(Pt 4): p. 733-5.

180. Pinheiro, C., et al., *Increasing expression of monocarboxylate transporters 1 and 4 along progression to invasive cervical carcinoma.* Int J Gynecol Pathol, 2008. **27**(4): p. 568-74.

181. Gopal, E., et al., *Expression of slc5a8 in kidney and its role in Na(+)-coupled transport of lactate.* J Biol Chem, 2004. **279**(43): p. 44522-32.

182. Miyauchi, S., et al., *Functional identification of SLC5A8, a tumor suppressor down-regulated in colon cancer, as a Na(+)-coupled transporter for short-chain fatty acids.* J Biol Chem, 2004. **279**(14): p. 13293-6.

183. Srinivas, S.R., et al., *Cloning and functional identification of slc5a12 as a sodium-coupled low-affinity transporter for monocarboxylates (SMCT2).* Biochem J, 2005. **392**(Pt 3): p. 655-64.

184. Ganapathy, V., et al., *Sodium-coupled monocarboxylate transporters in normal tissues and in cancer.* Aaps J, 2008. **10**(1): p. 193-9.

185. Hashimoto, T., et al., *Immunohistochemical analysis of MCT1, MCT2 and MCT4 expression in rat plantaris muscle.* J Physiol, 2005. **567**(Pt 1): p. 121-9.

186. Kirk, P., et al., *CD147 is tightly associated with lactate transporters MCT1 and MCT4 and facilitates their cell surface expression.* Embo J, 2000. **19**(15): p. 3896-904.

187. Hashimoto, T., R. Hussien, and G.A. Brooks, *Colocalization of MCT1, CD147, and LDH in mitochondrial inner membrane of L6 muscle cells: evidence of a mitochondrial lactate oxidation complex.* Am J Physiol Endocrinol Metab, 2006. **290**(6): p. E1237-44.

188. Deora, A.A., et al., *Mechanisms regulating tissue-specific polarity of monocarboxylate transporters and their chaperone CD147 in kidney and retinal epithelia.* Proc Natl Acad Sci U S A, 2005. **102**(45): p. 16245-50.

189. Philp, N.J., et al., *Loss of MCT1, MCT3, and MCT4 expression in the retinal pigment epithelium and neural retina of the 5A11/basigin-null mouse.* Invest Ophthalmol Vis Sci, 2003. **44**(3): p. 1305-11.

190. Dubouchaud, H., et al., *Endurance training, expression, and physiology of LDH, MCT1, and MCT4 in human skeletal muscle.* Am J Physiol Endocrinol Metab, 2000. **278**(4): p. E571-9.

191. Lin, J., C. Handschin, and B.M. Spiegelman, *Metabolic control through the PGC-1 family of transcription coactivators.* Cell Metab, 2005. **1**(6): p. 361-70.

192. Boidot, R., et al., *Regulation of monocarboxylate transporter MCT1 expression by p53 mediates inward and outward lactate fluxes in tumors.* Cancer Res. **72**(4): p. 939-48.

193. Borthakur, A., et al., *Regulation of monocarboxylate transporter 1 (MCT1) promoter by butyrate in human intestinal epithelial cells: involvement of NF-kappaB pathway.* J Cell Biochem, 2008. **103**(5): p. 1452-63.

194. Enoki, T., et al., *Testosterone increases lactate transport, monocarboxylate transporter (MCT) 1 and MCT4 in rat skeletal muscle.* J Physiol, 2006. **577**(Pt 1): p. 433-43.

195. Fanelli, A., et al., *MCT1 and its accessory protein CD147 are differentially regulated by TSH in rat thyroid cells.* Am J Physiol Endocrinol Metab, 2003. **285**(6): p. E1223-9.

196. Mathupala, S.P., P. Parajuli, and A.E. Sloan, *Silencing of monocarboxylate transporters via small interfering ribonucleic acid inhibits glycolysis and induces cell death in malignant glioma: an in vitro study.* Neurosurgery, 2004. **55**(6): p. 1410-9; discussion 1419.

197. Ishihara, H., et al., *Overexpression of monocarboxylate transporter and lactate dehydrogenase alters insulin secretory responses to pyruvate and lactate in beta cells.* J Clin Invest, 1999. **104**(11): p. 1621-9.

198. Maekawa, F., et al., *Basal and stimulated lactate fluxes in primary cultures of astrocytes are differentially controlled by distinct proteins.* J Neurochem, 2008. **107**(3): p. 789-98.

199. Cuff, M.A., D.W. Lambert, and S.P. Shirazi-Beechey, *Substrate-induced regulation of the human colonic monocarboxylate transporter, MCT1.* J Physiol, 2002. **539**(Pt 2): p. 361-71.

200. Clausen, M.R., H. Bonnen, and P.B. Mortensen, *Colonic fermentation of dietary fibre to short chain fatty acids in patients with adenomatous polyps and colonic cancer.* Gut, 1991. **32**(8): p. 923-8.

201. Scheppach, W., H.P. Bartram, and F. Richter, *Role of short-chain fatty acids in the prevention of colorectal cancer.* Eur J Cancer, 1995. **31A**(7-8): p. 1077-80.

202. Kruh, J., *Effects of sodium butyrate, a new pharmacological agent, on cells in culture.* Mol Cell Biochem, 1982. **42**(2): p. 65-82.

203. Asada, K., et al., *Reduced expression of GNA11 and silencing of MCT1 in human breast cancers.* Oncology, 2003. **64**(4): p. 380-8.

204. Cuff, M., et al., *The human colonic monocarboxylate transporter Isoform 1: its potential importance to colonic tissue homeostasis.* Gastroenterology, 2005. **128**(3): p. 676-86.

205. Lambert, D.W., et al., *Molecular changes in the expression of human colonic nutrient transporters during the transition from normality to malignancy.* Br J Cancer, 2002. **86**(8): p. 1262-9.

206. Li, H., et al., *SLC5A8, a sodium transporter, is a tumor suppressor gene silenced by methylation in human colon aberrant crypt foci and cancers.* Proc Natl Acad Sci U S A, 2003. **100**(14): p. 8412-7.

207. Su, J., X. Chen, and T. Kanekura, *A CD147-targeting siRNA inhibits the proliferation, invasiveness, and VEGF production of human malignant melanoma cells by down-regulating glycolysis.* Cancer Lett, 2009. **273**(1): p. 140-7.

208. Pinheiro, C., et al., *Monocarboxylate transporter 1 is up-regulated in basal-like breast carcinoma.* Histopathology. **56**(7): p. 860-7.

209. Koukourakis, M.I., et al., *Lung cancer: a comparative study of metabolism related protein expression in cancer cells and tumor associated stroma.* Cancer Biol Ther, 2007. **6**(9): p. 1476-9.

210. Ladanyi, M., et al., *The precrystalline cytoplasmic granules of alveolar soft part sarcoma contain monocarboxylate transporter 1 and CD147.* Am J Pathol, 2002. **160**(4): p. 1215-21.

211. Fang, J., et al., *The H+-linked monocarboxylate transporter (MCT1/SLC16A1): a potential therapeutic target for high-risk neuroblastoma.* Mol Pharmacol, 2006. **70**(6): p. 2108-15.

212. Chenal, J., K. Pierre, and L. Pellerin, *Insulin and IGF-1 enhance the expression of the neuronal monocarboxylate transporter MCT2 by translational activation via stimulation of the phosphoinositide 3-kinase-Akt-mammalian target of rapamycin pathway.* Eur J Neurosci, 2008. **27**(1): p. 53-65.

213. Chenal, J. and L. Pellerin, *Noradrenaline enhances the expression of the neuronal monocarboxylate transporter MCT2 by translational activation via stimulation of PI3K/Akt and the mTOR/S6K pathway.* J Neurochem, 2007. **102**(2): p. 389-97.

214. Wahl, M.L., et al., *Regulation of intracellular pH in human melanoma: potential therapeutic implications.* Mol Cancer Ther, 2002. **1**(8): p. 617-28.

215. Mahoney, B.P., et al., *Tumor acidity, ion trapping and chemotherapeutics. I. Acid pH affects the distribution of chemotherapeutic agents in vitro.* Biochem Pharmacol, 2003. **66**(7): p. 1207-18.

216. Manning Fox, J.E., D. Meredith, and A.P. Halestrap, *Characterisation of human monocarboxylate transporter 4 substantiates its role in lactic acid efflux from skeletal muscle.* J Physiol, 2000. **529 Pt 2**: p. 285-93.

217. Meredith, D. and H.C. Christian, *The SLC16 monocaboxylate transporter family.* Xenobiotica, 2008. **38**(7-8): p. 1072-106.

218. Jackson, V.N. and A.P. Halestrap, *The kinetics, substrate, and inhibitor specificity of the monocarboxylate (lactate) transporter of rat liver cells determined using the fluorescent intracellular pH indicator, 2',7'-bis(carboxyethyl)-5(6)-carboxyfluorescein.* J Biol Chem, 1996. **271**(2): p. 861-8.

219. Carpenter, L. and A.P. Halestrap, *The kinetics, substrate and inhibitor specificity of the lactate transporter of Ehrlich-Lettre tumour cells studied with the intracellular pH indicator BCECF.* Biochem J, 1994. **304 (Pt 3)**: p. 751-60.

220. Wilson, M.C., et al., *Lactic acid efflux from white skeletal muscle is catalyzed by the monocarboxylate transporter isoform MCT3.* J Biol Chem, 1998. **273**(26): p. 15920-6.

221. Halestrap, A.P. *Inhibiting lactate oxidation in tumor cells*. eLetters 2008; Available from: http://www.jci.org/eletters/view/36843#sec1.

222. Halestrap, A.P., *The mitochondrial pyruvate carrier. Kinetics and specificity for substrates and inhibitors.* Biochem J, 1975. **148**(1): p. 85-96.

223. Halestrap, A.P. and R.M. Denton, *The specificity and metabolic implications of the inhibition of pyruvate transport in isolated mitochondria and intact tissue preparations by alpha-Cyano-4-hydroxycinnamate and related compounds.* Biochem J, 1975. **148**(1): p. 97-106.

224. Bueno, V., et al., *The specific monocarboxylate transporter (MCT1) inhibitor, AR-C117977, a novel immunosuppressant, prolongs allograft survival in the mouse.* Transplantation, 2007. **84**(9): p. 1204-7.

225. Fishbein, W.N., *Lactate transporter defect: a new disease of muscle.* Science, 1986. **234**(4781): p. 1254-6.

226. Mitalipov, S. and D. Wolf, *Totipotency, pluripotency and nuclear reprogramming.* Adv Biochem Eng Biotechnol, 2009. **114**: p. 185-99.

227. da Silva Meirelles, L., P.C. Chagastelles, and N.B. Nardi, *Mesenchymal stem cells reside in virtually all post-natal organs and tissues.* J Cell Sci, 2006. **119**(Pt 11): p. 2204-13.

228. Kalluri, R. and R.A. Weinberg, *The basics of epithelial-mesenchymal transition.* J Clin Invest, 2009. **119**(6): p. 1420-8.

229. Kurrey, N.K., A. K, and S.A. Bapat, *Snail and Slug are major determinants of ovarian cancer invasiveness at the transcription level.* Gynecol Oncol, 2005. **97**(1): p. 155-65.

230. Yang, J., et al., *Twist, a master regulator of morphogenesis, plays an essential role in tumor metastasis.* Cell, 2004. **117**(7): p. 927-39.

231. Moen, I., et al., *Hyperoxic treatment induces mesenchymal-to-epithelial transition in a rat adenocarcinoma model.* PLoS ONE, 2009. **4**(7): p. e6381.

232. Jiang, J., Y.L. Tang, and X.H. Liang, *EMT: a new vision of hypoxia promoting cancer progression.* Cancer Biol Ther, 2011. **11**(8): p. 714-23.

233. Evans, S.M., et al., *Detection of hypoxia in human squamous cell carcinoma by EF5 binding.* Cancer Res, 2000. **60**(7): p. 2018-24.

234. Geradts, J., et al., *Nuclear Snail1 and nuclear ZEB1 protein expression in invasive and intraductal human breast carcinomas.* Hum Pathol. **42**(8): p. 1125-31.

235. Moody, S.E., et al., *The transcriptional repressor Snail promotes mammary tumor recurrence.* Cancer Cell, 2005. **8**(3): p. 197-209.

236. Hu, C.T., et al., *The transcriptional factor Snail simultaneously triggers cell cycle arrest and migration of human hepatoma HepG2.* J Biomed Sci, 2008. **15**(3): p. 343-55.

237. Zhang, A., et al., *Antisense-Snail transfer inhibits tumor metastasis by inducing E-cadherin expression.* Anticancer Res, 2008. **28**(2A): p. 621-8.

238. Zeisberg, E.M., et al., *Discovery of endothelial to mesenchymal transition as a source for carcinoma-associated fibroblasts.* Cancer Res, 2007. **67**(21): p. 10123-8.

239. Zeisberg, E.M., et al., *Endothelial-to-mesenchymal transition contributes to cardiac fibrosis.* Nat Med, 2007. **13**(8): p. 952-61.

240. Zeisberg, M., et al., *Fibroblasts derive from hepatocytes in liver fibrosis via epithelial to mesenchymal transition.* J Biol Chem, 2007. **282**(32): p. 23337-47.

241. Trabold, O., et al., *Lactate and oxygen constitute a fundamental regulatory mechanism in wound healing.* Wound Repair Regen, 2003. **11**(6): p. 504-9.

242. Khalil, N., et al., *Macrophage production of transforming growth factor beta and fibroblast collagen synthesis in chronic pulmonary inflammation.* J Exp Med, 1989. **170**(3): p. 727-37.

243. Cho, H.J., et al., *Snail is required for transforming growth factor-beta-induced epithelial-mesenchymal transition by activating PI3 kinase/Akt signal pathway.* Biochem Biophys Res Commun, 2007. **353**(2): p. 337-43.

244. Julien, S., et al., *Activation of NF-kappaB by Akt upregulates Snail expression and induces epithelium mesenchyme transition.* Oncogene, 2007. **26**(53): p. 7445-56.

245. Miller, A.M., et al., *Lactate treatment causes NF-kappaB activation and CD44 shedding in cultured trabecular meshwork cells.* Invest Ophthalmol Vis Sci, 2007. **48**(4): p. 1615-21.

246. Vegran, F., et al., *Lactate influx through the endothelial cell monocarboxylate transporter MCT1 supports an NF-kappaB/IL-8 pathway that drives tumor angiogenesis.* Cancer Res. **71**(7): p. 2550-60.

247. Martinez-Outschoorn, U.E., et al., *Ketones and lactate increase cancer cell "stemness," driving recurrence, metastasis and poor clinical outcome in breast cancer: achieving personalized medicine via Metabolo-Genomics.* Cell Cycle. **10**(8): p. 1271-86.

248. Mothersill, C., et al., *A role for lactate in the differentiation of cultured sheep thyroid cells.* Cell Biol Int Rep, 1981. **5**(9): p. 877-86.

249. Lee, S.Y., et al., *Wnt/Snail signaling regulates cytochrome C oxidase and glucose metabolism.* Cancer Res. **72**(14): p. 3607-17.

250. Zieker, D., et al., *Lactate modulates gene expression in human mesenchymal stem cells.* Langenbecks Arch Surg, 2008. **393**(3): p. 297-301.

251. Clough, J.R. and D.G. Whittingham, *Metabolism of [14C]glucose by postimplantation mouse embryos in vitro.* J Embryol Exp Morphol, 1983. **74**: p. 133-42.

252. Biggers, J.D., D.G. Whittingham, and R.P. Donahue, *The pattern of energy metabolism in the mouse oocyte and zygote.* Proc Natl Acad Sci U S A, 1967. **58**(2): p. 560-7.

253. Aomatsu, K., et al., *Slug is upregulated during wound healing and regulates cellular phenotypes in corneal epithelial cells.* Invest Ophthalmol Vis Sci. **53**(2): p. 751-6.

254. Thiery, J.P., *Epithelial-mesenchymal transitions in tumour progression.* Nat Rev Cancer, 2002. **2**(6): p. 442-54.

255. Barrallo-Gimeno, A. and M.A. Nieto, *The Snail genes as inducers of cell movement and survival: implications in development and cancer.* Development, 2005. **132**(14): p. 3151-61.

256. Dressman, H.K., et al., *Gene expression profiles of multiple breast cancer phenotypes and response to neoadjuvant chemotherapy.* Clin Cancer Res, 2006. **12**(3 Pt 1): p. 819-26.

257. Nolen, B.M., et al., *Serum biomarker profiles and response to neoadjuvant chemotherapy for locally advanced breast cancer.* Breast Cancer Res, 2008. **10**(3): p. R45.

258. Mueller-Klieser, W. and S. Walenta, *Geographical mapping of metabolites in biological tissue with quantitative bioluminescence and single photon imaging.* Histochem J, 1993. **25**(6): p. 407-20.

259. Schwickert, G., S. Walenta, and W. Mueller-Klieser, *Mapping and quantification of biomolecules in tumor biopsies using bioluminescence.* Experientia, 1996. **52**(5): p. 460-3.

260. Singletary, S.E., et al., *Staging system for breast cancer: revisions for the 6th edition of the AJCC Cancer Staging Manual.* Surg Clin North Am, 2003. **83**(4): p. 803-19.

261. Valero, V.V., A.U. Buzdar, and G.N. Hortobagyi, *Locally Advanced Breast Cancer.* Oncologist, 1996. **1**(1 & 2): p. 8-17.

262. El Saghir, N.S., et al., *Locally advanced breast cancer: treatment guideline implementation with particular attention to low- and middle-income countries.* Cancer, 2008. **113**(8 Suppl): p. 2315-24.

263. Newman, L.A., *Management of patients with locally advanced breast cancer.* Curr Oncol Rep, 2004. **6**(1): p. 53-61.

264. Hortobagyi, G.N. and A.U. Buzdar, *Management of locally advanced breast cancer.* Am J Clin Oncol, 1988. **11**(5): p. 597-601.

265. Vujaskovic, Z., et al., *A phase I/II study of neoadjuvant liposomal doxorubicin, paclitaxel, and hyperthermia in locally advanced breast cancer.* Int J Hyperthermia, 2010. **26**(5): p. 514-21.

266. Craciunescu, O.I., et al., *DCE-MRI parameters have potential to predict response of locally advanced breast cancer patients to neoadjuvant chemotherapy and hyperthermia: a pilot study.* Int J Hyperthermia, 2009. **25**(6): p. 405-15.

267. Goodwin, M.L., et al., *Blood lactate measurements and analysis during exercise: a guide for clinicians.* J Diabetes Sci Technol, 2007. **1**(4): p. 558-69.

268. Zetterstrom, R., *C. Cori (1896-1984), G. Cori (1896-1957) and B. Houssay (1887-1971) Nobel Prize in 1947 for discoveries of glycogen metabolism with relevant and irrelevant clinical implications.* Acta Paediatr, 2007. **96**(6): p. 935-8.

269. Cori, C.F., *Mammalian Carbohydrate Metabolism.* Physiol Rev, 1931. **11**(2): p. 143-275.

270. Oshida, M., et al., *Predicting the prognoses of breast carcinoma patients with positron emission tomography using 2-deoxy-2-fluoro[18F]-D-glucose.* Cancer, 1998. **82**(11): p. 2227-34.

271. Gatenby, R.A., et al., *Cellular adaptations to hypoxia and acidosis during somatic evolution of breast cancer.* Br J Cancer, 2007. **97**(5): p. 646-53.

272. Sauer, L.A. and R.T. Dauchy, *In vivo lactate production and utilization by Jensen sarcoma and Morris hepatoma 7288CTC.* Cancer Res, 1986. **46**(2): p. 689-93.

273. Sauer, L.A. and R.T. Dauchy, *Lactate release and uptake in hepatoma 7288CTC perfused in situ with L-[(U)-14C]lactate or D-[(U)-14C]glucose.* Metabolism, 1994. **43**(12): p. 1488-97.

274. Suarez, M., et al., *Early diagnosis of recurrent breast cancer with FDG-PET in patients with progressive elevation of serum tumor markers.* Q J Nucl Med, 2002. **46**(2): p. 113-21.

275. Dose Schwarz, J., et al., *Early prediction of response to chemotherapy in metastatic breast cancer using sequential 18F-FDG PET.* J Nucl Med, 2005. **46**(7): p. 1144-50.

276. Emmering, J., et al., *Preoperative [18F] FDG-PET after chemotherapy in locally advanced breast cancer: prognostic value as compared with histopathology.* Ann Oncol, 2008. **19**(9): p. 1573-7.

277. Gallagher, B.M., et al., *Metabolic trapping as a principle of oradiopharmaceutical design: some factors resposible for the biodistribution of [18F] 2-deoxy-2-fluoro-D-glucose.* J Nucl Med, 1978. **19**(10): p. 1154-61.

278. Vazquez, A., et al., *Catabolic efficiency of aerobic glycolysis: the Warburg effect revisited.* BMC Syst Biol. **4**: p. 58.

279. Parra-Bonilla, G., et al., *Critical role for lactate dehydrogenase A in aerobic glycolysis that sustains pulmonary microvascular endothelial cell proliferation.* Am J Physiol Lung Cell Mol Physiol. **299**(4): p. L513-22.

280. Bulik, M., et al., *Potential of MR spectroscopy for assessment of glioma grading.* Clin Neurol Neurosurg, 2013. **115**(2): p. 146-53.

281. Lodi, A., S.M. Woods, and S.M. Ronen, *Treatment with the MEK inhibitor U0126 induces decreased hyperpolarized pyruvate to lactate conversion in breast, but not prostate, cancer cells.* NMR Biomed, 2013. **26**(3): p. 299-306.

282. Harris, T., et al., *Kinetics of hyperpolarized 13C1-pyruvate transport and metabolism in living human breast cancer cells.* Proc Natl Acad Sci U S A, 2009. **106**(43): p. 18131-6.

283. Albers, M.J., et al., *Hyperpolarized 13C lactate, pyruvate, and alanine: noninvasive biomarkers for prostate cancer detection and grading.* Cancer Res, 2008. **68**(20): p. 8607-15.

284. Carey, F.A., *Organic Chemistry*. Sixth ed2006, 1221 Avenue of the Americas, New York, NY: McGraw-Hill.

285. Kaplan, O. and J.S. Cohen, *Metabolism of breast cancer cells as revealed by non-invasive magnetic resonance spectroscopy studies.* Breast Cancer Res Treat, 1994. **31**(2-3): p. 285-99.

286. Gribbestad, I.S., et al., *In vitro proton NMR spectroscopy of extracts from human breast tumours and non-involved breast tissue.* Anticancer Res, 1993. **13**(6A): p. 1973-80.

287. Krebs, H.A. and D. Bellamy, *The interconversion of glutamic acid and aspartic acid in respiring tissues.* Biochem J, 1960. **75**: p. 523-9.

288. Reitzer, L.J., B.M. Wice, and D. Kennell, *Evidence that glutamine, not sugar, is the major energy source for cultured HeLa cells.* J Biol Chem, 1979. **254**(8): p. 2669-76.

289. Zielke, H.R., et al., *Lactate: a major product of glutamine metabolism by human diploid fibroblasts.* J Cell Physiol, 1980. **104**(3): p. 433-41.

290. Kennedy, K.M., Scarbrough, P. M., Ribeiro, A., Richardson, R., Yuan, H., Sonveaux, P., Landon, C. D., Chi, J., Pizzo, S., Schroeder, T., Dewhirst, M. W., *Exogenous lactate is well-tolerated and utilized in breast cancer.* PloS ONE, 2013, in press.

291. Hussien, R. and G.A. Brooks, *Mitochondrial and plasma membrane lactate transporter and lactate dehydrogenase isoform expression in breast cancer cell lines.* Physiol Genomics. **43**(5): p. 255-64.

292. Di Donato, L., et al., *Rates of gluconeogenesis and citric acid cycle in perfused livers, assessed from the mass spectrometric assay of the 13C labeling pattern of glutamate.* J Biol Chem, 1993. **268**(6): p. 4170-80.

293. Majumdar, A. and H.M. Sonawat, *A two-dimensional 1H detected 13C NMR investigation of pyruvate metabolism in Halobacterium salinarium.* J Biochem, 1998. **123**(1): p. 115-9.

294. Marjanska, M., et al., *In vivo 13C spectroscopy in the rat brain using hyperpolarized [1-(13)C]pyruvate and [2-(13)C]pyruvate.* J Magn Reson, 2010. **206**(2): p. 210-8.

295. Gallagher, C.N., et al., *The human brain utilizes lactate via the tricarboxylic acid cycle: a 13C-labelled microdialysis and high-resolution nuclear magnetic resonance study.* Brain, 2009. **132**(Pt 10): p. 2839-49.

296. Rodrigues, T.B., et al., *Futile cycling of lactate through the plasma membrane of C6 glioma cells as detected by (13C, 2H) NMR.* J Neurosci Res, 2005. **79**(1-2): p. 119-27.

297. Sonveaux, P., et al., *Targeting the lactate transporter MCT1 in endothelial cells inhibits lactate-induced HIF-1 activation and tumor angiogenesis.* PLoS ONE, 2012. **7**(3): p. e33418.

298. Varani, J., W. Orr, and P.A. Ward, *A comparison of the migration patterns of normal and malignant cells in two assay systems.* Am J Pathol, 1978. **90**(1): p. 159-72.

299. Zhao, R., et al., *Hepatoma cell line HepG2.2.15 demonstrates distinct biological features compared with parental HepG2.* World J Gastroenterol, 2011. **17**(9): p. 1152-9.

300. ATCC. *MEF-1.* Available from: http://www.atcc.org/Products/All/CRL-2214.aspx.

301. Thomson, J.A., et al., *Embryonic stem cell lines derived from human blastocysts.* Science, 1998. **282**(5391): p. 1145-7.

302. Rafii, S., et al., *Angiogenic factors reconstitute hematopoiesis by recruiting stem cells from bone marrow microenvironment.* Ann N Y Acad Sci, 2003. **996**: p. 49-60.

303. Tavor, S., et al., *CXCR4 regulates migration and development of human acute myelogenous leukemia stem cells in transplanted NOD/SCID mice.* Cancer Res, 2004. **64**(8): p. 2817-24.

304. Herrero, P., et al., *L-3-11C-lactate as a PET tracer of myocardial lactate metabolism: a feasibility study.* J Nucl Med, 2007. **48**(12): p. 2046-55.

305. Birsoy, K., et al., *MCT1-mediated transport of a toxic molecule is an effective strategy for targeting glycolytic tumors.* Nat Genet, 2013. **45**(1): p. 104-8.

306. Dhup, S., et al., *Multiple biological activities of lactic acid in cancer: influences on tumor growth, angiogenesis and metastasis.* Curr Pharm Des. **18**(10): p. 1319-30.

307. Diers, A.R., et al., *Pyruvate fuels mitochondrial respiration and proliferation of breast cancer cells: effect of monocarboxylate transporter inhibition.* Biochem J. **444**(3): p. 561-71.

308. Mendes-Mourao, J., et al., *The involvement of mitochondrial pyruvate transport in the pathways of gluconeogenesis from serine and alanine in isolated rat and mouse liver cells.* FEBS Lett, 1975. **53**(1): p. 29-32.

309. Colen, C.B., et al., *Metabolic remodeling of malignant gliomas for enhanced sensitization during radiotherapy: an in vitro study.* Neurosurgery, 2006. **59**(6): p. 1313-23; discussion 1323-4.

310. Colen, C.B., et al., *Metabolic targeting of lactate efflux by malignant glioma inhibits invasiveness and induces necrosis: an in vivo study.* Neoplasia. **13**(7): p. 620-32.

311. Gatenby, R.A., *The potential role of transformation-induced metabolic changes in tumor-host interaction.* Cancer Res, 1995. **55**(18): p. 4151-6.

312. Gatenby, R.A. and E.T. Gawlinski, *The glycolytic phenotype in carcinogenesis and tumor invasion: insights through mathematical models.* Cancer Res, 2003. **63**(14): p. 3847-54.

313. Gatenby, R.A. and R.J. Gillies, *A microenvironmental model of carcinogenesis.* Nat Rev Cancer, 2008. **8**(1): p. 56-61.

314. Grotius, J., et al., *Impact of exogenous lactate on survival and radioresponse of carcinoma cells in vitro.* Int J Radiat Biol, 2009. **85**(11): p. 989-1001.

315. Wohnsland, S., et al., *Neurons and neuronal stem cells survive in glucose-free lactate and in high glucose cell culture medium during normoxia and anoxia.* Neurochem Res, 2010. **35**(10): p. 1635-42.

316. Cooper, G., *Chapter 14: The Eukaryotic Cell Cycle*, in *The cell: a molecular approach*2000, ASM Press: Washington D.C.

317. Liotta, L.A. and E. Kohn, *Anoikis: cancer and the homeless cell.* Nature, 2004. **430**(7003): p. 973-4.

318. Demidenko, Z.N., et al., *Paradoxical suppression of cellular senescence by p53.* Proc Natl Acad Sci U S A, 2010. **107**(21): p. 9660-4.

319. Ahmad, I.M., et al., *Mitochondrial O2*- and H2O2 mediate glucose deprivation-induced stress in human cancer cells.* J Biol Chem, 2005. **280**(6): p. 4254-63.

320. Blackburn, R.V., et al., *Metabolic oxidative stress activates signal transduction and gene expression during glucose deprivation in human tumor cells.* Free Radic Biol Med, 1999. **26**(3-4): p. 419-30.

321. Hsiao, Y.P., et al., *Antiproliferative effects of lactic acid via the induction of apoptosis and cell cycle arrest in a human keratinocyte cell line (HaCaT).* J Dermatol Sci, 2009. **54**(3): p. 175-84.

322. Lampe, K.J., et al., *Impact of lactic acid on cell proliferation and free radical-induced cell death in monolayer cultures of neural precursor cells.* Biotechnol Bioeng, 2009. **103**(6): p. 1214-23.

323. Simpson, C.D., K. Anyiwe, and A.D. Schimmer, *Anoikis resistance and tumor metastasis.* Cancer Lett, 2008. **272**(2): p. 177-85.

324. Cairns, R.A., T. Kalliomaki, and R.P. Hill, *Acute (cyclic) hypoxia enhances spontaneous metastasis of KHT murine tumors.* Cancer Res, 2001. **61**(24): p. 8903-8.

325. Dewhirst, M.W., *Mechanisms underlying hypoxia development in tumors.* Adv Exp Med Biol, 2003. **510**: p. 51-6.

326. Tannock, I.F., *The relation between cell proliferation and the vascular system in a transplanted mouse mammary tumour.* Br J Cancer, 1968. **22**(2): p. 258-73.

327. Batchelder, R.M., et al., *Oxygen dependence of the cytotoxicity of the enediyne anti-tumour antibiotic esperamicin A1.* Br J Cancer Suppl, 1996. **27**: p. S52-6.

328. Comerford, K.M., et al., *Hypoxia-inducible factor-1-dependent regulation of the multidrug resistance (MDR1) gene.* Cancer Res, 2002. **62**(12): p. 3387-94.

329. Brown, J.M. and W.R. Wilson, *Exploiting tumour hypoxia in cancer treatment.* Nat Rev Cancer, 2004. **4**(6): p. 437-47.

330. Chou, C.W., et al., *Tumor cycling hypoxia induces chemoresistance in glioblastoma multiforme by upregulating the expression and function of ABCB1.* Neuro Oncol. **14**(10): p. 1227-38.

331. Hsieh, C.H., et al., *Cycling hypoxia increases U87 glioma cell radioresistance via ROS induced higher and long-term HIF-1 signal transduction activity.* Oncol Rep. **24**(6): p. 1629-36.

332. Hsieh, C.H., et al., *NADPH oxidase subunit 4-mediated reactive oxygen species contribute to cycling hypoxia-promoted tumor progression in glioblastoma multiforme.* PLoS One. **6**(9): p. e23945.

333. Hsieh, C.H., et al., *NADPH oxidase subunit 4 mediates cycling hypoxia-promoted radiation resistance in glioblastoma multiforme.* Free Radic Biol Med. **53**(4): p. 649-58.

334. Ullah, M.S., A.J. Davies, and A.P. Halestrap, *The plasma membrane lactate transporter MCT4, but not MCT1, is up-regulated by hypoxia through a HIF-1alpha-dependent mechanism.* J Biol Chem, 2006. **281**(14): p. 9030-7.

335. Pinheiro, C., et al., *Expression of monocarboxylate transporters 1, 2, and 4 in human tumours and their association with CD147 and CD44.* J Biomed Biotechnol. **2010**: p. 427694.

336. Martinive, P., et al., *Preconditioning of the tumor vasculature and tumor cells by intermittent hypoxia: implications for anticancer therapies.* Cancer Res, 2006. **66**(24): p. 11736-44.

337. Dewhirst, M.W., *Intermittent hypoxia furthers the rationale for hypoxia-inducible factor-1 targeting.* Cancer Res, 2007. **67**(3): p. 854-5.

338. Yuan, G., et al., *Ca2+/calmodulin kinase-dependent activation of hypoxia inducible factor 1 transcriptional activity in cells subjected to intermittent hypoxia.* J Biol Chem, 2005. **280**(6): p. 4321-8.

339. Brurberg, K.G., B.A. Graff, and E.K. Rofstad, *Temporal heterogeneity in oxygen tension in human melanoma xenografts.* Br J Cancer, 2003. **89**(2): p. 350-6.

340. Achermann, R.E., et al., *Oxygenation of spontaneous canine tumors during fractionated radiation therapy.* Strahlenther Onkol, 2004. **180**(5): p. 297-305.

341. Pigott, K.H., et al., *Microregional fluctuations in perfusion within human tumours detected using laser Doppler flowmetry.* Radiother Oncol, 1996. **40**(1): p. 45-50.

342. Kimura, H., et al., *Fluctuations in red cell flux in tumor microvessels can lead to transient hypoxia and reoxygenation in tumor parenchyma.* Cancer Res, 1996. **56**(23): p. 5522-8.

343. Lin, Z., et al., *The influence of changes in tumor hypoxia on dose-painting treatment plans based on 18F-FMISO positron emission tomography.* Int J Radiat Oncol Biol Phys, 2008. **70**(4): p. 1219-28.

344. Saunders, L.R. and E. Verdin, *Sirtuins: critical regulators at the crossroads between cancer and aging.* Oncogene, 2007. **26**(37): p. 5489-504.

345. Lim, J.H., et al., *Sirtuin 1 modulates cellular responses to hypoxia by deacetylating hypoxia-inducible factor 1alpha.* Mol Cell. **38**(6): p. 864-78.

346. Nemoto, S., M.M. Fergusson, and T. Finkel, *SIRT1 functionally interacts with the metabolic regulator and transcriptional coactivator PGC-1{alpha}.* J Biol Chem, 2005. **280**(16): p. 16456-60.

347. Yang, H., et al., *Nutrient-sensitive mitochondrial NAD+ levels dictate cell survival.* Cell, 2007. **130**(6): p. 1095-107.

348. Alano, C.C., W. Ying, and R.A. Swanson, *Poly(ADP-ribose) polymerase-1-mediated cell death in astrocytes requires NAD+ depletion and mitochondrial permeability transition.* J Biol Chem, 2004. **279**(18): p. 18895-902.

349. Ying, W., *NAD+ and NADH in cellular functions and cell death.* Front Biosci, 2006. **11**: p. 3129-48.

350. Kingsley-Hickman, P.B., et al., *31P NMR measurement of mitochondrial uncoupling in isolated rat hearts.* J Biol Chem, 1990. **265**(3): p. 1545-50.

351. Dranka, B.P., B.G. Hill, and V.M. Darley-Usmar, *Mitochondrial reserve capacity in endothelial cells: The impact of nitric oxide and reactive oxygen species.* Free Radic Biol Med, 2010. **48**(7): p. 905-14.

352. Hill, B.G., et al., *Importance of the bioenergetic reserve capacity in response to cardiomyocyte stress induced by 4-hydroxynonenal.* Biochem J, 2009. **424**(1): p. 99-107.

353. Oberley, L.W. and G.R. Buettner, *Role of superoxide dismutase in cancer: a review.* Cancer Res, 1979. **39**(4): p. 1141-9.

354. Mohazzab, H.K., P.M. Kaminski, and M.S. Wolin, *Lactate and PO2 modulate superoxide anion production in bovine cardiac myocytes: potential role of NADH oxidase.* Circulation, 1997. **96**(2): p. 614-20.

355. Wiseman, H. and B. Halliwell, *Damage to DNA by reactive oxygen and nitrogen species: role in inflammatory disease and progression to cancer.* Biochem J, 1996. **313 (Pt 1)**: p. 17-29.

356. Porporato, P.E., et al., *Anticancer targets in the glycolytic metabolism of tumors: a comprehensive review.* Front Pharmacol. **2**: p. 49.

357. Kato, M., et al., *Distinct structural mechanisms for inhibition of pyruvate dehydrogenase kinase isoforms by AZD7545, dichloroacetate, and radicicol.* Structure, 2007. **15**(8): p. 992-1004.

358. Bonnet, S., et al., *A mitochondria-K+ channel axis is suppressed in cancer and its normalization promotes apoptosis and inhibits cancer growth.* Cancer Cell, 2007. **11**(1): p. 37-51.

359. Papandreou, I., T. Goliasova, and N.C. Denko, *Anticancer drugs that target metabolism: Is dichloroacetate the new paradigm?* Int J Cancer, 2011. **128**(5): p. 1001-8.

360. Michelakis, E.D., et al., *Metabolic modulation of glioblastoma with dichloroacetate.* Sci Transl Med, 2010. **2**(31): p. 31ra34.

361. Robey, I.F. and N.K. Martin, *Bicarbonate and dichloroacetate: evaluating pH altering therapies in a mouse model for metastatic breast cancer.* BMC Cancer, 2011. **11**: p. 235.

362. Kim, H.S., et al., *Carbohydrate restriction and lactate transporter inhibition in a mouse xenograft model of human prostate cancer.* BJU Int, 2012. **110**(7): p. 1062-9.

363. Thornton, S. *Deleterious effect of targeting lactate transporters in tumuor cells*. eLetters 2009; Available from: http://www.jci.org/eletters/view/36843#sec1.

364. Cantor, J.R. and D.M. Sabatini, *Cancer cell metabolism: one hallmark, many faces.* Cancer Discov, 2012. **2**(10): p. 881-98.

365. Neve, R.M., et al., *A collection of breast cancer cell lines for the study of functionally distinct cancer subtypes.* Cancer Cell, 2006. **10**(6): p. 515-27.

366. Ibrahim, E., et al., *Basal vs. luminal A breast cancer subtypes: a matched case-control study using estrogen receptor, progesterone receptor, and HER-2 as surrogate markers.* Med Oncol, 2009. **26**(3): p. 372-8.

367. Rouzier, R., et al., *Breast cancer molecular subtypes respond differently to preoperative chemotherapy.* Clin Cancer Res, 2005. **11**(16): p. 5678-85.

368. Komarova, E.A., et al., *Intracellular localization of p53 tumor suppressor protein in gamma-irradiated cells is cell cycle regulated and determined by the nucleus.* Cancer Res, 1997. **57**(23): p. 5217-20.

369. Filyak, O.S. and R.S. Stoika, *Comparative study of p53 expression in human carcinoma cell lines A549 and MCF7 under anticancer drug treatment.* Ukr Biokhim Zh, 2005. **77**(2): p. 136-40.

370. Kellen, J.A. and A. Mirakian, *The effect of toremifene on the expression of genes in a rat mammary adenocarcinoma.* In Vivo, 1996. **10**(5): p. 511-3.

371. Hui, L., et al., *Mutant p53 in MDA-MB-231 breast cancer cells is stabilized by elevated phospholipase D activity and contributes to survival signals generated by phospholipase D.* Oncogene, 2006. **25**(55): p. 7305-10.

372. Katayose, D., et al., *Cytotoxic effects of adenovirus-mediated wild-type p53 protein expression in normal and tumor mammary epithelial cells.* Clin Cancer Res, 1995. **1**(8): p. 889-97.

373. Maddocks, O.D. and K.H. Vousden, *Metabolic regulation by p53.* J Mol Med (Berl), 2011. **89**(3): p. 237-45.

374. Walenta, S. and W.F. Mueller-Klieser, *Lactate: mirror and motor of tumor malignancy.* Semin Radiat Oncol, 2004. **14**(3): p. 267-74.

375. Walenta, S., et al., *Tissue gradients of energy metabolites mirror oxygen tension gradients in a rat mammary carcinoma model.* Int J Radiat Oncol Biol Phys, 2001. **51**(3): p. 840-8.

376. Ege, G.N., et al., *Effects of a metastatic (13762) and nonmetastatic (R3230AC) mammary adenocarcinoma on radiocolloid localization in regional lymph nodes in Fischer 344 rats.* J Reticuloendothel Soc, 1983. **34**(6): p. 449-62.

377. Pavlides, S., et al., *The reverse Warburg effect: aerobic glycolysis in cancer associated fibroblasts and the tumor stroma.* Cell Cycle, 2009. **8**(23): p. 3984-4001.

378. Witkiewicz, A.K., et al., *Stromal caveolin-1 levels predict early DCIS progression to invasive breast cancer.* Cancer Biol Ther, 2009. **8**(11): p. 1071-9.

379. Witkiewicz, A.K., et al., *An absence of stromal caveolin-1 expression predicts early tumor recurrence and poor clinical outcome in human breast cancers.* Am J Pathol, 2009. **174**(6): p. 2023-34.

380. Pavlides, S., et al., *Loss of stromal caveolin-1 leads to oxidative stress, mimics hypoxia and drives inflammation in the tumor microenvironment, conferring the "reverse Warburg effect": a transcriptional informatics analysis with validation.* Cell Cycle. **9**(11): p. 2201-19.

381. Pavlides, S., et al., *Transcriptional evidence for the "Reverse Warburg Effect" in human breast cancer tumor stroma and metastasis: similarities with oxidative stress, inflammation, Alzheimer's disease, and "Neuron-Glia Metabolic Coupling".* Aging (Albany NY). **2**(4): p. 185-99.

382. Pavlides, S., et al., *Warburg meets autophagy: cancer-associated fibroblasts accelerate tumor growth and metastasis via oxidative stress, mitophagy, and aerobic glycolysis.* Antioxid Redox Signal. **16**(11): p. 1264-84.

383. Ariazi, E.A., G.M. Clark, and J.E. Mertz, *Estrogen-related receptor alpha and estrogen-related receptor gamma associate with unfavorable and favorable biomarkers, respectively, in human breast cancer.* Cancer Res, 2002. **62**(22): p. 6510-8.

384. Suzuki, T., et al., *Estrogen-related receptor alpha in human breast carcinoma as a potent prognostic factor.* Cancer Res, 2004. **64**(13): p. 4670-6.

385. Stein, R.A., et al., *Estrogen-related receptor alpha is critical for the growth of estrogen receptor-negative breast cancer.* Cancer Res, 2008. **68**(21): p. 8805-12.

386. Stein, R.A., S. Gaillard, and D.P. McDonnell, *Estrogen-related receptor alpha induces the expression of vascular endothelial growth factor in breast cancer cells.* J Steroid Biochem Mol Biol, 2009. **114**(1-2): p. 106-12.

387. Stein, R.A. and D.P. McDonnell, *Estrogen-related receptor alpha as a therapeutic target in cancer.* Endocr Relat Cancer, 2006. **13 Suppl 1**: p. S25-32.

388. Benton, C.R., et al., *PGC-1alpha increases skeletal muscle lactate uptake by increasing the expression of MCT1 but not MCT2 or MCT4.* Physiol Genomics, 2008. **35**(1): p. 45-54.

389. Cai, Q., et al., *Regulation of glycolysis and the Warburg effect by estrogen-related receptors.* Oncogene, 2012.

390. Gaillard, S., M.A. Dwyer, and D.P. McDonnell, *Definition of the molecular basis for estrogen receptor-related receptor-alpha-cofactor interactions.* Mol Endocrinol, 2007. **21**(1): p. 62-76.

391. Schena, M., et al., *Quantitative monitoring of gene expression patterns with a complementary DNA microarray.* Science, 1995. **270**(5235): p. 467-70.

392. Kulesh, D.A., et al., *Identification of interferon-modulated proliferation-related cDNA sequences.* Proc Natl Acad Sci U S A, 1987. **84**(23): p. 8453-7.

393. *Concepts of genetics* 10 ed2012, San Francisco: Pearson Education.

394. Anderson, N.L. and N.G. Anderson, *Proteome and proteomics: new technologies, new concepts, and new words.* Electrophoresis, 1998. **19**(11): p. 1853-61.

395. *Metabolic Profiling: Its Role in Biomarker Discovery and Gene Function Analysis*2003, Boston: Kluwer Academic Publishing.

396. Krebs, H.A., et al., *The fate of isotopic carbon in kidney cortex synthesizing glucose from lactate.* Biochem J, 1966. **101**(1): p. 242-9.

397. Mani, S.A., et al., *The epithelial-mesenchymal transition generates cells with properties of stem cells.* Cell, 2008. **133**(4): p. 704-15.

398. Al-Hajj, M., et al., *Prospective identification of tumorigenic breast cancer cells.* Proc Natl Acad Sci U S A, 2003. **100**(7): p. 3983-8.

399. Sleeman, K.E., et al., *CD24 staining of mouse mammary gland cells defines luminal epithelial, myoepithelial/basal and non-epithelial cells.* Breast Cancer Res, 2006. **8**(1): p. R7.

400. Sheridan, C., et al., *CD44+/CD24- breast cancer cells exhibit enhanced invasive properties: an early step necessary for metastasis.* Breast Cancer Res, 2006. **8**(5): p. R59.

401. B. Perez White, D.T., *T47D/PKC Cells Are Nonmigratory and Noninvasive In Vitro Despite Tamoxifen Resistance In Vivo*, in *Thirty-Second Annual CTRC-AACR San Antonio Breast Cancer Symposium*2009, Cancer Research: San Antonio, TX.

Biography

Kelly Marie Kennedy was born Wednesday, May 19, 1982.She grew up in Bucks County, PA with her loving and devoted parents, Thomas and Florene Kennedy, and her talented and entertaining brothers, Thomas and Donald Kennedy. She attended Council Rock High School until 2000. Following which, she attended Millersville University in Lancaster, PA for undergraduate studies. She earned a B.S. in Biology with an option in Medical Technology/Clinical Laboratory Science (MT/CLS) and a minor in English in 2005. Also in 2005, she earned her certification for MT/CLS from the American Society for Clinical Pathology (ASCP); however, she decided to dedicate her young adulthood to research. In 2005, she was admitted to the Pathology department at Duke University to pursue her PhD in Pathology, focusing on tumor metabolism.

She currently lives in Durham, NC with her caring and handsome chemist boyfriend, Niko, and their 2 cats (Lily and Tucker) and husky (Sky). When funds allow, she enjoys indulging in vinyl records so that she may listen to the wailing guitar of Jimi Hendrix, the gritty compositions of Portishead and the rich voice of Freddie Mercury. She enjoys classic and contemporary literature, especially the works of Albert Camus and Fyodor Dostoyevsky. Yoga, art and Eastern philosophies like Taoism and Buddhism keep her balanced and grateful.